MAJORANA BOUND STATES

Readout, decoherence and generalizations

Munk, Morten Ib Kjærgaard

Publication date:
2020

Document version
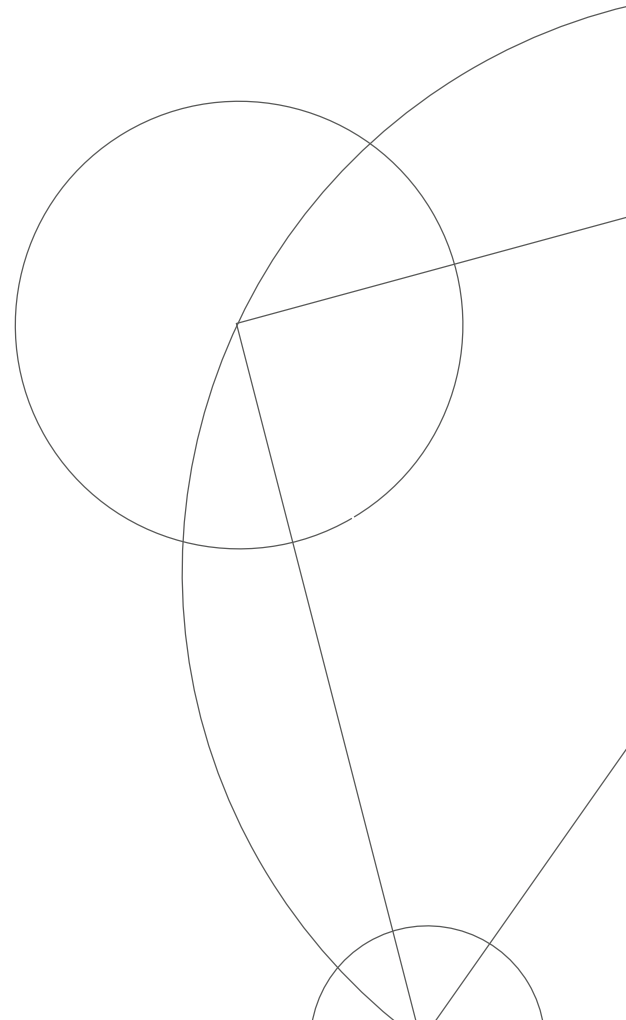Publisher's PDF, also known as Version of record

MAJORANA BOUND STATES:
Readout, decoherence and generalizations

PhD thesis
Morten Ib Kjærgaard Munk

April 2020

Preface

The work presented in this PhD thesis was carried out under the supervision of professor Karsten Flensberg at the Niels Bohr Institute, in the Condensed Matter Theory group at the University of Copenhagen. The work was done between september 2015 and April 2020 as part of an integrated master's and PhD programme. As such, a part of this thesis builds on the master's thesis titled *Dephasing of Majorana Box Qubits*, which was defended August 30$^{\text{th}}$ 2017.

The thesis is structured in three parts: An introduction providing the necessary concepts for following the projects, four research papers and an epilogue expanding upon the future research perspectives.

Project D was supervised by assistant professor Michele Burrello.

Morten Ib Kjærgaard Munk

Morten Ib Kjærgaard Munk
Frederiksberg, April 2020

Included projects:

Project A:

Parity-to-charge conversion in Majorana qubit readout
Morten I. K. Munk, Jens Schulenborg, Reinhold Egger and Karsten Flensberg
ArXiv preprint: arXiv:2004.02123. Submitted April 2020

Project B:

Dephasing of Majorana qubits due to classical noise
Morten I. K. Munk and Karsten Flensberg
Adapted from master's thesis, titled Dephasing of Majorana Box Qubits, defended August 30th 2017, supervised by Karsten Flensberg

Project C:

Fidelity and visibility loss in Majorana qubits by entanglement with environmental modes
Morten I. K. Munk, Reinhold Egger and Karsten Flensberg
Physical Review B 99, 155419 (2019)

Project D:

Dyonic zero-energy modes
Morten I. K. Munk, Asbjørn Rasmussen and Michele Burrello
Physical Review B 98, 245135 (2018)

Abstract

The study of topological phases has become one of the most active areas of the field of condensed matter physics. In the last decade, there has been immense experimental progress, owing to quantum leaps in materials science and the theoretical understanding of these systems. A remarkable example of topological phases is topological superconductors. These unusual superconductors are believed to host exotic Majorana quasiparticles whose underlying physics epitomizes the concept of "spooky action at a distance" in quantum mechanics: Simply moving them around one another can change the occupation of fermionic modes. In fact, by braiding them in a complicated fashion, most of the gates necessary for building a quantum computer may be implemented. Furthermore, since quantum information is stored in non-local degrees of freedom, qubits based on Majoranas are believed to be inherently resilient to noise. Along with other promising future applications, this motivates the need for a better understanding of Majorana quasiparticles, which is the overarching theme of this PhD dissertation. Apart from providing a review of the relevant background, the dissertation provides new insights and methods regarding the physics of Majorana bound states. The original contributions in the thesis are contained in four projects.

Project A tackles the problem of reading out the state of a Majorana box qubit, a minimal qubit where quantum information is stored in Majorana bound states. By using a novel Lindbladian approximation, we develop a Markovian theory of the dynamics of the reduced density matrix of a Majorana box qubit whose parity degrees of freedom has been converted to charge through the coupling of a quantum dot. This coupling splits the ground state degeneracy, and the dot is subjected to a fermion-number preserving interaction with environment modes during the readout. Our model contains the dynamics of the readout apparatus, and we find analytical expressions for the decay rates. These analytical expressions are easily applicable for a wide range of possible experiments, and we provide two experimentally relevant examples as case studies.

In Project B, we calculate the dephasing dynamics of an isolated Majorana box qubit subjected to electromagnetic fluctuations in a capacitively coupled electric circuit. These fluctuations are treated as classically oscillating fields, allowing for an intuitive picture of the dephasing as accrued non-adiabatic corrections to the time evolution due to the shifting of the Majorana zero-energy mode. Since the exact form of the noise term is unknown, the corrections are calculated by statistically averaging over different noise functions by using the fluctuation-dissipation theorem.

The problem of dephasing of Majorana qubits due to electromagnetic noise is refined in Project C, where we develop a model using a Bloch-Redfield approach, thus keeping the quantum mechanical nature of the environment modes. This allows us to go to low temperatures, and at zero temperatures we find a potential source of fidelity loss in Majorana parity readouts stemming from the fact that the zero-energy modes are dressed by the bosons, while the readout apparatus measures the bare Majorana modes. We calculate this fidelity loss for a projective measurement of the bare Majoranas, and we find that this can lead to a considerable source of errors. In proposals using measurement-based braiding of Majorana qubits, this error source thus enters into all stages of initialization, manipulation and readout of the qubits.

Finally, in project D we propose a model which generalizes Majorana zero-energy modes. It is constructed by starting from a bosonic model analogous to the Ising model, except where the local degrees of freedom and the global gauge symmetry are related to an arbitrary finite non-abelian group. By constructing a generalized Jordan-Wigner transformation, we map the model onto a local model with dyonic

degrees of freedom, meaning that they carry both a "magnetic charge" in the form of a group element index, as well as an "electric charge" corresponding to an irreducible representation of the group. We find that the model generically has a topological phase with zero-energy dyonic edge modes. The zero-energy modes are in general weak zero-energy modes, meaning that their degeneracy does not extend to all excited states. We discuss conditions under which the ground state is topologically ordered. When these conditions are not met, the ground states may be locally distinguishable, owing to the appearance of holographic symmetry operators localized on the boundary. The fusion rules of these dyonic zero-energy modes are discussed, but determining the braiding statistics remains an open problem.

Together the four projects expand upon our knowledge of Majorana physics in the context of topological quantum computation as well as our general understanding of emergent anyonic zero-energy modes. Hopefully, they will serve to guide theoretical and experimental condensed matter research towards establishing the existence of non-abelian anyons as a scientific fact.

Resumé

Studiet af topologiske faser er et af faststoffysikkens mest aktive forskningsområder. I det sidste årti er der sket store eksperimentelle fremskridt på grund af kvantespring i materialevidenskab og den teoretiske forståelse af disse systemer. Et bemærkelsesværdigt eksempel på topologiske faser er topologiske superledere. Disse usædvanlige superledere forventes at have eksotiske Majorana-kvasipartikler, hvis underliggende fysik understreger kvantemekanikkens forunderlige ikke-lokale natur: Ved blot at flytte disse partikler rundt om hinanden kan besættelsen af fermioniske tilstande ændres, og med den type processer kan man implementere de fleste af de gates, der er nødvendige for at bygge en kvantecomputer. Eftersom kvanteinformation lagres i ikke-lokale frihedsgrader, antages qubits, der er baseret på Majorana-kvasipartikler, at være modstandsdygtige over for støj. Sammen med andre lovende fremtidige anvendelser motiverer dette behovet for en bedre forståelse af Majorana-kvasipartikler, og dette er det overordnede tema i denne ph.d.-afhandling. De originale bidrag i afhandlingen er indeholdt i fire projekter.

Projekt A fremstiller en teori for aflæsningen af tilstanden af en såkaldt Majorana box qubit, hvor kvanteinformation er gemt i bundne Majorana tilstande. Ved at bruge en ny Lindblad approksimation udvikler vi en Markoviansk teori for dynamikken af den reducerede tæthedsmatrix af en Majorana box qubit, hvis paritetsfrihedsgrader er konverteret til ladning gennem koblingen af en kvantedot. Denne kobling splitter de udartede grundtilstande, og kvantedotten udsættes for bosoniske interaktioner under aflæsningen. Vores model indeholder dynamikken af målesudstyret, og vi udleder analytiske udtryk for henfaldsraterne. Disse analytiske udtryk kan anvendes til at beskrive mange forskellige eksperimenter, og vi præsenterer to eksperimentelt relevante eksempler som casestudier.

I Projekt B beregner vi dekohærensdynamikken for en isoleret Majorana box qubit udsat for elektromagnetiske fluktuationer i et kapacitivt koblet elektrisk kredsløb. Denne støj behandles som et klassisk felt, hvilket muliggør et intuitivt billede af dekohærens som ikke-adiabatiske korrektioner til tidsudviklingen på grund af en forskydning af Majorana-bølgefunktionen. Da den eksakte form af støjen er ukendt, beregnes korrektionerne ved en statistisk midling ved hjælp af fluktuations-dissipations teoremet.

Analysen af dekohærens i Majorana-qubits på grund af elektromagnetisk støj forfines i Projekt C, hvor vi udvikler en model ved hjælp af Bloch-Redfield teorien, og således bevarer den kvantemekaniske natur af frihedsgraderne. Dette giver os mulighed for at gå til lave temperaturer, og ved nul temperatur finder vi en potentiel kilde til fejl i Majorana paritetsudlæsninger, der skyldes, at Majorana-pariklerne er sammenfiltrede med bosonerne, mens måleapparatet måler de uperturberede Majorana-tilstande. Vi beregner udfaldene for projektive målinger af de uperturberede Majorana-tilstande, og vi finder at denne effekt kan medføre betydelig fejl. Dette kan potentielt spille en vigtig rolle i Majoranabaserede kvantecomputerarkitekturer baseret på såkaldt "measurement-based braiding", hvor alle operationer foregår gennem paritetsmålinger.

Endelig foreslår vi i projekt D en model, der generaliserer bundne Majorana-tilstande. Den er konstrueret ved at starte fra en bosonisk model, der er inspireret af Ising-modellen, bortset fra at de lokale frihedsgrader, samt den globale gaugesymmetri, er relateret til en vilkårlig, endelig, ikke-abelsk gruppe. Ved at konstruere en generaliseret Jordan-Wigner-transformation afbilder vi modellen til en lokal model med dyoniske frihedsgrader, hvilket betyder, at de både har en "magnetisk ladning", svarende til et gruppeelement, såvel som en "elektrisk ladning" svarende til en irreducibel repræsentation af gruppen. Vi finder her, at modellen generelt har en topologisk fase med dyoniske kanttilstande ved nul energi. Disse

kanttilstande er generelt svage nulenergitilstande, hvilket betyder, at deres udartethed ikke gælder for alle anslåede tilstande. Vi diskuterer forhold, under hvilke grundtilstanden er topologisk ordnet. Når disse betingelser ikke er opfyldt, kan grundtilstanden måles lokalt på grund af holografiske symmetrioperatorer, der opstår lokaliseret på kanten. Fusionsreglerne for disse dyoniske nulenergitilstande diskuteres, men deres "braiding" statistik er stadig et åbent spørgsmål.

Tilsammen udvider de fire projekter vores viden om Majorana-partiklernes fysik og deres anvendelse i topologiske kvantecomputere, såvel som vores generelle forståelse af emergente anyoner. Forhåbentlig vil disse projekter kunne vejlede teoretisk og eksperimentel forskning mod at etablere eksistensen af ikke-abelske anyoner.

Acknowledgements

I would like to thank Karsten Flensberg and Michele Burrello for being great and gentle supervisors. I have always felt welcome with my many questions and left discussions inspired. I'm grateful for our work together and I hope that we can keep collaborating in the future. Furthermore, I would like to thank Karsten for being an excellent mountain bike teacher and Michele for loyally showing up to my concerts.

It has been a real pleasure to do my PhD in the CMT group. It is an inspiring work environment, full of enthusiastic discussions and drawn-out group meetings due to too many questions. I'm particularly grateful for all my past and present colleagues. All the physics discussions have been stimulating, and I highly value the many friendships I have made. Writing my thesis mostly during the strange time that has been the spring of 2020, I have come to realize just how important it is to me. During my more than four years in the group, a lot of people have come and left, but all iterations of the group have been special. One had the CMT Chess Club, another parkour and climbing and a third afternoon tea parties. I would also like to highlight the CMT lunch club, which has made every lunch break an opportunity for experimental culinary experiences while enjoying ludicrous discussion topics.

I would like to thank Ida Egholm Nielsen for help with proofreading of this thesis.

Lastly, but certainly not least, I want to thank my wife Kamilla, who has been a big support throughout my PhD and who has managed to put up with a very busy version of me for the last six months.

Contents

Motivation and scope of thesis

The quote "more is different" by the late legendary physicist Philip Anderson [9] summarizes the philosophy of the field of condensed matter physics in just three words. Through the complex interplay of many ordinary electrons, order can emerge which is completely unrecognizable from its constituents.

In some cases this manifests itself in striking behaviour observable in macroscopic systems, a good example being superconductors levitating in a magnetic field. But other times, one would have to look through the tip of a tunneling scanning microscope to appreciate the curious effects. However, the results can be no less dramatic. A beautiful example of this is Majorana bound states, predicted to emerge in exotic superconductors under the right circumstances. These bizarre quasiparticles in a sense behave as half electrons, with two of them needed to define a normal fermionic particle. They are their own antiparticles and are ideally bound to zero energy. But the property for which they are most famous is their non-abelian braiding statistics. By simply moving Majoranas around one another in various patterns, non-trivial transformations can be made on the ground state manifold. This property is a feature of the topology of the ground state many-body wavefunction, and the result of such a process is independent of the fine geometric details of the paths the Majoranas travel around one another, even if the Majoranas are very far from each other. Thus, they offer a very clear demonstration of the non-local nature of quantum mechanics. Presently, Majorana bound states are believed to have been observed, but actually braiding them and demonstrating their topological properties has yet to be achieved.

The motivation for studying Majorana bound states is two-fold. Firstly, from the perspective of fundamental science, they behave unlike any known elementary particle, and proving their topological nature would be a major scientific discovery. Secondly, they have been proposed as a candidate for implementing topological quantum computation. With this is meant quantum computation carried out using non-local degrees of freedom, that are inherently resilient to noise, and where operations are implemented using fault-tolerant procedures. Drawing upon the resources of quantum entanglement and quantum contextuality [42], quantum computers and have been theoretically shown to be able to efficiently solve certain problems that regular classical computers cannot. Because of this, building a quantum computer could potentially have far-reaching consequences for society.

This thesis is dedicated to the study of Majorana bound states, and contributes to our knowledge of how to read out their quantum information, how that information leaks out when they are subjected to electromagnetic noise, and how to generalize them to new Majorana-like states with richer structure. It contains four projects, two of which are published, one which has recently been submitted and one which is unpublished. It is structured in the following way:

Chapter 1: Introduction reviews the physics of Majorana bound states and where to find them. It is described how qubits can be built from Majorana bound states, and how operations may be performed on them to achieve universal quantum computation. The chapter also provides a brief discussion of previous dephasing studies of Majorana qubits. Next, the mathematical tools used for studying the open quantum systems in Project A and C are detailed. Finally, the necessary background is given to motivate Project D. As that project is based upon extending a generalization of Majoranas, known as parafermions, an introduction to parafermions is provided.

Chapter 2: Project A contains the first scientific paper of the thesis, titled *Parity-to-charge conversion in Majorana qubit readout*. The project presents a flexible theory of the readout dynamics of Majorana qubits. The theory uses a novel Lindbladian approximation, guaranteeing complete positivity.

Chapter 3: Project B contains a study of the dephasing dynamics of Majorana qubits subjected to electromagnetic noise, modeled as classically varying potentials in an electric circuit.

Chapter 4: Project C contains the second scientific paper of the thesis, titled *Fidelity and visibility loss in Majorana qubits by entanglement with environmental modes*, which studies the dephasing dynamics of Majorana qubits and the fidelity reduction of Majorana qubit readouts due to quantum electromagnetic noise.

Chapter 5: Project D contains the third scientific paper, titled *Dyonic zero-energy modes*. This project introduces a family of models generalizing the Ising model from $\mathbb{Z}_2$ degrees of freedom to those given by a finite non-abelian group G. A generalized version of the Jordan-Wigner transformation maps the models to dyonic models, which are shown to have topological phases with dyonic zero-energy edge modes, whose anyonic structure is richer than that of Majorana zero-energy modes.

Chapter 6: Epilogue finally concludes the thesis, summarizing the findings of the four projects and reflecting on future research prospects.

Chapter 1

Introduction

1 Majorana zero-energy modes

The ground-breaking idea that many phases of matter may be understood from spontaneous symmetry breaking has led to a deep understanding of a wide variety of macroscopic phenomena, such as magnetism, solids and superconductors as well as microscopic phenomena, such as the Anderson-Higgs mechanism in particle physics. But over the last two decades, there has been a major shift in the condensed matter community towards studying a new group of phases called topological phases. In contrast with most ordinary phases, they are characterized by quantum phase transitions, also occuring at zero temperature, and continuous symmetries largely don't play a role. These phases typically have physical features which are encoded in the many-body wavefunctions of the ground states, and which are resilient to most local perturbations, as long as the gap to the excited states doesn't close. Two examples of such features are the edge currents in the integer quantum Hall effect [34] and the chiral counterpropagating edge modes of the quantum spin Hall effect [70]. In the former case, the edge current is unaffected by local perturbations in the bulk of the system and doesn't backscatter on impurities on the edge. In the latter case, the edge currents are also resilient, but not against magnetic impurities; the topological features are only protected from perturbations respecting time-reversal symmetry. Many topological systems share similar behaviour, and the topological features are only robust against perturbations so long as they don't break certain discrete symmetries.

A truly striking feature of some topological phases is the emergence of non-abelian anyons. These are quasiparticles which behave completely different from ordinary fermions and bosons. Majorana zero-energy modes is an example of such novel quasiparticles, and are the central object of this section, and indeed, the entire thesis. Before we turn to reviewing the properties and physics of Majorana zero-energy modes, we would like to dwell for a moment on why anyons are expected to exist in the first place. The standard textbook introduction to the quantum theory of identical particles argues that the exchange of two particles shouldn't affect the probabilities, and together with the constraint that two swaps should be the identity, fermionic and bosonic statistics are derived as the only possibilities [36]. So why should there be any room for non-abelian anyons?

In 2D, a more careful argument reveals that there are a host of other options [51, 79, 61]. A mathematically beautiful argument was first outlined in Ref. [51] and is concisely explained in Ref. [21]. It takes some very rudimentary algebraic topology, but to the author of this thesis, the aesthetics of the simplicity with which it leads to the possibility of non-abelian anyons compels him to present it in Section 1.1.

After this, in the rest of this section we will cover the basics of Majorana bound states, as relevant to this thesis. In Section 1.2 we discuss the formal definition and their properties, as well as how they can be used in topological quantum computation. In section 1.3 we discuss prerequisites for finding Majorana bound states in 1D systems, and we will focus on the Oreg-Lutchyn model for Majorana nanowires [62, 54] as the main example. Lastly, in section 1.4 we review the role of charging energy in building useful qubits for topological quantum computation using Majorana nanowires. The Majorana box qubit is introduced and we discuss how to manipulate and read out the qubit.

3

1.1 A very short introduction to anyons

First, we should carefully define the notion of a configuration space $\mathcal{C}_n(\mathcal{M})$ for a group of n identical particles moving on a manifold $\mathcal{M}$. For the classification of particles, we will exclude the measure-0 subspace D_n in which the position of two or more of the n particles coincide, and by virtue of the particles being identical, we identify points in configuration space which are obtained by permuting the n particles. Thus we write

$$\mathcal{C}_n = (\mathcal{M}^n - D_n)/S_n, \tag{1.1}$$

where S_n is the n-element permutation group, whose group elements act on configuration space by permuting the particles' positions. We would like to find a way to describe how the wavefunctions behave when the particles are rearranged from an initial configuration $x \in \mathcal{C}_n$ into an indistinguishable one. That is, we define a loop $p : [0,1] \to \mathcal{C}_n$, such that $p(0) = p(1) = x$. We are looking for properties independent of the details of the particular path, so we say that the loops $p(s)$ and $p'(s)$ are equivalent if one can be continuously deformed into the other. This equivalence defines an equivalence relation $\sim$, and the equivalence classes of loops can be given a group structure by defining the following product:

$$(p * p')(s) = \begin{pmatrix} p(2s) & : & 0 \le s \le 1/2 \\ p'(2s) & : & 1/2 < s \le 1 \end{pmatrix}. \tag{1.2}$$

The set of loop equivalence classes on $\mathcal{C}_n(\mathcal{M})$ equipped with the product $*$ forms a group $\pi_1(\mathcal{C}_n(\mathcal{M}))$ called the fundamental group of $\mathcal{C}_n(\mathcal{M})$. The identity element of $\pi_1(\mathcal{C}_n(\mathcal{M}))$ is the equivalence class of contractible loops, and inverse element $[p]_\sim^{-1}$ of an equivalence class $[p]_\sim$ of a loop p is defined as the equivalence class of the function $p(1-s)$; intuitively, the loop is run backwards.

Now, the identification of possible species of identical particles amounts to finding the unitary irreducible representations of $\pi_1(\mathcal{C}_n(\mathcal{M}))$. This is a fancy way of saying that we want to figure out which unitary operation the Hilbert space transforms under when one or more particles are exchanged any number of times, and in any order. In 1D, $\pi_1(\mathcal{C}_n(\mathbb{R}))$ itself becomes trivial, since it is not possible for the particles to avoid one another. In 3D or higher, loops in configuration space are only non-contractible when particles are exchanged, and there is no notion of an orientation during such an exchange. This implies that $\pi_1(\mathcal{C}_n(\mathbb{R}^m)) = S_n$ for $m \ge 3$. It turns out that only the one-dimensional unitary irreducible representations should be considered for fundamental particles[1], which gives two type of particles: Those that transform under the trivial representation, meaning bosonic statistics, and those that transform under the antisymmetric, meaning fermionic statistics. In 2D, however, there are many more non-contractible loops. All non-contractible loops can be generated by considering sequential exchange of particles and keeping track of the direction of the exchange. For visualization, imagine rotating the plane so the n particles appear to be positioned on a line next to each other, as shown on Figure 1, and we then label the particles from left with $i = 1, \ldots, n$. Any non-contractible loop in configuration space can then be constructed by a series of neighbor exchanges, and we draw the worldlines of the particles by letting time increase in the direction perpendicular to the plane. If we define the operators τ_i that exchanges the position r_i and r_{i+1}, with particle i passing in front of particle $i + 1$, then those operators generate $\pi_1(\mathcal{C}_n(\mathbb{R})^2)$. In Figure 1 the worldlines corresponding to the braid $\tau_i^{-1}\tau_{i-1}\tau_i$ are drawn. Formally, the τ_i are defined by the relations

$$\tau_i\tau_{i+1}\tau_i = \tau_i\tau_{i+1}\tau_i \tag{1.3a}$$

$$\tau_i\tau_j = \tau_j\tau_i, \quad |i - j| \ge 2. \tag{1.3b}$$

This defines the so-called *braid-group* $\mathcal{B}_n = \pi_1(\mathcal{C}_n(\mathbb{R}^2))$, and non-abelian anyons are defined as particles that transform under non-abelian unitary irreducible representations of the braid group under exchange. Note that if the number of particles $n = 2$ the braid group itself is abelian, so there has to always be more than 2 particles in order for the many-body wavefunction to transform in a non-abelian way. The Majorana modes, which are the concern of the majority of this thesis, are the simplest examples of non-abelian anyons, allowing for a description using a fermionic Fock space.

Non-abelian anyons still haven't been discovered as fundamental particles, but they have been predicted to emerge as quasiparticles in condensed matter systems. Since such systems ultimately consist

---

[1]Higher dimensional representations correspond to so-called parastatistics. It has been conjectured, however, that every free theory of particles with para-bosonic or para-fermionic statistics is equivalent to a gauge theory of regular bosons or fermions, which is a possible argument why they should not be considered fundamental [11]. We will nevertheless familiarize ourselves with parafermions in section 3, as they form the simplest generalization of Majoranas.

of interacting electrons, the many-body wavefunction of such an anyonic system must encode the non-abelian braiding statistics in the global entanglement structure. Thus one would maybe suspect that they should emerge in strongly interacting systems. Indeed, the first proposed physical system with anyons was the fractional quantum Hall system with filling fraction $\nu = 5/2$ [56]. Incidentally, this system is predicted to host Majoranas, and by now a whole zoo of anyons have been predicted to emerge for different filling fractions. These systems all have a "long-range entanglement", meaning that the ground state cannot be transformed into a product state by a series of local unitary transformations [17].

Short-range entangled systems may also have phases with emergent anyonic quasiparticles, but that requires the system to obey a discrete symmetry, usually time-reversal, particle-hole or chiral symmetry [8] or crystalline symmetries, such as inversion or discrete rotations [32]. Such a phase is called a symmetry-protected topological phases.

Asoundingly, this fact provides a ground for realizing Majoranas in mesoscopic systems by cleverly combining ingredients which in principle have been available for over 60 years. Experimentally, the first sign of Majorana modes were seen in Delft in 2012 [58], just two years after the theoretical proposal had been put forward [62, 54]. By 2016, radical development in material science allowed for much clearer signatures of the zero-bias conductance peak associated with the Majorana bound states, while simultaneously demonstrating the exponential suppression of the energy splitting of the Majoranas in the system size [4, 22]. It remains to be explicitly demonstrated that these states are really the theoretically predicted Majorana modes, although evidence is mounting. For example, last year transport through the supposed Majorana zero-energy modes was demonstrated to be coherent [78], in accordance with the theoretical prediction [31].
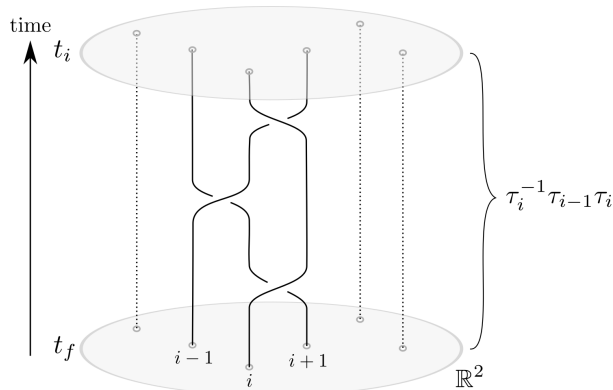

Figure 1: Representation of how an arbitrary braiding operation in $\mathbb{R}^2$ is generated from braiding neighbors. The worldlines of the particles are drawn with time moving in the upwards direction, and in this figure they represent the braiding operation $\tau_i^{-1}\tau_{i-1}\tau_i$ (note the opposite orientation of τ_i and τ_i^{-1} in the figure).

1.2 Formal properties of Majorana modes

In condensed matter systems, Majorana modes are mutually anti-commuting quasiparticles which are their own antiparticles. For a pair of Majorana modes, this means that their second quantized operators γ_1, γ_2 are Hermitian and anticommute:

$$\gamma_i^\dagger = \gamma_i, \tag{1.4a}$$
$$\{\gamma_i, \gamma_j\} = 2\delta_{i,j}. \tag{1.4b}$$

Because of the relations (1.4), one cannot define the occupation of a single Majorana mode, but a pair of Majorana modes γ_1, γ_2 define one single Dirac fermionic degree of freedom. If we define

$$f_{12} = \frac{\gamma_1 \pm i\gamma_2}{2}, \tag{1.5}$$

then f_{12} is an ordinary Dirac fermionic annihilation operator. Note that there is an inherent gauge freedom in choosing the sign in Eq. (1.5). This has important implications for the physics of Majorana systems: The number of fermions is only conserved modulo 2.

In systems consisting of several Majoranas, there is a further ambiguity in how to pair the Majoranas and form the fermionic states. This simple observation is actually at the heart of the remarkable topological properties which Majoranas are famous for. To understand this, let us consider a system consisting of four Majoranas $\gamma_1, \gamma_2, \gamma_3$ and γ_4. We assume for now that these four Majoranas constitute all degrees of freedom of the system, and as long as they are far away from each other, they don't interact in any way possible. Hence, the ground states are four-fold degenerate. One basis of the Hilbert space is $|n\rangle_{12}|n'\rangle_{34}$, where the states are defined as the eigenvectors of the fermionic number operator, $f_{ij}^\dagger f_{ij}|n\rangle_{ij} = n|n\rangle_{ij}$, and we use the sign convention

$$f_{34}^\dagger f_{12}^\dagger|0\rangle_{12}|0\rangle_{34} = |1\rangle_{12}|1\rangle_{34}. \tag{1.6}$$

We will now examine what happens to the state when we exchange two Majoranas, which is known as a *braid* [27]. We can derive the effect on the state of the system by noticing that the process is essentially a basis change. Assume for concreteness that the system is initially in the state $|0\rangle_{12}|0\rangle_{34}$ and consider the process sketched in Figure 2. First, γ_2 and γ_3 are exchanged, which is equivalent to changing to the basis $|n\rangle_{13}|n'\rangle_{24}$. Due to the conservation of fermionic parity, we write

$$|0\rangle_{12}|0\rangle_{34} = \alpha|0\rangle_{13}|0\rangle_{24} + \beta|1\rangle_{13}|1\rangle_{24}. \tag{1.7}$$

We may then calculate α and β by writing f_{12} and f_{34} in terms of f_{13} and f_{24} and impose

$$f_{12}|0\rangle_{12}|0\rangle_{34} = f_{34}|0\rangle_{12}|0\rangle_{34} = 0. \tag{1.8}$$

To do so, we need to be careful with the definitions of the fermionic operators. If we define all operators the same way, say $f_{ij} = (\gamma_i + i\gamma_j)/2$, then Eq. (1.8) cannot be consistently solved for α and β. If we define

$$f_{12} = \frac{\gamma_1 + i\gamma_2}{2}, \quad f_{34} = \frac{\gamma_3 + i\gamma_4}{2}, \tag{1.9}$$

then choosing to define $f_{13} = (\gamma_1 \mp i\gamma_3)/2$ imposes $f_{34} = (\gamma_2 \pm i\gamma_4)/2$. We associate the sign choice with the direction of the exchange. For the clockwise direction indicated in Figure 2 we choose

$$f_{13} = \frac{\gamma_1 - i\gamma_3}{2}, \quad f_{34} = \frac{\gamma_2 + i\gamma_4}{2}, \tag{1.10}$$

which implies that the Majorana operators may be written as

$$\gamma_1 = f_{13} + f_{13}^\dagger, \quad \gamma_2 = f_{24} + f_{24}^\dagger, \quad \gamma_3 = i(f_{13} - f_{13}^\dagger), \quad \gamma_4 = i(f_{24}^\dagger - f_{24}). \tag{1.11}$$

With this, Eq. (1.8) leads to

$$|0\rangle_{12}|0\rangle_{34} = \frac{1}{\sqrt{2}}\left(|0\rangle_{13}|0\rangle_{24} + i|1\rangle_{13}|1\rangle_{24}\right) = \frac{1}{\sqrt{2}}(1 - \gamma_2\gamma_3)|0\rangle_{12}|0\rangle_{34}. \tag{1.12}$$

As can be straightforwardly verified, braiding any two Majorana modes γ_i and γ_j clockwise amounts to applying the *braid operator*

$$B_{ij} \equiv \frac{1}{\sqrt{2}}(1 - \gamma_i\gamma_j). \tag{1.13}$$

Therefore braiding allows for non-trivial transformation of the ground-state manifold, implemented in a purely topological way, without any interactions between the individual Majoranas. If B_{ij} and B_{kl} share a Majorana, they don't commute, and the braid operators in Eq. (1.13) can be shown to form a unitary irreducible representation of the braid group, satisfying the defining relations in Eq. (1.3). We can visualize the effect of the braid in Eq. (1.12) on the Bloch sphere, as seen in Figure 2. We take the state $|00\rangle$ to be the north pole on the z axis, and the state $|11\rangle$ on the south pole. Braiding γ_2 and γ_3 clockwise therefore amounts to a rotation around the x-axis by an angle $\pi/2$. This immediately leads us to a stunning conclusion: A successive clockwise braid of γ_3 and γ_2 does not return the system to the initial state; rather, it changes the occupation of both fermionic states,

$$B_{23}^2|0\rangle_{12}|0\rangle_{34} = i|1\rangle_{12}|1\rangle_{34}. \tag{1.14}$$

With braiding, Clifford gates, that is Paulies, Hadamard and phase gate, can be implemented in a topologically protected way. In particular, for four Majoranas with an overall even fermionic parity, we can represent the basis states as

$$|0\rangle_{12}|0\rangle_{34} \equiv \begin{pmatrix} 1 \\ 0 \end{pmatrix}, \qquad |1\rangle_{12}|1\rangle_{34} \equiv \begin{pmatrix} 0 \\ 1 \end{pmatrix}, \tag{1.15}$$

and define a Pauli algebra as

$$\sigma_x = i\gamma_1\gamma_3, \quad \sigma_y = -i\gamma_2\gamma_3, \quad \sigma_z = i\gamma_1\gamma_2. \tag{1.16}$$

In this basis we find

$$B_{13}^2 = i\sigma_x, \quad B_{32}^2 = i\sigma_y, \quad B_{12}^2 = i\sigma_z, \tag{1.17}$$

and the Hadamard gate $\hat{H}$ and phase gate $\hat{S}$ are formed as

$$B_{12} = e^{i\pi/4} \begin{pmatrix} 1 & 0 \\ 0 & -i \end{pmatrix} = e^{i\pi/4}\hat{S}, \tag{1.18a}$$

$$B_{12}B_{13}B_{12} = \frac{i}{\sqrt{2}} \begin{pmatrix} 1 & 1 \\ 1 & -1 \end{pmatrix} = i\hat{H}. \tag{1.18b}$$

Universal quantum computation is not possible using only braiding. The reason is that braiding Majorana modes does not produce entanglement [13]. This statement can be intuitively understood from our discussion above, since braiding was derived from basis changes. It turns out that CNOT may be implemented in protected ways by using other means than braiding. But even so, a non-Clifford gate is needed for running algorhithms which cannot be efficiently simulated on a classical computer [35]. Different gates, such as T-gate, has to be implemented in a non-protected way, such as by magic state distillation.

The picture we have used to derive the braiding rules is also useful for explaining the process of *Majorana fusion*. The definition of this is a projective measurement of the combined parity of a pair of Majorana modes. This can for example be implemented by bringing a pair close together, allowing them to overlap and obtain a charge which can be measured, collapsing the state to being either empty or filled. The possible fusion channels can be found by doing a basis change. From Eq. (1.12), if the state $|0\rangle_{12}|0\rangle_{34}$ is prepared and γ_1 and γ_3 are fused, the possible outcomes are the vacuum state $|0\rangle_{13}$ and the occupied state $|1\rangle_{13}$, both with probability 1/2.

In the next section we will see how solid-state systems hosting Majorana modes may be constructed. In all the projects in this thesis, we study the dynamics of one-dimensional systems. The reason is that by far the greatest experimental progress has been made here, and currently the expectation seems to be that if we should realize topological quantum computation using Majorana modes, it will most likely be to be successful using either 1D systems or effectively 1D systems[2]. For this reason, we will exclusively focus on 1D in the following section.

1.3 Physical realization in 1D: The Majorana nanowire

Where should we expect these extraordinary quasiparticles to emerge? We need a solid-state system whose ground state allows for fluctuations of the number of pairs of fermions, and furthermore, in order to have quasiparticles which are their own anti-particles, there has to be a coupling between electrons and holes. These conditions are qualitatively fulfilled by superconductors. As we shall see, very particular superconductors do allow for topological phases where Majorana zero-energy modes are present. In 1D they are bound to the boundary of the system or at interfaces between parts of the system in the topological and trivial phase. For this reason, they are refered to as Majorana bound states.

Whether Majorana bound states can emerge in a particular superconductor depends crucially on the symmetries of the Cooper-pair- and bogoliubon wavefunctions, or equivalently of the pairing potential Δ_k. Conventional s-wave superconductors where the electrons pair up into spin-singlet states do not

---

[2]Based on the previous section, non-abelian anyons should not appear in 1D. The reconciliation happens when one considers the fact that in order to access the topological properties of Majoranas in 1D systems, one has to effectively extend the system to 2D, for instance by moving the Majoranas in both dimensions, or through couplings between distant Majoranas.
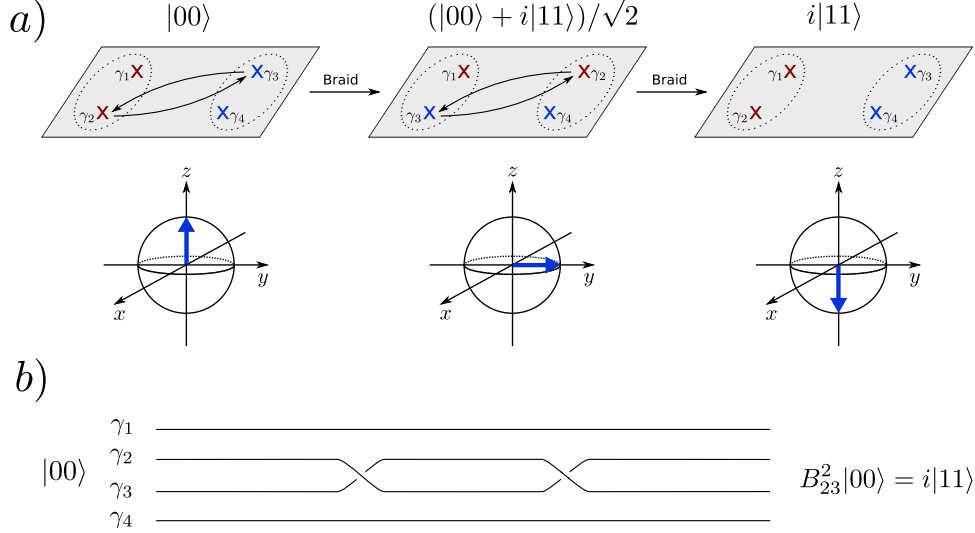
Figure 2: Sketch of a braiding process. Panel $a)$ depicts a system of four Majoranas, $\gamma_1, \gamma_2, \gamma_3, \gamma_4$ subjected to two successive braids, exchanging γ_2 and γ_3 twice in a clockwise fashion. Through the process, the chosen basis is always that of the occupancy of the left-most and right-most pairs of Majoranas. The initial state is $|00\rangle$, and after braiding γ_2 and γ_3 once, the state is now $(|00\rangle + i|11\rangle)/\sqrt{2}$. After the final braid, the state is proportional to $|11\rangle$. These steps are indicated on the Bloch sphere, with $|00\rangle$ and $|11\rangle$ being the north- and south poles, respectively. Each braid results in a counter-clockwise rotation by an angle of $\pi/2$ around the x-axis of the Bloch sphere. Panel $b)$ shows the braiding diagram for the process in panel $a)$, with time increasing in the right direction.

allow for Majorana bound states. Instead, one needs to procure a more exotic pairing, where the pairs form spin-triplets. Such pairings can happen for example in the presence of ferromagnetic interactions [19], but in general, it is hard to procure an intrinsic triplet pairing. But in mesoscopic systems, where materials with different properties are combined, it is theoretically simpler. The idea is essentially that if a semiconductor with a strong spin-orbit coupling and a strong Zeeman splitting is proximitized by an s-wave superconductor, it develops a pairing in a single helical band. Since there is only a single band, this is qualitatively like a spin-triplet pairing. Thus, it is possible to engineer the exotic superconductive pairing needed for Majorana bound states using readily available ingredients from mesoscopic physics.

Before we turn to this system in more detail, let us familiarize ourself a bit more with unconventional pairings and the consequences for subgap states. First, to understand the correspondence between the pairing symmetry and the Cooper-pair wavefunction consider the following BCS Hamiltonian for a general spin-independent repulsion [19]:

$$H_{\text{BCS}} = \sum_{k,\sigma} \xi_k c_{k\sigma}^\dagger c_{k\sigma} + \sum_{k,k'} V_{k,k'} c_{k\uparrow}^\dagger c_{-k\downarrow}^\dagger c_{-k'\downarrow} c_{k'\uparrow}. \tag{1.19}$$

Here, σ denotes spin-z projection and $\xi_k = k^2/(2m) - \mu$ with μ denoting the chemical potential. We focus on the inversion-symmetric case where $V_{-k,-k'} = V_{k,k'}$. The interaction in the BCS Hamiltonian is understood to only involve states close to the Fermi energy. Up to a constant energy shift, in the mean-field approximation Eq. (1.19) becomes

$$H_{\text{BCS}} \approx \sum_k \Psi_k^\dagger H_{\text{BdG},k} \Psi_k, \tag{1.20}$$

where the BdG Hamiltonian is

$$H_{\text{BdG},k} = \begin{pmatrix} \frac{k^2}{2m} - \mu & \Delta_k \\ \Delta_k^* & -\frac{k^2}{2m} + \mu \end{pmatrix}, \tag{1.21}$$

the Nambu spinor Ψ_k is defined by

$$\Psi_k \equiv \begin{pmatrix} c_{k,\uparrow} \\ c_{-k,\downarrow}^\dagger \end{pmatrix}, \tag{1.22}$$

8

and the pairing potential Δ_k is determined self-consistently through the expression [16]

$$\Delta_k = -\sum_{k'} V_{k,k'} \langle c_{-k'\downarrow} c_{k'\uparrow} \rangle . \tag{1.23}$$

In Eq. (1.23), the expectation value is taken with respect to the ground states, which is a coherent state for the pair creation operator

$$|\Psi_0^{\mathrm{BCS}}\rangle \propto \exp\left(\sum_k w_k c_{k,\uparrow}^{\dagger} c_{-k,\downarrow}^{\dagger}\right) |FS\rangle, \tag{1.24}$$

where $|FS\rangle$ is the Fermi sea, containing filled states up to the Fermi level. For the present example, the gap equation Eq. (1.23) can be cast in the form of the BCS gap equation [19]:

$$\Delta_k = -\sum_{k'} V_{k,k'} \frac{\Delta_{k'}}{2E_{k'}} \tanh\left(\frac{\beta E_{k'}}{2}\right), \tag{1.25}$$

where $E_k = \sqrt{\xi_k^2 + |\Delta_k|^2}$. Note that there is no a priori reason that the BdG Hamiltonian in Eq. (1.21) should imply that the pairing in Eq. (1.25) should turn out to be an even or an odd function of k. One should therefore be cautious when concluding from the BCS Hamiltonian in Eq. (1.19) whether the pairing is singlet or triplet, even though at first glance it appears to be pairing electrons into spin-singlets. The reason is that the state $|k,\uparrow\rangle|-k\downarrow\rangle$ is neither a spin-singlet or triplet. One has to respectively take the antisymmetric or the symmetric state under spin-exchange. To explicitly see that a generic k-dependent interaction $V_{k,k'}$ has pairing in both a singlet and triplet channel, we rewrite the pairing term in the BCS Hamiltonian before mean-field, casting Eq. (1.19) into the form

$$H_{\mathrm{BCS}} = \sum_{k,\sigma} \xi_k c_{k\sigma}^{\dagger} c_{k\sigma} + \frac{1}{4} \sum_{k,k'} \left(V_{k,k'}^S \Lambda_{S,k}^{\dagger} \Lambda_{S,k} + V_{k,k'}^T \Lambda_{T,k}^{\dagger} \Lambda_{T,k}\right), \tag{1.26a}$$

$$V_{k,k'}^{S/T} = \frac{V_{k,k'} \pm V_{-k,k'}}{2}, \tag{1.26b}$$

$$\Lambda_{S/T,k} = c_{-k\downarrow} c_{k\uparrow} \mp c_{-k\uparrow} c_{k\downarrow}, \tag{1.26c}$$

where we have made use of the inversion symmetry $V_{-k,-k'} = V_{k,k'}$. Hence, there are two different terms projecting onto singlet- and triplet pairing. In the standard introductory textbook treatment $V_{k,k'}$ is taken to be the Coulomb electron-electron repulsion, renormalized by electron-phonon interactions to yield an effective interaction which is k-independent and attractive for k and k' sufficiently close to the Fermi momenta, and zero otherwise. The gap equation Eq. (1.25) then implies that Δ_k becomes independent of k, and based on the above discussion, the electrons pair up into spin-singlet states since this interaction has $V_{k,k'}^T = 0$. The leading contribution to the Cooper-pair wave function has zero orbital angular momentum, meaning that the pair form an s-orbital, which is the origin for the term s-wave superconductor. With different interactions, there also exist spin-singlet superconductors with pairings where the Cooper-pairs have an angular momentum. An example is d-wave superconductors where the Cooper-pairs form d-orbitals. By using a different possibly spin-dependent interaction, it is possible to have the pairing predominantly be in the triplet channel. Such a pairing is called p-wave when the Cooper-pairs form p-orbital with a single unit of total angular momentum.

Let us briefly pause to comment on the relation between the Cooper-pair wave function and the pairing symmetry. Analogous to the above discussion, singling out the term in Eq. (1.24) corresponding to the factor in the product with wavenumber k does not constitute a properly symmetrized wavefunction, and one should also include the pair corresponding to $-k$. We may thus identify the state $|\psi_k^{\mathrm{CP}}\rangle$ with wavenumber k as

$$|\psi_k^{\mathrm{CP}}\rangle = \left(w_k c_{k,\uparrow}^{\dagger} c_{-k,\downarrow}^{\dagger} + w_{-k} c_{-k,\uparrow}^{\dagger} c_{k,\downarrow}^{\dagger}\right) |FS\rangle. \tag{1.27}$$

Hence, if $w_{-k} = w_k$ the Cooper-pair is bound in a spin-singlet state, but if $w_{-k} = -w_k$, then the state would spin-triplet with zero spin-z projection. Using Eq. (1.24) to evaluate Eq. (1.23), we see

$$\Delta_k \propto \sum_{k'} V_{k,k'} \prod_{k,k'} \left\langle FS \left| e^{w_k^* c_{-k',\downarrow} c_{k',\uparrow}} c_{-k,\downarrow} c_{k,\uparrow} e^{w_k c_{k,\uparrow}^{\dagger} c_{-k,\downarrow}^{\dagger}} \right| FS \right\rangle = \sum_{k'} V_{k,k'} w_{k'}. \tag{1.28}$$

9

Using $V_{-k,-k'} = V_{k,k'}$, we thus see that if $\Delta_{-k} = \pm\Delta_k$ then $w_{-k} = \pm w_k$, and we conclude that a spatially even pairing results in a spin-singlet pairing while a spatially odd pairing results in a spin-triplet pairing. For different interactions where electrons and holes with the same spin are paired the same result would follow.

Next, we turn to the nature of subgap states for the case of purely even or odd Δ_k, that is, for the singlet and triplet pairing, separately. These cases are described by BdG Hamiltonians in the form of Eq. (1.21), but their corresponding bases of Nambu spinors differ. Specifically, for the triplet case, we assume that pairing only happens with spins oriented in one particular direction, say $\sigma = \uparrow$. We write the BdG Hamiltonians in the singlet/triplet case as

$$H_{\text{BdG},k}^{S/T} = \begin{pmatrix} \frac{k^2}{2m} - \mu & \Delta_k^{S/T} \\ (\Delta_k^{S/T})^* & -\frac{k^2}{2m} + \mu \end{pmatrix}, \tag{1.29}$$

and the corresponding Nambu spinors are

$$\Psi_k^S = \begin{pmatrix} c_{k\uparrow} \\ c_{-k\downarrow}^\dagger \end{pmatrix}, \quad \Psi_k^T = \begin{pmatrix} c_{k\uparrow} \\ c_{-k\uparrow}^\dagger \end{pmatrix}, \tag{1.30}$$

respectively. The eigenvalues E_k of the BdG Hamiltonian in Eq. (1.29) are

$$E_k = \pm\sqrt{\left(\frac{k^2}{2m} - \mu\right)^2 + \left|\Delta_k^{S/T}\right|^2}. \tag{1.31}$$

For real k, these energies are always larger than a superconducting gap, $|E_k| \geq \Delta_{\text{SC}}$, and this energy corresponds to the minimum energy of a freely propagating fermionic quasiparticle. There are sometimes solutions with energies below the gap. Such states are collectively called *Andreev-bound states* [64], which in many cases arise in the vicinity of for example impurities, magnetic domains and interfaces outside of the superconductor. In particular, by definition, there are no states with real wavenumber k below the superconducting gap. Instead, a sub-gap state requires complex k. Note that for $(\Delta_k^{S/T})^*$ in Eq. (1.29), conjugation should happen before evaluating k. The reason is that the momentum operator is Hermitian, so $p^\dagger$ and p evaluated on a plane wave with imaginary wavenumber should give the same eigenvalue. The same is true for the expression $\left|\Delta_k^{S/T}\right|^2 = (\Delta_k^{S/T})^*\Delta_k^{S/T}$, which enters in Eq. (1.31).

For sub-gap states, the non-zero imaginary value of k implies that the state must be localized inside the superconductor near for instance a defect or an interface, hence the terminology "bound state". The Majorana states that we are looking for are special subgap states, whose energies are pinned to zero and whose hole and electron components have equal magnitude. This is guaranteed because of particle-hole symmetry, which exists for all superconductors, whenever there is only a single state at zero energy, or if such a state is completely isolated from other zero-energy states. For that to happen, the pairing needs to be in the triplet channel, as we shall see. For singlet/triplet pairing respectively, the particle-hole symmetry is described by the simple anti-unitary operator

$$\mathcal{P}_{S/T} = \eta_{y/x} K, \tag{1.32}$$

where η_i are the usual Pauli operators acting on the two-level system defined by $H_{\text{BdG},k}^{S/T}$, and K is complex conjugation. In terms of electrons and holes, both $\mathcal{P}_S$ and $\mathcal{P}_T$ change and electron operator with wavenumber k into a hole operator with wavenumber $-k$, where we remember that the complex conjugation operator K on the k-space Hamiltonian flips the sign of k, since $Kp = -p$. But furthermore $\mathcal{P}_S$ also flips the spin. We explicitly see that

$$KH_{\text{BdG},k}^{S/T} = \left[\left(\frac{k^2}{2m} - \mu\right)\eta_z + \text{Re}(\Delta_{-k}^{S/T})\eta_x + \text{Im}(\Delta_{-k}^{S/T})\eta_y\right]K, \tag{1.33}$$

meaning that $\{\mathcal{P}_{S/T}, H_{\text{BdG},k}^{S/T}\} = 0$ in the case of even/odd pairing, which defines particle-hole symmetry. If there exists a single isolated sub-gap state at zero energy, then that state is pinned to zero energy for an extended parameter range. In fact, this pinning is topological; it is not possible to move the state away from zero energy by continuous deformation of the Hamiltonian without closing the gap or breaking

the symmetry, as long as no other zero-energy solutions are nearby. For that reason, a phase with such an isolated zero energy state is an example of symmetry-protected topological phases.

To unpack the above claims, assume that $|\psi_E\rangle$ is a sub-gap eigenstate of $H_{\mathrm{BdG},k}^T$ with energy E. The particle-hole symmetry then implies that $\mathcal{P}_T|\psi_E\rangle$ is an eigenstate with energy $-E$. As mentioned above, we need a boundary in order to have a normalizable solution, so we will assume that the $1D$ system is described by the Hamiltonian $H(x) = H_{\mathrm{BdG},k}^T$ for positions $x \geq 0$, and the vacuum $H(x) = \infty$ for $x < 0$, which is equivalent to imposing the Dirichlet boundary condition $\psi_E(x=0) = 0$ for the real-space wavefunction $\psi_E(x) = \langle x|\psi_E\rangle$. If we write

$$\psi_E(x) = \begin{pmatrix} u_E(x) \\ v_E(x) \end{pmatrix}, \tag{1.34}$$

then the field operator $\hat{\Psi}_E(x)$ related to $|\psi_E\rangle$ can be written as

$$\hat{\Psi}_E = \int_0^\infty dx \begin{pmatrix} u_E(x) & v_E(x) \end{pmatrix} \begin{pmatrix} \hat{\Psi}(x) \\ \hat{\Psi}^\dagger(x) \end{pmatrix} = \int_0^\infty dx (u_E(x)\hat{\Psi}(x) + v_E(x)\hat{\Psi}^\dagger(x)), \tag{1.35}$$

where $\hat{\Psi}(x)$ is the annihilation operator for an electron at position x. On the other hand, the field operator $\hat{\Psi}'_E$ for the state $\mathcal{P}_T|\psi_E\rangle$ is

$$\hat{\Psi}'_E = \int_0^\infty dx (v_E^*(x)\hat{\Psi}(x) + u_E^*(x)\hat{\Psi}^\dagger(x)) = \hat{\Psi}_E^\dagger. \tag{1.36}$$

Now here is the punchline: If there only is a single solution at $E = 0$, then

$$\mathcal{P}_T|\psi_0\rangle = e^{i\theta}|\psi_0\rangle, \tag{1.37}$$

and through an appropriate gauge transformation, we can get rid of the complex phase, after which we may write

$$\hat{\Psi}_0 = \hat{\Psi}_0^\dagger. \tag{1.38}$$

Thus the zero-energy solution is really a Majorana zero-energy bound state! Notice that the condition in Eq. (1.37) is only possible to fulfill because the components of Ψ_k^T in Eq. (1.30) have the same spin. Searching for single zero-energy solutions for singlet-pairing would show that there are no solutions since $\mathcal{P}_S$ flips the spin of each component.

Suppose there are two isolated zero-energy solutions, localized at very distant boundaries so there is zero overlap between the two. Then each state still has to individually be eigenstates of the particle-hole operator since it doesn't involve any spatial transformations. Thus, both solutions are also Majorana zero modes. If the two states overlap, however, the two solutions will acquire a finite energy of $\pm E_0$. This energy splitting has to be exponentially suppressed in the system size, because the sub-gap states decay exponentially, as described above.

If the Hamiltonian with completely isolated Majorana zero-energy modes is continuously deformed using local perturbations, since particle-hole symmetry would otherwise imply that a new solution appeared, spontaneously changing the dimension of the Hilbert space. Thus, the gap has to close before the Majorana solutions can disappear.

It should be stressed that the first-quantized Majorana solution $|\psi_0\rangle$ does not describe a fermionic state in the Fock space. Instead, it describes the profile of the Majorana. In order to have a meaningful fermionic Fock space, one needs to have an even number of Majoranas, so fermionic states may be defined between the pairs. Importantly, there is no way to establish the topological nature of the modes through the spectrum alone. In order to experimentally test whether sub-gap states are majoranas or not, one ultimately needs to actually demonstrate their non-abelian statistics.

The simplest example with odd pairing is the so-called p-wave superconductor. In 1D, a p-wave superconductor is governed by the Hamiltonian H_{pw} obtained from $H_{\mathrm{BdG},k}^T$ in Eq. (1.29) when only the lowest order dependency of k is included in the pairing. Through a gauge transformation the pairing can be made real valued, meaning $\Delta_k^T = vk$. Explicitly, the Hamiltonian is defined as

$$H_{\mathrm{pw}} = \begin{pmatrix} \frac{p^2}{2m} - \Delta & vp \\ vp & -\frac{p^2}{2m} + \Delta \end{pmatrix}. \tag{1.39}$$

This Hamiltonian is used extensively in Chapter 3 and 4, and we will explicitly solve for the eigenstates in the half-infinite case. As explicitly calculated there, there is a zero-energy solution whenever the gap is positive $\Delta > 0$. As Δ decreases and passes zero, the gap closes and reopens, and there is a topological phase transition to the trivial phase $\Delta < 0$ with no Majorana zero-energy modes.

Although the Hamiltonian H_{pw} looks simple, there are no known simple materials which are intrinsically p-wave superconductors. In their seminal paper in 2008, Fu and Kane demonstrated that the proximity effect from a conventional s-wave superconductor can in principle be used to generate an effective spin-triplet pairing [33]. Their idea was to proximitize a single band, where the spin is locked to the momentum. Such a spin-momentum locked system can be found, for instance in the chiral edge modes of an integer quantum Hall liquid. This setup is still connected with considerable experimental difficulty, because quantum Hall systems need a large magnetic field compared to the critical field of most superconductors. Two years later, Oreg *et al.* and Lutchyn *et al.* independently came up with an approach which would spark a large experimental and theoretical interest [62, 54]. The idea was to use systems with a large spin-orbit coupling in order to procure the spin-momentum locking. One realization of this is the so-called *Majorana nanowire*, which is sketched in Figure 3. Here, a semiconducting material with a large spin-orbit coupling, usually InAs or InSb, is grown in a hexagonal shape, usually about 100 nm wide and with a length $\gtrsim 1\mu$m [4]. Along two of the facets, a thin layer of aluminium is grown epitaxially, meaning that the lattice of the Al matches that of the InAs. When the system is cooled down and the aluminium becomes superconducting, the epitaxial interface ensures that the induced superconducting pairing Δ_{SC} gives rise to a hard superconducting gap. Lastly, a magnetic field is applied along the wire. Figure 4 demonstrates what happens when these three ingredients are successively added in the case where the spin-orbit interaction dominates. Note that this limit is only taken for the purpose of visualization. The conclusions that Majorana zero modes emerge is valid regardless of the relationship between the spin-orbit and Zeeman interaction [62]. The spin-orbit coupling splits the spin degeneracy, and when the magnetic field is added perpendicular to the spin-orbit direction, it generates a Zeeman splitting B which causes the dispersion to separate into two helical bands. Importantly, if the Fermi momentum is large, the spins at the Fermi momenta are approximately anti-aligned, so the system may be proximitized by an s-wave superconductor. In order to have just a single effective p-wave superconducting band, the nanowire must have a low electronic density. Specifically, as long as the chemical potential μ is small compared with the Zeeman splitting $\mu \ll B$, there is effectively only a single band, and therefore there exists only a single zero-energy solution at domain walls. The system should therefore be expected to be in the topological phase for these parameters. However, as it turns out, the Zeeman splitting must also dominate over the pairing $B > \Delta_{\text{SC}}$ for the zero modes to exist.

Let us examine these statements in a bit closer detail. We describe the proximitized nanowire by the second quantized Hamiltonian

$$H_{\text{nw}} = \sum_k \Psi_k^\dagger H_{\text{BdG},k} \Psi_k \tag{1.40a}$$

$$H_{\text{BdG},k} = H_{0,k} + H_\Delta, \tag{1.40b}$$

$$H_{0,k} = \xi_k \tau_z + B\sigma_x \tau_z + \alpha k \sigma_z \tau_z, \tag{1.40c}$$

$$H_\Delta = \Delta_{\text{SC}} \sigma_z \tau_x, \tag{1.40d}$$

$$\Psi_k^\dagger = \begin{pmatrix} c_{k\uparrow}^\dagger, & c_{k\downarrow}^\dagger, & c_{-k\downarrow}, & c_{-k\uparrow} \end{pmatrix}, \tag{1.40e}$$

where $\xi_k = \frac{k^2}{2m^*} - \mu$, m^* is the effective electron mass, μ is the chemical potential, α is the spin-orbit coupling parameter and τ_i and σ_i are Pauli operators in particle-hole- and spin-space, respectively. The eigenvalues $E^{e/h\pm}$ of $H_{0,k}$ are

$$E_\pm^e = \xi_k \pm \lambda_k, \quad E_\pm^h = -\xi_k \pm \lambda_k, \tag{1.41a}$$

$$\lambda_k = \sqrt{B^2 + \Delta_{\text{SC}}^2}. \tag{1.41b}$$

The goal is to derive an effective theory for the lowest energetic bands E_-^e and E_+^h when the superconducting pairing H_Δ is added. To do so, one can express $H_{\text{BdG},k}$ in the eigenbasis of $H_{0,k}$ and define projectors P and Q respectively onto the lowest energetic eigenstates of $H_{0,k}$ with energy E_-^e and E_-^h, and the highest energetic states with energy E_+^e and E_+^h. When the pairing is added, the projection of
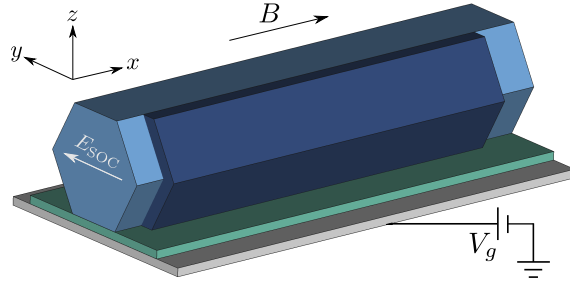
Figure 3: Sketch of a Majorana nanowire. A semiconductor, usually InAs or InSb, is grown in a hexagonal shape, here shown in light blue. The wire has a width of around 100 nm and a length on the order of several µm. Along two facets, a thin shell of Al, shown in dark blue, is grown epitaxially, providing a clean interface and a hard induced superconducting gap. This interface induces a Rashba spin-orbit coupling due to the electric field E_{SOC} from the Al interface. This coupling is described by a Hamiltonian term $\alpha(\boldsymbol{p} \times \hat{\boldsymbol{y}}) \cdot \boldsymbol{\sigma} = \alpha k \sigma_z$. The system is cooled below the critical temperature where the Al becomes superconducting and a magnetic field B perpendicular to the spin-orbit direction is applied. In this way, the induced superconductivity in the nanowire can be made effectively p-wave. Thus, in the topological regime the system hosts two Majorana bound states at the opposite ends of the wire. The nanowire is placed on a dielectric, shown in green, and gated with a voltage V_g, which allows for Coulomb blockading the system. This is crucial to isolate the zero-energy Majorana degrees of freedom from environment fermions. This last ingredient is described in Section 1.4.
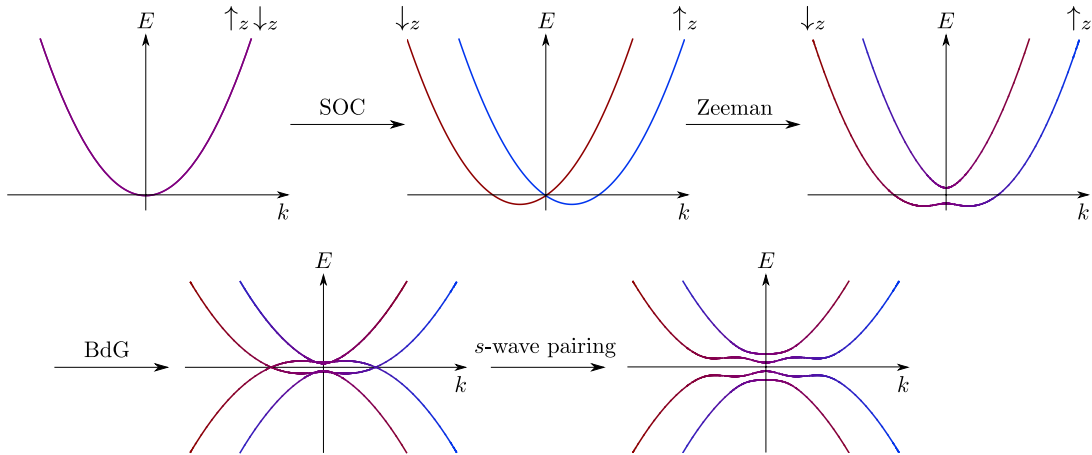

Figure 4: The effect of adding the ingredients for generating topological superconductivity step by step. The first graph shows the dispersion of free electrons with spin degeneracy. Next, a spin-orbit coupling is added in the negative z-direction, splitting the bands according to the spin-z projection. Adding a Zeeman interaction lifts the degeneracy at $k = 0$. There are now two helical bands, with the spin-z projection varying smoothly as a function of k. If $B \ll \alpha k_F$, where α is the spin-orbit parameter and k_F is the Fermi momentum, then at k_F the spins are still approximately anti-aligned in the z-direction. Next, going to a BdG representation the spectrum is doubled and mirrored, introducing the holes as separate degrees of freedom. Here, we see that electrons- and hole bands are degenerate at opposite wavenumber and opposite spin. Adding superconductivity therefore splits the remaining degeneracies, and it does so in a way that the lowest band effectively doesn't have a spin-degree of freedom, since the band is helical. Because of this, the pairing is effectively spinless, which is akin to triplet pairing, leading to topological superconductivity.

13

the eigenstates onto the lowest bands is exactly described by the energy-dependent Hamiltonian $H_P(E)$, given by

$$H_P(E) = PH_{\text{BdG},k}P + PH_{\text{BdG},k}Q\left(EQ - QH_{\text{BdG},k}Q\right)^{-1}QH_{\text{BdG},k}P. \tag{1.42}$$

We demand that B is the largest energy scale, and we notice that solutions to the nonlinear equation $H_P(E)|\psi(E)\rangle = E|\psi(E)\rangle$ have eigenvalues $E = \mathcal{O}(E_-^e, E_+^h) + \mathcal{O}(\Delta)$. Using this, we can Taylor expand $H_P(E)$ to leading order in Δ/B, and the dependence of E drops out, yielding the effective low-energy Hamiltonian H_{eff} given by

$$H_{\text{eff}} = \begin{pmatrix} \left(\frac{1}{2m^*} - \frac{\alpha^2}{2B}\right)k^2 - \mu - B + \frac{\Delta_{\text{SC}}^2}{B} & \frac{\alpha\Delta_{\text{SC}}}{B}k \\ \frac{\alpha\Delta_{\text{SC}}}{B}k & -\left(\frac{1}{2m} - \frac{\alpha^2}{2B}\right)k^2 + \mu + B - \frac{\Delta_{\text{SC}}^2}{B} \end{pmatrix}. \tag{1.43}$$

Thus we see that when B is the dominating energy scale, the proximitized nanowire is a p-wave superconductor, described by a Hamiltonian of the form in Eq. (1.39), with the parameters

$$m = \left(\frac{1}{m^*} - \frac{\alpha^2}{B}\right)^{-1}, \quad \Delta = \mu + B - \frac{\Delta_{\text{SC}}}{B}, \quad v = \frac{\alpha\Delta_{\text{SC}}}{B}. \tag{1.44}$$

In this limit, where B dominates, $\Delta > 0$, so we expect a single exponentially localized Majorana bound state to be present at each end of the wire. From the above discussion, we know that the Majorana modes are robust against continuous deformations, as long as the gap doesn't close. The gap of the full Hamiltonian H_{BdG} can be shown to close only when $\mu = \pm\sqrt{B^2 - \Delta_{\text{SC}}}$, so whenever $B > \Delta_{\text{SC}}$, we can extend the conclusions to the statement which was given above, that we expect a single Majorana whenever $|\mu| < \sqrt{B^2 - \Delta_{\text{SC}}}$, and this parameter range, along with $B > \Delta_{\text{SC}}$, thus defines the topological regime.

1.4 Charging energy and a minimal Majorana qubit

Now that we have an idea of how 1D systems hosting Majorana bound states may be constructed using experimentally available building blocks, we turn our attention to the next obvious question: How do we use this to construct a useful qubit?

The first obstacle is to protect the quantum information. The energy cost of switching the Majorana parity is zero, so one could rightfully worry that fermions from the environment could tunnel into the p-wave superconductor, causing flips of the Majorana parity. Such processes are called *quasiparticle poisoning*. The system may be engineered to have a very small capacitance, in which case Coulomb repulsion can energetically restrict such processes when the system is carefully gated. This introduces a different problem, however, since it is not possible to form superpositions of a single Majorana pair between having odd and even parity without including the quasiparticle continuum, defeating the whole purpose of the topological qubit. The problem will be fixed by connecting two nanowires by a conventional superconducting backbone, resulting in the system displayed in Figure 5, which has been dubbed the Majorana box qubit [63]. This system is in a way a minimal qubit one can construct out of Majorana nanowires, and it is a key system in this thesis, since it is the central object of study in Project A, B and C.

But before getting ahead of ourselves, let us first discuss how to isolate the system from the environment. This is achieved by engineering the system to have a large charging energy E_C. This enters from Coulomb repulsion in the system, and is described by the Hamiltonian H_C given by

$$H_C = \frac{e^2}{2C}N^2 - V_g eN, \tag{1.45}$$

where N is the operator associated with the total number of electrons on the island and the potential V_g is tunable by a gate voltage. Up to an irrelevant constant shift, H_C may be cast in the following form

$$H_C = E_C(N - n_g)^2, \tag{1.46}$$

where the charging energy $E_C = e^2/(2C)$ and the dimensionless parameter $n_g = CV_g/e$ can be tuned to control the number of electrons in the system. In particular, when n_g is an integer, and E_C dominates all environmental energy scales, the system is said to be *Coulomb blockaded*. When superconductivity is
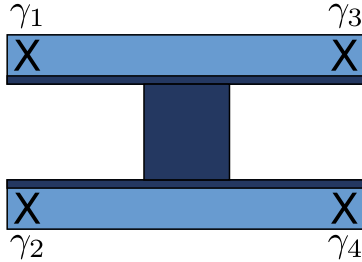
Figure 5: Sketch of the Majorana box qubit: Two parallel Majorana nanowires, shown in light blue with a dark blue edge to indicate the Al shell from Fig. (3), are strongly coupled by an s-wave superconducting backbone, shown in dark blue. This effectively joins the systems together, giving them a common sea of Cooper-pairs and a common charging energy. The wires are assumed to be in the topological regime, so the system hosts 4 Majorana fermions, $\gamma_1, \ldots, \gamma_4$.

added, if n_g is odd, the ground state has an unpaired quasiparticle, and if n_g is even, the ground state has no quasiparticles.

If the superconductor is p-wave and in the topological regime, then there is no difference in the energy of the ground state whether n_g is even or odd, since the unpaired fermion may now occupy the zero-energy state spanned by the Majoranas.

As a side note, one should in principle be careful when adding interactions, as they can completely change the topological properties of the system. All the above arguments were made in reference to an effectively non-interacting problem. Adding interactions may in principle cause gap-closings which can take the system out of the topological regime, or drastically change the topological behaviour [26]. Adding charging energy, however, never closes the quasiparticle gap, although, depending on n_g, it may move the Majorana state away from zero energy. When E_C dominates, the charging energy simply restricts the total number of fermions in the system, but is otherwise still described by the same non-interacting mean-field Hamiltonian. Thus it doesn't affect the existence of the Majoranas, but can be thought of as a constraint on the occupations.

In Chapter 4, when we look at decoherence of isolated Majorana systems, we will have to account for a thermal distribution of the fermionic quasiparticles, constrained by the charging energy to be either even or odd. Finding the Fermi distribution function when subject to a parity constraint is in principle a straightforward, albeit tedious, exercise in thermodynamics. Historically, it was first pointed out by Tuominen et $al.$ [74, 75, 50] that the free energy $F_{e/o}$ in the even/odd parity sectors differ by an amount $\delta F = F_o - F_e$ approximately equal to [40, 71]

$$\delta F = -k_B T \ln \tanh[N_{\text{eff}} e^{-\beta \Delta}] \approx \Delta - k_B T \ln(N_{\text{eff}}), \tag{1.47}$$

where $\beta = 1/(k_B T)$. The effective number of quasiparticle states N_{eff} for a BCS superconductor with gap Δ is

$$N_{\text{eff}} = 2 \int_\Delta^\infty dE \frac{\rho_D E}{\sqrt{E^2 - \Delta^2}} e^{-\beta(E-\Delta)} \approx \rho_D \sqrt{2\pi k_B T \Delta}, \tag{1.48}$$

where ρ_D is the normal state density of states at the Fermi energy. All the above approximations are valid at low temperatures $\Delta/(k_B T) \gg 1$. This difference in free energy implies a parity dependent occupation $n_F^{e/o}(E)$ of the continuum quasiparticle states at energy $E \geq \Delta$ in the even/odd sector. A direct calculation shows [4]

$$n_F^{e/o}(E) = \frac{1}{\exp \beta(E \pm \delta F) + 1}, \tag{1.49}$$

where the sign is plus for the even sector, and minus for the odd.

With the ability to Coulomb blockade Majorana nanowires, we now understand how to protect the ground-state parity from quasiparticle poisoning. In order to form superpositions of different ground-state parities, we need a way for two Majorana nanowires to have a common large charging energy. This can be done by connecting them by a conventional s-wave superconductor [63]. Heuristically, this allows the two nanowires to share a common sea of Cooper-pairs, which may be split at zero energy cost, if the two electrons can be placed in the Majorana ground states. For example, if the total fermionic parity

is even, then the states $|00\rangle$ and $|11\rangle$ in the ground states differ by one Cooper-pair. The reason why it works can be formally understood by first considering two s-wave superconductors connected by a Josephson junction and with separate charging energies. Let N_1 and N_2 be the number of Cooper-pairs in the respective superconductors and let Φ_1 and Φ_2 the phase of their pairing, conjugate to the number operators $[\Phi_i, N_i] = i$ [39]. When the two superconductors are tunneling coupled, the Hamiltonian H_{1-2} describing the combined system is given by [16]

$$H_{1-2} = E_{C_1}(2N_1 - n_{g_1})^2 + E_{C_2}(2N_2 - n_{g_2})^2 - E_J \cos\Phi, \tag{1.50}$$

where $\Phi = \Phi_1 - \Phi_2$, E_J is the Josephson energy, E_{C_i} is the charging energy of the i'th superconductor and n_{g_i} is the corresponding gate parameter. In Eq. (1.50) we have neglected all quasiparticles, which would otherwise appear separately in the charging energy terms, as well as mutual capacitances, which we assume to be much smaller than the individual charging energies. Up to a constant energy shift, the Hamiltonian may be rewritten as

$$H_{1-2} = E_C(N - n_g^+)^2 + E_C(n - n_g^-)^2 + \Delta E_C nN - E_J \cos\Phi, \tag{1.51}$$

where

$$N = N_1 + N_2, \tag{1.52a}$$
$$n = N_1 - N_2, \tag{1.52b}$$
$$E_C = E_{C_1} + E_{C_2}, \tag{1.52c}$$
$$\Delta E_C = \frac{E_{C_1} - E_{C_2}}{2}, \tag{1.52d}$$
$$n_g^\pm = \frac{2(n_{g_1}E_{C_1} \pm n_{g_2}E_{C_2})}{E_{C_1} + E_{C_2}}. \tag{1.52e}$$

Notice that $[N, \Phi] = [N, n] = 0$. This implies that if n_g^+ is an integer and $E_C \gg \Delta E_C$, then the first term in (1.51) can pin N be equal to n_g^+. We will consider the case $\Delta E_C \ll E_C$, where the interaction term leads to a small shift of n. Because $[n, \Phi] = 2i$, in the weakly coupled case $E_J \ll E_C$, n is pinned to n_g^-, and the phase difference Φ fluctuates. In the opposite strong coupling limit $E_J \gg E_C$, the Josephson energy term pins phase difference to $\Phi = 0$, making n fluctuate so the number of Cooper-pairs in the two superconductors is undetermined. Strong Josephson coupling evidently allows for two s-wave superconductors to obtain a common charging energy.

For topological superconductors with Majorana modes, the occupancy of the zero mode appears in the charging energy term. However, they may be removed from there by a gauge transformation, after which the parity of the zero-energy mode is encoded in the boundary conditions of many-body wavefunction in phase space. Explicitly, for a topological superconductor with Majorana modes γ_1, γ_2, the charging energy term is [1, 12, 31, 39]

$$H_C = E_C\left(\frac{2}{i}\frac{\partial}{\partial\Phi} + n_{12} - n_g\right)^2, \tag{1.53}$$

where $n_{12} = \frac{1 - i\gamma_1\gamma_2}{2}$ is the occupation of the zero-energy fermionic state the Cooper-pair number operator N has been written explicitly in terms of the superconducting phase Φ. By unitarily transforming H_C by the operator

$$U = e^{i\Phi n_{12}/2}, \tag{1.54}$$

we see

$$UH_CU^\dagger = E_C\left(\frac{2}{i}\frac{\partial}{\partial\Phi} - n_g\right)^2. \tag{1.55}$$

The effect of the unitary transformation can be understood in the phase basis

$$|\Phi, n_{12}\rangle = \frac{1}{\sqrt{2\pi}}\sum_N e^{-i\Phi N}|N, n_{12}\rangle, \tag{1.56}$$

which is the Fourier transform of the number basis, defined through $\Lambda^\dagger\Lambda|N\rangle = N|N\rangle$, where the Cooper-pair operator $\Lambda = \sum_{k,\sigma,\sigma'} w_{k,\sigma,\sigma'} c_{k,\sigma}^\dagger c_{-k,\sigma'}$ is is defined in analogy with Eq. (1.24), except the pairing is
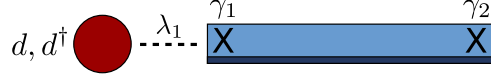
Figure 6: A quantum dot with a single level is tunnel coupled to a Majorana nanowire in the topological regime, with a coupling strength λ_1. The lowest energetic processes are governed by tunneling through the Majorana mode γ_1.

allowed to be in the triplet channel. After the unitary transformation, the phase basis states are

$$U|\Phi, n_{12}\rangle = \frac{1}{\sqrt{2\pi}} \sum_N e^{-i\Phi(2N-n_{12})/2} |N, n_{12}\rangle. \tag{1.57}$$

After the transformation, all operators look the same, except for Majorana operators, which are transformed according to

$$\gamma_i \rightarrow e^{i\Phi(i\gamma_1\gamma_2)/2}\gamma_i, \tag{1.58}$$

and the phase factor reflects the fact that when γ_i flips the ground state from $|n_{12} = 0/1\rangle$ to $|n_{12} = 1/0\rangle$ the charge on the superconductor is increased/decreased by e. The result of this exercise is that when a topological superconductor is connected to a conventional superconductor, the result is algebraically completely similar to Eq. (1.51), albeit with the states on the topological superconductor transformed according to Eq. (1.54). As a side point, when two topological superconductors with phases Φ_L and Φ_R are connected, say with the junction between the Majorana zero modes γ_L and γ_R, then the same argument can be made, except Eq. (1.51) is modified by the addition of the so-called fractional Josephson term H_{FJ}, which tends to dominate over the regular Josephson coupling and is equal to [39]

$$H_{FJ} = E_{FJ} \cos\left(\frac{\Phi_L - \Phi_R}{2}\right) i\gamma_L\gamma_R. \tag{1.59}$$

This term is responsible for the 4π periodic Josephson current measured in topological Majorana nanowires. The appearance of the fractional Josephson term does not alter the argument, however, and if $E_{FJ} \gg E_C$, then the two topological superconductors may be brought to effectively share a common charging energy.

The last point we need to address before turning to the Majorana box qubit is what happens when a Coulomb blockaded p-wave superconductor is tunnel coupled to a quantum dot. Such a setup will be important for controlling the Majorana qubit. Since we want to manipulate fermionic paritites, it is important that there is only one state on each dot. This constraint is motivated by the large magnetic fields needed to drive the nanowires into the topological regime, since these will gap out the spin degree of freedom on the dot. Suppose a quantum dot with a single level described by the annihilation operator d is connected by a tunnel coupling λ_1 in the vicinity of Majorana γ_1, as sketched on Fig. 6. After performing the unitary transformation in Eq. (1.54), the system is described by the Hamiltonian

$$H_{d-\text{pw}} = \epsilon d^\dagger d + E_C \left(\frac{2}{i}\frac{\partial}{\partial\Phi} - n_g\right)^2 + \left(\lambda_1 d^\dagger e^{-i\Phi/2}\gamma_1 + \text{H.c.}\right). \tag{1.60}$$

This Hamiltonian is obtained after projecting to the energetically lowest states, discarding processes where the dot electron tunnels to or from continuum quasiparticle states[3]. After this projection, we have also discarded the bare Hamiltonian of the p-wave superconductor, since the Majorana states have zero energy. Transforming Eq. (1.60) by the unitary operator $U_d = e^{id^\dagger d\Phi/2}$, and using

$$U_d d^\dagger U_d^\dagger = d^\dagger e^{i\Phi/2}, \quad U_d d U_d^\dagger = d e^{-i\Phi/2}, \tag{1.61}$$

we find

$$U_d H_{d-\text{pw}} U_d^\dagger = \epsilon d^\dagger d + E_C \left(\frac{2}{i}\frac{\partial}{\partial\Phi} - d^\dagger d - n_g\right)^2 + \left(\lambda_1 d^\dagger\gamma_1 + \text{H.c.}\right)$$

$$= \tilde{\epsilon} d^\dagger d + E_C \left(\frac{2}{i}\frac{\partial}{\partial\Phi} - n_g\right)^2 + \left(\lambda_1 d^\dagger\gamma_1 + \text{H.c.}\right) + \text{const.} \tag{1.62}$$

---

[3]The tunneling amplitude λ_i in Eq. (1.60) is the result after this projection.

Thus, the Coulomb blockade leads to a shift of the dot energy to $\tilde{\epsilon} = \epsilon + E_C(1 + 2n_g)$. In this gauge, Eq. (1.62) allows for only having to consider the occupation of the zero mode and the dot. To understand this, note that the number basis states have been transformed to

$$|N, n_{12}, n_d\rangle \rightarrow |\Phi, n_{12}, n_d\rangle' \equiv U_d U |\Phi, n_{12}, n_d\rangle = e^{i\Phi(n_d + n_{12})/2}|N, n_{12}, n_d\rangle, \qquad (1.63)$$

where we denoted the occupation of the zero mode and dot by n_{12} and n_d, respectively. The term in the Hamiltonian $\lambda_i d^\dagger \gamma_i + \text{H.c.}$ connects states with the same charging energy but with a different number of Cooper pairs. To see this, we explicitly calculate

$$d^\dagger \gamma_1 |N, 0, 0\rangle'' \propto |N, 1, 1\rangle = e^{-i\Phi} U_d U |N, 1, 1\rangle = |N - 1, 1, 1\rangle', \qquad (1.64)$$

where we used that $e^{\pm i\Phi}$ is the translation operator for N by ± 1. Similar calculations show

$$
\begin{aligned}
d\gamma_1 |N - 1, 1, 1\rangle' &\propto |N, 0, 0\rangle', \\
d^\dagger |N, 0, 1\rangle' &\propto |N, 1, 0\rangle', \\
d\gamma_1 |N, 1, 0\rangle' &\propto |N, 0, 1\rangle'.
\end{aligned} \qquad (1.65)
$$

Apparently, the Cooper-pair number is a slave to n_d and n_{12}, and the Hamiltonian is block-diagonal, with the block corresponding to the parity of the dot and the Majorana mode. Also, the charging energy only differs between these blocks, with the eigenvalue $E_C(N - n_g)^2$ in the even block and $E_C(N + 1 - n_g)^2$ in the odd. The conclusion is, that if charging energy dominates and n_g is tuned to an integer, the effect of the charging energy is simply to restrict the Hilbert space to a two-level system, and the Cooper pairs can be forgotten.

Having discussed all the necessary ingredients, we are finally ready to introduce the *Majorana box qubit* [63], which is displayed on Figure 5. It essentially consists of two parallel Majorana nanowires, connected by an s-wave superconducting backbone. The system has four Majorana zero-energy states γ_1, γ_2, γ_3 and γ_4 and it has a large overall charging energy, meaning that ground state space is subjected to the parity constraint $\gamma_1 \gamma_2 \gamma_3 \gamma_4 = \pm 1$. Throughout this thesis, we will always assume that the charging energy is sufficiently large to completely protect it from quasiparticle poisoning from the outside. Thus, for example if the overall parity is even, we could choose the basis for the ground states given by $\{|00\rangle, |11\rangle\}$, where $|n_{12}n_{34}\rangle$ is defined through the occupations of the two independent fermionic modes corresponding to the Majorana pairs γ_1, γ_2 and γ_3, γ_4. We use the Pauli algebra defined in Eq. (1.16).

This architecture is not useful for implementing operations where Majoranas are physically braided around one another. Rather, initialization, readout and manipulation of the Majorana box qubit involves carefully controlling couplings to external quantum dots with single electronic levels. An intuitively simple way to implement Pauli operations on the system is outlined in panel a) of Figure 7. The idea is to couple quantum dots to the system and carefully tune dot levels so an electron is forced to tunnel through, resulting in a *tunneling braid operation* [29]. It is important that only a single state is hosted by the quantum dot. Since sequential tunneling is energetically unfavorable, owing to the large charging energy, the dominant contribution is due to co-tunneling. Close to the boundaries, the electron annihilation- and creation operators may be written in terms of the corresponding Majorana mode and the continuum quasiparticles. If the energy gap is large, the dominant contribution will involve only the Majoranas, and the tunneling braid results in the action of a Majorana bilinear on the Majorana box qubit ground states, meaning that the Pauli operation in Eq. (1.16) may be implemented. In Figure 7 panel a) the left dot is coupled to two Majoranas γ_1 and γ_2 through tunable tunnel couplings λ_1 and λ_2. The right dot is just connected to one Majorana γ_3. Suppose the left dot is initially occupied while the right dot is empty. By slowly tuning the dot levels $\epsilon_{L/R}$, the final state can be made to have the right dot occupied and the left empty. If $\lambda_2 = 0$, the only way for the left dot to co-tunnel through the system is via γ_1 and γ_3, and thus the state of the qubit is transformed by $\gamma_1 \gamma_3 \propto \sigma_x$. If both tunnel couplings $\lambda_1, \lambda_2 \neq 0$ then the co-tunneling process instead applies a superposition of $\gamma_1 \gamma_3$ and $\gamma_2 \gamma_3$. The relative weight can be controlled by the relationship $|\lambda_1/\lambda_2|$ and the phase can be controlled by inserting a magnetic flux ϕ through the resulting loop, see Figure 7a). Such a general transformation is not topologically protected.

The drawbacks of this method is that it relies on very acute control of both the quantum dot energies, the tunneling amplitudes as well as the phases. It turns out, however, that if we know how to measure and initialize the parity of a Majorana pair, then all braiding operations may be implemented through a
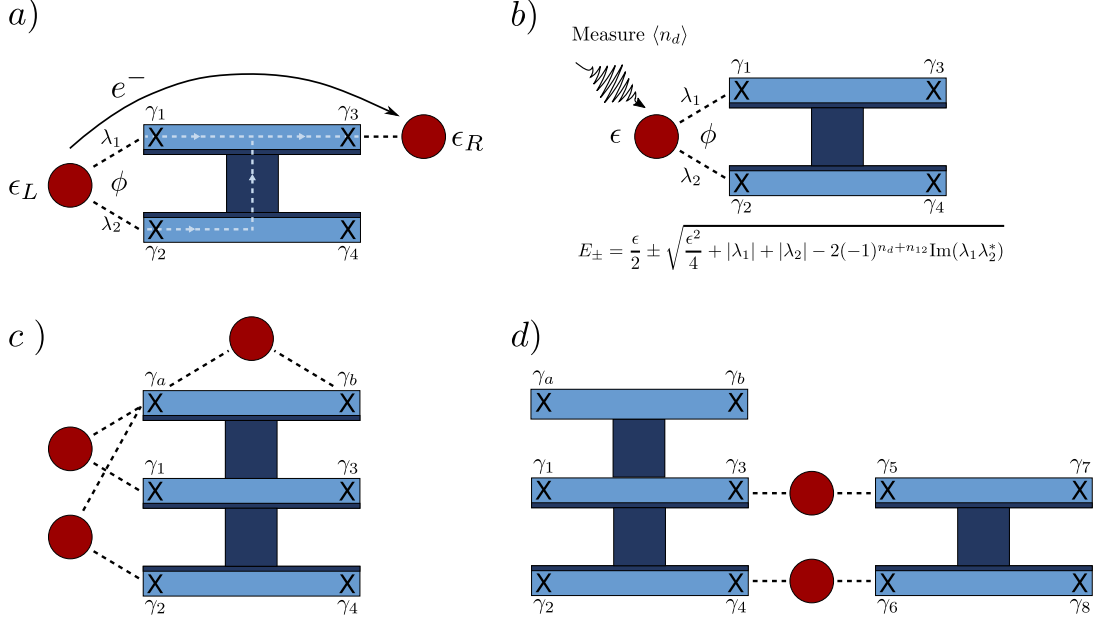
Figure 7: Control of a Majorana box qubit using quantum dots. All dots are assumed to host only a single electronic level.

Panel a) shows a proposed way of implementing Pauli operators as well as arbitrary rotations of the box qubit state. Two quantum dots are connected to the qubit. The left is connected to both γ_1 and γ_2 with tunneling amplitudes λ_1 and λ_2, respectively, and a magnetic flux ϕ is inserted in the loop, resulting in a non-zero complex phase between the tunneling amplitudes. The right dot is connected to just γ_3. By slowly adjusting the two dot energy levels, $\epsilon_{L/R}$, an electron can be made to co-tunnel through the system. Co-tunneling is dominant because of the large charging energy. If $\lambda_2 = 0$ the process applies the operator $\gamma_1\gamma_3 \propto \sigma_x$ on the state of the box qubit. For non-zero λ_2, arbitrary linear combinations of $\gamma_1\gamma_3$ and $\gamma_2\gamma_3$ can be achieved, although these operations are not topologically protected.

Panel b) depicts a setup used for measuring the parity $i\gamma_1\gamma_2$. A quantum dot is tunnel coupled to both γ_1 and γ_2, splitting the ground state degeneracy. The energies of the system depend on the combined parity of the dot and the coupled Majorana pair, which is a conserved quantity. Measuring the dot occupation through a fermion-number preserving interaction with a readout device will reflect this joined parity. Thus, measuring dot population gives a projective measurement of the joined dot- and Majorana pair parity. Lastly, by adjusting the dot energy level ϵ to empty or fill the dot, the system can be prepared in a specific parity state.

Panel c) depicts a setup for performing the measurement-based braiding $B_{12} = (1-\gamma_1\gamma_2)/\sqrt{2}$ using quantum dots. To do so, an auxiliary Majorana pair γ_a and γ_b needs to be introduced, sharing a common charging energy with the box qubit. This is achieved through another Majorana nanowire, connected through an s-wave superconductor with the box qubit. The braid can be performed by measuring the parities $i\gamma_a\gamma_b$, $\gamma_a\gamma_1$ and $i\gamma_2\gamma_a$ and postselecting for the positive outcomes. To accommodate these measurements, three quantum dots are tunnel coupled to the respective Majoranas, so the above-mentioned protocol of measuring the pairities may be used.

Panel d) shows a setup for measuring the joint parity $\gamma_3\gamma_4\gamma_5\gamma_6$ of two separate Majorana box qubits. This effect is achieved by tunnel coupling one dot to γ_3 and γ_5 and another dot to γ_4 and γ_6. Let's say that the bottom dot has a very high energy. Then the leading non-trivial process co-tunnels an electron all the way around in the loop, implementing the operator $\gamma_3\gamma_4\gamma_5\gamma_6$. Thus, the energy of the system depends on the combination of this number and the dot occupation, and by measuring the top dots occupation, the joint parity may be projectively measured. Such a measurement can be used for implementing a measurement-based entanglement generating gate on the two qubits.

19

process called *measurement-based braiding* [44, 49, 61, 63, 76], which we will elaborate on below. Thus, if we know how to read out Majorana parities, we can also initialize and perform all one-qubit Clifford gates, and we will therefore begin with elaborating on how such a readout is envisioned.

To read out the parity of a Majorana pair, one must first find a way to break the degeneracy of the ground state. One of the most commonly suggested strategies is to connect a quantum dot to a Majorana pair in a tunable way, as shown in panel *b*) of Figure 7. Once a quantum dot has been connected, the parity of the Majorana pair is no longer a good quantum number, since the combined Dirac fermion is free to tunnel to and from the dot. The combined parity $s = (-1)^{n_d + n_{12}}$ of the dot and the Majorana pair is, however, still a good quantum number. If the dot energy is ϵ and the dot state is tunnel coupled to γ_1 and γ_2 with tunneling amplitudes λ_1 and λ_2, then the energies of the combined dot and box qubit is

$$E_\pm^s = \frac{\epsilon}{2} \pm \sqrt{\frac{\epsilon^2}{4} + |\lambda_1|^2 + |\lambda_2|^2 - 2s \operatorname{Im}(\lambda_1 \lambda_2^*)}. \tag{1.66}$$

Thus the ground state energy is split only if there is a non-zero complex phase between λ_1 and λ_2, which can be ensured by applying a magnetic flux ϕ through the loop. Since only the dot occupation depends on ϵ, the expected dot occupation $\langle n_d \rangle = \langle dH/d\epsilon \rangle$. So, for instance at zero temperature, the dot expectation is found from the derivative of the energies E_-^s with respect to ϵ. If the initial parity of the dot is known, fermionic-parity conserving interactions on the dot will tend to decohere the Majorana system, leading to a projective measurement of the combined parity of the dot and the Majorana pair. If the coupling is in such a way that it is sensitive to $\langle n_d \rangle$ the value of s can be read out. If the dot is finally decoupled in a way that leaves it in a state of definite occupation, then a readout can be infered on the isolated Majorana system. The details and dynamics of how this happens, including an explicit modeling of measurement devices, is the subject of Project A in Chapter 2. Here we also discuss the statements above regarding the energies of the Majorana box qubit split by a dot in detail. It is also possible to read out the quantum capacitance of the dot $\langle d^2H/d\epsilon^2 \rangle$. This can be done dispersively, by driving the system far away from resonance, so no transitions are caused in the box qubit system. A way to understand this readout physically is that the capacitance corresponds to the boundary conditions for a reflected wave. A high capacitance leads to a phase shift of π, just like how sound waves reflect with a phase shift at the end of an open tube, while a small capacitance does not lead to a phase shift. By measuring the phase shift, the value of s can be deduced. If there is dissipation in the system, the amplitude reduction of the reflected wave can also be used as a readout.

Understanding how to read out Majorana parities, we are now in position to understand how measurement-based braiding can be implemented physically. We here present a conceptually simple argument put forward by Vijay and Fu [76]. Figure 7*c*) shows a setup for implementing the braiding operation B_{12} using the process described above for reading out parities via quantum dots.

Measurement-based braiding takes an additional ancillary pair of Majorana states γ_a, γ_b connected with the box-qubit, meaning the 6 Majoranas share a common charging energy. Perhaps it is not a priori obvious why the Majorana may be braided through a measurement scheme. Physically, it originates from a topological relation between non-trivial fusion rules and non-trivial braiding statistics. If we define the operators $P_{ij}^\pm = (1 + i\gamma_i\gamma_j)/2$, which project onto the $\pm$ eigenstates of $i\gamma_i\gamma_j$, then we have for $i, j = 1, \ldots 4$

$$P_{ab}^+ P_{ai}^+ P_{ja}^+ = \frac{1}{8}(1 + i\gamma_a\gamma_b - \gamma_i\gamma_j(1 + i\gamma_a\gamma_b) - i\gamma_i(\gamma_a - i\gamma_b) + i\gamma_j(\gamma_a - i\gamma_b)). \tag{1.67}$$

The measurement-based braiding scheme requires the ancillary Majorana pair to be initialized in a state with definite parity as well as post-selecting for of the outcomes of intermediate measurements. The latter means that specific outcomes of the measurements are required for the braiding to work. Since the measurement outcomes are known, it is also known whether the measurement-based braid was successful or not, and there are ways to undo undesirable measurements without starting all over in a complicated braiding operation. Suppose the initial state of the four logical Majoranas $\gamma_1, \ldots, \gamma_4$ is $|\psi\rangle$ and the ancillary Majorana pair is initialized in the state $|i\gamma_a\gamma_b = +1\rangle$. The punchline is now simply that

$$P_{ab}^+ P_{ai}^+ P_{ja}^+ |\psi\rangle |i\gamma_a\gamma_b = +1\rangle \propto \frac{1}{\sqrt{2}}(1 - \gamma_i\gamma_j)|\psi\rangle |i\gamma_a\gamma_b = +1\rangle = B_{ij}|\psi\rangle |i\gamma_a\gamma_b = +1\rangle. \tag{1.68}$$

This implies that if $i\gamma_j\gamma_a$, $i\gamma_a\gamma_i$ and $i\gamma_a\gamma_b$ are subsequently measured in that specific order and the measurement outcomes are all $+1$, then the effect is the same as braiding γ_i and γ_j. The mismatch in

normalization in Eq. (1.68) simply has to do with the important fact, that measurements in quantum mechanics always require a normalization by hand after the measurement[4]. Importantly, since all the measurements include γ_a, if the undesirable outcome -1 is returned by any of the measurements, it is always possible to recreate the state before the measurement by measuring an appropriate Majorana bilinear. For example, suppose $i\gamma_j\gamma_a$ returns the unwanted outcome P_{ja}^-. Then observe

$$P_{ab}^+ P_{ja}^- |\psi\rangle|0\rangle_{ab} = \frac{1}{4}(1 + i\gamma_a\gamma_b - i\gamma_j\gamma_a - i\gamma_a\gamma_j i\gamma_a\gamma_b)|\psi\rangle|0\rangle_{ab} \propto |\psi\rangle|0\rangle_{ab}, \tag{1.69}$$

so if $i\gamma_a\gamma_b$ is measured with the outcome $+1$, then the unwanted measurement $i\gamma_j\gamma_a = -1$ is undone. This potentially implies a bit of back-and-forth action when doing measurement-based-braiding, but since the speedup from doing quantum computation is exponential, this should not be a major concern in practice.

In Figure 7c) a setup is shown which allows the measurement-based braiding of γ_1 and γ_2. The top dot connects the distant Majoranas γ_a and γ_b, which may be infeasible to do in a coherent manner, since the tunnel junctions have to be long. To circumvent this problem, one can use a separate Majorana nanowire, which can function as a non-localized quantum dot, allowing for short tunneling junctions at the end. This is possible because transport through Majorana nanowires is coherent [31].

For building a quantum computer, one can either do the non-Clifford gate, like T-gate, using magic state distillation [44] or using the possibility of arbitrary rotations by tunneling braiding [29, 63]. The only missing ingredient now for universal quantum computation is an entangling operation. One way to do so is analogous to measurement-based braiding[44], and it requires the ability to measure the joint parity $\gamma_3\gamma_4\gamma_5\gamma_6$ of four Majoranas. A schematic for how to do this is shown in Figure 7, panel d). Here, two Majorana box qubits are connected through two quantum dots. Each dot connects to just one Majorana from each qubit and it is assumed that no tunneling happens from one dot to the other. If one of the dots is tuned close to resonance and the other is tuned to a very large energy, comparable with the charging energy, then transport from the resonant dot through the qubits happens by co-tunneling processes through all Majoranas and the dot. This means that the energy of the combined system depends on the value of $\gamma_3\gamma_4\gamma_5\gamma_6$, and, similarly to the Majorana pair parity readout, one can read out the joint parity of the four Majorana by measuring either the charge or capacitance of the dot close to resonance. Defining the joint parity projection operator $P_{3456}^\pm = (1 \mp \gamma_3\gamma_4\gamma_5\gamma_6)/2$, an explicit calculation shows

$$W_{3456} \equiv P_{ab}^+ P_{a3}^+ P_{3456}^- P_{b3}^+ P_{ab}^+ \propto (1 - i\gamma_3\gamma_4\gamma_5\gamma_6), \tag{1.70}$$

and the controlled Z gate $C(Z)$ can then be formed in conjunction with braiding as [44]

$$C(Z) = B_{12}B_{56}W_{3456}. \tag{1.71}$$

Thus, complete scalable quantum computation is possible with Majorana box qubits.

In Project B and C, we will investigate the decoherence properties of Majorana box qubits when they are subject to electromagnetic fluctuations, but are otherwise ideal. With this is meant that they are perfectly protected from quasiparticle poisoning and the wires are infinitely long with neither overlap, nor errors inside the ground state space originating from excited quasiparticles propagating down the system from Majorana to Majorana and implementing Pauli errors. To get a better feeling for what is known regarding the dephasing properties of Majorana qubits, in the next section we give a brief and non-extensive review of the results from previous studies.

1.5 Dephasing mechanisms for Majorana qubits

We have already encountered one source of dephasing in the previous section in the context of Majorana parity readouts. This happened when a quantum dot was coupled to two of the four Majorana zero modes of a Majorana box qubit (MQB), splitting the degerency and converting the parity degree of freedom to charge. Fluctuating electromagnetic fields in an environment or measurement apparatus could then destroy the coherence between the different parity sectors of the Majorana system. An example which is studied in detail in Project A of Chapter 2 has the quantum dot capacitively coupled to a quantum point contact (QPC). The conductance through the QPC then depends on the charge of the dot. In

---

[4]This innocent-looking fact is at the heart of the "measurement problem".

this example, fermions never enter the system, which is important, since the readout procedure hinges on fermionic parity of the combined dot-MBQ system being constant. A different setup has also been proposed [63, 66] where the current is allowed to pass through the system. Here, two quantum dots are tunneling coupled to one Majorana each. A flux ϕ is inserted through the loop defined by the MBQ and the two dots. In this system, when a current runs into one dot and out the other, the electrons will either pass directly from dot to dot, or they will co-tunnel through the MBQ, picking up a phase depending on the parity of the Majorana pair. The interference between the two paths leads to a detectable difference in conductance depending on the state of the qubit, and since the degeneracy of the qubit is lifted, the state dephases to one where the coupled Majorana pair has a definite parity.

The dephasing mechanisms discussed above are all intentional, reflecting the need of the experimenter to collapse the wavefunction at will. They can theoretically be switched off when this is wanted. Not all sources of dephasing are wanted though, but reflect obstacles that any useful implementation will have to overcome. The goal is to engineer the system so the dephasing times from all sources are long enough that all relevant experiments may be run on a much shorter time scale.

One dephasing mechanism is qualitatively related to the readout procedure detailed in the previous section. When a Majorana nanowire has a finite length, the two Majorana states will overlap, and this generically splits the degeneracy and gives charge to the Dirac fermionic state composed of the two Majoranas. Analogously to how the charge of the dot could couple to electromagnetic fluctuations in the environment, so can the charge of the zero-mode in small systems. Interestingly, interactions between such Majorana overlap and bound charges in dielectric surroundings have been theoretically predicted to push the charge and energy of the Majorana modes towards zero [24]. With this in mind, Knapp *et al.* studied decoherence due to couplings to the dipole moment of the overlapping Majoranas [48] and found that the dominant source of dephasing then is $1/f$ noise. Theoretically, the lifetime could thus potentially be significantly extended by implementing a form of spin-echo procedure, which is efficient for $1/f$ noise [20]. Since the Majorana overlap is exponentially suppressed in the system size, the coherence time increases exponentially with the length of the wires.

The large charging energy of the Majorana systems was imposed in order to restrict quasiparticle poisoning, where fermions from the environment tunnel into the Majorana system and flips the parity. Some degree of quasiparticle poisoning is unavoidable, however. An early study that theoretically investigated the rate of quasiparticles entering from the outside was carried out by Rainis *et al.* [67]. They point out, that even though the population of quasiparticles should be exponentially suppressed in the ratio between the superconducting gap and temperature, the lifetime of the quasiparticles scale inversely with this, and thus if the tunneling rate is sizable at low temperatures, even though there will tend to be few quasiparticles around, those that are there will have a long time to wreak havoc by tunneling into and out of the Majorana system. As experiments have been catching up since then, a better grasp of the issues of quasiparticle poisoning has since been established. Through observations of negative differential conductance, Higginbotham *et al.* [40] estimated a parity lifetime of $\gtrsim 0.1\mu s$ in their nanowire sample. Later, Albrecht *et al.* [3] put a more optimistic bound of a parity-state lifetime of $\gtrsim 1\mu s$ for strongly coupled systems. By comparing the expected $2e$-periodic conductance peaks for a Coulomb blockaded nanowire with "shadow peaks", off-set by $1e$ corresponding to sequential tunneling through the sub-gap state which is occupied there unless a quasiparticle is excited, they were able to fit a model which bounded the lifetime for weakly coupled systems by $\gtrsim 10\mu s$.

Quasiparticle poisoning doesn't need to originate from outside quasiparticles tunneling into the system. For example, it is possible for environment phonons or photons to excite a single quasiparticle and flip the parity of a zero-energy state. In finite-size systems, this can lead to logical errors if the quasiparticle then recombines with a different Majorana. However, it is also a source of error in otherwise ideal systems of infinite size. We will be investigating the latter type of error in detail in Chapter 3 and 4.

Two early studies of such errors are due to Schmidt *et al.* in 2012 [69] and Shih-Hao *et al.* in 2014 [41]. The former uses a Markovian treatment by adopting a Lindblad formalism, while the latter retains some aspects of non-Markovianity by applying a Feynman-Vernon influence functional approach. In Chapter 4, we will recover many of their qualitative conclusions, and our model will also allow for a calculation of the non-Markovian dynamics at zero temperature, which leads to a qualitatively new source of errors.

If the chemical potential fluctuates throughout the system, localized Andreev bound states may appear in the vicinity of Majoranas. In that case, the energy of the excitations is much lower, and errors are much more likely to happen. Such a system was studied by Aseev *et al.* in 2018 [10], who showed that non-uniform chemical potentials may drastically limit the lifetime of Majorana qubits, which could

provide a serious challenge for proposed braiding experiments that use varying chemical potentials as a means to move the Majorana zero modes.

Lastly, a recent paper suggests that the dephasing dynamics of Majorana box qubits may depend qualitatively on the topological nature of the system, and that studying dephasing times could serve as a first test of whether the zero modes are really Majorana bound states, or rather non-topological Andreev bound states with energies close to zero [55]. This study suggests that an experimental investigation of the dephasing dynamics of Majorana qubits should perhaps be a near-time goal which could provide more evidence to the topological nature of the found zero-energy modes.

2 Open quantum systems

One of the most famous features of quantum mechanics is that coherence between different states is destroyed in measurements and that the outcome is probabilistic. The so-called measurement problem of how one can possibly get to a probabilistic outcome from a deterministic theory was a very divisive problem in the early days of quantum mechanics, and to some extent still is. But a mathematical theory has since been formulated that seems to now satisfy most physicists, and which forms the basis of our modern understanding of quantum measurements. This is the theory of open quantum systems. Although it doesn't decisively solve the measurement problem [2], it's a beautiful and powerful theory that treats the classical world on equal footing as the microscopic and shows that no new physics than the Schrödinger equation is needed bridge the gap between the two. It relies on the simple observation that when a quantum system S interacts with an environment E, entanglement between the two builds up leading to a non-unitary time evolution of S. If the environment consists of many more degrees of freedom than the system, this has the effect of giving the system a classical behaviour by destroying the quantum coherence in the system. The state is then said to decohere. Sometimes, a distinction is made between relaxation, where states evolve towards lower energy and as such is often thermal in nature, and dephasing, which purely concerns the coherence. In that case decoherence is a common term for both processes. We will use the words decoherence and dephasing synonymously. A substantial part of the work in this thesis is concerned with the dynamics of open quantum systems and the resulting decoherence.

The system S and the environment E are described by Hamiltonians H_S and H_E, respectively, which act on Hilbert spaces $\mathcal{H}_S$ and H_E. The coupling is mediated by a Hamiltonian H_I, which generates the entanglement. The object of interest is the reduced density matrix ρ_S, whose time dependence is governed by the dynamical map

$$\rho_S(t) = \mathrm{tr}_E[\rho(t)] = \mathrm{tr}_E[U(t,t_0)\rho(t_0)U^\dagger(t,t_0)], \tag{2.1}$$

with the time evolution operator

$$U(t,t_0) = e^{-i(H_S + H_E + H_I)(t-t_0)}, \tag{2.2}$$

when all Hamiltonians are time-independent. At some initial time t_0, the density matrix $\rho(t_0)$ on the full Hilbert space is often taken to be a product state on $\mathcal{H}_S \otimes \mathcal{H}_E$, allowing us to write

$$\rho_S(t) = \mathrm{tr}_E[U(t,t_0)\rho_S(t_0) \otimes \rho_E(t_0)U^\dagger(t,t_0)], \tag{2.3}$$

where $\rho_E(t_0)$ is the initial state of the environment. Because of the entanglement generated by H_I, the time evolution of the reduced density matrix is in general not unitary, which can lead to decoherence of the system.

An important distinction in the theory of open quantum systems is whether the dynamics is Markovian or not. The physical intuition for Markovian dynamics is when the environment doesn't have a substantial memory. In this case, the equations of motion are vastly simplified. Simply imposing a Markovian approximation can break unitarity on the combined system, leading to unphysical behaviour especially at late times. This problem can be avoided if the equation of motion of the reduced density matrix can be cast into Lindblad form. In Project A of Chapter 2 we will apply a novel approximation which guarantees Lindblad form. This approximation has been highlighted a few times over the last couple of years [46, 59], and has recently been put on a solid theoretical footing by Nathan and Rudner [60].

In Project C, we use the more familiar Bloch-Redfield theory. Here, we will be both interested in decoherence at finite temperature, which is well-described by a Markovian approximation, but also in entanglement build-up due to quantum fluctuations at zero temperature. For the latter purpose, Markovian approximations break down.

In the following sections we will review the techniques that we need for those two projects. But first, let us address the concept of Markovian dynamics of open quantum systems in some detail.

2.1 Markovian master equations

Physically, the dynamics of an open quantum system is said to be Markovian when the environment has very short memory compared to the characteristic time scales of the system. This implies that the rate

of change in the state of the system doesn't depend on its history, which again means that entanglement build-up does not contribute to the change in the system state, and that the change is therefore not dominated by virtual processes. Formally, the dynamics of a quantum system is said to be Markovian when the equations of motion of the reduced density matrix $\rho_S(t)$ is time-local, meaning that we may write

$$\dot{\rho}_S(t) = \mathcal{L}(t)\rho_S(t), \tag{2.4}$$

where $\mathcal{L}(t)$ is the *Liouvillian superoperator*, acting on $\rho_S(t)$ with operator multiplication from both sides. In the literature, a Markovian equation of motion is often called *master equation*. The master equation (2.4) is a simple differential equation and has the formal solution

$$\rho_S(t) = \mathcal{T}e^{\int_{t_0}^t ds\mathcal{L}(s)}\rho_S(t_0), \tag{2.5}$$

where $\mathcal{T}$ denotes time ordering,

$$\mathcal{T}A(t_1)B(t_2) = \theta(t_1 - t_2)A(t_1)B(t_2) + \theta(t_2 - t_1)B(t_2)A(t_1), \tag{2.6}$$

for arbitrary superoperators A and B. We will only need the theory for cases where H_S, H_E and H_I are all time-independent, so we assume this from now on. This implies that the Liouvillian $\mathcal{L}$ also becomes time-independent. The dynamical map $\rho_S(t_0) \mapsto \rho_S(t)$ needs to preserve Hermiticity, trace and complete positivity. As proven by Lindblad [52], this turns out to be true for Markovian systems if and only if the Liouvillian has a very particular form, called *Lindblad form*. The Lindblad form is defined by

$$\mathcal{L}\mathcal{O} = -i[H, \mathcal{O}] + \sum_k \gamma_k \left(-\frac{1}{2}\{L_k^\dagger L_k, \mathcal{O}\} + L_k\mathcal{O}L_k^\dagger \right), \tag{2.7}$$

where the decay rates γ_k are non-negative and the "jump operators" L_k are traceless and orthonormal in the sense that

$$\text{tr}[L_i^\dagger L_j] = \delta_{i,j}. \tag{2.8}$$

It's straightforward to see that Eq. (2.7) preserves Hermiticity and trace, but it is more suprising a priori that complete positivity is also quaranteed.

Many established approximations, such as the Bloch-Redfield master equation which we will turn to in Section 2.2, do not guarantee a Lindblad form. Sometimes this is not a big problem, since unphysical behaviour, such as having an eigenvalue of $\mathcal{L}$ with a small positive real value, most often appears at late times. But depending on which questions are being asked, it is potentially dangerous not to have the time-evolution on Lindblad form. A standard remedy is to apply further system-dependent approximations that enforce the Lindblad form. The rotating-wave approximation is a famous example [15]. Alternatively, when such approximations are not applicable, phenomenological models are often used, where jump operators are derived for instance based on detailed balance.

The Lindblad form (2.7) may seem peculiar at first glance, but to see how it naturally emerges in Markovian dynamics, for the rest of this section we will present an argument [65, 72], which shows how any Markovian time evolution due to time evolution of the form in Eq. (2.3) must be writable using a Lindblad form[5].

The argument begins by noting that the time evolution in Eq. (2.3) has a neat operator expansion in terms of so-called *Kraus operators*. If $\{|b_j\rangle\}_{j=1}^{\dim \mathcal{H}_E}$ is an orthonormal basis of $\mathcal{H}_E$ diagonalizing $\rho_E(t_0)$, then we may write

$$\rho(t_0) = \sum_j \lambda_j \rho_s(t_0) \otimes |b_j\rangle\langle b_j|, \tag{2.9}$$

where $\{\lambda_j\}$ are the eigenvalues of $\rho_E(t_0)$. This may be used to rewrite Eq. (2.3) for the time evolution of the system's reduced density matrix as

$$\rho_S(t) = \sum_{k,p} A_{k,p}(t, t_0)\rho_S(t_0)A_{k,p}^\dagger(t, t_0), \tag{2.10}$$

---

[5]Note that this argument doesn't prove the more useful true statement that Lindbladian time-evolution implies completely positive and trace-preserving dynamical map.

where the Kraus operators $A_{k,p}(t, t_0)$ are defined by

$$A_{k,p}(t, t_0) = \sqrt{\lambda_p} \langle b_k | U(t, t_0) | b_p \rangle. \tag{2.11}$$

Note that the Kraus operators are unital

$$\sum_{k,p} A_{k,p}^\dagger(t, t_0) A_{k,p}(t, t_0) = \sum_{k,p} \lambda_p \langle b_p | U^\dagger(t, t_0) | b_k \rangle \langle b_k | U(t, t_0) | b_p \rangle = \mathbb{1}_S, \tag{2.12}$$

and they depend on the initial state. We wish to construct a similar operator expansion for infinitesimal time evolution from any later time $t_1 > t_0$. The above Kraus operators were derived from a product state, but at later times the system will be entangled with the environment. There still exist Kraus operators for the time evolution starting from $\rho(t_1)$, which is not a product state. This can for instance be seen by using Stinespring's dilation theorem, which posits the existence of an auxiliary Hilbert space $\tilde{\mathcal{H}}$, a pure state $|\tilde{1}\rangle \in \tilde{\mathcal{H}}$, and a unitary operator $\tilde{\mathcal{U}}(t, t_1)$ such that

$$\rho_S(t) = \operatorname{tr}_{\tilde{\mathcal{H}}}[\tilde{\mathcal{U}}(t, t_1) \left(\rho_S(t_1) \otimes |\tilde{1}\rangle\langle\tilde{1}| \right) \tilde{\mathcal{U}}^\dagger(t, t_1)], \tag{2.13}$$

which, completely analogous to the case above, implies the existence of Kraus operators $\{\tilde{A}_k(t, t_0)\}$ such that $\rho_S(t) = \sum_k \tilde{A}_k(t, t_1) \rho_S(t_0) \tilde{A}_k(t, t_1)$. These Kraus operators are again unital,

$$\sum_k \tilde{A}_k^\dagger(t, t_1) \tilde{A}_k(t, t_1) = \mathbb{1}_S, \tag{2.14}$$

just as in the unentangled case. Since the Hamiltonian is time-independent, if the dynamics is Markovian, we should expect to recover a simple differential equation for $\rho(t)$, and we may get this by using the Kraus operators to implement an infinitesimal time increment,

$$\rho_S(t + dt) = \sum_k A_k(dt) \rho_S(t) A_k(dt), \tag{2.15}$$

and only keep contributions linear in dt, before taking the limit $dt \to 0$. Comparing it with a Taylor expansion of Eq. (2.1) for infinitesimal time evolution,

$$\begin{aligned} \rho_S(t + dt) &= \sum_k \langle b_k | U(t + dt, t) \rho(t) U^\dagger(t + dt, t) | b_k \rangle \\ &\approx \rho_S(t) - i \sum_k \langle b_k | [H, \rho(t)] | b_k \rangle dt, \end{aligned} \tag{2.16}$$

we see that the Kraus operators may consist both of non-trivial operators acting from only one side, but also operators acting from both sides, implying that $A_k(dt)$ has contributions proportional to $\sqrt{dt}$. For convenience, we may collect all terms proportional to the identity as well as all terms linear in dt in one of the Kraus operators, say $A_0(t + dt, t)$, and write

$$A_{k=0}(dt) = \mathbb{1} + dt(-iH_L + K), \tag{2.17a}$$
$$A_{k \neq 0}(dt) = \sqrt{dt} L_k, \tag{2.17b}$$

where $H_L^\dagger = H_L$ is an effective Hamiltonian generating unitary evolution for $\rho_S(t)$, and $K^\dagger = -K$. Eqs. (2.17) imply that

$$\rho_S(t + dt) = \rho_S(t) + dt \left(-i[H_L, \rho_S(t)] + \{K, \rho_S(t)\} + \sum_{k>0} L_k \rho_S(t) L_k^\dagger \right), \tag{2.18}$$

and using unitality, Eq. (2.14), we see that

$$K = -\frac{1}{2} \sum_{k>0} L_k^\dagger L_k. \tag{2.19}$$

Taking $dt \to 0$ gives the Lindblad equation

$$\dot{\rho}_S(t) = -i[H_L, \rho_S(t)] + \sum_{k>0} \left(-\frac{1}{2}\{L_k^\dagger L_k, \rho_S(t)\} + L_k \rho_S(t) L_k^\dagger \right). \qquad (2.20)$$

The orthogonality of L_k can be established from the fact that the Kraus operators may always be chosen to be orthogonal. Thus, we see that when open quantum systems are governed by a Markovian master equation, it has to be on Lindblad form. If one forces time-evolution into a Markovian form in a way that does not yield a master equation on Lindblad form, there is a risk of having secular terms which for instance can lead to an exponentially slow growth of the density matrix elements, leading to a useless theory for late time behaviour.

In the following section, we will review the Bloch-Redfield theory of open quantum systems. This will be useful for deriving a Markovian theory, which will have Lindblad form only in a limited set of cases, but luckily one that applies to Project C. The theory allows for calculating non-Markovian dynamics of open quantum systems, which we will also need in Project C. It should be noted, however, that since there is no equivalent to Lindblad's theorem for non-Markovian evolution, one should be wary of model breakdown at late times.

2.2 Bloch-Redfield theory

In the previous section, we took an abstract view on what Markovian dynamics entails, and in this section we will review a commonly used Markovian approximation. The discussion on the validity is saved for the next section, where we will review the recent work by Nathan and Rudner [60]. In this section, we will develop the standard Bloch-Redfield master equation for the reduced density matrix $\rho_S(t)$.

We write the time-independent Hamiltonian H as

$$H = H_0 + H_I, \qquad (2.21)$$
$$H_0 = H_S + H_E, \qquad (2.22)$$
$$H_I = X\Phi, \qquad (2.23)$$

where H_S and H_E are quadratic Hamiltonians acting on the system and environment, respectively, and H_I is for simplicity taken to be a product of Hermitian operators X and Φ acting on on the system and environment, respectively. We will also assume that Φ is linear in the creation/annihilation operators corresponding to the environment modes. The quadratic bath is characterized purely by its two-point correlation function $B(t)$ in these creation/annihilation operators. We take an initial product state

$$\rho(t_0) = \rho_S(t_0) \otimes \rho_E(t_0), \qquad (2.24)$$

assuming that ρ_E is a steady state of H_E. Thus, the correlation function is defined in the interaction picture as

$$B(t - t') = \langle \Phi(t)\Phi(t') \rangle = \text{tr}_E[\Phi(t)\Phi(t')\rho_E], \qquad (2.25)$$

where we take the interaction picture with respect to the interaction H_I, meaning

$$\Phi(t) = e^{iH_E t}\Phi e^{-iH_E t}. \qquad (2.26)$$

The environment may be either fermionic or bosonic, and we denote the annihilation operator of the environmental modes by a_q. In terms of these, we write

$$H_E = \sum_q \omega_q a_q^\dagger a_q, \qquad (2.27a)$$

$$H_I = \sum_q X(M_q a_q \pm M_q^* a_q^\dagger), \qquad (2.27b)$$

with the convention of $+$ in Eq. (2.27b) for bosons, and $-$ for fermions. We take $\omega_q \geq 0$ for simplicity and stress that the operator X acts only on the system and not on the bath. In the interaction picture

the Heisenberg equation of motion gives $a_q(t) = e^{-i\omega_q t} a_q$. Thus, we have

$$
B(t) = \sum_{q,q'} \left\langle \left(e^{-i\omega_q t} M_q a_q \pm e^{i\omega_q t} M_q^* a_q^\dagger \right) \left(M_{q'} a_{q'} \pm M_{q'}^* a_{q'}^\dagger \right) \right\rangle
$$

$$
= \pm \sum_q |M_q|^2 \left(e^{i\omega_q t} \left\langle a_q^\dagger a_q \right\rangle + e^{-i\omega_q t} (1 \pm \left\langle a_q^\dagger a_q \right\rangle) \right). \tag{2.28}
$$

This may be conveniently expressed in terms of the spectral function (or density of states)[6]

$$
J(\omega) = \sum_q |M_q|^2 \, \delta(\omega - \omega_q). \tag{2.29}
$$

In thermal equilibrium at temperature $1/\beta$, we have

$$
\left\langle a_q^\dagger a_q \right\rangle = \begin{cases} n_{\rm B}(\omega) & : \text{bosons} \\ n_{\rm F}(\omega) & : \text{fermions} \end{cases}, \tag{2.30}
$$

where the Bose and Fermi functions are defined as $n_{\rm B}(\omega) = (\exp(\beta\omega)-1)^{-1}$ and $n_{\rm F}(\omega) = (\exp(\beta\omega)+1)^{-1}$, respectively. With this, $B(t)$ becomes

$$
B(t) = \int_0^\infty d\omega J(\omega) \begin{cases} e^{-i\omega t}(n_B(\omega) + 1) + e^{i\omega t} n_B(\omega) & : \text{bosons} \\ e^{-i\omega t}(1 - n_F(\omega)) + e^{i\omega t} n_F(\omega) & : \text{fermions.} \end{cases} \tag{2.31}
$$

For bosons, a useful rewriting of the correlation function $B(t)$ is

$$
B(t) = \int_0^\infty d\omega J(\omega) \left(\coth\left(\frac{\beta\omega}{2} \right) \cos(\omega t) - i\sin(\omega t) \right), \qquad \text{(bosons)} \tag{2.32}
$$

and in frequency space, Eq. (2.32) becomes

$$
B(\omega) = \int_0^\infty d\nu \, J(\nu) \int_{-\infty}^\infty dt e^{i\omega t} \left(\coth\left(\frac{\beta\nu}{2} \right) \cos(\nu t) - i\sin(\nu t) \right)
$$

$$
= \frac{1}{2} \int_0^\infty d\nu \, J(\nu) 2\pi \left[\left(\delta(\omega + \nu) + \delta(\omega - \nu) \right) \coth\left(\frac{\beta\nu}{2} \right) - \left(\delta(\omega + \nu) - \delta(\omega - \nu) \right) \right]
$$

$$
= \pi \begin{cases} J(\omega) \left(\coth\left(\frac{\beta\omega}{2} \right) + 1 \right) & : \omega > 0 \\ 2\beta^{-1} \lim_{\omega \to 0} \frac{J(\omega)}{\omega} & : \omega = 0 \\ J(-\omega) \left(\coth\left(\frac{-\beta\omega}{2} \right) - 1 \right) & : \omega < 0, \end{cases} \qquad \text{(bosons)} \tag{2.33}
$$

where we used in the third line that $\int_0^\infty d\nu \delta(\nu) = 1/2$. In all situations we consider, $J(\omega)$ will be ohmic, meaning proportional to ω for small frequencies, so the limit in (2.33) is well-defined. Hence, we write

$$
B(\omega) = \pi J(|\omega|) \text{sgn}(\omega) \left(\coth\left(\frac{\beta\omega}{2} \right) + 1 \right), \qquad \text{(bosons)} \tag{2.34}
$$

which is a form we will see again in Chapter 2. When $J(\omega)$ is an odd function, we will often absorb the $\text{sgn}(\omega)$ into $J(|\omega|)$. As an example of an ohmic environment, in Chapter 2 we study the dynamics when a split Majorana box qubit is subjected to a bosonic environment with the generic ohmic spectral density $J(\omega) = \omega \exp(-|\omega|/\omega_c)/2$, where ω_c is an ultraviolet cutoff. We may gain some intuition about $B(\omega)$ for bosons when we rewrite it as

$$
B(\omega) = 2\pi J(|\omega|) \text{sgn}(-\omega) n_{\rm B}(-\omega). \qquad \text{(bosons)} \tag{2.35}
$$

The form of $B(\omega)$ in Eq. (2.35) is suggestive that transition rates in the system due to the bath should be proportional to $B(\omega)$, since it contains both the density of states and the occupancy of the environment modes. This is precisely what Fermi's golden rule implies, and this observation is helpful in motivating

---

[6]Note, that in Chapter 4, the spectral function is defined with an extra factor of π.

the jump operators in the next section. We will return to discuss this in Section 2.3, but for now, we note that $B(\omega)$ is non-negative and is not an even function of ω, which reflects the fact that for low temperatures, transitions from higher to lower energetic states happen more frequently than the reverse.

Although we have included just a single coupling in Eq. (2.23), it is straightforward to generalize the following theory to contain several distinct bath couplings $X_i \Phi_i$ as long as the separate bath operators Φ_i commute.

The starting point for deriving the Bloch-Redfield master equation is the Heisenberg equation of motion, written in the interaction picture as

$$\dot{\rho}(t) = -i[H_I(t), \rho(t)]. \tag{2.36}$$

Eq. (2.36) can be integrated to get

$$\rho(t) = \rho(t_0) - i \int_{t_0}^{t} dt' [H_I(t'), \rho(t')], \tag{2.37}$$

which can be inserted back into (2.36), giving

$$\dot{\rho}(t) = -i[H_I(t), \rho(t_0)] - \int_{t_0}^{t} dt' [H_I(t), [H_I(t'), \rho(t')]]. \tag{2.38}$$

For initial product state defined in Eq. (2.24), we assume that

$$\mathrm{tr}[\Phi \rho_E(t_0)] = 0. \tag{2.39}$$

We can then find a master equation for $\rho_S(t)$ by tracing Eq. (2.38) over the environment degrees of freedom:

$$\dot{\rho}_S(t) = -\int_{t_0}^{t} dt' \, \mathrm{tr}_E[H_I(t), [H_I(t'), \rho_E(t')]]$$

$$\equiv \int_{t_0}^{t} dt' \Delta(t, t') \rho(t'). \tag{2.40}$$

The superoperator $\Delta(t, t')$ is denoted the memory kernel, and the standard step is now to perform the Born approximation, which amounts to approximating the density matrix under the integral in Eq. (2.40) with a product state at all times, ignoring backaction on the environment. Since we assumed that ρ_E is a steady state, the Born approximation implies taking the state

$$\rho(t) \approx \rho_S(t) \otimes \rho_E \tag{2.41}$$

for all times t in the integrand of Eq. (2.40). This results in a memory-kernel superoperator $\Delta_B(t, t')$ in the Born approximation, acting just on the system's reduced density matrix:

$$\dot{\rho}_S(t) = \int_{t_0}^{t} dt' \Delta_B(t, t') \rho_S(t'). \tag{2.42}$$

The approximation is computationally very useful, since it implies that all terms in the integrand of Eq. (2.40) are proportional to the environment correlation function either with $B(t - t')$ or $B(t' - t)$.

We may conveniently write $\Delta_B(t, t')$ explicitly by introducing the following superoperator notation [60]: For ordinary operators A and $\mathcal{O}$, let $\hat{A}_{L/R}$ denote the superoperator obtained by left/right multiplication of A with the sign convention

$$\hat{A}_L \mathcal{O} = A\mathcal{O}, \tag{2.43a}$$

$$\hat{A}_R \mathcal{O} = -\mathcal{O}A, \tag{2.43b}$$

where the sign is useful for notational brevity thanks to the commutators in Eq. (2.40). Using this notation, along with the Einstein summation convention, we can write

$$\Delta_B(t, t') = -\hat{X}_\mu(t) \hat{X}_\nu(t') B_{\mu\nu}(t - t'), \tag{2.44a}$$

$$B_{\mu\nu}(t - t') = \mathrm{tr}_E[\hat{\mathbb{1}}_\mu \hat{\mathbb{1}}_\nu \hat{\Phi}_\mu(t) \hat{\Phi}_\nu(t') \rho_E]. \tag{2.44b}$$

Note that $B_{\mu\nu}(t)$ doesn't depend on μ because of the cyclicity of the trace, and also that the role of the identity operators is to adjust for the sign. Since $B(-t) = B^*(t)$, we have

$$B_{\mu,L}(t) = B_{\mu,R}(-t) = B(t). \tag{2.45}$$

Returning to the derivation, $B(t)$ will tend to be a decaying function of $|t|$ with some characteristic time scale τ_c. If $t - t_0 \gg \tau_c$, we may extend the integration limit t_0 to $-\infty$ in Eq. (2.42). This step is often done to remove the dependency on t_0, but it is strictly speaking not necessary. If τ_c is very short compared to the rate of changes in $\rho_S(t)$, the only substantial contribution in the integrand of Eq. (2.40) is picked up for $t' \approx t$. In that case we can implement a Markovian approximation by replacing $\rho_S(t')$ with $\rho_S(t)$ under the integral. With the full Born-Markov approximation, we arrive at the Bloch-Redfield master equation

$$\dot{\rho}_S(t) = \mathcal{D}_R(t)\rho_S(t), \tag{2.46}$$

where the "retarded", or "right", dissipator is defined as

$$\mathcal{D}_R(t) = \int_{-\infty}^{t} dt' \Delta_B(t, t'). \tag{2.47}$$

There is no a priori reason why Eq. (2.46) should necessarily be on Lindblad form, except in the special case where $H_S = 0$. This exception is relevant for Project C of Chapter 4 where H_0 will describe an ideal system of Majoranas, which are exactly at zero energy, and the quasiparticle states are treated as separate fermionic environments. When $H_S = 0$, the time-evolution of X is trivial, and therefore, in superoperator notation, the retarded dissipator becomes time-independent and is given by

$$\mathcal{D}_R(t) = -\hat{X}_\mu \hat{X}_\nu \int_{-\infty}^{t} dt' B_{\mu\nu}(t - t') = -\hat{X}_\mu \hat{X}_\nu \int_{0}^{\infty} dt' B_{\mu\nu}(t'), \tag{2.48}$$

and writing Eq. (2.48) out in terms of regular operators yields the simple Lindblad form

$$\mathcal{D}_R \rho_S = -i\Omega[X^2, \rho_S] + \Gamma\left(-\frac{1}{2}\{X^2, \rho_S\} + X\rho_S X\right), \tag{2.49}$$

where we defined

$$\text{Re}\left[\int_{0}^{\infty} dt' B(t')\right] = \frac{1}{2}\Gamma, \qquad \text{Im}\left[\int_{0}^{\infty} dt' B(t')\right] = \Omega. \tag{2.50}$$

The first term in (2.49) is a term that renormalizes the bare Hamiltonian H_S, which is absent from the commutator since we are using the interaction picture. When the environment is bosonic, this renormalization is often denoted the Lamb shift. Strictly speaking, only the second term in Eq. (2.49) should be referred to as the dissipator, since this is the part that contributes to non-unitary evolution of ρ_S.

If one were interested in non-Markovian dynamics, Eq. (2.42) serves as a useful starting point. After switching to the Scrhödinger picture, the equation of motion is

$$\begin{aligned}
\dot{\rho}_S(t) = -i[H_S, \rho_S(t)] - \int_{t_0}^{t} dt' \Big[& X e^{-iH_S(t-t')} X \, \rho_S(t') \, e^{iH_S(t-t')} B(t - t') \\
& + e^{-iH_S(t-t')} \rho_S(t') \, X e^{iH_S(t-t')} X B(t' - t) \\
& - e^{-iH_S(t-t')} X \, \rho_S(t') \, e^{iH_S(t-t')} X B(t - t') \\
& - X e^{-iH_S(t-t')} \rho_S(t') \, X e^{iH_S(t-t')} B(t' - t) \Big] \\
\equiv -i[H_S, \rho_S(t)] - (\hat{R} * \rho_S)(t),
\end{aligned} \tag{2.51}$$

where $(\hat{R} * \rho_S)(t) = \int_{t_0}^{t} dt' \hat{R}(t - t')\rho_S(t')$ denotes convolution with respect to the initial time t_0. The convolution theorem for Laplace transforms may then be used to get

$$\rho_S(s) - s\rho_S(t_0) = -i[H_S, \rho_S(s)] - \hat{R}(s)\rho_S(s), \tag{2.52}$$

meaning

$$\rho_S(s) = s\mathcal{K}^{-1}(s)\rho_S(t_0), \tag{2.53a}$$

$$\mathcal{K}(s) = 1 + \hat{R}(s) - i \sum_{\mu=L,R} (\hat{H}_S)_\mu. \tag{2.53b}$$

While Eq. (2.53) is formally simple to write down, the inverse Laplace transform can be a nightmare to evaluate, especially since the poles are not necessarily isolated. If one is only interested in the non-Markovian effects at late times, a simplification can sometimes be to approximate $\mathcal{K}(s)$ by its form for $s \approx 0$ and analytically continue to the whole complex plane, although one should be careful with branch cuts. This can guarantee simple poles, but even so the problem may be intractable, especially at finite temperatures. This method will be employed in Chapter 4 for Project C.

In Project A in Chapter 2 when we want to study the readout of a Majorana box qubit in the Markovian limit, the technique in the preceding section is not useful, since it does not yield a Lindblad form in that case. In the following section we will turn to the novel Lindbladian master equation, recently treated by Nathan and Rudner [60]. Following their work, we also discuss error bounds for both the Bloch-Redfield master equation and the effective Lindbladian approximation.

2.3   Effective Lindbladian approximation

In this section, we will discuss an effective Lindbladian master equation which we use in Chapter 2. The approximation prescribes a specific jump operator L of the form

$$L = \sum_{m,n} \sqrt{B(E_n - E_m)} \langle m|X|n\rangle \, |m\rangle\langle n| \,, \tag{2.54}$$

such that the dynamics is given by the master equation

$$\dot{\rho}_S(t) = \mathcal{L}\rho_S(t) \equiv -i[H_S + H_{LS}, \rho_S(t)] + \left(-\{L^\dagger L, \rho_S(t)\} + L\rho_S(t)L^\dagger\right), \tag{2.55}$$

where H_{LS} is the Lamb shift. The jump operator in Eq. (2.54) has been seen sparingly in the literature, see for example [46, 59], and recently the approximation has been put on theoretically solid ground [60], providing a strict bound for the error introduced by the approximation. Although this form may seem surprising at first glance, it is actually quite natural since Fermi's golden rule naturally follows. From Eq. (2.55), the transition rate $\Gamma_{a \to b}$ between two eigenstates $|a\rangle\langle a|$ and $|b\rangle\langle b|$ of H_S becomes

$$\Gamma_{a \to b} = \frac{d}{dt} |\langle b|a(t)\rangle|^2 \Big|_{t=0} = \langle b|\left(\mathcal{L}|a\rangle\langle a|\right)|b\rangle = |\langle b|X|a\rangle|^2 B(E_a - E_b). \tag{2.56}$$

As an example, let us check that (2.56) exactly reproduces Fermi's golden rule for the case of thermalized bosons, with the bath- and coupling Hamiltonians given by (2.27a) and (2.27b), respectively, and where the operators a_q are bosonic fields. We denote the bath eigenstates by $|\{n_i\}\rangle$. If initially, the reduced density matrix is $\rho_S(0) = |a\rangle\langle a|$ and the environment state is thermal, $\rho_E(0) = \sum_{\{n_i\}} e^{-\beta E_{\{n_i\}}}/Z_E$, then the transition probability $P_{a \to b}(t)$ is

$$P_{a \to b}(t) = \langle b|\rho_S(t)|b\rangle = \sum_{\{n'_j\}} \langle b, \{n'_j\}|\rho(t)|\{n'_j\}\rangle$$

$$= \frac{1}{Z_E} \sum_{\{n_i\},\{n'_j\}} e^{-\beta E_{\{n_i\}}} \left|\langle b, \{n'_j\}|U(t)|a, \{n_i\}\rangle\right|^2, \tag{2.57}$$

where $U(t)$ is the time-evolution operator. To the lowest order in H_I, we find the transition rate using Fermi's golden rule [16],

$$\Gamma_{a,\{n_i\} \to b,\{n'_j\}} = \frac{d}{dt} \left|\langle b, \{n'_j\}|U(t)|a, \{n_i\}\rangle\right|^2 \approx 2\pi \left|\langle b, \{n'_j\}|H_I|a, \{n_i\}\rangle\right|^2 \delta(E_b + E_{\{n'_j\}} - E_a - E_{\{n_i\}}). \tag{2.58}$$

With the coupling H_I given by Eq. (2.27b), this can be shown to imply

$$\Gamma_{a \to b} = 2\pi |\langle b|X|a\rangle|^2 J(|E_a - E_b|)\mathrm{sgn}(E_b - E_a)n_{\mathrm{B}}(E_b - E_a). \tag{2.59}$$

If we use the expression for $B(\omega)$ in Eq. (2.35), we recover the transition rate predicted by the effective Lindbladian approximation in Eq. (2.56).

In Project A in Chapter 2, we make use of this Lindbladian approximation. The work was carried out based on a private communication with Nathan and Rudner before the publication of their paper. Since then, they have made some changes in the derivation, leading to a slightly different formula for the Lamb shift than the one we use in our paper. The two formulas are not equal, but as they are based off approximations whose validity is governed by the same small parameter, their difference should also only be of that order. But because of the discrepancies, we will provide a sketch of their earlier derivation leading to the formula for the Lamb shift used in Project A.

At the heart of the argument lies the observation that the standard implementation of Born-Markov from the previous section is not unique. A whole family of Born-Markov approximations exist, all equally valid in the following sense: The difference between the exact value of $\dot{\rho}_S(t)$ and that calculated through any of these Born-Markov approximation is bounded by the same number. A special symmetric Born-Markov approximation forms the basis from which a final approximation unveils the Lindblad form. As we shall see, the validity of this final approximation depends on a different parameter than the other Born-Markov approximations, however there exists a single quantity which serves as an error bound for the Born-, Markovian- and effective Lindblad approximations.

The family of equivalent Born-Markov approximations can be derived by finding an "advanced" version of Eq. (2.46)

$$\dot{\rho}_S(t) = \mathcal{D}_A(t)\rho_S(t), \tag{2.60}$$

where the "advanced" dissipator is

$$\mathcal{D}_A(t) = \int_t^\infty dt' \Delta_B(t', t), \tag{2.61}$$

and showing that the advanced Born-Markov approximation is just as valid as the retarded. After this, the family of Markov approximations can be parametrically formed by taking combinations of the form

$$\mathcal{D}_\alpha(t) = \alpha \mathcal{D}_R(t) + (1 - \alpha)\mathcal{D}_A(t), \tag{2.62}$$

with $\alpha \in [0, 1]$. The combination with $\alpha = 1/2$ is the above-mentioned symmetric case, from which the final approximation can be done, obtaining a master equation on Lindblad form. Let's first address what is being meant by "equally valid". For all error analysis, a normalization is used such that $||X|| \leq 1$ in the singular value norm. This can always be achieved by rescaling Φ.

Nathan and Rudner show the following exact bound for the rate of change of the reduced density matrix:

$$\dot{\rho}_S(t) \leq \Gamma_0, \tag{2.63}$$

$$\Gamma_0 \equiv 4 \int_0^\infty dt \, |B(t)|. \tag{2.64}$$

Note that Γ_0 only depends on details of the environment. They then demonstrate that the Born approximation introduces an error $\mathcal{E}_B$, which can be shown to be bounded as

$$\mathcal{E}_B \leq \tau_c \Gamma_0^2, \tag{2.65}$$

$$\tau_c \equiv \frac{4}{\Gamma_0} \int_0^\infty dt \, t \, |B(t)|. \tag{2.66}$$

The derivation of this error bound hinges on the environment being quadratic. The time τ_c can be thought of as a characteristic decay time of $B(t)$, which can be heuristically verified in the special case $B(t) \sim \frac{\Gamma_0}{4\tau_c} e^{-|t|/\tau_c}$.

The error bound for the Markovian approximation can be found by writing

$$\dot{\rho}_S(t) = \int_{t_0}^t dt' \Delta_B(t, t')\rho(t') = \int_{t_0}^t dt' \Delta_B(t, t')\rho(t) + \int_{t_0}^t dt' \Delta_B(t, t')(\rho(t') - \rho(t)). \tag{2.67}$$

The first term is what is kept in the Markovian approximation, and using the bound in Eq. (2.63), the triangle inequality, as well as expression (2.44a), the norm of the second term can be shown also to be bounded by $\tau_c \Gamma_0^2$. The Markov approximation apparently entails an error of the same size as the one

already made by invoking the Born approximation. Thus, the full Born-Markov approximation leading to the Bloch-Redfield master equation (2.46) introduces an error

$$\mathcal{E}_M \leq 2\tau_c \Gamma_0^2. \tag{2.68}$$

It is in this sense that the advanced Born-Markov approximation may be shown to be equivalent to the retarded [60]; it comes with an error also bounded by $\mathcal{E}_M$.

We now to take the symmetric combination with $\alpha = 1/2$ and extend the integration limits to $\pm\infty$, which introduces a Lamb shift:

$$\mathcal{D}_{1/2}(t) = \frac{1}{2} \int_{-\infty}^{t} dt' \Delta_B(t, t') + \frac{1}{2} \int_{t}^{\infty} dt' \Delta_B(t', t)$$
$$= \frac{1}{4} \left(\overline{\mathcal{D}}_R(t) + \overline{\mathcal{D}}_A(t) \right) - \frac{i}{4} \left(\Lambda_R(t) + \Lambda_A(t) \right). \tag{2.69}$$

Here, we defined

$$\overline{\mathcal{D}}_R = \int_{-\infty}^{\infty} dt' \Delta_B(t, t'), \qquad \overline{\mathcal{D}}_A = \int_{-\infty}^{\infty} dt' \Delta_B(t', t), \tag{2.70a}$$

$$\Lambda_R(t) = i \int_{-\infty}^{\infty} dt' \theta(t' - t) \left(\Delta_B(t', t) - \Delta_B(t, t') \right), \tag{2.70b}$$

$$\Lambda_A(t) = i \int_{-\infty}^{\infty} dt' \theta(t - t') \left(\Delta_B(t, t') - \Delta_B(t', t) \right), \tag{2.70c}$$

where $\theta(t)$ is the Heaviside step function. Using the expression for $\Delta_B(t, t')$ in Eq. (2.44a), the action of the dissipator in (2.69) can be written as

$$D_{1/2}(t)\rho_S = \frac{1}{4} \left(\overline{\mathcal{D}}_R(t) + \overline{\mathcal{D}}_A(t) \right) \rho_S - i[H_{LS}, \rho_S], \tag{2.71}$$

and the Lamb shift may be written as

$$H_{LS} \equiv \frac{1}{4} \left(\Lambda_R(t) + \Lambda_A(t) \right) = \frac{i}{4} \int_{-\infty}^{\infty} ds \, \text{sgn}(t - s) X(t) X(s) B(t - s) + \text{H.c.} \tag{2.72}$$

Evaluating this term gives the Lamb shift we use in Project A. Before doing so, let us briefly comment on how the derivation continues, as it is relevant for the error discussion. The square root in the jump operators appear due to a rewriting of $B(t)$,

$$B(t - t') = \int_{-\infty}^{\infty} ds \, g(t - s) g(s - t'), \tag{2.73}$$

where

$$g(t) = \frac{1}{2\pi} \int_{-\infty}^{\infty} d\omega \sqrt{B(\omega)} e^{-i\omega t}. \tag{2.74}$$

Starting from Eq. (2.71), the Lindblad form is uncovered by showing

$$D_{1/2}(t)\rho_S = \mathcal{L}\rho_S(t) + \mathcal{O}_\mathcal{L}, \tag{2.75}$$

where $\mathcal{L}$ is the Liouvillian superoperator from Eq. (2.55). The norm of the error term $\mathcal{O}_\mathcal{L}$ satisfies the bound

$$||\mathcal{O}_\mathcal{L}|| \leq \Gamma_J \tau_J \Gamma_0, \tag{2.76}$$

where new time- and energy scales, defined through $g(t)$ rather than $B(t)$ have been introduced:

$$\Gamma_J \equiv \left(\int_0^{\infty} dt \, |g(t)| \right)^2, \tag{2.77}$$

$$\tau_J \equiv \frac{\int_0^{\infty} dt \, t \, |g(t)|}{\int_0^{\infty} dt \, |g(t)|}. \tag{2.78}$$

33

By now, we have two separate bounds that both need to be satisfied in order for the effective Lindblad approximation to be valid. The first is the usual Born-Markov limit $\tau_c \Gamma_0 \ll 1$, and the second is the new condition $\tau_J \Gamma_J \ll 1$. It is possible to express both bounds in terms of a single one. To see this, we rewrite

$$\Gamma_0 = \int_0^\infty dt\, |B(t)| \leq \int_{-\infty}^\infty dt \int_{-\infty}^\infty dt'\, |g(t-t')|\,|g(t')| = \overline{\Gamma}_J, \tag{2.79}$$

where we introduced the rate

$$\overline{\Gamma}_J = \left(\int_{-\infty}^\infty dt\, |g(t)| \right)^2. \tag{2.80}$$

Furthermore,

$$\tau_c = \frac{1}{\Gamma_0} \int_0^\infty dt\, t\, |B(t)| \leq \frac{1}{\Gamma_0} \int_0^\infty dt\, t \int_{-\infty}^\infty dt'\, |g(t-t')|\,|g(t')|$$

$$\leq \frac{1}{\Gamma_0} \int_{-\infty}^\infty dt \int_{-\infty}^\infty dt'(|t-t'|+|t'|)\,|g(t-t')|\,|g(t')| = \frac{2}{\Gamma_0} \overline{\Gamma}_J \overline{\tau}_J \tag{2.81}$$

where

$$\overline{\tau}_J = \frac{\int_{-\infty}^\infty dt\, |t|\,|g(t)|}{\int_{-\infty}^\infty dt\, |g(t)|}. \tag{2.82}$$

This implies that

$$\Gamma_0 \tau_c \leq 2\overline{\Gamma}_J \overline{\tau}_J, \tag{2.83}$$

and also

$$\Gamma_J \tau_J \leq 8\overline{\Gamma}_J \overline{\tau}_J. \tag{2.84}$$

This means that if $8\overline{\Gamma}_J \overline{\tau}_J \ll 1$, then both the Bloch-Redfield and the subsequent Nathan-Rudner approximation are valid. We emphasize that the above limits assume $||X|| = 1$.

Finally, let us derive the expression for the Lamb shift, starting from Eq. (2.72). We write this equation as

$$H_{LS}(t) = \frac{i}{4} X(t) K(t) + \text{H.c.}, \tag{2.85}$$

where we introduced the function

$$K(t) = \int_{-\infty}^\infty ds\, \text{sgn}(t-s) X(s) B(t-s). \tag{2.86}$$

We may rewrite $K(t)$ by shifting the integrals, using the Fourier transforms $X(\nu)$ and $B(\omega)$ of $X(t)$ and $B(t)$ and by using the fact that $B(t)$ decays in order to shift the frequencies of $B(\omega)$ with an infinitesimal for explicit convergence of the integrals:

$$K(t) = \int_0^\infty ds X(t-s) B(s) + \int_0^{-\infty} ds X(t-s) B(s)$$

$$= \frac{1}{4\pi^2} \int_{-\infty}^\infty d\omega d\nu X(\nu) \left[\int_0^\infty ds B(\omega + i0^-) e^{-i(t-s)\nu} e^{-i(\omega+i0^-)s} + \int_0^{-\infty} ds B(\omega + i0^+) e^{-i(t-s)\nu} e^{-i(\omega+i0^+)s} \right]$$

$$= -\frac{i}{4\pi^2} \int_{-\infty}^\infty d\omega d\nu X(\nu) \left[\frac{B(\omega + i0^-)}{\omega - \nu + i0^-} + \frac{B(\omega + i0^+)}{\omega - \nu + i0^+} \right] e^{-i\nu t}$$

$$= -\frac{i}{2\pi} \int_{-\infty}^\infty d\nu X(\nu) e^{-i\nu t} Q(\nu) \tag{2.87}$$

Here, we defined

$$Q(\nu) \equiv \frac{1}{\pi} \mathcal{P} \int_{-\infty}^\infty d\omega \frac{B(\omega)}{\omega - \nu}, \tag{2.88}$$

where $\mathcal{P}$ denotes Cauchy principal value of the integral. Thus, we may rewrite the Lamb shift as

$$H_{LS}(t) = \frac{1}{16\pi^2} \int_{-\infty}^\infty d\nu d\xi X(\xi) X(\nu) Q(\nu) e^{-i(\xi+\nu)t} + \text{H.c.}, \tag{2.89}$$

34

and using that $X^\dagger(\nu) = X(-\nu)$ as well as $Q^*(\nu) = Q(-\nu)$ we find

$$H_{LS}(t) = \frac{1}{16\pi^2} \int_{-\infty}^{\infty} d\nu d\xi X(\xi) X(\nu) e^{-i(\xi+\nu)t} \big(Q(\nu) + Q(\xi)\big). \tag{2.90}$$

In the eigenbasis $\{|m\rangle\}$ of H_0, we can rewrite this in the Schrödinger picture as

$$H_{LS} = \frac{1}{4} \sum_{m,l,n} \langle m\,|X|\,l\rangle \langle l\,|X|\,n\rangle \big(Q(E_m - E_l) + Q(E_l - E_n)\big) |m\rangle\langle n|, \tag{2.91}$$

which follows from the fact that

$$X(\xi) = 2\pi \sum_{mn} \delta(\xi - E_m + E_n) \langle m\,|X|\,n\rangle |m\rangle\langle n|. \tag{2.92}$$

This concludes our discussion of the effective Lindbladian. We had to go to some detail to recover this equation for the Lamb shift which is used in Project A. But as the dust settles, let us reflect on what we have learned.

In the preceding two sections we have developed powerful mathematical tools for calculating the dynamics of open quantum systems, when the bath is described by a quadratic Hamiltonian. One only needs to know the bath correlation function $B(\omega)$ to use the techniques. If the system Hamiltonian is zero, Markovian dynamics is captured by the Bloch-Redfield master equation, but when it isn't the master equation doesn't have Lindblad form, implying a risk of model breakdown at late times. This problem can be remedied by using the effective Lindblad approximation, which is less accurate, but whose accuracy, like Bloch-Redfield, is controllable through a parameter that only depends on the details of the environment. Finally, non-Markovian dynamics may sometimes be calculated in the Born approximation by going to Laplace space, although it can be hard to obtain analytical results when doing the inverse Laplace transform.

In the next section we will derive the form of the spectral density when the environment consists of modes in an electric circuit to which the system is capacitively coupled. We will use this result quite extensively, as it is used in Chapter 2 and is central to Chapter 3 and 4.

2.4 Electromagnetic environments

A returning theme in the projects of this thesis will be dealing with the decoherence of Majorana systems who are subjected to the presence of a dissipative electromagnetic environment. Such noise results for instance from fluctuations in electronic components used to tune and manipulate the Majorana experiments. The systems are cooled to a low temperature and electric signals are passed through attenuators to limit the noise, but it is impossible to completely eliminate it. In this section, we assume that the system is capacitively coupled to an electric circuit and derive a relation between the correlation function $B(\omega)$ of the modes in the circuit and the impedance $Z(\omega)$ of the circuit. With that, the techniques of the previous sections can be applied to calculate the decoherence of the system.

Figure 8 shows how we imagine the coupling: A capacitor C is coupled to an environment impedance $Z_{\text{env}}(\omega)$. The electric potential φ over the capacitor fluctuates both due to thermal- and quantum effects. The fluctuation in potential energy then couples to our system, playing the role of Φ in Eq. (2.23). Our method will be useful only when we ignore backaction from the system onto the circuit, meaning that the fluctuations of charge and the electric dipole moment of the system must be significantly smaller than those of the capacitor. If a small external voltage $\delta V(t)$ is applied to the system, we may use linear response theory to relate the retarded current-current correlation function $G_{II}^R(\omega)$ to the total impedance $Z(\omega)$ of the system [16]. The relation is

$$\text{Re}\,\frac{1}{Z(\omega)} = -\frac{1}{\omega}\,\text{Im}\left[G_{II}^R(\omega)\right], \tag{2.93}$$

with

$$G_{II}^R(t,t') = -i\theta(t-t')\,\langle[I(t), I(t')]\rangle. \tag{2.94}$$

The total impedance of the circuit displayed in Figure 8 is

$$Z(\omega) = \frac{1}{\frac{1}{i\omega C} + Z_{\text{env}}(\omega)}. \tag{2.95}$$
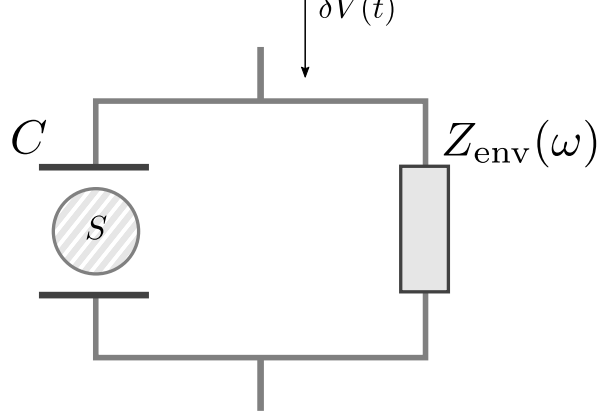
Figure 8: Schematic of the coupling of a system, denoted by S on the figure, to an electromagnetic environment, modeled as an electric circuit. The system is capacitively coupled to a frequency-dependent environment impedance $Z_{\mathrm{env}}(\omega)$. Temperature and quantum fluctuations cause the system to feel a time-dependent potential $\delta V(t)$, which enters the coupling Hamiltonian.

By definition, $\delta V(\omega) = Z(\omega) I(\omega)$, and we have $\delta V(t) = \varphi(t)$, so the retarded potential-potential correlation function $G^R_{\varphi\varphi}(\omega)$ is related to $G^R_{II}(\omega)$ through

$$G^R_{\varphi\varphi}(\omega) = |Z(\omega)|^2 \, G^R_{II}(\omega). \tag{2.96}$$

We can use the fluctuation-dissipation theorem to arrive at an expression for $B(\omega)$. For completeness, we derive the result here, following Ref. [16]. The trick is to write the correlation functions in the Lehmann representation, in terms of the exact eigenstates $|n\rangle$ of H_B. For the thermal Gibbs state $\rho_B = \sum_n e^{-\beta E_n} |n\rangle\langle n| / \mathcal{Z}$, where $\mathcal{Z}$ is the partition function, we have

$$
\begin{aligned}
B(\omega) &= \frac{1}{\mathcal{Z}} \int_{-\infty}^{\infty} dt e^{i\omega t} \sum_n e^{-\beta E_n} \langle n|\Phi(t)\Phi(0)|n\rangle \\
&= \frac{1}{\mathcal{Z}} \int_{-\infty}^{\infty} dt e^{i\omega t} \sum_{nn'} e^{-\beta E_n} |\langle n|\Phi|n'\rangle|^2 \, e^{i(E_n - E_{n'})t} \\
&= \frac{2\pi}{\mathcal{Z}} \sum_{nn'} e^{-\beta E_n} |\langle n|\Phi|n'\rangle|^2 \, \delta(\omega + E_n - E_{n'}).
\end{aligned}
\tag{2.97}
$$

Equivalently, using $\varphi = \Phi/e$, the retarded correlation function is

$$
\begin{aligned}
G^R_{\varphi\varphi}(\omega) &= \int_{-\infty}^{\infty} dt e^{i(\omega + i\eta)t} \left(-i\theta(t) \, \langle [\varphi(t), \varphi(0)] \rangle \right) = -i \int_0^{\infty} dt e^{i(\omega + i\eta)t} \left(\langle \varphi(t)\varphi(0) \rangle - \langle \varphi(0)\varphi(t) \rangle \right) \\
&= -\frac{i}{\mathcal{Z}} \int_0^{\infty} dt e^{i(\omega + i\eta)t} \sum_{nn'} e^{-\beta E_n} |\langle n|\varphi|n'\rangle|^2 \left(e^{i(E_n - E_{n'})t} - e^{-i(E_n - E_{n'})t} \right) \\
&= \frac{1}{e^2 \mathcal{Z}} \sum_{nn'} e^{-\beta E_n} |\langle n|\Phi|n'\rangle|^2 \left(\frac{1}{\omega + E_n - E_{n'} + i\eta} - \frac{1}{\omega - E_n + E_{n'} + i\eta} \right).
\end{aligned}
\tag{2.98}
$$

Using $\frac{1}{x + i\eta} = \mathcal{P}\frac{1}{x} - i\pi\delta(x)$ in the limit $\eta \to 0^+$, we find

$$
\begin{aligned}
\mathrm{Im}\left(G^R_{\varphi\varphi}(\omega) \right) &= -\frac{\pi}{e^2 \mathcal{Z}} \sum_{nn'} e^{-\beta E_n} |\langle n|\Phi|n'\rangle|^2 \left(\delta(\omega + E_n - E_{n'}) - \delta(\omega - E_n + E_{n'}) \right) \\
&= -\frac{1}{2e^2} B(\omega) + \frac{\pi}{e^2 \mathcal{Z}} \sum_{nn'} e^{-\beta(E_n + \omega)} |\langle n|\Phi|n'\rangle|^2 \, \delta(\omega + E_n - E_{n'}) \\
&= \frac{1}{2e^2} \left(e^{-\beta\omega} - 1 \right) B(\omega).
\end{aligned}
\tag{2.99}
$$

Putting everything together, the correlation function is

$$B(\omega) = e^2 \omega \, \text{Re} \left(\frac{1}{Z(\omega)} \right) |Z(\omega)|^2 \left(\coth \left(\frac{\beta \omega}{2} \right) + 1 \right), \qquad (2.100)$$

and using Eq. (2.34), we can read off the spectral density

$$J(\omega) = \frac{1}{\pi} e^2 \omega \, \text{Re} \left(\frac{1}{Z(\omega)} \right) |Z(\omega)|^2. \qquad (2.101)$$

This concludes our discussion of open quantum systems. Before we are ready to get into the projects of the thesis, we need to set the stage for Project D, in which we discuss generalizations of Majoranas. In order to appreciate the choices in the model and how they were motivated, we will need to familiarize ourselves with the simplest generalization of Majoranas, known as parafermions. The next section, therefore, is a discussion of parafermions and in which sense they generalize Majorana.

3 Generalizing Majorana bound states

The Majorana modes that we have dealt with so far, have very rich physics. With their non-abelian braiding statistics, their behaviour is unlike any observed for elementary particles, and the fact that pairs provide non-local fermionic levels, impervious to local interactions, gives rise to promising architectures for quantum computation. Majoranas, however, are in a way the simplest possible example of non-abelian anyons, and one could imagine anyonic systems transforming under more complicated unitary irreducible representations of the braid group. One theoretical example is Fibonacci anyons [73], whose braiding group, contrary to that of Majorana fermions, is complete. For applications in quantum computation, the realization of these complicated anyons would be of immense interest, since all operations could then be carried out in a way that is topologically protected. Experimentally, we are far away from achieving this, but theoretical investigations may eventually help pave the way for new breakthroughs.

In Project D of Chapter 5 the story will depart from the subject of readouts and lifetimes of Majorana architectures, and investigate if new anyons may be theoretically predicted as zero-energy modes in one-dimensional systems akin to the Majorana nanowires. The simplest generalization of Majoranas is called parafermions, and architectures for realizing these have been proposed [18, 53]. Mathematically, parafermions generalize Majoranas in a very intriguing way. As it turns out, Majorana zero-energy modes appear in the context of the Ising model through a bijective mapping, called the Jordan-Wigner transformation. This maps the Ising model onto the celebrated Kitaev chain toy model of spinless fermions jumping on a one-dimensional lattice with superconducting pairing [47]. This model has a phase, corresponding to the ferromagnetically ordered phase on the Ising side, which has one unpaired Majorana mode at each end. The Ising model is symmetric under flipping all spins, and on the fermionic side, this $\mathbb{Z}_2$ symmetry corresponds to fermionic number conservation.

The generalization to parafermions happens, when one considers an Ising-like model, called a clock model, with N states at each site, such that the global symmetry is $\mathbb{Z}_N$ instead. There exists a transformation generalizing the Jordan-Wigner transformation, but now the result is not a fermionic model, but rather a "parafermionic" model, consisting of operators with fractional exchange statistics. The ground states of the new model in a sense consists of fractional fermions, implying that physical realizations of the model have to involve fractionally charged particles in fractional quantum Hall systems. Again, there is a parameter regime where there are edge zero-energy modes, and these are now parafermions. Compared to the Ising model however, more care needs to be taken when classifying these zero energy modes. In particular, when a complex phase is introduced that breaks chiral symmetry, the degeneracy of the ground state may extend into the excited states.

In Chapter 5, we will introduce a model, which we dub the chiral gauge flux ladder, which neatly generalizes the clock model for arbitrary finite non-abelian groups G. By introducing a non-abelian version of Jordan-Wigner transformation we find new zero-energy modes, which are dyonic, meaning that they are characterized by both a group element and an irreducible representation of G. In the language of lattice gauge theory, the anyons are both magnetically and electrically charged.

In this section we will review in some detail the story outlined above for Majoranas and parafermions. It is useful to understand the intricacies in the chiral clock model and the resulting parafermions in order to appreciate the choices made when constructing our chiral gauge flux ladder model. Finally, we will review some of the techniques which will be useful for following the story of the paper.

Though we won't delve deeper into the braiding rules for parafermions and their potential future application in topological quantum computation, it is still useful to get a better grasp on what parafermions physically represent, and which physical quantity their fusion correspond to. The next section is therfore dedicated to defining $\mathbb{Z}_N$ parafermions and unpacking one particular physical realization of them. This particular realization only allows for $\mathbb{Z}_N$ parafermions where $N = 2m$.

3.1 A physical realization of $\mathbb{Z}_{2m}$ parafermions

A major conceptual simplicity with Majoranas lies in the fact that they can be thought of as non-interacting anyons. For a system with two Majorana zero-energy modes, γ_1 and γ_2, the ground states are given by the eigenstates of $P_{12} = i\gamma_1\gamma_2$, which counts the fermionic parity of the fermionic mode shared by the two Marjoranas. The fact that there exists a nice Fock space for the ground states makes it particularly simply to understand their fusion rules and braiding statistics. $\mathbb{Z}_N$ parafermions generalize Majoranas when $N > 2$. Denoting a $\mathbb{Z}_N$ parafermionic operators by α, the generalization lies firstly in

the fact that

$$\alpha^N = 1, \tag{3.1}$$

and secondly that in 1D they obey the commutation relation [6]

$$\alpha(x_1)\alpha(x_2) = e^{i\frac{2\pi}{N}\text{sgn}(x_1-x_2)}\alpha(x_2)\alpha(x_1). \tag{3.2}$$

When $N > 2$, the fact that they don't anticommute indicates that there is no hope for producing them as simple linear combinations of holes and electrons in 1D as we could with Majoranas. Luckily, there exists a fairly simple physical model, proposed by Clarke, Alicea and Shtengel in 2012 [18], which gives a good intuition for the differences between parafermionic- and Majorana zero-energy bound states. The basic intuition is to use the edge states of a fractional quantum hall system with filling factor $\nu = 1/m$, and have m be an odd integer. These states are gapless modes which inherently have the pairwise commutation relation of (3.2) [34], and they are described by creation operators ψ_{edge} obeying the commutation relation

$$\psi_{\text{edge}}(x_1)\psi_{\text{edge}}(x_2) = e^{i\frac{\pi}{m}\text{sgn}(x_1-x_2)}\psi_{\text{edge}}(x_2)\psi_{\text{edge}}(x_1). \tag{3.3}$$

Then similar ingredients to what we saw in the construction of the Majorana nanowire in Section 1.3 are added. Figure 9 is adapted from Clarke *et al.* [18], and shows their proposed setup: Two fractional quantum Hall systems are connected resulting in counter propagating modes at their interface. The two systems have opposite g-factors, so the spins of the edge currents are opposite. This allows an ordinary s-wave superconductor at the interface, shown in green in the figure, to pair the electronic part of one mode with the hole part of the other, allowing for bound states near the boundary. Insulating regions, shown on the figure in blue, can be introduced for example by engineering a strong spin-orbit coupling perpendicular to the magnetic field, since this causes back scattering between the two edge modes. Zero-energy modes α may then appear in very short trenches between superconducting and insulating regions, as indicated on Figure 9, panel b). In the analogy with the Majorana nanowires, the backscattering here plays the same role here as the Zeeman coupling did then, and will ensure that only a single zero-energy mode exists in the trench. In order to have a pair of parafermionic zero energy modes, we could then imagine having either a case as on Figure 9, with two insulating regions flanking a central superconducting region, or interchanging the superconducting and insulating regions. In the former case the ground states will have a bound fractional charge in the central island, and in the latter the central island instead has a bound fractional spin. For concreteness, we consider the former setup with the superconductor in the middle. The following discussion is directly adapted from Clarke *et al.* [18].

The gapless edge modes allow for a useful bosonized representation. The creation operator $\psi^\dagger_{\text{edge},R/L}(x)$ for a right/left-moving edge mode at position x may be written as [34]

$$\psi^\dagger_{\text{edge},R/L}(x) \propto e^{im\Phi_{R/L}(x)}. \tag{3.4}$$

The fields $\Phi_{R/L}(x)$ are not bosonic, but rather satisfy the so-called Kac-Moody commutation relations [28]

$$[\Phi_R(x), \Phi_R(x')] = -[\Phi_L(x), \Phi_L(x')] = i\frac{\pi}{m}\text{sgn}(x - x'), \tag{3.5a}$$

$$[\Phi_L(x), \Phi_R(x')] = i\frac{\pi}{m}, \tag{3.5b}$$

and they are related to the densities $\rho_{R/L}(x)$ of the corresponding edge modes through

$$\rho_{R/L}(x) = \pm\frac{1}{\pi}\frac{d}{dx}\Phi_{R/L}(x). \tag{3.6}$$

The fields $\Phi_{R/L}(x)$ may be rewritten in terms of new fields, $\varphi(x)$ and $\theta(x)$ in the following way

$$\Phi_{R/L}(x) = \varphi(x) \pm \theta(x), \tag{3.7}$$

and from the Kac-Moody commutation relations, $\varphi(x)$ and $\theta(x)$ inherit the commutation relations

$$[\varphi(x), \theta(x')] = i\frac{\pi}{m}\Theta(x - x'), \tag{3.8}$$
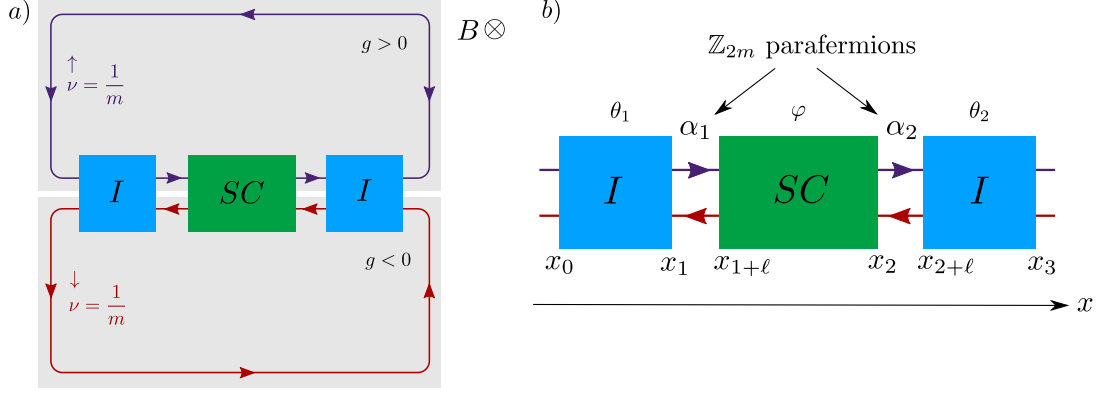
39

Figure 9: Proposal for an experiment featuring parafermions, adapted from Clarke *et al.* [18]. Panel *a*) shows two fractional quantum Hall systems, driven to a filling factor $\nu = 1/m$ by a magnetic field B. The two systems have opposite sign of the *g*-factor, which means that the resulting edge currents have opposite spin. The two systems are connected, resulting in counter propagating modes. These modes are alternately gapped out in insulating regions shown in blue, resulting for instance from a large spin-orbit interaction, and subjected to an *s*-wave superconductive pairing in the green regions. Panel *b*) shows the emergent $\mathbb{Z}_{2m}$ parafermionic zero-energy modes α_1 and α_2, which appear in the junctions between the superconducting and insulating regions. In terms of the bosonized fields, the insulating regions pin $\theta_i = \pi n_\theta^{(i)}/m$ while the superconducting region in the middle pins $\varphi = \pi n_\varphi/m$, where $n_\theta^{(i)}$ and n_φ are integers.

where $\Theta(x)$ is the Heaviside step function, while φ and θ commute

$$[\varphi(x), \varphi(x')] = [\theta(x), \theta(x')] = 0. \tag{3.9}$$

The derivatives of the new fields have a nice physical interpretation based Eq. (3.6) in terms of the total charge- and spin density $\rho(x)$ and $s(x)$ (note, since the counter propagating modes have different spin, $s(x)$ is also equal to the current density):

$$s(x) = j(x) = \rho_R(x) - \rho_L(x) = \frac{1}{\pi}\frac{d}{dx}\varphi(x), \tag{3.10}$$

$$\rho(x) = \rho_R(x) + \rho_L(x) = \frac{1}{\pi}\frac{d}{dx}\theta(x). \tag{3.11}$$

In the absence of superconducting or insulating regions, the gapless modes are describable by a Hamiltonian quadratic in the current- and charge densities [34]:

$$H_0 = \frac{mv}{2\pi}\int dx \left[\left(\frac{d}{dx}\varphi(x)\right)^2 + \left(\frac{d}{dx}\theta(x)\right)^2\right]. \tag{3.12}$$

Using the coordinates in Figure 9*b*), the superconducting region $x \in X_{\mathrm{SC}} = [x_1 + l, x_2]$ is governed by the Hamiltonian

$$H_{\mathrm{SC}} = \Delta \int_{X_{\mathrm{SC}}} dx\ \psi_{\mathrm{edge},R}(x)\psi_{\mathrm{edge},L}(x) + \mathrm{H.c.}$$

$$\propto -\Delta \int_{X_{\mathrm{SC}}} dx \cos(2m\varphi), \tag{3.13}$$

and the two insulating regions $x \in X_{\mathrm{I}}^{(1)} = [x_0, x_1]$ and $x \in X_{\mathrm{I}}^{(2)} = [x_2 + l, x_3]$ are governed by a Hamiltonian H_{I} given by

$$H_{\mathrm{I}} = M \sum_{i=1,2}\int_{X_{\mathrm{I}}^{(i)}} dx \sum_{j=R,L} \psi_{\mathrm{edge},j}^\dagger(x)\psi_{\mathrm{edge},j}(x) + \mathrm{H.c.}$$

$$\propto -M \sum_{i=1,2}\int_{X_{\mathrm{I}}^{(i)}} dx \cos(2m\theta). \tag{3.14}$$

40

We assume that Δ and M dominate in the regions where they appear. The point with the whole bosonization procedure is that the effect of the interactions is then very simple. In superconducting regions $x \in X_{\mathrm{SC}}$, φ gets pinned to the values

$$\varphi = \frac{\pi}{m} n_\varphi, \tag{3.15}$$

where n_φ is an integer valued operator. Conversely, in insulating regions $x \in X_{\mathrm{I}}^{(i)}$, θ gets pinned to values

$$\theta = \frac{\pi}{m} n_\theta^{(i)}, \tag{3.16}$$

where again the operator $n_\theta^{(i)}$ has integer eigenvalues. Thus the effective Hamiltonian describing the setup is simply

$$H_{\mathrm{eff}} = \sum_{i=1,2} H_{\mathrm{eff},i} \tag{3.17}$$

$$H_{\mathrm{eff},i} = \frac{mv}{2\pi} \int_{x_i}^{x_i+\ell} dx \left[\left(\frac{d}{dx} \varphi(x) \right)^2 + \left(\frac{d}{dx} \theta(x) \right)^2 \right], \tag{3.18}$$

subject to the boundary conditions set by $n_\theta^{(i)}$ and n_φ. Clarke *et al.* demonstrated that the effective Hamiltonian $H_{\mathrm{eff},i}$ in (3.18) has an exact zero-energy mode α_i. When ℓ is short compared to the coherence length of the induced superconducting pairing, the mode is simply equal to

$$\alpha_i \propto e^{i \frac{\pi}{m} \left(n_\theta^{(i)} + n_\varphi \right)}. \tag{3.19}$$

The pair α_1 and α_2 are $\mathbb{Z}_N$ parafermions with $N = 2m$, satisfying the defining relations Eq. (3.1) and (3.2). This may be verified by using

$$[n_\theta^{(1)}, n_\varphi] = -i \frac{m}{\pi}, \qquad [n_\varphi, n_\theta^{(2)}] = 0, \tag{3.20}$$

which follows directly from (3.8) and (3.9). Just like the case with Majorana zero-energy modes, the ground states of the system are given by eigenstates of the product of the two parafermions

$$P_{12} = \alpha_1^\dagger \alpha_2 = e^{-i \frac{\pi}{m} \left(n_\theta^{(1)} - n_\theta^{(2)} + \frac{1}{2} \right)}, \tag{3.21}$$

which follows by using the Baker-Cambell-Hausdorff formula. Hence, the ground state is $N = 2m$ fold degenerate. Labeling the ground states by $|n\rangle$ such that $P_{12}|n\rangle = e^{i(n-1/2)\pi/m}|n\rangle$, we may examine the effect of α_i on them by using the Baker-Cambell-Hausdorff formula twice to see that

$$\begin{aligned} P_{12} e^{-i \frac{\pi}{m} n_\varphi} |n\rangle &= e^{i \frac{\pi}{m} \left(n_\theta^{(1)} - n_\theta^{(2)} - \frac{1}{2} \right)} e^{-i \frac{\pi}{m} n_\varphi} |n\rangle \\ &= e^{i \frac{\pi}{m} \left(n_\theta^{(1)} - n_\theta^{(2)} - n_\varphi - \frac{1}{2} \right) + i \frac{\pi}{2m}} |n\rangle \\ &= e^{i \frac{\pi}{m}} e^{-i \frac{\pi}{m} n_\varphi} P_{12} |n\rangle \\ &= e^{i(n+1/2)\pi/m} e^{-i \frac{\pi}{m} n_\varphi} |n\rangle, \end{aligned} \tag{3.22}$$

which implies

$$e^{-i \frac{\pi}{m} n_\varphi} |n\rangle = |n + 1 \bmod 2m\rangle. \tag{3.23}$$

Since $\alpha_i^\dagger \sim e^{-i \frac{\pi}{m} n_\varphi}$, we see that the zero-energy modes, just like in the case of Majoranas, cycle through the ground states. Because of the relation (3.11), the total charge q between the insulating islands is

$$q = e \int_{x_1}^{x_2+\ell} dx \rho(x) = \frac{e}{m} \left(n_\theta^{(2)} - n_\theta^{(1)} \right). \tag{3.24}$$

This means that in a fusion experiment, where the two parafermions α_1 and α_2 are made to interact with each other (possibly through a dot like in the Majorana readouts), if the state $|n\rangle$ is measured, a

fractional charge $q = \frac{e}{m} n$ is trapped in the superconducting island

If the insulating and superconducting regions were swapped, then the analysis would follow in exactly the same way, but φ and θ would swap roles, and from (3.10), one would find instead that the middle insulating region traps a fractional spin. It should be pointed out that the expression for the parafermionic zero-energy modes in Eq. (3.19) is not exact for finite ℓ. Here, there are contributions from quasiparticles with an energy gap $\sim 1/\ell$. Thus it is only in the limit $\ell \to 0$ that the zero-energy mode exactly commutes with the effective Hamiltonian.

Now that we have a bit of a physical feeling about parafermions, we will now depart from physical descriptions and work towards the chiral clock model mentioned in the preceding section. Before we get there, we should first define a few key concepts that will be important for generalizing the clock model.

3.2 About topological order and zero-energy modes

The ground state manifold in both the Majorana nanowires and in the parafermionic system described in the previous section are topologically ordered. We adopt the definition of topological order provided by Alexandradinata *et al.* [5]. In Chapter 5 the precise definition will be provided, so for now it will suffice to state intuitively what topological order means in the context of Majorana or parafermionic zero-energy modes. In both cases, the system has a global symmetry $\mathcal{Q}$ as well as the boundary zero-energy modes α_1 and α_2 at the left- and right boundary, respectively. It is simplest to phrase what topological order entails in the case of Majoranas. Here, the superconducting pairing means that the number of electrons is not preserved, but fluctuates modulo 2. The global symmetry $\mathcal{Q} = (-1)^{N_f}$ measures the fermionic parity, and the two edge zero-energy modes cycle between even and odd fermionic parity. In the ground states, the total fermionic parity is given just by the occupancy of the zero-energy fermionic mode, so $\mathcal{Q} = i\gamma_1\gamma_2$. This operator is non-local, meaning that is not expressible in terms of any local operators. In fact, no local observable can distinguish the ground states. This important property is called *local indistinguishability*. Furthermore, operators with support only in the bulk do not cause transitions between the ground states (but they may cause transitions to excited states). These two properties are taken as the definition of topologically ordered ground states in 1D systems: i) transitions between ground states are only caused close to the boundary, and ii) the ground states are locally indistinguishable.

The definition of topological order is intimately tied to the notion of locality. A Hamiltonian obeying the above two conditions has a ground state degeneracy which is protected under local perturbations when they do not close the gap to the excited states. If the gap closes, then operators in the bulk can cause transitions between the ground states. In this way, the definition is compatible with the discussion about symmetry-protected topological phases in Section 1: No continuous deformations preserving the energy gap and respecting the symmetry (in Majorana systems the symmetry being fermionic parity conservation) can remove the feature. For interacting systems, the support of operators, as measured with respect to the non-interacting system's modes, will tend to extend. For this reason the definition of topological order should be refined with the notion of *quasi-local* operators, whose support exponentially decays with some characteristic length scale much smaller than the system size.

For the parafermions, the story is very similar, except the global symmetry $\mathcal{Q}$ is now the fractional $\mathbb{Z}_N$ charge (or spin), which, as we saw in the previous section, is distinguished by the operator $\mathcal{Q} = P_{12}$. Note that for the parafermions, P_{12} is not Hermitian, but its eigenvectors are still orthogonal. We know from the preceding section that P_{12} is diagonalizable and that the eigenvalues have the form $e^{i2\pi n/N}$. It will be useful for later to note, that this follows directly from the identity

$$P_{12}^N = \mathbb{1}, \tag{3.25}$$

which immediately gives that P_{12} is diagonalizable and unitary. Denoting again the eigenvector of P_{12} with the eigenvalue $e^{i2\pi(n-1/2)/N}$ by $|n\rangle$, then consequently

$$\langle n'|n\rangle = e^{-i\frac{2\pi(n-1/2)}{N}} \langle n'|P_{12}|n\rangle = e^{i\frac{2\pi(n'-n)}{N}} \langle n'|n\rangle, \tag{3.26}$$

so when $n' \neq n \bmod N$, then $\langle n'|n\rangle = 0$. Importantly, this confirms that the N degenerate ground states may indeed be found as orthogonal eigenvectors of P_{12}.

So far we have relied on the intuition from Majorana bound states when discussing zero-energy modes. These have been taken as operators γ, exponentially localized near the boundaries, which in

second quantization translates to

$$[\gamma, H] \propto e^{-\xi_M/L}, \qquad (-1)^{N_f}\gamma = -\gamma(-1)^{N_f}, \tag{3.27}$$

where ξ_M is the Majorana coherence length. In his seminal paper, Fendley extended this to the case of parafermionic modes α with the symmetry $\mathcal{Q}$ given by the $\mathbb{Z}_N$ charges, also localized near the boundary. These modes satisfy [25]

$$[\alpha, H] \propto e^{-\xi_{pf}/L}, \qquad \mathcal{Q}\alpha = e^{i\frac{2\pi}{N}}\alpha\mathcal{Q}, \tag{3.28}$$

where ξ_{pf} is the parafermion coherence length. But since our definition of topological order only involves the ground state, the definition in (3.28) is stronger than needed, as it implies that the degeneracies also hold for all the excited states. Zero-modes satisfying (3.28) are therefore said to be *strong zero-energy modes*. If the condition is relaxed instead, so α only commutes with H projected onto the ground state manifold, then α is said to be a *weak zero-energy mode* [6], and the effect is that some of the excited states (usually all excited states with an energy above some threshold) have an energy splitting decaying polynomially in the system size.

When we generalize $\mathbb{Z}_N$ to a general finite group G, the condition of having strong zero-energy modes will turn out to be so restrictive, that it seemingly almost never happens. But we will find an extended regime with weak zero-energy modes.

3.3 The Jordan-Wigner transformation: A map from bosons to anyons

Now that we have a firmer grasp on when ground states are topologically ordered, let us turn to the proposition from the beginning of the section, that there should be a connection between $\mathbb{Z}_N$ parafermions and bosonic lattice models with global $\mathbb{Z}_N$ symmetry. We start by making some observations regarding the simpler case of Majorana modes.

In 1-dimensional systems with a pair of Majorana zero-energy modes, there is a global $\mathbb{Z}_2$ symmetry, counting the total number of fermions modulo 2, and we have the edge modes that cycle through the ground states. Another model with very similar characteristics is the Ising model, consisting of L sites with a $\mathbb{Z}_2$ degree of freedom at each site. The Ising model Hamiltonian is

$$H_{\text{IM}} = -J\sum_{i=1}^{L} \sigma_i^z \sigma_{i+1}^z - \mu\sum_i \sigma_i^x. \tag{3.29}$$

In the ordered ferromagnetic regime $J > 0$ and $|\mu| \ll J$ and in the thermodynamic limit, the ground states consist of all sites having spin up $|\uparrow\rangle_1|\uparrow\rangle_2\ldots$ or down $|\downarrow\rangle_1|\downarrow\rangle_2\ldots$, while for finite size systems, the ground states are the symmetric or antisymmetric combination of the two. The ground state may distinguished by any σ_j^z operator, in particular those at the edges. In this model, there is no local operator that can switch between the ground states, a fact that leads to exponentially small splitting of the ground state energies in the system size. Perturbation theory shows that the splitting $\Delta E_0 \sim (\mu/J)^L$. The Ising model, like the Majorana system, has a global $\mathbb{Z}_2$ symmetry, generated by the operator $\mathcal{Q} = \prod_i \sigma_i^x$ which flips all spins. Though the two models at first glance have nothing to do with one another, the similarities between them is not coincidental. There exists a bijective non-local mapping, called the Jordan-Wigner transformation [6], which maps the Ising model to the Kitaev chain toy model, which for low-energies is nothing else than the 1D p-wave superconducting Hamiltonian in Eq. (1.39) that we studied in Section 1. Throughout this section we will refer to a "bosonic" and "anyonic" side. For the Ising model, the bosonic side is the one in Eq. (3.29), where the operators and states are bosonic spins. The "anyonic", or "Majorana side", is the Kitaev model considered after the Jordan-Wigner transformation. The transformation consists of defining [25]

$$a_i = \left(\prod_{j=1}^{i-1} \sigma_j^x\right)\sigma_i^z, \tag{3.30a}$$

$$b_i = -i\left(\prod_{j=1}^{i} \sigma_j^x\right)\sigma_i^z, \tag{3.30b}$$

which are Majorana operators since $\{a_i, a_j\} = \{b_i, b_j\} = 2\delta_{ij}$ and $\{a_i, b_j\} = 0$. Using Eqs. (3.30), we may write the Ising Hamiltonian from Eq. (3.29) as

$$H_{\mathrm{IM}} = iJ \sum_{i=1}^{L-1} b_i a_{i+1} + i\mu \sum_{i=1}^{L} a_i b_i. \tag{3.31}$$

If we define fermionic annihilation operators $c_i = (a_i + ib_i)$ we can equivalently write it up to a constant as

$$H_{\mathrm{IM}} = 2\mu \sum_i c_i^\dagger c_i - \left[J \sum_i \left(c_i^\dagger c_{i+1} + c_i^\dagger c_{i+1}^\dagger \right) + \mathrm{H.c.} \right], \tag{3.32}$$

which is a model of spinless fermions jumping on a chain with superconducting pairing. If we instate a lattice spacing a, then lattice Fourier transformation gives

$$H_{\mathrm{IM}} = -2 \sum_k \left(J\cos(ak) - \mu \right) c_k^\dagger c_k - J \sum_k \left[i\sin(ak) c_k^\dagger c_{-k}^\dagger + \mathrm{H.c.} \right]. \tag{3.33}$$

This Hamiltonian may be made real by a gauge transformation, and if we consider just the low energy subspace with $k \ll a$, then it becomes

$$H_{\mathrm{IM,eff}} = \sum_k \left[\left(\frac{Ja^2 k^2}{2} - (J-\mu) \right) c_k^\dagger c_k + aJk c_k^\dagger c_{-k}^\dagger \right] + \mathrm{H.c.}, \tag{3.34}$$

which is, as advertised, the Hamiltonian for a p-wave superconductor with mass $1/Ja^2$, chemical potential $J - \mu$ and superconducting pairing aJ. From the discussion of Section 1 we thus expect the model to have Majorana zero-energy modes whenever $J > \mu$. In terms of the Majoranas, the global symmetry $\mathcal{Q}$ becomes

$$\mathcal{Q} = \prod_j (-ia_j b_j), \tag{3.35}$$

so on the Majorana side, $\mathcal{Q} = (-1)^{N_f}$ measures the fermionic parity, as expected. When $\mu = 0$, a_1 and b_L are strong zero-energy modes, since they commute with H_{IM}, and they distinguish the fermionic parity. If Π_{GS} is the projector on the ground state space, then we see that the symmetry operator on the ground state space concerns only the edge modes:

$$\Pi_{\mathrm{GS}} \mathcal{Q} \, \Pi_{\mathrm{GS}} = -ia_1 b_L. \tag{3.36}$$

When a small μ is introduced, these expressions don't hold anymore, since the zero-energy modes become perturbed. They remain strong, and the perturbed zero-energy modes can be constructed using an iterative procedure. For ease of notation let H_J and H_μ be the first and second term in (3.29), respectively. Roughly, the construction of the left strong zero mode Γ goes like this: First we define $\Gamma^{(0)} = a_1$, which satisfies

$$[H, \Gamma^{(0)}] = [H_\mu, \Gamma^{(0)}] = -2i\mu b_1. \tag{3.37}$$

By choosing $\Gamma^{(1)}$ such that $[H_J, \Gamma^{(1)}] = 2i\mu b_1$, we then have that

$$[H, \Gamma^{(0)} + \Gamma^{(1)}] = [H_\mu, \Gamma^{(1)}] \propto \frac{\mu}{J}\mu. \tag{3.38}$$

$\Gamma = \sum_{i=0}^{L} \Gamma^{(i)}$ is then iteratively constructed by demanding $[H_J, \Gamma^{(i+1)}] = -[H_\mu, \Gamma^{(i)}]$. If this construction is well-defined, then

$$[H, \Gamma] = [H_\mu, \Gamma^{(L)}] \sim \left(\frac{\mu}{J} \right)^L \mu, \tag{3.39}$$

which proves the exponential localization of Γ. Note that to all iteration levels i, $\Gamma^{(i)}$ changes the total fermionic parity. This follows from the fact that $\Gamma^{(i)}$ will always be odd in a_i and b_i operators.

Let us take a step back and review what has happened. Through a non-local mapping, the bosonic operators in the Ising model have been mapped onto Majorana fermionic operators. The Hamiltonian is local both on the bosonic side, where locality is measured by operators being formed of local products of σ^z and σ^x, and on the Majorana fermionic side, where locality is measured by operators being formed by

local products of the Majorana operators a_i and b_i. Let us take a look at the roles of the global symmetry $\mathcal{Q}$ and the edge modes on the Ising- and Majorana side. On both sides, $\mathcal{Q}$ is a non-local operator related to the global $\mathbb{Z}_2$ symmetry. On the bosonic side in the ordered phase, it cycles between the ground states in the basis of eigenstates of σ_z, and on the Majorana side, it distinguishes the ground states' fermionic parity. Also, in the ordered phase, for simplicity when $\mu = 0$, the ground state is distinguished by any operator σ_i^z. On the Majorana side, these operators cycle between the ground states by switching the fermionic parity, but only the edge operators σ_1^z and σ_L^z may be written as local combinations of the Majorana operators.

The simplest generalization of the above discussion comes when the group $\mathbb{Z}_2$ is changed to $\mathbb{Z}_N$. This suggests that we should be able to repeat the above procedure starting now from an Ising-like model where the local $\mathbb{Z}_2$ degrees of freedom are replaced with $\mathbb{Z}_N$. This is done by labeling the states $|n\rangle$, for $n \in \{0, \ldots, N-1\}$. In place of σ^z and σ^x, we take the operators σ and τ, defined by their action on the basis states:

$$\sigma|n\rangle = \omega^n |n\rangle, \qquad \omega = e^{i\frac{2\pi}{N}}, \tag{3.40}$$

$$\tau|n\rangle = |n+1 \bmod N\rangle, \tag{3.41}$$

implying the commutation relations $\sigma\tau = \omega\tau\sigma$. The Ising model is then generalized to what is called the $\mathbb{Z}_N$ chiral clock Potts model, whose Hamiltonian is[7]

$$H_{\text{Potts}} = -J \sum_{i=1}^{L} (e^{i\phi}\sigma_i^\dagger \sigma_{i+1} + e^{-i\phi}\sigma_i \sigma_{i+1}^\dagger) - \mu \sum_{n=1}^{N-1}\sum_{i=1}^{L} \tau_i^n \tag{3.42}$$

This Hamiltonian has a global $\mathbb{Z}_N$ symmetry given by $\mathcal{Q} = \prod_i \tau_i$, which winds all the states once. For simplicity, let us take $J, \mu \geq 0$. In analogy to the Ising case described above, this model can be mapped to another local model through a Jordan-Wigner-like transformation, first introduced by Fradkin and Kadanoff [30], and here the resulting degrees of freedom will be parafermionic. The phase ϕ will turn out to be important for the nature of the zero-energy modes. Let us first study the ordered case $\mu = 0$. On states $|m\rangle_i|n\rangle_{i+1}$, the first term in (3.42) gives

$$-J\left(e^{i\phi}\sigma_i^\dagger \sigma_{i+1} + e^{-i\phi}\sigma_i \sigma_{i+1}^\dagger\right)|m\rangle_i|n\rangle_{i+1} = -2J\cos\left(\frac{2\pi}{N}(m-n) - \phi\right)|m\rangle_i|n\rangle_{i+1}. \tag{3.43}$$

When $\phi = 0$, then the ground state is "ferromagnetic" as it consists simply of the N states $\prod_{i=1}^{L} |m\rangle_i$ which spontaneously break the global $\mathbb{Z}_N$ symmetry. When ϕ is non-zero, the system is chiral, meaning that it breaks spatial inversion symmetry. For example, if $\phi = \frac{2\pi}{N}$ the ground states are "anti-ferromagnetic", and in fact helical, as they wind with a relative phase of ϕ down the length of the system. So ϕ allows for continuous deformation between the ferromagnetically and anti-ferromagnetically ordered ground states. The role of ϕ for retaining the N-fold ground state degeneracy into the excited states is simply understood when picturing excitations as domain walls [6]. The first excited states have form $|\ldots aaabbb\ldots\rangle$. When $\phi = 0$ these states are all degenerate, and by application of the μ term, the kink may be moved down to the boundary $|\ldots aaab\rangle$, where it can change into a different kink type $|\ldots aaac\rangle$, and eventually be moved back to the initial location $|\ldots aaaccc\ldots\rangle$. The coupling between the states within the degenerate subspace leads to a power law splitting (transitions occur already to first order in the degenerate perturbation theory), but when ϕ gets switched on, the different kink types have different energy, which leads instead to a splitting exponentially suppressed in the system size [43]. Since the degeneracy is lost for $\phi = 0$, the zero-energy modes cannot be strong.

The Jordan-Wigner transformation for the chiral clock model is very similar to the one for the Ising

---

[7]Fendley writes the Hamiltonian more generally, namely as [25]

$$H_{\text{Potts}} = -J\sum_{i=1}^{L}\sum_{m=1}^{N-1} C_m(\sigma_i^\dagger \sigma_{i+1})^m - \mu\sum_{i=1}^{L}\sum_{m=1}^{N-1} D_m\tau_i^m,$$

but for the purpose of this discussion, we don't need the full generality.

model. It consists of defining

$$\alpha_i = \left(\prod_{j=1}^{i-1} \tau_j\right) \sigma_i, \tag{3.44}$$

$$\beta_i = \omega^{(N+1)/2} \left(\prod_{j=1}^{i} \tau_j\right) \sigma_i, \tag{3.45}$$

which are parafermions, obeying for $i \neq j$

$$\alpha_i \beta_j = \omega^{\text{sgn}(j-i)} \beta_j \alpha_i, \quad \alpha_i \alpha_j = \omega^{\text{sgn}(j-i)} \alpha_j \alpha_i, \quad \beta_i \beta_j = \omega^{\text{sgn}(j-i)} \beta_j \beta_i, \tag{3.46}$$

while $\alpha_i \beta_i = \omega \beta_i \alpha_i$, so the β_i behaves as a parafermion located at a later site than α_i. On the parafermionic side, the Hamiltonian becomes [25]

$$H_{\text{Potts}} = -J \sum_{i=1}^{L-1} \left[e^{i\phi} \omega^{(1-N)/2} \beta_i^{N-1} \alpha_{i+1} + e^{-i\phi} \omega^{(1-N)/2} \beta_i \alpha_{i+1}^{N-1} \right] - \mu \sum_{i=1}^{L} \sum_{m=1}^{N-1} \omega^{(m-N)m/2} \alpha_i^{N-m} \beta_i^m. \tag{3.47}$$

The funny looking factors of ω are needed to make sure that the Hamiltonian is Hermitian. Again, when $\mu = 0$, the system has strong zero-energy modes α_1 and β_L. Analogously to the Majorana case, the symmetry operator may be written $\mathcal{Q} = \prod_i \omega^{(1-N)/2} \alpha_i^\dagger \beta_i$, and on the ground state space

$$\Pi_{\text{GS}} \mathcal{Q} \, \Pi_{\text{GS}} = \omega^{(1-N)/2} \alpha_1^\dagger \beta_L, \tag{3.48}$$

so drawing on the physical discussion of Section 3.1, the symmetry operator distinguishes the fractional charge or spin of the ground states on the parafermionic side. Through an iterative construction, a strong zero-energy mode may be defined for $\mu > 0$, but as Fendley showed [25], the first correction now scales as $\mu/2J \sin(N\phi)$. Thus the zero-energy mode cannot be strong whenever $\phi = \pi n$ for integer n. But otherwise the procedure can be formally carried out. The radius of convergence of the series $\Gamma = \sum_i \Gamma^{(i)}$ is ϕ-dependent and was later numerically studied by Moran *et al.* [57]. They found that resonances could emerge between excited states when $\phi \neq \pi n$, turning the zero-energy modes into weak modes, although only potentially at very high energies. Moran *et al.* show that such resonances always happen when N is not a prime number, except at special "anti-resonant" points. For prime N the resonances occur only at isolated values of ϕ, but in the thermodynamic limit the resonance points of ϕ become dense. This underlines that strong zero-energy modes are exceptionally hard to procure for more complicated anyonic systems than Majoranas.

That the weak zero-energy modes survive for $\mu > 0$ and finite ϕ was shown by Alexandradinata *et al.* [5] by using the technique of quasi-adiabatic continuation, first introduced by Hastings *et al.* [37]. The idea is to construct an operator $\mathcal{V}(\mu)$ that commutes with $\mathcal{Q}$, preserves quasi-locality and maps the ground states $|\psi_0(0)\rangle$ of $H(\mu = 0)$ to the ground states $|\psi_0(\mu)\rangle$ of $H(\mu)$. The projector $\Pi_{\text{GS}}(\mu)$ onto the ground states for finite μ is then simply related to projector $\Pi_{\text{GS}}(\mu = 0)$ by

$$\Pi_{\text{GS}}(\mu) = \mathcal{V}^\dagger(\mu) \Pi_{\text{GS}}(\mu = 0) \mathcal{V}(\mu). \tag{3.49}$$

For Eq. (3.49) to make sense, the gap $\Delta(\mu')$ of $H(\mu')$ needs to be non-zero for all $\mu' \in [0, \mu]$. Otherwise, it is not guaranteed that $\Pi_{\text{GS}}(\mu)$ projects on the ground state manifold of $H(\mu)$. The fundamental idea is that all quasi-local operators that commute with $\mathcal{Q}$ must obey

$$\Pi_{\text{GS}}(\mu = 0) \mathcal{O} \Pi_{\text{GS}}(\mu = 0) = c(\mathcal{O}) \Pi_{\text{GS}}(\mu = 0), \tag{3.50}$$

for some complex number $c(\mathcal{O})$. If $\mathcal{V}(\mu)$ satisfies (3.49), preserves quasi-locality and commutes with $\mathcal{Q}$, then $\mathcal{V}^\dagger(\mu) \alpha \mathcal{V}(\mu)$ and $\mathcal{V}^\dagger(\mu) \beta \mathcal{V}(\mu)$ are weak zero-energy modes of $H(\mu)$, since for instance

$$
\begin{aligned}
[\mathcal{V}^\dagger(\mu) \alpha \mathcal{V}(\mu), \Pi_{\text{GS}}(\mu) H(\mu) \Pi_{\text{GS}}(\mu)] &= \mathcal{V}^\dagger(\mu) [\alpha_1, \Pi_{\text{GS}}(\mu = 0) \mathcal{V}(\mu) H(\mu) \mathcal{V}^\dagger(\mu) \Pi_{\text{GS}}(\mu = 0)] \mathcal{V}(\mu) \\
&= c\left(\mathcal{V}(\mu) H(\mu) \mathcal{V}^\dagger(\mu)\right) \mathcal{V}^\dagger(\mu) [\alpha_1, \Pi_{\text{GS}}(\mu = 0)] \mathcal{V}(\mu) \\
&= 0,
\end{aligned} \tag{3.51}
$$

where we used Eq. (3.50) in the second line, and the fact that α_1 permutes the unperturbed ground states in the last. $\mathcal{V}(\mu)$ takes the explicit form [38]

$$\mathcal{V}(\mu) = \mathcal{T}_\mu \exp\left(i \int_0^\mu d\mu' \mathcal{D}(\mu')\right), \tag{3.52}$$

where $\mathcal{T}$ is the path-ordering operator of μ, and the generator is

$$\mathcal{D}(\mu) = -i \int_{-\infty}^{\infty} dt F(\Delta(\mu)t) e^{iH(\mu)t} \left(\partial_\mu H(\mu)\right) e^{-iH(\mu)t}, \tag{3.53}$$

for a suitable even filter function $F(t)$, whose Fourier transform obeys $F(\omega = 0) = 1$. The purpose of the filter function is to cut off the time evolution of $\partial_\mu H(\mu)$ for large $|t|$. As shown by Hastings [38], this operator preserves quasi-locality, and furthermore, he proves the following bound using linear perturbation theory[8]:

$$\left|\partial_\mu|\psi_0(\mu)\rangle - i\mathcal{D}(\mu)|\psi_0(\mu)\rangle\right| \leq C(\mu) \left|\left|\partial_\mu H(\mu)\right|\right|, \tag{3.54}$$

for a suitable function $C(\mu)$, which depends on the filter function and the gap $\Delta(\mu)$. Eq. (3.54) then gives in the adiabatic regime the relation $\mathcal{V}(\mu)|\psi(0)\rangle = |\psi(\mu)\rangle$. Lastly, the quasi-adiabatic continuation $\mathcal{V}(\mu)$ preserves the symmetry by $\mathcal{Q}$, as can be straightforwardly checked.

3.4 Towards general groups

In the previous sections, we studied in detail how parafermions mathematically (and physically) are generalizations of Majorana fermions. In Chapter 5 we will generalize this further by upgrading the $\mathbb{Z}_N$ symmetry to one generated by a finite non-abelian group G. To do this, we employ a Hilbert space which is particularly suited for the task by considering a basis of states $|g\rangle$ labeled by group elements g of G, and unitary operators θ_h and $\tilde{\theta}_h$ corresponding respectively to left- and right multiplication of h:

$$\theta_h|g\rangle = |hg\rangle, \tag{3.55}$$

$$\tilde{\theta}_h|g\rangle = |gh\rangle. \tag{3.56}$$

These operators generalize the σ^x from the Ising model, as it generates transitions between the states. In order to generalize the operator σ^z we use the representation operators U_{mn}^F defined by

$$U_{mn}|g\rangle = D_{mn}^F(g)|g\rangle, \tag{3.57}$$

where $D^F(g)$ is the matrix representation of g in the irreducible representation F. Occasionally we will use the representation basis, defined by

$$|Jmn\rangle = \sqrt{\frac{\dim J}{|G|}} \sum_{g \in G} D_{mn}^J(g)|g\rangle \tag{3.58}$$

for an irreducible representation J. One useful fact is, that the representation basis states are orthogonal

$$\langle Jmn|J'm'n'\rangle = \delta_{JJ'}\delta_{mm'}\delta_{nn'}, \tag{3.59}$$

which follows from Schur's orthogonality theorem, which states

$$\sum_g \sqrt{\frac{\dim J}{|G|}} \sqrt{\frac{\dim J'}{|G|}} D_{n'm'}^{J'}(g^{-1}) D_{mn}^J = \delta_{JJ'}\delta_{mm'}\delta_{nn'}. \tag{3.60}$$

In order to generalize the Potts clock model Hamiltonian (3.42) one could write

$$H = -J \sum_i \left(\text{Tr}(U^F(i)U^{F\dagger}(i+1)) + \text{H.c.}\right) - \mu \sum_i \sum_{g \in G} \theta_g(i), \tag{3.61}$$

---

[8]This is an extension of Lemma 6 in Reference [38]. The Lemma is stated in terms of Gaussian filter functions, but that is only used in the third line of his Eq. (74). The proof holds for different filter functions, with the effect of changing the constant C. Furthermore, Hastings proves it for μ close to zero, but it can be straightforwardly extended to give (3.54). Alternatively, Eq. (3.49) is proven in Ref. [14]

where the trace is over the matrix indices of U. Note that the last term includes all possible transitions, a separate term with right multiplication doesn't change anything. As can be checked, Eq. (3.61) has a global left- and right symmetry $\mathcal{Q} = \prod_i \theta_g(i)$ and $\tilde{\mathcal{Q}} = \prod_i \tilde{\theta}_g(i)$. If we pick $G = \mathbb{Z}_N$, this reduces to the non-chiral Potts clock model with $\phi = 0$ if we take F to be the fundamental representation, $D^F(m) = e^{i2\pi m/N}$. There are several options for making (3.61) chiral, since we may include matrix products under the trace. Doing so will tend to break either the left or the right global symmetry. The last term in (3.61) may also be generalized, but we go into details about this in the paper in Chapter 5. The trick is now to find an appropriate Jordan-Wigner transformation, find the edge modes, classify their properties and figure out if they survive for finite μ as either weak or strong zero-energy modes. This is the subject of Chapter 5.

Chapter 2

Project A:
Parity-to-charge conversion in
Majorana qubit readout

One of the central experimental goals in the field Majorana research is being able to reliably read out the parity of a Majorana pair. This would allow for a topologically protected implementation of the full set of single-qubit Clifford gates through measurement-based braiding protocols. Thus, it would present a way to finally test once and for all if the zero-bias conductance peaks, reported in proximitized nanowires for almost a decade, truly stem from Majorana bound states.

A solid theoretical understanding of the readout dynamics of Majorana qubits is therefore important to reach these goals, but presently, the problem has received surprisingly little attention. By using a novel Lindbladian approximation, which has recently been put on a mathematically rigorous ground, we propose a flexible and powerful theoretical framework for calculating the readout dynamics for a paradigmatic Majorana qubit, whose degeneracy has been split by coupling of a quantum dot. Our theory provides general analytical expressions, useful for generic environments. We provide explicit examples in the form of decoherence from coupling to thermal bosonic modes in an environment LC circuit, as well as coupling to a quantum point contact in a conductance measurement. The latter case yields measurement-induced dephasing, and serves as a readout of the Majorana parity through the charge of the quantum dot.

Parity-to-charge conversion in Majorana qubit readout

Morten I. K. Munk,[1] Jens Schulenborg,[1] Reinhold Egger,[2] and Karsten Flensberg[1]

[1]*Center for Quantum Devices, Niels Bohr Institute,*
University of Copenhagen, 2100 Copenhagen, Denmark
[2]*Institut für Theoretische Physik, Heinrich-Heine-Universität, 40225 Düsseldorf, Germany*
(Dated: April 12, 2020)

We study the time-dependent effect of Markovian readout processes on Majorana qubits whose parity degrees of freedom are converted into the charge of a tunnel-coupled quantum dot. By applying a recently established effective Lindbladian approximation [1–3], we obtain a completely positive and trace preserving Lindblad master equation for the combined dot-qubit dynamics, describing relaxation and decoherence processes beyond the rotating-wave approximation. This approach is applicable to a wide range of weakly coupled environments representing experimentally relevant readout devices. We study in detail the case of thermal decay in the presence of a generic Ohmic bosonic bath, in particular for potential fluctuations in an electromagnetic circuit. In addition, we consider the nonequilibrium measurement environment for a parity readout using a quantum point contact capacitively coupled to the dot charge.

I. INTRODUCTION

In the pursuit of reliable and scalable qubits, Majorana bound states (MBSs) have received a substantial amount of attention in the previous decade [4–8]. Using zero-energy Majorana states, non-abelian many-body braiding statistics could be implemented [9–16], and quantum information may be encoded in nonlocal degrees of freedom which are robust to local noise [4, 11, 16–23]. Several physical Majorana platforms have been proposed and studied over the years [11, 24–35]. Experiments aiming to verify the presence of MBSs have so far focused primarily on measuring zero-bias conductance peaks [36–43] and the fractional Josephson effect [44–46]. These phenomena represent key physical effects of zero-energy Majorana end states in one-dimensional (1D) topological superconductors [11, 25, 26, 47–49]. However, despite providing necessary indicators, and with the benefit of readily being experimentally accessible even in the coherent transport regime [50], neither zero-bias peaks nor unconventional Josephson relations have so far provided conclusive evidence for the presence of MBSs [51–61]. The ultimate goal thus remains to demonstrate non-abelian braiding statistics, see also Ref. [62].

The crux of the latter problem may be solved by developing a reliable readout procedure for the fermion parity of a MBS pair. Indeed, whereas braiding Majoranas locally in space is very challenging from an experimental perspective, see also Refs. [12, 63], alternative schemes have been proposed which simulate braiding purely through parity measurements [22, 64–66]. In order to read out the parity of a MBS pair, however, parity has to be converted to a physically observable quantity, such as flux, charge, or capacitance [67]. This paper focuses on the perhaps simplest Majorana qubit, called the Majorana box qubit (MBQ) [21, 22], see Fig. 1. The two-fold degenerate ground state of the MBQ is spanned by the parities of MBS pairs in a system where one has four MBSs with constant total parity. As depicted in Fig. 1 and detailed in Sec. II, one can read out the par-
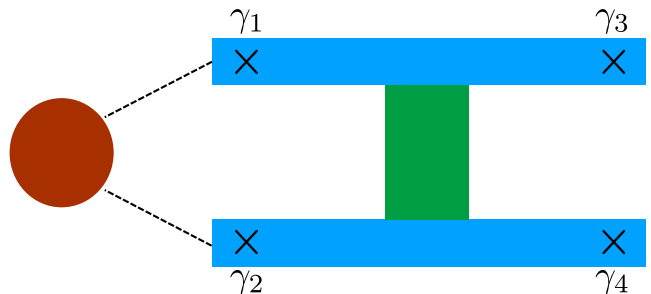

FIG. 1. Schematic of a Majorana box qubit (MBQ), consisting of two topologically superconducting nanowires (shown in blue), hosting Majorona zero-energy states (γ_i) at their ends. The nanowires are strongly coupled to a common superconducting ground (green) that effectively provides a common charging energy for the island. The ground-state degeneracy is split by a tunnel-coupled single-level quantum dot (red).

ity of a MBS pair for any initially prepared qubit state by tunnel-coupling a quantum dot to the respective two MBSs on the island, since this parity in general will affect the outcome of a dot charge measurement [13, 21, 22, 68].

However, a successful readout crucially relies on the total parity in the combined dot-MBQ system being constant over a sufficiently long measurement time. This means that (i) the readout device itself should not exchange particles with the dot-MBQ system, and (ii) the decoherence due to the readout should be fast compared to decoherence caused by external noise sources which *do* affect the total parity. Previous theoretical studies of measurement-induced decoherence in Majorana qubits [21, 22, 69–72] have analyzed related questions but without taking into account the detailed quantum dynamics of the dot and thereby, in particular, neglecting quantum backaction effects [73]. In this paper, we propose and study a flexible and powerful theoretical approach which can ultimately provide a unified and quite realistic description of the parity-to-charge conversion process and the corresponding readout dynamics in such a topo-

logically protected system.

In the main sections II and III of this work, we discuss how a solely capacitively coupled environment representing the readout device causes a prepared quantum state of the dot-MBQ system with fixed total parity to decohere in time. To describe the decay dynamics, in Sec. II, we derive a Markovian quantum master equation [74–79] for the reduced density operator, $\rho(t)$, describing the dot and the two coupled Majorana states. To achieve this, we employ a recently established [1–3] effective Lindbladian approximation. Unlike the common secular approximation [78, 79], this approximation retains nontrivial effects due to the coupling of coherence and population dynamics, i.e., off-diagonal elements of ρ in the local energy eigenbasis couple to diagonal elements, see also Ref. [80]. Moreover, unlike, e.g., the Wangsness-Bloch-Redfield approximation [74, 75, 81], this scheme is guaranteed to yield completely positive trace-preserving (CPTP) dynamics [76, 77] — an essential requirement for a physical, probabilistic interpretation of the reduced density matrix $\rho(t)$. As we are particularly interested in decoherence, i.e., the decay of off-diagonal elements of $\rho(t)$, this approximation is particularly well suited here. In contrast to previous works [21, 22, 69–72], our approach is able to capture quantum backaction effects on the MBQ state since the quantum dynamics of the dot fermion is taken into account.

Experimentally relevant estimates for relaxation and decoherence rates in this dot-MBS system will be derived for two different types of measurement environments in Sec. III. The first is a thermal bath of bosonic modes [82, 83], for which we discuss electromagnetic potential fluctuations in an electric circuit as a concrete example. This case also accounts for the fact that even if the measurement process does not provide the experimentalist with any information, the mere coupling to the measurement device already leads to decoherence due to the inevitable noise in the measurement apparatus. Second, as an example for a nonequilibrium environment that does provide information about the system state, we consider a voltage-biased, capacitively coupled quantum point contact (QPC) acting as a dot-charge sensor [84–87]. In the outlook section IV, we then lay out how future work can extend this analysis to a quantitative description, taking into account also other relaxation mechanisms. Such mechanisms could possibly involve particle exchange such as quasiparticle poisoning. The paper closes with some concluding remarks in Sec. V. Finally, we note that technical details have been delegated to two appendices.

II. KEY CONCEPTS OF MBQ READOUT

A. Model

The MBQ device of interest is depicted in Fig. 1. It consists of two topological superconductor nanowires [25, 26], hosting altogether four zero-energy MBSs at their ends, and an effectively spinless, single-level quantum dot tunnel-coupled to two of the nanowire ends. With the superconducting bridge, the two nanowires form a single floating island subject to Coulomb charging effects. We assume that on the island, the superconducting gap is so large that the influence of quasiparticles and subgap (Andreev) states beyond MBSs can be neglected. The low-energy Hamiltonian then reads

$$H = H_0 + H_B + H_I, \tag{1}$$

$$H_0 = \epsilon\, n_d + \sum_{i=1,2} \gamma_i \left(\lambda_i d - \lambda_i^* d^\dagger \right), \tag{2}$$

$$H_I = \sqrt{g}\, n_d \varphi. \tag{3}$$

The Hamiltonian H_0 describes both the local coherent dynamics of the dot, with level position ϵ, occupation number operator $n_d = d^\dagger d$, and fermionic annihilation operator d, and of the two tunnel-coupled MBSs. The latter are described by Majorana operators, $\gamma_i = \gamma_i^\dagger$, with anticommutation relations $\{\gamma_i, \gamma_j\} = 2\delta_{ij}$. The amplitudes $\lambda_{i=1,2}$ for tunneling between dot and γ_i are, without loss of generality, parametrized by the real-valued quantities λ, a, and ϕ,

$$\lambda_1 = \lambda \geq 0, \qquad \lambda_2 = a\lambda e^{i\phi}, \qquad 0 \leq a \leq 1. \tag{4}$$

Importantly, the phase difference ϕ is controllable by, e.g., a variable magnetic flux inside the loop constituted by the tunneling links and the superconducting backbone. As we show in Sec. II B, one can tune this phase to split the energies of the MBQ in such a way that it is possible to read out the MBQ state. For this to work, however, we furthermore require that the charging energy of the superconducting island is large enough to constrain the total fermion parity of the MBQ, $(-1)^{n_L+n_R}$, where $n_{L/R} = f_{L/R}^\dagger f_{L/R}$ denotes the occupation of the left/right fermionic state with $f_{L/R} = (\gamma_{1/3} + i\gamma_{2/4})/2$. We assume Coulomb valley conditions such that all other charge states of the superconducting island in Fig. 1 cost a large excitation energy at least of the order of the charging energy of the island [21, 22].

The term H_B in Eq. (1) describes the environment, e.g., representing a measurement device, and H_I is a capacitive coupling between the dot charge and the environment. Concrete implementations of H_B and the specific degrees of freedom, φ, coupling to the dot charge via H_I are discussed in Sec. II C. In general terms, the dimensionless coupling constant g in H_I is determined by the ratio between a capacitive interaction energy, E_{int}, and a model-specific reference energy, E_{ref}. We require that this reference energy is large in comparison, $0 < E_{\text{int}}/E_{\text{ref}} \ll 1$, such that $g \ll 1$ quantifies a weak system-environment coupling, justifying a perturbative expansion in H_I. Furthermore, we here only consider environments H_B which are quadratic in field operators, and that are effectively bosonic from the point of view of the fermions in the dot-MBQ system. As detailed in

Sec. II C, this case includes, for example, photons in a thermal electromagnetic environment as well as the effective bosonic modes originating from the Coulomb interaction between the dot charge and the local electronic charge density in a fermionic environment.

B. Readout principle and fidelity

To explain the readout principle for the MBQ state in concrete terms, in the following we always consider the sector with even total parity, where the total parity of the superconducting island is assumed to be conserved during the entire measurement. In this case, the MBQ has two basis states, $|0_L 0_R\rangle$ with $n_L = n_R = 0$ and $|1_L 1_R\rangle$ with $n_L = n_R = 1$. Given this total-parity constraint, the readout principle and its fidelity rely mostly on the fact that fermionic parity is exchanged through the tunnel couplings between the dot and the tunnel-coupled left Majorana pair, corresponding to γ_1 and γ_2 in Fig. 1. Importantly, the full Hamiltonian (1) conserves the joined parity of the dot and these two MBSs,

$$s = (-\mathbb{1})^{n_d + n_L}. \tag{5}$$

We next observe that due to the presence of the phase ϕ in the tunneling amplitudes (4), eigenstates of the dot-MBQ system Hamiltonian H_0 (defined in the absence of the environment) in general have different energies for $s = +1$ and $s = -1$. Denoting the eigenstates of H_0 by $|p, s\rangle$, with $p = \pm$, we have

$$H_0|p,s\rangle = E_{p,s}|p,s\rangle, \quad E_{\pm,s} = (\epsilon \pm E_s)/2,$$
$$E_{s=\pm} = \sqrt{\epsilon^2 + 4\lambda^2(1 + a^2 + sa\sin\phi)}. \tag{6}$$

Since s is a conserved quantity, an initial MBQ state with $s = +1$ will dynamically relax towards a stationary state with $s = +1$ when coupled to the measurement device. By Eq. (6), this stationary state has an energy different from the energy of the state to which an initial state with $s = -1$ relaxes. In addition, also the average dot occupation number,

$$\langle n_d \rangle = \frac{d\langle H \rangle}{d\epsilon}, \tag{7}$$

depends on this energy difference in the long-time limit. This fact ultimately enables one to read out the parity number $s = \pm 1$ via measurements of the dot charge, see Eq. (7), or via its quantum-capacitive effect $\sim d^2\langle H \rangle / d\epsilon^2$, see Ref. [22].

Suppose now that the dot is initially empty, $n_d = 0$, and the MBQ has been prepared in the initial state

$$|\psi_0\rangle = \alpha_0|0_L 0_R\rangle + \beta_0|1_L 1_R\rangle, \tag{8}$$

with complex-valued coefficients α_0 and β_0 subject to $|\alpha_0|^2 + |\beta_0|^2 = 1$. In general, the initial state of the combined dot-MBQ system thus corresponds to a superposition of states with different values of $s = \pm 1$. Since the
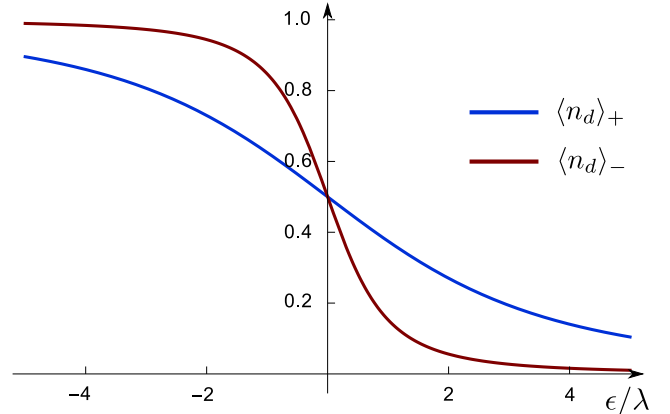

FIG. 2. Readout principles for the MBQ device in Fig. 1: Average steady-state dot occupation number, $\langle n_d \rangle_s$, vs ϵ/λ for different parities $s = \pm 1$ in Eq. (5). Here $\langle n_d \rangle_s$ has been calculated for the ground state with energy $E_{-,s}$ in Eq. (6), using $a = 1$ and $\phi = \pi/3$. Calculating $\langle n_d \rangle_s$ instead for the thermal states $\rho_{st,s}$ in Eq. (10), the two curves approach the constant curve $\langle n_d \rangle = 1/2$ with increasing temperature. Thereby the readout visibility, i.e., the ability to distinguish the values $s = \pm 1$, will be gradually lost.

energies (6) of the system depend on s, decoherence due to the coupled bath representing the measurement device should relax the reduced density matrix of the dot-MBQ system, $\rho(t)$, to the stationary limit according to

$$\rho(t) = \begin{pmatrix} |\alpha_0|^2 \rho_{s=+} & \alpha_0\beta_0^* \rho_c \\ \alpha_0^*\beta_0 \rho_c^\dagger & |\beta_0|^2 \rho_{s=-} \end{pmatrix}$$
$$\xrightarrow{t\to\infty} \rho_{st} = \begin{pmatrix} |\alpha_0|^2 \rho_{st,s=+} & 0 \\ 0 & |\beta_0|^2 \rho_{st,s=-} \end{pmatrix}. \tag{9}$$

The diagonal blocks here describe the density matrix projected to the respective subspace with parity $s = \pm 1$, while the off-diagonal part ρ_c describes coherences between both parity sectors. The steady-state distributions, $\rho_{st,+}$ and $\rho_{st,-}$, may in practice be distinguished by measuring $\langle n_d \rangle$ or $d\langle n_d \rangle/d\epsilon$, averaged over some time interval. In this way, one performs a projective measurement of the initial MBQ state, where $s = +1$ $(s = -1)$ occurs with probability $|\alpha_0|^2$ $\left(|\beta_0|^2\right)$. Once the dot is effectively decoupled from the MBSs by adiabatically adjusting ϵ towards the limit of zero occupation $n_d = 0$, one knows that the MBQ state equals $|0_L 0_R\rangle$ $(|1_L 1_R\rangle)$ if $s = +1$ $(s = -1)$ has been measured.

To better understand the fidelity and limitations of this readout, Fig. 2 shows the dependence of $\langle n_d \rangle_s$ on the dot level energy ϵ, as determined by Eq. (7) for the ground states corresponding to the energies $E_{-,s}$. We observe that for $\epsilon/\lambda \neq 0$, the ground states in the $s = \pm 1$ sectors *can* be distinguished by measuring the charge on the dot. If the system is instead prepared in a thermal state,

$$\rho_{st,s} = \frac{1}{Z_s} \sum_{p=\pm} e^{-\beta E_{p,s}} |p,s\rangle\langle p,s|, \tag{10}$$

with Eq. (6) and $\beta = (k_B T)^{-1}$, the curves in Fig. 2 would flatten towards $\langle n_d \rangle_s = 1/2$ as temperature is increased. Evidently, a charge readout of the dot can still measure $s = \pm 1$ provided that the system has thermalized at a sufficiently low temperature.

We note that for a more general environment, the long-term limit need not be represented by a thermal distribution. Nevertheless, as long as the dot charge $\sim d \langle H \rangle / d\epsilon$ and/or, depending on the setup, its quantum capacitance $\sim d^2 \langle H \rangle / d\epsilon^2$, differ for $s = +1$ and $s = -1$, the value of s may in principle still be distinguished if the system decoheres to a block-diagonal state as in Eq. (9).

By developing a Lindbladian master equation for the above model, we show in Sec. II E below that block-diagonal relaxation similar to Eq. (9) does indeed generically happen. The missing ingredient for arriving at this master equation is — as covered in Sec. II C below — a physical specification of the environment, H_B, and its coupling to the dot, H_I. A key advantage of the jump operator approximation established in Refs. [1–3], and summarized in Sec. II E, is that we may simply write down the master equation once we have determined the environmental correlation function,

$$B(t) = \langle \varphi(t) \varphi \rangle . \tag{11}$$

This correlator is defined with respect to the initial state of the bath before the measurement begins, where $\varphi(t) = e^{iH_B t} \varphi e^{-iH_B t}$ is taken in the interaction picture. We note that this procedure directly works only for a vanishing linear moment, $\langle \varphi(t) \rangle = 0$. For $\langle \varphi(t) \rangle \neq 0$, the linear moment needs to be time-independent, $\langle \varphi(t) \rangle = \langle \varphi \rangle$. In that case, one can remove the linear moment, $\varphi \to \varphi - \langle \varphi \rangle$, by a shift of the dot energy, $\epsilon \to \epsilon + \langle \varphi \rangle$, in Eq. (1). As this shift does not introduce an explicit time dependence, the effective Lindbladian approximation in Sec. II E will still apply upon using the bath correlator

$$B(t) = \langle [\varphi(t) - \langle \varphi \rangle][\varphi - \langle \varphi \rangle] \rangle \tag{12}$$

instead of Eq. (11).

C. Physical realizations of environments

Let us now precisely formulate the physical systems representing the readout device. As announced in Sec. I, we consider two different cases. The first is an Ohmic thermal bath of bosonic modes. This can be seen as a simple phenomenological model for the effects of a measuring apparatus on the dot-MBQ system, such as capacitive noise due to voltage fluctuations in the electronic circuit coupled to the dot, see Fig. 3. A bosonic bath can, however, also be taken at face value, as a microscopic model of thermal relaxation of the system which will invariably be present due to charge couplings with the environment. The second addressed case is that of a nonequilibrium measurement environment, formed by two voltage-biased electronic leads coupled by a QPC.
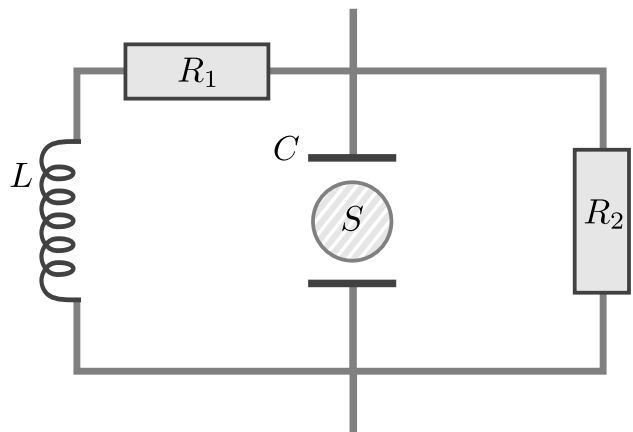

FIG. 3. Schematic circuit representing a typical electromagnetic environment. The dot-MBQ system (S) is capacitively coupled to the environmental inductance and resistances. The resulting potential φ on the capacitor C enters as a charge coupling in the Hamiltonian (18).

Since the QPC is also capacitively coupled to the dot, see Fig. 4, the QPC transmission is affected by the Coulomb interaction with the dot. By monitoring the conductance through the QPC, one can thereby measures the dot charge and hence the parity $s = \pm 1$.

1. Thermal bath of bosons

Let us first consider a bosonic environment in thermal equilibrium. This model is useful both for describing the inherent decoherence due to electromagnetic radiation, but also as a simple phenomenological model for understanding the dynamics of the system under a generic readout. The environmental Hamiltonian,

$$H_B = \sum_q \omega_q \left(b_q^\dagger b_q + \frac{1}{2} \right), \tag{13}$$

in this case consists of non-interacting bosons characterized by quantum numbers q and energies ω_q, where $b_q^\dagger$ and b_q are the corresponding creation and annihilation operators. We assume that the dot charge capacitively couples to these bosons,

$$H_I = \sqrt{g} n_d \varphi, \quad \varphi = \sum_q \left(M_q b_q^\dagger + M_q^* b_q \right). \tag{14}$$

The bath operator φ is determined by the mode-dependent coupling energies M_q. The small dimensionless coupling constant g, which we have introduced in Eq. (1), is physically related to the ratio of the capacitive interaction energy, E_{int}, of the dot-environment coupling and the typical frequency ω_0 of the environmental oscillators, $g = g(E_{\text{int}}/\omega_0)$. The spectral density associated with the coupling is assumed to be Ohmic with some cut-off function $\mathcal{C}(\omega, \omega_c)$ determined by a cutoff frequency ω_c

(where $\omega_c \approx \omega_0$),

$$J(\omega) = \sum_q |M_q|^2 \delta(\omega - \omega_q) = \omega \mathcal{C}(\omega, \omega_c). \quad (15)$$

An Ohmic spectral density occurs in many different scenarios [82, 83], including, e.g., the capacitive coupling of the system to an electromagnetic transmission line [79]. The precise form of the cutoff function $\mathcal{C}$ depends on the physical nature of the bath, as we further discuss below. At this stage, it is only relevant in so far as it will regularize integrals at high frequencies in what follows.

The initial density operator of the bath, ρ_B, taken before the dot couples to the environment at times $t \geq 0$, is assumed to be thermal, $\rho_B = e^{-\beta H_B}/\text{Tr}\left[e^{-\beta H_B}\right]$. The expectation value $\langle \varphi(t_1) \ldots \varphi(t_N) \rangle$ with respect to ρ_B thus disappears by virtue of Wick's theorem for any odd number N of bath operators, with $\varphi(t) = e^{iH_B t}\varphi e^{-iH_B t}$. As stated above and detailed in Sec. II E, the relaxation of the dot-MBQ system then only depends on the autocorrelation function,

$$B_{\text{th}}(t) = \langle \varphi(t)\varphi(0) \rangle \quad (16)$$
$$= \int_0^\infty d\nu J(\nu) \left[e^{i\nu t}n_B(\nu) + e^{-i\nu t}(n_B(\nu) + 1)\right],$$

with the index "th" indicating the case of a thermal bath. Equation (16) derives from the vanishing two-point correlators $\langle b_q^\dagger b_q^\dagger \rangle = \langle b_q b_q \rangle = 0$, and the occupations $\langle b_q^\dagger b_q \rangle = \langle b_q b_q^\dagger \rangle - 1 = n_B(\omega_q)$, with the Bose-Einstein distribution, $n_B(\omega) = (e^{\beta\omega} - 1)^{-1}$. The relaxation of the dot-MBQ system is then determined by the Fourier transform of Eq. (16),

$$B_{\text{th}}(\omega) = \int_{-\infty}^\infty dt \, B_{\text{th}}(t)e^{i\omega t}$$
$$= \frac{\pi}{2}\omega \mathcal{C}(\omega, \omega_c)\left[\coth\left(\frac{\omega}{2k_B T}\right) + 1\right]. \quad (17)$$

To obtain physically meaningful estimates for g and for the cutoff function $\mathcal{C}$, we next observe that in many situations of practical interest, the dominant bosonic reservoir is represented by the electromagnetic modes in the electric circuit connected to the dot-MBQ system. In such cases, the specific form of g and $J(\omega)$ may often be derived from the electrodynamical properties of the equivalent classical circuit. As a specific example, consider the case sketched in Fig. 3, where the dot-MBQ system is placed in an LC circuit and couples through the voltage drop φ/e over the capacitor C to the bath. The interaction Hamiltonian may then be written as

$$H_I = n_d \varphi. \quad (18)$$

In thermal equilibrium, the correlation function $B(t) = \langle \varphi(t)\varphi \rangle$ may be calculated by using the Kubo formula and the fluctuation-dissipation theorem. The impedance of the circuit in Fig. 3 is given by

$$Z(\omega) = \left(\frac{1}{R_2} + \frac{1}{R_1 + i\omega L} + i\omega C\right)^{-1}, \quad (19)$$

and $B(\omega)$ follows as (see also Ref. [83])

$$B_{LC}(\omega) = e^2 \omega \, \text{Re}\left(\frac{|Z(\omega)|^2}{Z(\omega)}\right)\left[\coth\left(\frac{\omega}{2k_B T}\right) + 1\right]. \quad (20)$$

Rescaling $\varphi \mapsto \sqrt{g}\varphi$ in Eq. (18) and $B_{LC}(\omega) \mapsto B_{LC}(\omega)/g$ in Eq. (20), this expression matches the general result for a thermal bosonic bath with Ohmic spectral density in Eq. (17), where the coupling constant $g = g_{LC}$ and the bath cutoff frequency ω_c are given by

$$g_{LC} = \frac{e^2}{2C\omega_{LC}}, \quad \omega_c = \omega_{LC} = \frac{1}{\sqrt{LC}}, \quad (21)$$

and ω_{LC} is the LC resonance frequency of the circuit in Fig. 3. As expected, the dimensionless small system-bath coupling, g_{LC}, follows as the ratio between the capacitive interaction energy, $E_{\text{int}} = e^2/2C$, and the reference energy set by the LC resonance frequency, $E_{\text{ref}} = \omega_{LC}$. Equation (20) predicts a cutoff function $\mathcal{C}(\tilde{\omega})$, with $\tilde{\omega} = \omega/\omega_c$, of the form

$$\mathcal{C}(\tilde{\omega}) = \frac{4}{\pi} \frac{\tilde{\omega}_2 + \frac{\tilde{\omega}_1}{1 + \tilde{\omega}_1^2 \tilde{\omega}^2}}{\left(\tilde{\omega}_2 + \frac{\tilde{\omega}_1}{1 + \tilde{\omega}_1^2 \tilde{\omega}^2}\right)^2 + \tilde{\omega}^2\left(1 - \frac{1}{\tilde{\omega}_1^{-2} + \tilde{\omega}^2}\right)^2}, \quad (22)$$

with $\tilde{\omega}_{i=1,2} = (R_i C \omega_{LC})^{-1}$. Evidently, $\mathcal{C}(\tilde{\omega})$ approaches a constant for $\tilde{\omega} \to 0$ but decays $\propto 1/\tilde{\omega}^2$ for $\tilde{\omega} \to \infty$. This limiting behavior is characteristic for a Lorentzian cutoff function.

2. QPC detector

Next we consider a measurement apparatus defined by a QPC that weakly couples together two voltage-biased electronic leads, see Fig. 4. The QPC is also capacitively coupled to the dot charge. This coupling mechanism in turn affects the QPC transparency, and hence the measured conductance through the QPC. One can thereby perform a readout of the parity $s = \pm 1$ in Eq. (5). As explained above, the outcome of this measurement also determines the eigenvalue of the MBS parity operator $i\gamma_1\gamma_2$.

To good accuracy, the setup in Fig. 4 can be modeled by [84–87]

$$H_B = \sum_{k;\ell=L,R} \epsilon_{\ell k} c_{\ell k}^\dagger c_{\ell k} \quad , \quad H_I = \sqrt{g}n_d\varphi, \quad (23)$$
$$g = (E_{\text{int}}/E_{\text{ref}})^2 \quad , \quad \varphi = E_{\text{ref}}V\hat{\rho}.$$

The bath here corresponds to the left and right electronic leads together with their mutual coupling via the QPC. The Hamiltonian H_B contains the annihilation (creation) operators $c_{\ell k}^{(\dagger)}$ for electrons in single-particle eigenstates of the combined lead-QPC-lead system. The corresponding eigenenergies, $\epsilon_{\ell k}$, are labeled by the wave vector k and
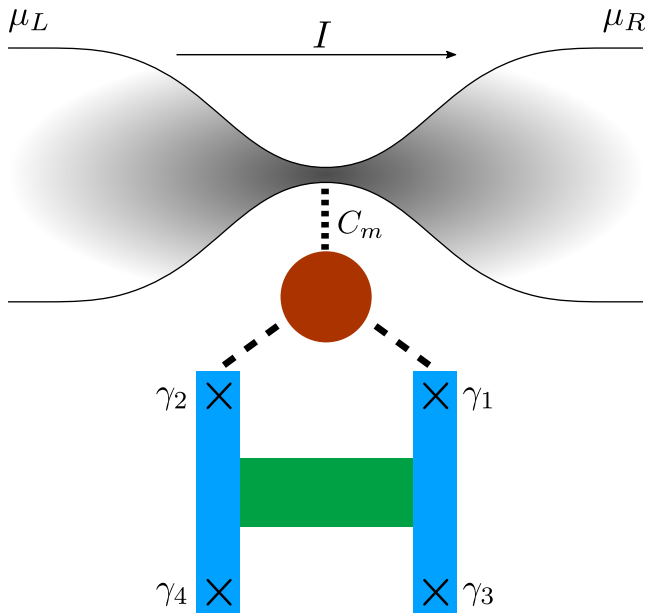
FIG. 4. Schematic Majorana parity readout using a quantum point contact (QPC) connecting two voltage-biased leads. The dot-MBQ system capacitively couples to the QPC through a mutual capacitance C_m between the charge density in the QPC and the charge on the dot. This coupling decoheres the dot-MBQ system and perturbs the potential that the QPC feels, leading to a parity-dependent shift of the conductance through the QPC.

the index $\ell = L, R$. This index specifies whether the scattering state originates from the left or the right lead. The bath operator φ in Eq. (23) contains the local electron density operator $\hat{\rho}$ in the small (essentially point-like) region representing the central QPC region, with volume V. We assume that the capacitive interaction between $\hat{\rho}$ and the dot charge represents the dominant coupling between the QPC and the dot-MBQ system, see also App. A. The corresponding interaction energy, $E_{\text{int}} = 2e^2/(C_m V)$, is determined by the mutual dot-QPC capacitance C_m per volume V, where the factor 2 accounts for the electron spin. To justify the weak-coupling approximation, $g \ll 1$, the energy E_{int} must be small compared to a reference energy E_{ref}. The latter energy is obtained from the following analysis.

We assume that scattering states originating from the left/right lead thermalize according to Fermi-Dirac distributions with equal temperatures, $T_L = T_R = T$, but different chemical potentials, $\Delta\mu = \mu_L - \mu_R \geq 0$. This potential bias induces a stationary charge current across the QPC. The envisioned readout relies on the fact that the capacitive coupling of the QPC to the dot affects the QPC transparency, and hence the current response to the potential bias depends on the dot occupation [84–86]. As detailed in App. A, the bath correlators describing the time-dependent effect of this readout on the dot-MBQ system are obtained by expressing $\hat{\rho}$ in terms of the op-

erators $c_{\ell k}$ and $c^\dagger_{\ell k}$. We find a time-independent linear moment, $\langle \varphi(t) \rangle = \langle \varphi \rangle \neq 0$. As pointed out in Sec. II B, one can absorb $\langle \varphi \rangle$ by a shift of the dot level energy ϵ. The Fourier transform of the auto-correlation function (12) is then found as

$$B_{\text{QPC}}(\omega) = \int_{-\infty}^{\infty} dt \, B_{\text{QPC}}(t) e^{i\omega t} \qquad (24)$$

$$= \pi \sum_{\ell,\ell'=L,R} J_{\ell\ell'}(\omega) \left[\coth\left(\frac{\omega + \mu_{\ell\ell'}}{2k_B T} \right) + 1 \right],$$

with the lead-dependent spectral densities

$$J_{\ell\ell'}(\omega) = \int_{-\infty}^{\infty} d\Omega \, \Gamma_{\ell\ell'} \left(\Omega + \mu_{\ell\ell'} - \frac{\omega}{2}, \Omega + \mu_{\ell\ell'} + \frac{\omega}{2} \right)$$

$$\times \left[n_{\text{F}} \left(\Omega - \frac{\Delta\mu_{\ell\ell'} + \omega}{2} \right) - n_{\text{F}} \left(\Omega + \frac{\Delta\mu_{\ell\ell'} + \omega}{2} \right) \right], \qquad (25)$$

where we use the Fermi-Dirac distribution, $n_{\text{F}}(\omega) = (e^{\beta\omega} + 1)^{-1}$, the lead-averaged chemical potentials $\mu_{\ell\ell'} = (\mu_\ell + \mu_{\ell'})/2$, and the potential differences $\Delta\mu_{\ell\ell'} = \mu_\ell - \mu_{\ell'}$. The coupling function

$$\Gamma_{\ell\ell'}(\omega, \omega') = E_{\text{ref}}^2 \sum_{kk'} |\tau_{\ell k,\ell'k'}|^2 \delta(\omega - \epsilon_{\ell k}) \delta(\omega' - \epsilon_{\ell'k'}) \quad (26)$$

describes how the QPC scatters electrons from lead ℓ with energy ω into lead ℓ' with energy ω'. In App. A, we explicitly evaluate Eq. (26) for the case of 1D leads with the QPC approximated by a δ-peak potential. In general, Γ scales with the energetic densities of states in the respective lead, $D_\ell = D_\ell(E = \mu_\ell)$, and with the typical transmission coefficient τ of the QPC, $\Gamma \sim \tau^2(E_{\text{ref}} D_\ell)(E_{\text{ref}} D_{\ell'})$. A small coupling g can then be realized in two different ways: The first is to have low QPC transparency $\tau \ll 1$, as set by precise implementation of the QPC. Alternatively, one needs a reference scale E_{ref} that is small compared to $1/D_{L,R}$ but at the same time large compared to the capacitive energy E_{int}, thus leading to $g = (E_{\text{int}}/E_{\text{ref}})^2 \ll 1$ according to Eq. (23). Physically, this corresponds to either a relatively low density of states or to a large mutual capacitance $C_m V$.

To understand how $\Gamma_{\ell\ell'}$ in Eq. (25) behaves as a function of Ω, and hence how it enters the spectral densities $J_{\ell\ell'}$, we note that the Fermi functions in Eq. (25) will effectively restrict the support of the integrand to the window

$$-\frac{\omega + |\Delta\mu_{\ell\ell'}|}{2} < \Omega < \frac{\omega + |\Delta\mu_{\ell\ell'}|}{2}. \qquad (27)$$

Under the assumption that the applied voltage bias and any internal energy scale determining the QPC transparency (e.g., a potential barrier height) are much smaller than the average chemical potential with respect to the band bottom of the leads, $\Delta\mu_{\ell\ell'} \ll \mu_{\ell\ell'}$, we can distinguish two limits, namely the cases $|\omega| \ll \mu_{\ell\ell'}$ and $|\omega| \gg \mu_{\ell\ell'}$. For small frequencies, $|\omega| \ll \mu_{\ell\ell'}$,

the coupling profile $\Gamma_{\ell\ell'}$ in Eq. (25) can be assumed Ω-independent within the region (27) where the integrand has significant support, $\Gamma_{\ell\ell'} \sim [E_{\text{ref}}D_\ell(\mu_{\ell\ell'})]^2 \sim (E_{\text{ref}}/\mu_0)^2$, with the average chemical potential $\mu_0 = (\mu_L + \mu_R)/2$. We here assumed a form of the density of states as appropriate for a 1D electron gas with $|\Delta\mu_{\ell\ell'}| \ll \mu_{\ell\ell'}$, where one finds $D_\ell(\mu_{\ell\ell'}) \sim 1/\mu_{\ell\ell'}$. For large frequencies, $|\omega| \gg \mu_{\ell\ell'}$, on the other hand, the coupling factor $\Gamma_{\ell\ell'}(\Omega + \mu_{\ell\ell'} - \omega/2, \Omega + \mu_{\ell\ell'} + \omega/2)$ in Eq. (25) is expected to decay as $1/|\omega|$ for most Ω. One can rationalize this fact by noting that the density of states decreases, similarly to the case of a 1D Fermi gas, with $1/\sqrt{|\omega|}$ for sufficiently strong lateral electron confinement in the QPC. Importantly, to regularize Eq. (24) at high frequencies, we also need to account for the finite electronic bandwidth that eventually cuts off the integral.

To qualitatively include all the above-mentioned effects, we now set $E_{\text{ref}} = \mu_0/2$ with $\mu_0 = (\mu_L + \mu_R)/2$ and introduce an exponential cutoff. We thus consider the simplified coupling function

$$\Gamma_{\ell\ell'}\left(\Omega + \mu_{\ell\ell'} - \frac{\omega}{2}, \Omega + \mu_{\ell\ell'} + \frac{\omega}{2}\right) \to \frac{1}{4}e^{-\frac{|\omega|}{\omega_c}}, \quad (28)$$

with $\omega_c \simeq \mu_0$. The dimensionless coupling constant introduced in Eq. (1) then equals

$$g = (2E_{\text{int}}/\mu_0)^2, \quad (29)$$

where $E_{\text{int}} = 2e^2/(C_m V)$. The weak-coupling assumption holds for $E_{\text{int}} \ll \mu_0$. For a quantitatively more precise calculation, one can resort to a specific QPC model as shown, e.g., in App. A, followed by a numerical evaluation of Eq. (25).

Here we proceed by inserting Eq. (28) into Eq. (25). We then obtain an Ohmic spectral density with a potential shift and an exponential cutoff,

$$J_{\ell\ell'}(\omega) \to \frac{1}{4}(\omega + \Delta\mu_{\ell\ell'})e^{-\frac{|\omega|}{\omega_c}}$$
$$\overset{\Delta\mu_{\ell\ell'} \ll \omega_c}{\approx} \frac{\omega + \Delta\mu_{\ell\ell'}}{4}e^{-\frac{|\omega + \Delta\mu_{\ell\ell'}|}{\omega_c}}. \quad (30)$$

Using this result in Eq. (24), summing over $\ell, \ell' = L, R$, and comparing the result to Eqs. (15) and (16), we observe that $B_{\text{QPC}}(\omega)$ becomes a lead average of bosonic bath correlators in thermal equilibrium, B_{th} in Eq. (17),

$$B_{\text{QPC}}(\omega) = \frac{2B_{\text{th}}(\omega) + B_{\text{th}}(\omega + \Delta\mu) + B_{\text{th}}(\omega - \Delta\mu)}{2} \tag{31}$$

with the potential bias $\Delta\mu = \mu_L - \mu_R$.

In summary, Eq. (31) states that the readout procedure represented by the potential gradient $\Delta\mu$ manifests itself analogously to the capacitive noise of thermal fluctuations. For $\Delta\mu \gg T$, and when lead-state energy differences $-\Delta\mu < \omega < \Delta\mu$ are most relevant for the readout, this contribution to the bath noise and to the relaxation of the dot-MBQ system becomes dominant. In this regime, we show in Sec. III B 2 that $\Delta\mu$ plays the role of an effective temperature for the decay rates. In the opposite high-temperature limit, $T \gg \Delta\mu$, the dynamics instead represents a purely thermal decay due to the two leads, $B_{\text{QPC}} \approx 2B_{\text{th}}$. However, the readout may still work if the dot charge, and hence the QPC conductance, depends on the final MBQ state, and thus on the parity of the initial MBQ state.

D. Mapping to spin-boson model

In this subsection, we show that our model (1) is intimately related to the celebrated spin-boson model, which is a paradigmatic model for describing the dissipative dynamics of two-level quantum systems [83]. To that end, we first observe that the joined parity s in Eq. (5) is conserved for the model in Eq. (1),

$$[H, s] = 0, \qquad s = (-\mathbb{1})^{n_d + n_L}. \quad (32)$$

Our system, defined by the dot and the two coupled MBSs, can be described in terms of two different two-level systems which are both coupled to a common bosonic bath. Below, we make this connection explicit. The dynamical properties of the spin-boson model have been thoroughly studied in the past [83, 88–91]. In contrast to those studies, we here encounter two copies of the spin-boson model, corresponding to the parity eigenvalues $s = \pm 1$, respectively. The dynamics of coherences between those two subsectors then represents the quantity of most interest. Note that such coherences do not violate parity superselection rules [92–94] since they comply with total parity conservation once the parity $(-\mathbb{1})^{n_R}$ of the uncoupled Majorana pair is accounted for.

Introducing the auxiliary Majorana operators $\eta_{1,2}$ for representing the dot fermion, $d = (\eta_1 + i\eta_2)/2$, we first define the Pauli operator algebra

$$\tilde{\sigma}_x = -i\gamma_1\eta_2, \quad \tilde{\sigma}_y = i\gamma_1\eta_1, \quad \tilde{\sigma}_z = -i\eta_1\eta_2. \quad (33)$$

Next we write the parity operator (5) as $s = -\gamma_1\gamma_2\eta_1\eta_2$ in order to express Eq. (1) as

$$H = -\frac{1}{2}(\epsilon + \sqrt{g}\varphi)\sigma_z - \frac{\Delta_s}{2}\sigma_x + H_B, \quad (34)$$
$$\Delta_{s=\pm 1} = 2\lambda\sqrt{1 + a^2 + 2sa\sin\phi},$$

where we use the rotated Pauli operators

$$\sigma_{\alpha=x,y,z} = e^{i\theta_s\tilde{\sigma}_z}\tilde{\sigma}_\alpha e^{-i\theta_s\tilde{\sigma}_z}, \quad (35)$$
$$\theta_s = -\frac{1}{2}\tan^{-1}\left(\frac{a\cos\phi}{s + a\sin\phi}\right).$$

We note that a constant energy shift has been neglected in Eq. (34), along with the term $\sqrt{g}\varphi/2$. Indeed, upon averaging over the bath degrees of freedom, the last term yields a contribution $\sim n_d\langle\varphi(t)\rangle$ up to order $\mathcal{O}((\sqrt{g})^2)$.

Since the average $\langle \varphi(t) \rangle$ is time-independent for all environments considered here, see Sec. II C, such a contribution only generates a shift of ϵ which can be calibrated away.

For $\Delta_+ \neq \Delta_-$ in Eq. (34), the system state relaxes to the stationary limit (9) for standard reasons. In particular, since the energies of the two blocks with $s = \pm 1$ do not match, there are no cancellations of dynamical phases in the off-diagonal entries of the density matrix. The large number of bosonic modes then implies that these terms will cancel out in the long-time limit. However, for $\Delta_+ = \Delta_-$, the evolution of the off-diagonals blocks is identical to the diagonal blocks, and the long-time limit of the density matrix is instead given by

$$\rho(t) \xrightarrow[\Delta_+ = \Delta_-]{t \to \infty} P_0 \, |0_d\rangle\langle 0_d| \, |\psi_0\rangle\langle\psi_0| \\ + P_1 \, |1_d\rangle\langle 1_d| \, |\overline{\psi}_0\rangle\langle\overline{\psi}_0| \,, \quad (36)$$

where n_d is the occupation of the dot, $P_{0,1}$ the probability to encounter $n_d = 0, 1$ in the readout, $|\psi_0\rangle$ has been specified in Eq. (8), and we use $|\overline{\psi}_0\rangle = \alpha_0|0_L 1_R\rangle + \beta_0|1_L 0_R\rangle$. Thus the dot occupation can be read out, but no information will be gained in this case. In fact, the final step of emptying the dot will simply restore the initial MBQ state.

E. Effective Lindbladian

We are now in a position to derive the quantum master equation governing the time evolution of the reduced density matrix, $\rho(t)$, describing the dot-MBQ system under the influence of the dissipative environment. In general, a master equation describing a CPTP Markovian time evolution of $\rho(t)$ can always be cast into Lindblad form [76–78],

$$\rho(t) = e^{\mathcal{L}t}\rho, \quad (37a)$$
$$\mathcal{L}\rho = -i[H_{LS} + H_0, \rho] \\ + \sum_k \Gamma_k \left(L_k \rho L_k^\dagger - \frac{1}{2}\{L_k^\dagger L_k, \rho\} \right), \quad (37b)$$

where the jump operators L_k describe dissipative transitions induced by the environment. The corresponding transition rates are non-negative, $\Gamma_k \geq 0$, thereby guaranteeing CPTP time evolution. Furthermore, the Lamb shift contribution appearing in the coherent part of the time evolution is captured by a Hamiltonian H_{LS}. This term encodes system energy renormalizations due to the dressing of system operators by environmental modes. Such effects may occur even at zero temperature.

Conventional recipes for deriving Markovian master equations for open quantum systems, such as the Wangsness-Bloch-Redfield approach [74, 75, 81], in general do not result in master equations of Lindblad form and hence do not necessarily yield CPTP evolution. In

contrast, the effective Lindbladian approximation, previously established in Refs. [1, 2] and very recently put on a rigorous footing by Nathan and Rudner [3], automatically stipulates a Lindbladian form, and thus does away with such problems. In this subsection, we give a brief overview of this approximation and apply it to our model. In effect, the approximation *prescribes* the form of the jump operator,

$$L = \frac{\sqrt{g}}{2} \sum_{m,n} \sqrt{B(E_n - E_m)} \, \langle m \, |{-}\sigma_z| \, n \rangle \, |m\rangle\langle n| \,, \quad (38)$$

where $B(\omega) = \int_{-\infty}^{\infty} dt \, e^{i\omega t} B(t)$. The states $|n\rangle = |p, s\rangle$ are energy eigenstates of the system Hamiltonian H_0, see Eq. (6), and σ_z has been defined in Eq. (35), see also App. B for a detailed discussion. The appearance of the square root of the Fourier transformed boson correlator (12) can be rationalized by noting that Fermi's Golden Rule is then immediately recovered for the transition rates between eigenstate populations. While jump operators of the form in Eq. (38) have been suggested before [1], one of the central contributions of Nathan and Rudner [3] is to put this approximation on solid theoretical grounds by providing an error bound on $\dot{\rho}(t)$. The approximation consists (i) of a familiar type of Markovian approximation, which is equivalent to the Wangsness-Bloch-Redfield approach in the sense that both approaches share the same error bound $\mathcal{E}_M$. However, Ref. [3] formulates (ii) another approximation that is not equivalent to the standard secular approximation [78, 79] but nevertheless yields the desired Lindblad form of the master equation. Importantly, this second approximation has a different error bound, $\mathcal{E}_L$, than the Wangsness-Bloch-Redfield approach. However, there exists a single quantity, $\mathcal{E}$, which is larger than both $\mathcal{E}_M$ and $\mathcal{E}_L$, which serves as error bound for the effective Lindbladian approximation.

In order to derive Eq. (37), one starts from the Wangsness-Bloch-Redfield approximation which can be written as [74, 75, 78, 81]

$$\dot{\rho}(t) = \mathcal{D}_R(t)\rho(t) + \mathcal{E}_M, \quad (39)$$

where $\mathcal{E}_M$ is the error introduced by this approximation. The retarded dissipator is given by

$$\mathcal{D}_R(t) = \int_{-\infty}^{t} dt' \Delta_1(t, t'), \quad (40)$$

where the bath memory kernel superoperator, $\Delta_1(t, t')$, is (in the interaction picture) defined by

$$\Delta_1(t, t')\mathcal{O} = -\text{tr}_B[H_I(t), [H_I(t'), \mathcal{O}]]. \quad (41)$$

Here tr_B indicates a trace over the bath degrees of freedom. We note that the Born (weak-coupling) approximation has been used to derive Eq. (39). The error of the approximation may be bounded as [95]

$$\mathcal{E}_M \leq 2g\tilde{\Gamma} \int_0^{\infty} dt \, t \, |B(t)|, \quad (42)$$

with

$$\tilde{\Gamma} = g \int_0^\infty dt \, |B(t)| . \qquad (43)$$

The latter quantity serves as bound for the rate of change of the reduced density matrix in the maximal eigenvalue norm,

$$||\dot{\rho}(t)|| \leq \tilde{\Gamma}. \qquad (44)$$

Nathan and Rudner [3] also show that the Born approximation alone introduces an error of size $\mathcal{E}_M/2$, and thus, in a sense, is already equivalent to the full Born-Markov approximation, which accounts for an additional error bounded by $\mathcal{E}_M/2$. We note that this argument only holds true on short time scales, since small deviations in $\dot{\rho}(t)$ may lead to very different long-time limits.

From the above starting point, one then derives the following bound [3]:

$$\dot{\rho}(t) = \mathcal{L}(t)\rho(t) + \mathcal{E}_M + \mathcal{E}_L. \qquad (45)$$

This equation is of Lindblad form, see Eq. (37), with the single jump operator L in Eq. (38) and the rate $\Gamma = 1$. The Lamb shift contribution H_{LS} is discussed in Sec. III C below. The new error term, $\mathcal{E}_L$, is bounded according to

$$\mathcal{E}_L \leq 2g\tilde{\Gamma} \int_0^\infty dt dt' \, t \, |h(t)| \, |h(t')| , \qquad (46)$$

$$h(t) = \frac{1}{2\pi} \int_{-\infty}^\infty d\omega \, \sqrt{B(\omega)} e^{-i\omega t}.$$

Moreover, one finds [3]

$$\mathcal{E}_M, \mathcal{E}_L \leq \mathcal{E}, \quad \mathcal{E} = \eta \tilde{\Gamma}, \qquad (47)$$

where we define the dimensionless number

$$\eta = 2g \int_{-\infty}^\infty dt dt' \, |t \, h(t)| \, |h(t')| . \qquad (48)$$

The effective Lindbladian approximation is then justified for $\eta \ll 1$.

We emphasize that the error bound $\mathcal{E}$ is conservative. Taking, e.g., a thermal bosonic bath, the error bound diverges in the infinite-temperature limit owing to the presence of $n_B(\nu)$ in Eq. (16), even though the Markovian approximation should be valid in this limit. Furthermore, $\mathcal{E}$ tends to be at least an order of magnitude larger than $\mathcal{E}_M$ in the cases considered below. For the numerical results shown in Sec. III, we have chosen model parameters in a conservative manner, such that $\mathcal{E}$ is at most comparable to the slowest non-vanishing decay rate of the problem. However, we expect that the effective Lindbladian approximation remains accurate even when less conservative parameters are chosen. Moreover, since $\mathcal{E} \propto g^2$, the error bound can always be made arbitrarily small against the relevant relaxation and decoherence rates by reducing g, since those rates already receive contributions $\propto g$. We discuss the error bound in more detail in Sec. III B 1.

III. RESULTS

A. Results for generic environments

Making use of the effective Lindbladian approximation, see Eqs. (37) and (38), we obtain an explicit expression for the Liouvillian, $\mathcal{L}$, that holds for an arbitrary bath correlation function $B(\omega)$. Just as the Hamiltonian is a block-diagonal operator, the Liouvillian is a block-diagonal superoperator. We parametrize the reduced density matrix as

$$\rho = \begin{pmatrix} \rho_+ & \rho_c \\ \rho_c^\dagger & \rho_- \end{pmatrix}, \quad \rho_i = \begin{pmatrix} a_i & b_i \\ c_i & d_i \end{pmatrix}, \quad i = \pm, c, \qquad (49)$$

where the diagonal blocks $\rho_\pm$ refer to the parity $s = \pm 1$ in Eq. (5). Noting that $b_\pm = c_\pm^*$, the time evolution is given by $(i = \pm, c)$

$$\rho_i(t) = e^{\mathcal{L}_i t}\rho_i(t = 0). \qquad (50)$$

We refer the reader to App. B for the explicit form of the superoperators $\mathcal{L}_i$. Their complex-valued eigenvalues, $\{\Lambda_j^i\}$, contain information about the rate of change in the corresponding density matrix block i. Specifically, the respective decay rates are given by

$$\Gamma_j^i = -\operatorname{Re}\Lambda_j^i. \qquad (51)$$

For the diagonal blocks $(i = s = \pm)$, the problem is formally identical to a single spin-boson model, see Sec. II D. There is one zero eigenvalue, $\Lambda_0^s = 0$, corresponding to the steady state reached at very long times. To lowest order in g and using Eq. (51), we obtain the decay rates describing the approach to the steady state,

$$\Lambda_1^s = -g\frac{\Delta_s^2}{4E_s^2}[B(E_s) + B(-E_s)] + \mathcal{O}(g^3), \qquad (52a)$$

$$\Lambda_{2,\pm}^s = -\frac{g}{8E_s^2}\left(\Delta_s^2[B(E_s) + B(-E_s)] + 4\epsilon^2 B(0)\right)$$
$$\pm iE_s + \mathcal{O}(g^2), \qquad (52b)$$

with Δ_s in Eq. (34) and E_s in Eq. (6). For a parity readout of the dot-MBS system, these rates describe how fast the dot charge (or the quantum capacitance) will reach its final value at long times. The respective density matrix block in this long-time limit is determined by the kernel of $\mathcal{L}_i$. For the diagonal block with $s = \pm 1$, using the energy eigenbasis (6), we obtain

$$\rho_s(\infty) = \frac{1}{A_s^+ + A_s^-} \begin{pmatrix} A_s^- & -i\frac{g}{E_s}A_s^c \\ i\frac{g}{E_s}A_s^c & A_s^+ \end{pmatrix}, \qquad (53)$$

with the quantities

$$A_s^\pm = \frac{\Delta_s^2}{4E_s^2}B(\pm E_s), \quad A_s^c = A_s^- n_s^+ - A_s^+ n_s^-, \qquad (54)$$

$$n_s^\pm = \frac{\Delta_s \epsilon}{8E_s^2}\sqrt{B(0)}\left(3\sqrt{B(\pm E_s)} - \sqrt{B(\mp E_s)}\right).$$

In addition, to order $\mathcal{O}(g)$, the steady-state expectation value for the dot occupation number in block $s = \pm 1$ is given by

$$\langle n_d(\infty) \rangle_s = \frac{1}{2} \left(1 - \langle \sigma_z(\infty) \rangle_s \right)$$

$$= \frac{1}{2} \left(1 - \frac{\epsilon}{E_s} \frac{B(E_s) - B(-E_s)}{B(E_s) + B(-E_s)} \right). \quad (55)$$

Similarly, the respective saturation value for the quantum capacitance follows as $\frac{d}{d\epsilon} \langle n_d(\infty) \rangle_s$.

Finally, for the coherence block $(i = c)$, one finds only non-zero eigenvalues. Up to order $\mathcal{O}(g^2)$ terms, with $p_1, p_2 = \pm 1$, they are given by

$$\Lambda^c_{p_1, p_2} = -\frac{g}{2} \left(A^{p_2}_{p_1} + A^{-p_1 p_2}_{-p_1} + 2 K^{p_1} \right) + i p_2 f^{p_1}, \quad (56)$$

with the quantities $A^{\pm}_s$ in Eq. (54) and

$$K^{\pm} = \frac{\epsilon^2 (f^{\pm})^2}{2 E_+^2 E_-^2} B(0), \quad f^{\pm} = \frac{1}{2}(E_+ \pm E_-). \quad (57)$$

We now proceed by illustrating these general results for the specific environments in Sec. II C.

B. Results for specific environments

One of the main results of this work is stated in Eq. (56), which yields the rates $\Gamma^c_{p_1 p_2} = -\operatorname{Re} \Lambda^c_{p_1 p_2}$ (with $p_1, p_2 = \pm 1$) governing the decay of quantum coherence shared by the two parity subblocks $s = \pm 1$, see Eq. (5). Along with the (known) relaxation rates for the spin-boson model [83], see Eqs. (52a) and (52b), these results allow one to obtain explicit estimates for the relaxation and/or decoherence time scales characterizing the dot-MBQ system coupled to a generic environment with the correlator $B(\omega)$. In this subsection, we examine these results for the specific environments in Sec. II C.

1. Thermal bath of bosons

We begin with a bosonic bath in thermal equilibrium, see Sec. II C 1. For an Ohmic bath, the correlator $B_{\text{th}}(\omega)$ is given by Eq. (17). We choose an exponential cutoff function, $\mathcal{C}(\omega, \omega_c) = e^{-|\omega|/\omega_c}$, where ω_c is the bath cutoff frequency.

First, in order to obtain the dimensionless number $\eta = \eta_{\text{th}}$, we have numerically computed the integrals in Eq. (48) as a function of $k_B T / \omega_c$. The error bounds discussed in Sec. II E imply the condition $\eta_{\text{th}} \ll 1$ for the effective Lindbladian approximation. Within the temperature range

$$0.001 \omega_c \lesssim k_B T \lesssim 10 \omega_c, \quad (58)$$

we find $\eta_{\text{th}} < 100g$, with a broad minimum at $\eta_{\text{th}} \approx 10g$ around $k_B T \approx 0.1 \omega_c$. For small system-bath couplings,

say, $g \lesssim 0.001$, we conclude that the effective Lindbladian approximation is safely controlled within the temperature window (58). The error bound $\mathcal{E}_{\text{th}} = \eta_{\text{th}} \tilde{\Gamma}$, see Eq. (47), is then smaller than the predicted decay rates. The error bound may, however, become larger for either very low or very high temperatures. The case of very high temperatures has already been discussed in Sec. II E. Moreover, in the zero-temperature limit, one generally expects the Lindblad equation to break down [78, 83]. However, let us also recall that this error bound is conservative, and the actual error introduced by the effective Lindbladian approximation may in fact be much smaller, see Sec. II E. Finally, we note that for the numerical calculation of η_{th}, we have used a long-time integration cutoff $t_{\max}$ in Eq. (48), which physically corresponds to the total duration of the measurement. Sending $t_{\max} \to \infty$, one encounters a weak logarithmic divergence of η_{th}, see also Refs. [2, 3].

For the diagonal blocks $\mathcal{L}_i$ with $i = s = \pm 1$, we recover from Eqs. (52a) and (52b) the known thermalization rates of the spin-boson model to lowest order in the coupling g [83],

$$\Gamma^s_{1,\text{th}} = \frac{\pi g \Delta_s^2}{4 E_s} e^{-E_s/\omega_c} \coth \left(\frac{E_s}{2 k_B T} \right),$$

$$\Gamma^s_{2,\text{th}} = \frac{1}{2} \Gamma^s_{1,\text{th}} + \frac{\pi g}{2} \frac{\epsilon^2}{E_s^2} k_B T. \quad (59)$$

These rates tell us how quickly thermalization occurs, i.e., on which time scales the density matrix of the combined dot-MBS system will approach the thermal state in Eq. (10). Turning to the coherences between the $s = +1$ and $s = -1$ sectors, Eq. (56) yields the corresponding four decay rates to order $\mathcal{O}(g)$. With $p_1, p_2 = \pm 1$, we find

$$\Gamma^c_{p_1, p_2, \text{th}} = \frac{\pi g}{8} \left\{ \frac{\Delta_{p_1}^2}{2 E_{p_1}} e^{-\frac{E_{p_1}}{\omega_c}} \left[\coth \left(\frac{E_{p_1}}{2 k_B T} \right) + p_2 \right] \right.$$

$$+ \frac{\Delta_{-p_1}^2}{2 E_{-p_1}} e^{-\frac{E_{-p_1}}{\omega_c}} \left[\coth \left(\frac{E_{-p_1}}{2 k_B T} \right) - p_1 p_2 \right]$$

$$\left. + \frac{\epsilon^2 (E_+ + p_1 E_-)^2}{E_+^2 E_-^2} k_B T \right\}. \quad (60)$$

Three of these rates approach a finite value as $T \to 0$ and therefore describe parity thermalization of the coupled dot-MBS system. However, the smallest rate, $\Gamma^c_{1,\text{th}} \equiv \Gamma^c_{+,-,\text{th}}$, vanishes in the $T \to 0$ limit and corresponds to a dephasing rate for inter-parity quantum coherence. From Eq. (60), we find the low-temperature behavior

$$\Gamma^c_{1,\text{th}}(T \to 0) \simeq \frac{\pi g}{8} \frac{\epsilon^2 (E_+ - E_-)^2}{E_+^2 E_-^2} k_B T. \quad (61)$$

Figures 5, 6, and 7 illustrate the above results. The decay rates in the diagonal sector, see Eq. (59), are shown in Fig. 5, while the decay of quantum coherence between the two parity sectors is shown in Fig. 6, see Eq. (60), and
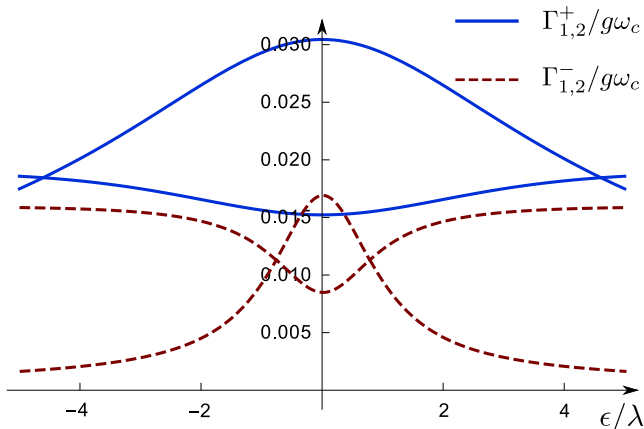
FIG. 5. Thermalization rates $\Gamma^s_{1/2,\text{th}}$ (in units of $g\omega_c$), see Eq. (59), vs ϵ/λ for a thermal boson bath. These rates describe thermalization of the diagonal density matrix blocks with parity $s = \pm 1$, where blue solid (red dashed) curves are for $s = +1$ ($s = -1$). We use the parameters $k_B T = \lambda = 0.01\omega_c$, $a = 1$, and $\phi = \pi/3$.
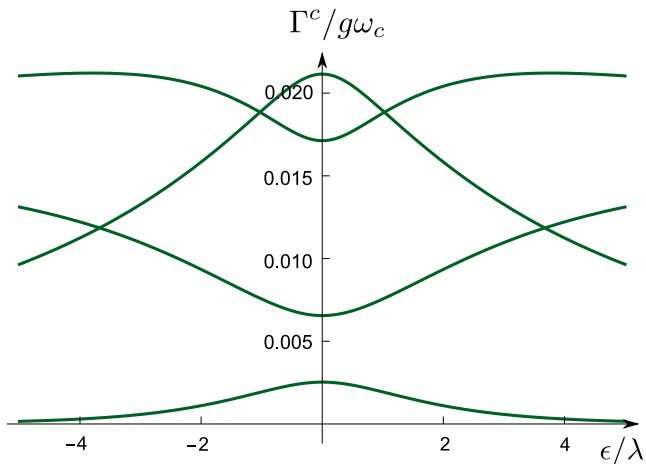

FIG. 6. Rates describing the decay of quantum coherence between different parity sectors, see Eq. (60), for a thermal bosonic bath. We show the four rates $\Gamma^c_{p_1 p_2,\text{th}}$ (in units of $g\omega_c$), see Eq. (60), vs ϵ/λ, for the parameters in Fig. 5.

in Fig. 7. In Figs. 5 and 6, we show the respective rates at fixed temperature as a function of the ratio ϵ/λ between the dot level energy ϵ and the overall tunneling strength λ. We observe that some of the inter-parity decay rates are of the same order of magnitude as the thermalization rates in the parity-diagonal sectors. These inter-parity rates also do not vanish in the $T \to 0$ limit and correspond to thermalization rates of the system. In the long-time limit, the smallest of the rates shown in Fig. 6 dominates the approach to the steady state. The dephasing rate in the off-diagonal parity sector, $\Gamma^c_{1,\text{th}}$, is shown in Fig. 7 and vanishes according to Eq. (61) as $T \to 0$. Our results show that quantum coherence between different parity sectors can persist for long time scales at
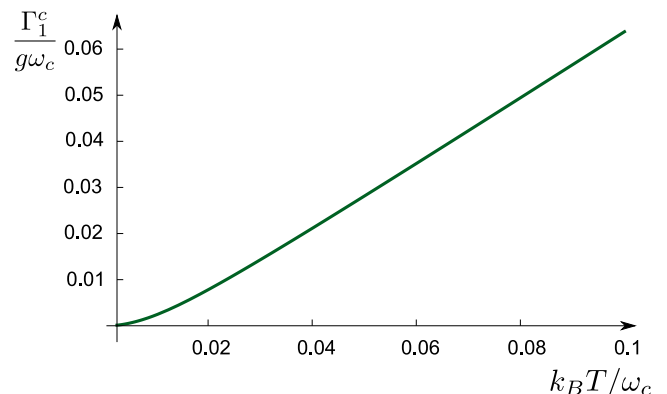

FIG. 7. Inter-parity dephasing rate, $\Gamma^c_{1,\text{th}} = \Gamma^c_{+-,\text{th}}$ (in units of $g\omega_c$), vs $k_B T/\omega_c$ for a thermal bosonic bath, see Eq. (60). We use the parameters in Figs. 5 and 6 with $\epsilon = \lambda/2$. The low-temperature behavior is given by Eq. (61).

low temperatures.

We also note that in the long-time limit, the expectation value of the dot occupation number approaches the thermal equilibrium value. Indeed, Eq. (55) yields

$$\langle n_d(\infty)\rangle_{s,\text{th}} = \frac{1}{2}\left[1 - \frac{\epsilon}{E_s}\tanh\left(\frac{E_s}{2k_B T}\right)\right]. \quad (62)$$

This result holds for arbitrarily small (but finite) g.

As concrete example for a thermal bosonic bath, we now consider the electromagnetic environment corresponding to the circuit in Fig. 3, where the bath correlator has been specified in Eq. (20). In effect, the respective decay rates can then be inferred from the above results by replacing

$$ge^{-\frac{E_s}{\omega_c}} \to g_{LC}\,\mathcal{C}\left(E_s/\omega_{LC}\right), \quad (63)$$

with the Lorentzian cutoff function $\mathcal{C}(\tilde{\omega})$ in Eq. (22). The coupling g_{LC} and the LC resonance frequency ω_{LC} have been specified in Eq. (21). For instance, the first of the two thermalization rates in Eq. (59), for the diagonal sector with parity $s = \pm 1$, is given by

$$\Gamma^s_{1,LC} = \frac{\pi g_{LC}\Delta_s^2}{4E_s}\mathcal{C}\left(\frac{E_s}{\omega_{LC}}\right)\coth\left(\frac{E_s}{2k_B T}\right), \quad (64)$$

with Δ_s in Eq. (34). Similarly, we find from Eq. (61) the low-temperature behavior of the dephasing rate for inter-parity quantum coherence,

$$\Gamma^c_{1,LC} \simeq \frac{g_{LC}}{4}\frac{\omega_{LC}}{\omega_1 + \omega_2}\frac{\epsilon^2(E_+ - E_-)^2}{E_+^2 E_-^2}k_B T, \quad (65)$$

with $\omega_{1,2} = 1/(R_{1,2}C)$.

2. QPC detector

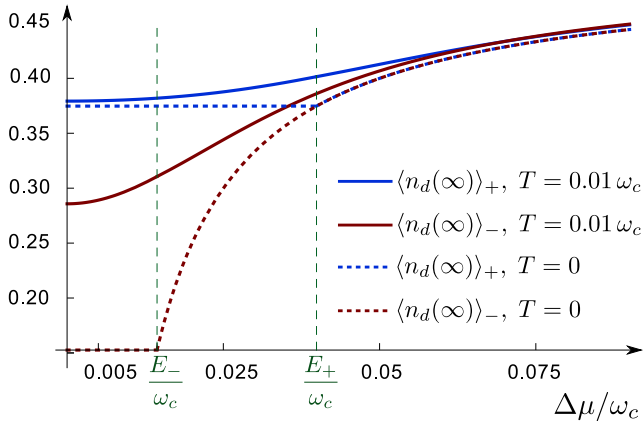We next turn to the nonequilibrium environment corresponding to the QPC measurement setup shown in Fig. 4,

FIG. 8. Steady-state dot occupation number, $\langle n_d(\infty)\rangle_s$, vs potential bias $\Delta\mu$ for the QPC parity readout with $s = \pm 1$, see Sec. III B 2, obtained from Eq. (55) with Eq. (66), $\epsilon = 0.01\omega_c$, $\lambda = \epsilon$, $a = 1$, and $\phi = \pi/3$. The system energies $E_\pm$ in Eq. (6) are shown as green vertical dashed lines. Blue (red) curves are for parity $s = +1$ ($s = -1$). Solid curves are for $k_B T = 0.01\omega_c$. The corresponding analytical $T = 0$ results, Eq. (68), are shown as dashed curves.

see Sec. II C 2. For this QPC charge readout of the parity of the dot-MBQ state, the bath correlator is given by Eq. (31). For simplicity, we focus on the effect of the potential gradient $\Delta\mu = \mu_L - \mu_R > 0$ across the QPC, and neglect the purely thermal contribution to $B_{\text{QPC}}(\omega)$, which on its own has already been studied in Sec. III B 1. For $\Delta\mu \ll \omega_c$, we thus take the bath correlator responsible for the QPC charge readout as

$$B_{\text{QPC}}(\omega) \simeq \frac{\pi}{2} \sum_{p=\pm} (\omega + p\Delta\mu) e^{-|\omega + p\Delta\mu|/\omega_c}$$
$$\times \left[\coth\left(\frac{\omega + p\Delta\mu}{2k_B T} \right) + 1 \right]. \quad (66)$$

In this case, our numerical analysis of Eq. (48) shows that with increasing potential bias $\Delta\mu$, the parameter η becomes smaller. In a sense, the bias $\Delta\mu$ acts like an effective temperature and by increasing its value, the memory time of the bath becomes shortened [96]. For example, using $\Delta\mu = 0.1\omega_c$ and $g = 0.001$, we find that in contrast to Eq. (58), the effective Lindbladian approximation stays accurate for all temperatures $k_B T \lesssim 10\omega_c$, down to zero temperature.

Let us now turn to the zero-temperature limit in order to study how decoherence in our system will depend on $\Delta\mu$. For $T = 0$ and $0 < E_s, \Delta\mu \ll \omega_c$, Eq. (66) simplifies to

$$B_{\text{QPC},T=0}(\omega) \approx \pi \sum_{p=\pm} |\omega + p\Delta\mu|\, \Theta(\omega + p\Delta\mu), \quad (67)$$

where $\Theta(x)$ is the Heaviside step function. Moreover, from Eq. (55), we obtain the average steady-state dot occupation number as

$$\langle n_d(\infty)\rangle_s = \begin{cases} \frac{1}{2}(1 - \epsilon/E_s), & \Delta\mu < E_s, \\ \frac{1}{2}(1 - \epsilon/\Delta\mu), & \Delta\mu \geq E_s. \end{cases} \quad (68)$$

In order to read out the parity $s = \pm 1$, we evidently cannot have $\Delta\mu \geq E_s$ for both values of s. On the other hand, if $\Delta\mu < E_s$ for both s, the dependence on $\Delta\mu$ drops out completely, resulting in the optimal case of maximum visibility. We illustrate the average steady-state dot occupation number in Fig. 9, where we observe that while the above $T = 0$ argument basically carries over to the finite temperature case, the sharp changes at $\Delta\mu = E_s$ in Eq. (68) are smeared out by thermal fluctuations.

The smallest non-vanishing decay rate at $T = 0$ in the diagonal block with parity $s = \pm 1$ is then given by

$$\Gamma_1^s = \frac{\pi g}{4} \frac{\Delta_s^2}{E_s^2} \times \begin{cases} E_s, & \Delta\mu < E_s, \\ \Delta\mu, & \Delta\mu \geq E_s. \end{cases} \quad (69)$$

For the optimal visibility case with $\Delta\mu < E_s$ for both values of s, this result formally coincides with the smallest thermal rate at zero temperature, see Eq. (59). Importantly, the decay rate is then insensitive to the value of the potential bias $\Delta\mu$. For the decay of the off-diagonal coherences, we find that the $T = 0$ dephasing rate, $\Gamma_1^c(\Delta\mu)$, depends linearly on the potential bias for $\Delta\mu < E_\pm$,

$$\Gamma_1^c(T = 0, \Delta\mu) \simeq \frac{\pi g}{16} \frac{\epsilon^2 (E_+ - E_-)^2}{E_+^2 E_-^2} \Delta\mu. \quad (70)$$

By comparing this result to the thermal rate in Eq. (61), we observe that the potential bias plays the role of an effective temperature, as expected on general grounds [96]. In the opposite limit, $k_B T \gg \Delta\mu$, the dephasing rate is basically described by the results in Sec. III B 1.

Figure 9 illustrates the dephasing rate Γ_1^c for the case of a QPC detector, as a function of both temperature and bias voltage. These results were obtained from Eq. (56). We first observe that at low temperatures, the dephasing rate increases with increasing potential bias. This behavior is expected because the potential bias acts as effective temperature. On the other hand, for $k_B T \gtrsim \Delta\mu$, the potential bias has little effect on the rate which now is dominated by thermal fluctuations. Next, we note that in the potential bias window where different parity states can be distinguished with good visibility, the time scale $\tau_M = 1/\Gamma_1^c$ for the off-diagonal coherence to decay, and hence the time it takes to make a projective measurement of the parity $s = \pm 1$, is limited to a time of the order $\tau_M \approx 10^6/\omega_c$. On the other hand, the readout time is determined by $\tau_R = \min_s 1/\Gamma_1^s$, i.e., in terms of the decay rates in the diagonal sector. Now τ_R is typically shorter than τ_M, which implies that if the system parameters are chosen such that the final state allows one to distinguish the two values of s, the time τ_M will effectively determine
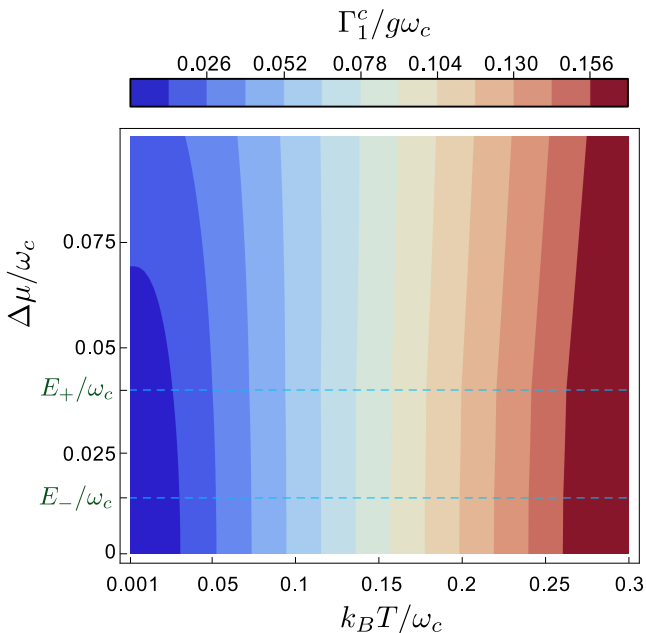
FIG. 9. Dephasing rate for parity off-diagonal quantum coherence, Γ_1^c (in units of $g\omega_c$), in the T-$\Delta\mu$ plane, for the case of a QPC readout environment with $\epsilon = \lambda = 0.01\omega_c, a = 1$, and $\phi = \pi/3$. The dashed horizontal lines correspond to $\Delta\mu = E_{s=\pm}$, see Eqs. (6) and (68).

the readout time of the measurement. Finally, we note that from Fig. 8, one observes that for good visibility, one needs $\Delta\mu \lesssim E_+$. This observation suggests that a readout procedure with an initially larger value of $\Delta\mu$ may be advantageous since in this manner one can speed up the off-diagonal decay. Subsequently using a smaller potential bias $\Delta\mu$, one can then maximize visibility.

C. Lamb shift

The Lamb shift can be thought of as a renormalization of the dot-MBQ energies by the bath modes. This renormalization does not contribute to decay rates but contributes to the effective Hamiltonian appearing in the Liouvillian. So far we have not discussed the corresponding term, H_{LS}, which appears in the coherent time evolution part of Eq. (37). The Lamb shift could potentially be important for the readout, for instance, by reducing the visibility in the readout via s-dependent shifts of the average dot occupation $\langle n_d \rangle_s$.

In this subsection, we show that for $E_\pm \ll \omega_c$, H_{LS} only causes an s-independent constant energy shift. As a consequence, the Lamb shift is not expected to affect the readout visibility for our dot-MBQ setups.

In the eigenbasis of H_0, defined by $H_0 |p, s\rangle = \left(\frac{\epsilon}{2} + \frac{p}{2} E_s\right) |p, s\rangle$ for $p = \pm 1$, see Eq. (6), the Lamb shift in the effective Lindbladian approximation takes the form

[3]

$$H_{LS} = \frac{g}{16} \sum_{p,q,r,s=\pm 1} Z_{pq,s} Z_{qr,s} \tag{71}$$

$$\times \left[Q\left(\frac{p-q}{2} E_s\right) + Q\left(\frac{q-r}{2} E_s\right) \right] |p, s\rangle\langle r, s|,$$

$$Q(\omega) = \frac{\mathcal{P}}{\pi} \int_{-\infty}^{\infty} d\nu \frac{B(\nu)}{\omega - \nu},$$

where $\mathcal{P}$ denotes the principal part of the integral and $B(\nu)$ is the bath correlator for the respective environment. We employ the quantities

$$Z_{pq,s} \equiv \langle p, s | \sigma_z | q, s \rangle = \begin{cases} -p\epsilon/E_s, & p = q, \\ \Delta_s/E_s, & p = -q, \end{cases} \tag{72}$$

with Δ_s in Eq. (34), such that Eq. (71) can be written as

$$H_{LS} = \frac{g}{8} \sum_s \left(\frac{\epsilon^2 Q(0)}{E_s^2} + \frac{\Delta_s^2 [Q(E_s) + Q(-E_s)]}{2E_s^2} \right) \Pi_s, \tag{73}$$

where Π_s is the projector onto the diagonal parity block with $s = \pm 1$. The Lamb shift therefore shifts the energies in each block.

We next discuss the form of H_{LS} for the different environments introduced above. Using Eq. (73) and symmetry relations obeyed by $B(\omega)$ corresponding to Eq. (12), we find that the Lamb shift H_{LS} is independent of temperature. Crucially, for $E_s \ll \omega_c$, we will show that the energy shift is s-independent for all these cases, and therefore it indeed is irrelevant with respect to the parity readout. The Lamb shift is also negligible with regard to the average dot occupation $\langle n_d(\infty)\rangle_s$, since Eq. (62) is already determined by contributions of order $\mathcal{O}(g^0)$.

1. Thermal boson bath

We first evaluate Eq. (73) for thermal bosons. For an Ohmic bath, using the bath correlator $B_{\text{th}}(\omega)$ in Eq. (17) with an exponential cutoff function, Eq. (73) yields the result

$$H_{LS} = \frac{g\omega_c}{8} \sum_{p,s=\pm} \left[1 + \frac{\Delta_s^2}{2E_s^2} \xi\left(\frac{E_s}{\omega_c}\right) \right] |p, s\rangle\langle p, s|, \tag{74}$$

where $\xi(x) = xe^x \text{Ei}(-x) - xe^{-x} \text{Ei}(x)$ with the exponential integral, $\text{Ei}(x) = -\int_x^\infty dt e^{-t}/t$. Using $\xi(x) \to 0$ for $x \to 0$, we find that for $E_\pm \ll \omega_c$, Eq. (74) reduces to the constant energy shift $g\omega_c/8$ which does not affect the parity readout.

Next we turn to the electromagnetic environment in Fig. 3, with the bath correlator $B_{LC}(\omega)$ in Eq. (20), where the Lamb shift takes a more complicated form. Using the cutoff function $\mathcal{C}(\tilde{\omega})$ in Eq. (20) with $\omega_c = \omega_{LC}$,

we find

$$Q(0) = \frac{e^2}{4C} \mathcal{P} \int_{-\infty}^{\infty} d\tilde{\omega}\, \mathcal{C}(\tilde{\omega})$$

$$Q(E_s) + Q(-E_s) = \frac{e^2}{4C} \mathcal{P} \int_{-\infty}^{\infty} d\tilde{\omega}\, \mathcal{C}(\tilde{\omega}) \qquad (75)$$

$$\times \left(\frac{\tilde{\omega}}{\tilde{\omega} + \frac{E_s}{\omega_{LC}}} + \frac{\tilde{\omega}}{\tilde{\omega} - \frac{E_s}{\omega_{LC}}} \right).$$

Using these expressions, we observe that the s-dependence drops out again in H_{LS} in the parameter regime $E_{\pm} \ll \omega_c = \omega_{LC}$.

2. Lamb shift for QPC

For the QPC case, we find the Lamb shift

$$H_{LS} = \frac{g\omega_c}{8} \sum_{p,s} \left(1 + \frac{\epsilon^2}{E_s^2} \xi\left(\frac{\Delta\mu}{\omega_c}\right) + \frac{\Delta_s^2}{E_s^2} \xi\left(\frac{E_s}{\omega_c}\right) \right)$$

$$\times |p,s\rangle\langle p,s|, \qquad (76)$$

where $\xi(x)$ has been defined after Eq. (74). As in the thermal case, in the limit $E_{\pm}, \Delta\mu \ll \omega_c$, the Lamb shift has no consequences for the parity readout.

IV. OUTLOOK

The model we have introduced provides a flexible framework, which may be adapted to study other experimental setups and dephasing mechanisms related to the parity-charge conversion process, see also Refs. [67, 97]. Below we sketch possible extensions of our work that we find particularly interesting. However, a more detailed study of these points goes beyond the scope of this paper.

A. Dispersive readout

One could use our framework to model the effect of dispersive readouts of Majorana qubits [21, 98]. To that end, we consider the electromagnetic environment shown in Fig. 3. To include the effects of the dispersive readout, however, one should explicitly include the driving fields into the model for the environment. This step will modify $B(t)$ significantly, leading to dephasing already at zero temperature. From this point on, our approach should then be applicable again. In particular, by calculating $\langle n_d(\infty)\rangle_s$, one can obtain the impedance shift of the system, from which the resulting amplitude and phase shifts of the reflected signal corresponding to the values $s = \pm 1$ can be deduced.

B. Other dephasing mechanisms

Above, we have studied dephasing caused by the measurement circuit during the MBQ readout. In this subsection, we describe how intrinsic sources of dephasing can be included in the formalism. In particular, we discuss how the time evolution of the density matrix will be changed due to residual Majorana overlap integrals and/or because of quasiparticle poisoning effects.

When allowing for quasiparticles to relax to or be excited from the zero-energy MBS sector, we need, because of total parity conservation, an additional quantum number describing whether the quasiparticle sector has even or odd occupancy. The total parity of the MBSs and the quantum dot is given by

$$p = -i\gamma_1\gamma_2\gamma_3\gamma_4\eta_1\eta_2, \qquad (77)$$

such that $p = \pm 1$ is the quantum number that keeps track of whether the quasiparticle number parity has changed. We can then define MBQ Pauli operators $\mathbf{s} = (s_x, s_y, s_z)$ as

$$\begin{aligned} s_x &= \gamma_1\gamma_3\eta_1\eta_2 = i\gamma_2\gamma_4 p, \\ s_y &= \gamma_1\gamma_4\eta_1\eta_2 = -i\gamma_2\gamma_3 p, \\ s_z &= \gamma_1\gamma_2\eta_1\eta_2 = i\gamma_3\gamma_4 p. \end{aligned} \qquad (78)$$

In a similar way, we can write the original Pauli operators $\tilde{\sigma}_\alpha$, see Eq. (33), as

$$\begin{aligned} \tilde{\sigma}_x &= -i\gamma_1\eta_2 = \gamma_2\gamma_3\gamma_4\eta_1 p, \\ \tilde{\sigma}_y &= i\gamma_1\eta_1 = \gamma_1\gamma_3\gamma_4\eta_1 p, \\ \tilde{\sigma}_z &= -i\eta_1\eta_2 = p\gamma_1\gamma_2\gamma_3\gamma_4. \end{aligned} \qquad (79)$$

The two sets of Pauli operators commute, $[s_\alpha, \tilde{\sigma}_{\alpha'}] = 0$ for all α, α'.

1. Majorana overlaps

Dephasing of a Majorana qubit due to finite MBS overlaps has been studied before by Knapp *et al.* [99]. The Majorana overlaps introduce a Hamiltonian term of the form

$$H_{\text{overlap}} = \sum_{i<j} t_{ij} i\gamma_i\gamma_j = \mathbf{s} \cdot [p\mathbf{d}_1 + \tilde{\sigma}_z \mathbf{d}_2], \qquad (80)$$

where the real-valued vectors $\mathbf{d}_1 = (t_{24}, -t_{23}, t_{34})$ and $\mathbf{d}_2 = (t_{13}, t_{14}, t_{12})$ contain the overlap matrix elements t_{ij}. We observe that the MBS overlaps basically cause the Bloch vector of the MBQ to precess around an axis defined by the vectors $\mathbf{d}_1$ and $\mathbf{d}_2$. It is straightforward to include Eq. (80) in the coherent part of the Liouvillian, see Eq. (37). For a detailed discussion of the resulting physics, see Ref. [99].

2. Quasiparticle poisoning

We now consider quasiparticle poisoning caused by excitations out of the MBS ground state sector and/or by the relaxation of thermally generated quasiparticles into the MBS sector. We will assume that the time scales for these two processes are slow, in particular much slower than relaxation within the quasiparticle continuum. Moreover, the time scale for the spatial equilibration of quasiparticles is also assumed to be much shorter than the typical time between subsequent poisoning events. These two assumptions imply that the quasiparticle distribution function is identical for all MBS positions. The Hamiltonian that describes the coupling between quasiparticles and MBSs is then given by [71]

$$H_{qp} = H_F + H_B + H_{pois}, \quad H_F = \sum_k E_k \alpha_k^\dagger \alpha_k,$$

$$H_B = \sum_q \omega_q b_q^\dagger b_q, \quad H_{pois} = \sum_{i=1}^4 \gamma_i \sum_{qk} \Gamma_{iqk} \varphi_q,$$

$$\Gamma_{iqk} = v_{iqk} \alpha_k - v_{iqk}^* \alpha_k^\dagger, \quad \varphi_q = b_q + b_q^\dagger, \qquad (81)$$

where α_k are fermionic annihiliation operators for above-gap Bogoliubov quasiparticles with energy E_k. Moreover, b_q are annihilation operators for bosonic modes (phonons and/or electromagnetic modes) which mediate the coupling between the two fermionic subsystems, ω_q are boson energies, and v_{iqk} are the coupling matrix elements. A key point is now that the quasiparticles have different distribution functions depending on the total quasiparticle number being even or odd. Of course, this statement only holds true for a finite system where parity is conserved, but for closed MBQs, this is indeed the case. The difference between the even and odd quasiparticle number sectors is only significant for temperatures $T \lesssim T^*$, where T^* is the characteristic temperature at which the probability of having a single quasiparticle on the island approaches unity. This cross-over temperature is inversely proportional to the volume V_S of the superconductor and given by [39, 71, 100, 101]

$$T^* \approx \frac{\Delta}{k_B N_{\rm eff}}, \quad N_{\rm eff} = d_S V_S \sqrt{2\pi k_B T \Delta}, \qquad (82)$$

where d_S is the density of states and Δ the pairing gap.

To take total parity conservation into account, we project the Hamiltonian (81) onto the sector with (say) total even occupancy, $H_{qp} \to P_e H_{qp} P_e$, where P_e is the projection operator to total even parity. We also define separate projection operators for quasiparticles and MBSs onto the respective even and odd parity sectors, $P_{e/o}^{qp,M}$. With $P_e = P_e^M P_e^{qp} + P_o^M P_o^{qp}$, the projected poi-

soning Hamiltonian becomes

$$P_e H_{pois} P_e = \sum_{i=1}^4 P_o^M \gamma_i P_e^M \sum_{qk} P_o^{qp} \Gamma_{iqk} \varphi_q P_e^{qp}$$

$$+ \sum_{i=1}^4 P_e^M \gamma_i P_o^M \sum_{qk} P_e^{qp} \Gamma_{iqk} \varphi_q P_o^{qp}. \qquad (83)$$

We can now identify two contributions in Eq. (83). The first term couples the MBQ via the operator $\gamma_{i,e\to o} = P_o^M \gamma_i P_e^M$ to a reservoir with an even number of quasiparticles, while the second term couples it via $\gamma_{i,o\to e} = \gamma_{i,e\to o}^\dagger$ to a reservoir with odd quasiparticle number. Equation (83) allows us to directly apply the effective Lindbladian approximation introduced in Sec. II E. To that end, we define a jump operator for each of the two terms in Eq. (83),

$$L_{e\to o} = \sum_i \sum_{mn} \langle m | \gamma_{i,e\to o} | n \rangle \sqrt{g_{ii}^e(E_n - E_m)} | m \rangle \langle n |,$$
$$(84a)$$

$$L_{o\to e} = \sum_i \sum_{mn} \langle m | \gamma_{i,o\to e} | n \rangle \sqrt{g_{ii}^o(E_n - E_m)} | m \rangle \langle n |,$$
$$(84b)$$

where the two bath functions are given by

$$g_{ij}^{e/o}(t) = -\sum_{qk} \langle \Gamma_{iqk}(t) \Gamma_{jqk}(0) \rangle_{e/o} \langle \varphi_q(t) \varphi_q(0) \rangle. \quad (85)$$

The fermionic expectation value is here taken over quasiparticle distributions in the respective sector with even or odd total occupation number. The functions (85) have also been discussed in Refs. [39, 71, 100–103]. Note that in Eqs. (84a) and (84b) we have neglected coherent transport of quasiparticles between the ends of the topological superconductors. If coherent quasiparticle transfer between the wire ends is important, it can be included by creating jump operators from the square roots of the matrices $g_{ij}^{e/o}(\omega)$ [3].

As final step, we now use the fact that because of the coupling to incoherent quasiparticle reservoirs, the total even and odd ($p = \pm 1$) sectors of the MBQ have no quantum-coherent coupling. We can therefore write the dynamical equations for the MBQ reduced density matrices with even or odd parity, $\rho_{e/o}$, as

$$\dot\rho_e = (\dot\rho_e)^{(0)} - \frac{1}{2} \{ L_{e\to o}^\dagger L_{e\to o}, \rho_e \} + L_{o\to e} \rho_o L_{o\to e}^\dagger, \; (86a)$$

$$\dot\rho_o = (\dot\rho_o)^{(0)} - \frac{1}{2} \{ L_{o\to e}^\dagger L_{o\to e}, \rho_o \} + L_{e\to o} \rho_e L_{e\to o}^\dagger, \; (86b)$$

where $(\dot\rho_{e/o})^{(0)}$ is the time derivative in the absence of quasiparticle poisoning. Finally, we note that the coupling of the MBS sector to the quasiparticle reservoirs will also give rise to Hamiltonian corrections of the same form as the residual overlaps in Eq. (80).

V. CONCLUSIONS

We have developed a flexible theory for calculating the thermalization and dephasing rates for arbitrary quantum states of a Majorana box qubit tunnel-coupled to a quantum dot for parity readout. Our analysis shows that this parity-to-charge conversion process sensitively depends on the choice of the readout device connected to the dot charge. The latter can be thought of as a generic Markovian bosonic environment (heat bath), either in thermal equilibrium or operated under nonequilibrium conditions. Particular care has been taken to properly account for the decay of coherences among blocks with different fermion number parity $s = \pm 1$, where s refers to the parity of the quantum dot together with the two tunnel-coupled Majorana states.

By employing a recently developed effective Lindbladian approximation, the resulting quantum master equation is by construction of Lindblad form, meaning that complete positivity of the density matrix is guaranteed during the entire time evolution. We have provided explicit results for decay rates when the environment consists of a generic thermal boson heat bath. An important special case is defined by the electromagnetic fluctuations in a macroscopic electric circuit connected to the Majorana qubit. In addition, we have examined the nonequilibrium environment corresponding to a Majorana parity readout via conductance measurements of a quantum point contact that is capacitively coupled to the dot. For all these examples, we have derived analytical expressions for decay rates, which in turn can be related to experimentally measurable quantities. By taking into account quasiparticle poisoning and Majorana overlap effects as sketched in Sec. IV, it stands to reason that this theoretical approach can allow for a realistic and powerful description of quantum decoherence in Majorana box qubits.

Note added: After completion of this manuscript, we were informed of a closely related independent manuscript by Steiner and von Oppen [104]. Their conclusions are consistent with our findings. Despite of the overlap between both works, they are largely complementary. While we employ the improved jump operators introduced in Refs. [1–3] and use them to investigate explicit models for the measurement apparatus, Ref. [104] focuses on the stochastic nature of quantum measurements and provides an in-depth analysis of the measurement current.

ACKNOWLEDGMENTS

Appendix A: Bath correlator for QPC detector

In this appendix, we derive the bath autocorrelator $B_{\mathrm{QPC}}(\omega)$ in Eq. (31) for a quantum point contact capacitively coupled to the dot-MQB system, see Fig. 4. We start from the interaction Hamiltonian (23),

$$H_I = \frac{2e^2}{C_m} \hat{\rho}\, n_d, \tag{A1}$$

where $\hat{\rho} = \psi^\dagger \psi$ is the electron density operator in a small (approximately point-like) volume V centered around the longitudinal coordinate $x = 0$ along the QPC. Near this point, the capacitive coupling between the QPC charge density and the dot charge will be most pronounced. Here, ψ is the electron annihilation operator for QPC electrons in this volume, and C_m is the mutual dot-QPC capacitance per volume. The electron spin is accounted for by the factor 2 in Eq. (A1).

As concrete example, we model the QPC as 1D fermion system connected to electron reservoirs on the left and right side, with chemical potentials μ_L and μ_R, respectively. We assume that the capacitive interaction involves the QPC charge density at $x = 0$ only, see Eq. (A1). The QPC itself is modeled by a δ-peak barrier of height $\mathcal{V}_0$ per unit length. The corresponding contribution to the first-quantized Hamiltonian is $V_{\mathrm{QPC}} = \mathcal{V}_0 \delta(x)$. We next express the local QPC fermion operator ψ as

$$\psi = \sum_{\ell = L/R, k} \Psi_{\ell k}(x = 0)\, c_{\ell k}, \tag{A2}$$

where the $c_{\ell k}$ are fermionic annihilation operators corresponding to the single-particle QPC scattering states $\Psi_{\ell k}(x)$ with wave number k originating from reservoir $\ell = L, R$. For the 1D QPC model with a δ-barrier, one finds [105]

$$\Psi_{\ell = L/R, k}(x) = \frac{1}{\sqrt{L_0}} \Big[\left(e^{\pm ikx} + r_k e^{\mp ikx} \right) \Theta(\mp x)$$
$$+ t_k e^{\pm ikx} \Theta(\pm x) \Big], \tag{A3}$$
$$r_k = \frac{1}{i\frac{k}{m\mathcal{V}_0} - 1}, \quad t_k = \frac{1}{1 + i\frac{m\mathcal{V}_0}{k}},$$

where L_0 is the QPC length, m the electron mass, and r_k and t_k are reflection and transmission amplitudes, respectively. The charge density at $x = 0$ follows as

$$\hat{\rho} = \frac{1}{V} \sum_{\ell, \ell' = L, R} \sum_{kk'} \tau_{\ell k, \ell' k'}\, c_{\ell k}^\dagger c_{\ell' k'}, \tag{A4}$$

where $\tau_{\ell k,\ell' k'}$ quantifies the overlap between $\Psi_{\ell k}$ and $\Psi_{\ell' k'}$. For the 1D model with Eq. (A3), we obtain

$$\tau_{\ell k,\ell' k'} = \frac{1}{4}(1 + r_k + t_k)(1 + r_{k'} + t_{k'}), \qquad \text{(A5)}$$

which is independent of the lead indices ℓ, ℓ'. For calculating the bath correlation function, we next assume

$$\left\langle c_{\ell k}^\dagger c_{\ell' k'} \right\rangle = \delta_{\ell\ell'}\delta_{kk'} n_{\mathrm{F},\ell}(\epsilon_{\ell k}), \qquad \text{(A6)}$$

with Fermi-Dirac distribution functions, $n_{\mathrm{F},\ell}(\epsilon) = 1/(e^{\beta(\epsilon-\mu_\ell)}+1)$, and the single-particle eigenenergies, $\epsilon_{\ell k}$, in the bath Hamiltonian H_B, see Eq. (23). Equation (A6) effectively enforces the constraint that electrons thermalize before entering the QPC. We then have

$$\langle \hat{\rho}(t) \rangle = \langle \hat{\rho} \rangle = \frac{1}{V} \sum_{\ell,k} \tau_{\ell k,\ell k}\, n_{\mathrm{F},\ell}(\epsilon_{\ell k}), \qquad \text{(A7)}$$

where $\hat{\rho}(t) = e^{iH_B t}\hat{\rho}e^{-iH_B t}$ and $\tau_{\ell k,\ell k} > 0$. For the 1D example with a δ-barrier, we have $\tau_{\ell k,\ell k} = |t_k|^2$ according to Eq. (A3). With the bath operator φ in Eq. (23), we now observe that Eq. (A7) implies a time-independent linear moment,

$$\langle \varphi(t) \rangle = \langle \varphi \rangle = E_{\mathrm{ref}} \sum_{\ell,k} \tau_{\ell k,\ell k} n_{\mathrm{F},\ell}(\epsilon_{\ell k}). \qquad \text{(A8)}$$

Rewriting the interaction Hamiltonian as

$$H_I = \sqrt{g}n_d(\varphi - \langle\varphi\rangle) + \sqrt{g}n_d \langle\varphi\rangle, \qquad \text{(A9)}$$

we observe that the linear moment in Eq. (A8) can be absorbed by a shift of the dot level energy ϵ,

$$H_I \to \sqrt{g}n_d(\varphi - \langle\varphi\rangle), \quad \epsilon \to \epsilon - \sqrt{g}\langle\varphi\rangle, \qquad \text{(A10)}$$

see Eqs. (2) and (23). With respect to the redefined interaction Hamiltonian, the time-dependent bath autocorrelator in Eq. (12), $B_{\mathrm{QPC}}(t)$, which enters the effective Lindbladian approximation, can be evaluated by using $c_{\ell k}(t) = e^{-i\epsilon_{\ell k}t}c_{\ell k}$ along with Wick's theorem and Eq. (A6). The result is

$$B_{\mathrm{QPC}}(t) = E_{\mathrm{ref}}^2 \sum_{\ell k,\ell' k'} \left|\tau_{\ell k,\ell' k'}\right|^2 e^{i(\epsilon_{\ell k}-\epsilon_{\ell' k'})t}$$
$$\times\, n_{\mathrm{F},\ell}(\epsilon_{\ell k})\left[1 - n_{\mathrm{F},\ell'}(\epsilon_{\ell' k'})\right]. \qquad \text{(A11)}$$

We now introduce the coupling profile function $\Gamma_{\ell\ell'}(\omega,\omega')$ as in Eq. (26), which for the 1D case with a δ-barrier is given by

$$\Gamma_{\ell\ell'}(\omega,\omega') = \frac{\frac{m}{4\pi^2}L_0^2 E_{\mathrm{ref}}^2\sqrt{\omega\omega'}}{\left(\frac{m\mathcal{V}_0^2}{2}+\omega\right)\left(\frac{m\mathcal{V}_0^2}{2}+\omega'\right)}\Theta(\omega)\Theta(\omega'), \qquad \text{(A12)}$$

where we use Eq. (A3) and $\frac{1}{L_0}\sum_k(\cdots) \to \frac{1}{2\pi}\int dk(\cdots)$. Identifying the general form (26) of Γ in Eq. (A11), we find

$$B_{\mathrm{QPC}}(t) = \sum_{\ell,\ell'} \int_{-\infty}^\infty d\omega d\omega'\, \Gamma(\omega,\omega')e^{i(\omega-\omega')t}$$
$$\times\, n_{\mathrm{B}}(\omega-\omega'-\mu_\ell+\mu_{\ell'})\left[n_{\mathrm{F},\ell'}(\omega')-n_{\mathrm{F},\ell}(\omega)\right], \quad \text{(A13)}$$

where we used the identity

$$n_{\mathrm{F}}(\xi)\left[1 - n_{\mathrm{F}}(\xi')\right] = n_{\mathrm{B}}(\xi - \xi')\left[n_{\mathrm{F}}(\xi') - n_{\mathrm{F}}(\xi)\right].$$

Changing variables in Eq. (A13) to $\Omega = (\omega+\omega')/2$ and $\nu = \omega - \omega'$, shifting Ω by $\mu_{\ell\ell'} = (\mu_\ell+\mu_{\ell'})/2$, and finally performing a Fourier transformation, we arrive at Eqs. (24) and (25).

Finally, we note that if we evaluate $\Gamma_{\ell\ell'}\left(\Omega+\mu_{\ell\ell'}-\frac{\omega}{2},\Omega+\mu_{\ell\ell'}+\frac{\omega}{2}\right)$ with the coupling function Eq. (A12) for $E_{\mathrm{ref}} = \mu_0/2$ with $\mu_0 = (\mu_L+\mu_R)/2$ and $m\mathcal{V}_0^2 \ll \mu_0$ as well as $1/(mL_0^2) \ll \mu_0$, we can qualitatively confirm the behavior of $\Gamma_{\ell\ell'}\left(\Omega+\mu_{\ell\ell'}-\frac{\omega}{2},\Omega+\mu_{\ell\ell'}+\frac{\omega}{2}\right)$ assumed below Eq. (26) in order to arrive at the simplification in Eq. (28). For all involved integrals to converge, Γ is here assumed to decay sufficiently fast at large frequencies due to the finite electronic bandwidth in the leads.

Appendix B: Matrix form of the Liouvillian

In this appendix, we specify the full matrix form of the Liouvillian. For a generic environmental correlation function, $B(\omega)$, using the energy eigenstates $|p, s\rangle$ of the combined dot-plus-coupled-MBS system in Eq. (6) and the quantities Δ_s in Eq. (34), the jump operator takes the general form

$$L = -\frac{\sqrt{g}}{2}\sum_{s=\pm 1}\left[\frac{\epsilon\sqrt{B(0)}}{E_s}(|-,s\rangle\langle -,s| - |+,s\rangle\langle +,s|)\right.$$
$$+ \frac{\Delta_s\sqrt{B(-E_s)}}{E_s}|+,s\rangle\langle -,s|$$
$$+ \left.\frac{\Delta_s\sqrt{B(E_s)}}{E_s}|-,s\rangle\langle +,s|\right]. \qquad \text{(B1)}$$

Using the basis in Eq. (49), the matrix form of the Liouvillian contains the blocks $\mathcal{L}_i$ with $i = \pm, c$,

$$\mathcal{L} = \begin{pmatrix} \mathcal{L}_+ & 0 & 0 & 0 \\ 0 & \mathcal{L}_c & 0 & 0 \\ 0 & 0 & \mathcal{L}_c^* & 0 \\ 0 & 0 & 0 & \mathcal{L}_- \end{pmatrix}, \qquad \text{(B2)}$$

with the parity-diagonal blocks ($s = \pm 1$),

$$\mathcal{L}_s = \begin{pmatrix} -gA_s^+ & -gm_s & -gm_s & gA_s^- \\ -gn_s^+ & -gB_s + iE_s & gC_s & gn_s^- \\ -gn_s^+ & gC_s & -gB_s - iE_s & gn_s^- \\ gA_s^+ & gm_s & gm_s & -gA_s^- \end{pmatrix}, \qquad \text{(B3)}$$

and the matrix

$$\mathcal{L}_c = \begin{pmatrix} \mathcal{L}_c^{++} & \mathcal{L}_c^{+-} \\ \mathcal{L}_c^{-+} & \mathcal{L}_c^{--} \end{pmatrix}. \tag{B4}$$

This matrix contains the following 2×2 blocks:

$$\mathcal{L}_c^{+-} = \begin{pmatrix} g j_+^- & g\sqrt{A_+^- A_-^-} \\ g\sqrt{A_-^+ A_+^-} & g q_+^- \end{pmatrix},$$

$$\mathcal{L}_c^{-+} = \begin{pmatrix} g q_+^+ & g\sqrt{A_-^- A_+^+} \\ g\sqrt{A_+^+ A_-^+} & g j_+^+ \end{pmatrix},$$

$$\mathcal{L}_c^{++} = -\begin{pmatrix} \frac{g}{2}\left(A_+^+ + A_-^+\right) + gK^- - if^- & -g j_-^- \\ -g q_-^+ & \frac{g}{2}\left(A_-^- + A_+^+\right) + gK^+ - if^+ \end{pmatrix},$$

$$\mathcal{L}_c^{--} = -\begin{pmatrix} \frac{g}{2}\left(A_+^- + A_-^+\right) + gK^+ + if^+ & -g q_-^- \\ -g j_-^+ & \frac{g}{2}\left(A_+^+ + A_-^-\right) + gK^- + if^- \end{pmatrix}.$$

In the above expressions, we have used the quantities $A_s^\pm$ and $n_s^\pm$ in Eq. (54), and $K^\pm$ and $f^\pm$ in Eq. (57). Moreover, we define

$$B_s = \frac{1}{8E_s^2}\left[\Delta_s^2\left(B(E_s) + B(-E_s)\right) + 4\epsilon^2 B(0)\right],$$

$$C_s = \frac{\Delta_s^2}{4E_s^2}\sqrt{B(E_s)B(-E_s)}, \tag{B5}$$

$$m_s = \frac{\Delta_s \epsilon}{8E_s^2}\sqrt{B(0)}\left(\sqrt{B(E_s)} + \sqrt{B(-E_s)}\right),$$

as well as

$$j_s^\pm = \pm\frac{\Delta_s \epsilon}{8E_s^2 E_{-s}}\sqrt{B(0)}\left[\sqrt{B(\pm E_s)}(2E_s - E_{-s})\right.$$
$$\left. + E_{-s}\sqrt{B(\mp E_s)}\right], \tag{B6}$$

$$q_s^\pm = \pm\frac{\Delta_s \epsilon}{8E_s^2 E_{-s}}\sqrt{B(0)}\left[-\sqrt{B(\pm E_s)}(2E_s + E_{-s})\right.$$
$$\left. + E_{-s}\sqrt{B(\mp E_s)}\right].$$

[1] Gediminas Kiršanskas, Martin Franckié, and Andreas Wacker, "Phenomenological position and energy resolving Lindblad approach to quantum kinetics," Phys. Rev. B **97**, 035432 (2018).

[2] Evgeny Mozgunov and Daniel Lidar, "Completely positive master equation for arbitrary driving and small level spacing," Quantum **4**, 227 (2020).

[3] Frederik Nathan and Mark S. Rudner, "Universal Lindblad equation for open quantum systems," arXiv (2020), 2004.01469.

[4] Chetan Nayak, Steven H. Simon, Ady Stern, Michael Freedman, and Sankar Das Sarma, "Non-Abelian anyons and topological quantum computation," Rev. Mod. Phys. **80**, 1083–1159 (2008).

[5] Frank Wilczek, "Majorana returns," Nat. Phys. **5**, 614–618 (2009).

[6] Marcel Franz, "Viewpoint: Race for Majorana fermions," Physics **3** (2010), 10.1103/Physics.3.24.

[7] Ady Stern, "Non-Abelian states of matter," Nature **464**, 187–193 (2010).

[8] Martin Leijnse and Karsten Flensberg, "Introduction to topological superconductivity and Majorana fermions," Semicond. Sci. Technol. **27**, 124003 (2012).

[9] N. Read and Dmitry Green, "Paired states of fermions in two dimensions with breaking of parity and time-reversal symmetries and the fractional quantum Hall effect," Phys. Rev. B **61**, 10267–10297 (2000).

[10] D. A. Ivanov, "Non-Abelian Statistics of Half-Quantum Vortices in p-Wave Superconductors," Phys. Rev. Lett. **86**, 268–271 (2001).

[11] A. Yu. Kitaev, "Fault-tolerant quantum computation by anyons," Ann. Phys. **303**, 2–30 (2003).

[12] Jason Alicea, Yuval Oreg, Gil Refael, Felix von Oppen, and Matthew P. A. Fisher, "Non-Abelian statistics and topological quantum information processing in 1D wire networks," Nat. Phys. **7**, 412–417 (2011).

[13] Karsten Flensberg, "Non-Abelian Operations on Majorana Fermions via Single-Charge Control," Phys. Rev. Lett. **106**, 090503 (2011).

[14] Jay D. Sau, David J. Clarke, and Sumanta Tewari, "Controlling non-Abelian statistics of Majorana fermions in semiconductor nanowires," Phys. Rev. B **84**, 094505 (2011).

[15] B. van Heck, A. R. Akhmerov, F. Hassler, M. Burrello, and C. W. J. Beenakker, "Coulomb-assisted braiding of Majorana fermions in a Josephson junction array," New J. Phys. **14**, 035019 (2012).

[16] David Aasen, Michael Hell, Ryan V. Mishmash, Andrew Higginbotham, Jeroen Danon, Martin Leijnse, Thomas S. Jespersen, Joshua A. Folk, Charles M. Marcus, Karsten Flensberg, and Jason Alicea, "Milestones Toward Majorana-Based Quantum Computing," Phys. Rev. X **6**, 031016 (2016).

[17] Barbara M. Terhal, Fabian Hassler, and David P. DiVincenzo, "From Majorana fermions to topological order," Phys. Rev. Lett. **108**, 260504 (2012).

[18] Sankar Das Sarma, Michael Freedman, and Chetan Nayak, "Majorana zero modes and topological quantum computation," Quantum Inf. **1**, 15001 (2015).

[19] L. A. Landau, S. Plugge, E. Sela, A. Altland, S. M. Albrecht, and R. Egger, "Towards Realistic Implementations of a Majorana Surface Code," Phys. Rev. Lett. **116**, 050501 (2016).

[20] S. Plugge, L. A. Landau, E. Sela, A. Altland, K. Flensberg, and R. Egger, "Roadmap to Majorana surface codes," Phys. Rev. B **94**, 174514 (2016).

[21] Stephan Plugge, Asbjørn Rasmussen, Reinhold Egger, and Karsten Flensberg, "Majorana box qubits," New J. Phys. **19**, 012001 (2017).

[22] Torsten Karzig, Christina Knapp, Roman M. Lutchyn, Parsa Bonderson, Matthew B. Hastings, Chetan Nayak, Jason Alicea, Karsten Flensberg, Stephan Plugge, Yuval Oreg, Charles M. Marcus, and Michael H. Freedman, "Scalable designs for quasiparticle-poisoning-protected topological quantum computation with Majorana zero modes," Phys. Rev. B **95**, 235305 (2017).

[23] Daniel Litinski, Markus S. Kesselring, Jens Eisert, and Felix von Oppen, "Combining Topological Hardware and Topological Software: Color-Code Quantum Computing with Topological Superconductor Networks," Phys. Rev. X **7**, 031048 (2017).

[24] Liang Fu and C. L. Kane, "Superconducting Proximity Effect and Majorana Fermions at the Surface of a Topological Insulator," Phys. Rev. Lett. **100**, 096407 (2008).

[25] Roman M. Lutchyn, Jay D. Sau, and S. Das Sarma, "Majorana Fermions and a Topological Phase Transition in Semiconductor-Superconductor Heterostructures," Phys. Rev. Lett. **105**, 077001 (2010).

[26] Yuval Oreg, Gil Refael, and Felix von Oppen, "Helical Liquids and Majorana Bound States in Quantum Wires," Phys. Rev. Lett. **105**, 177002 (2010).

[27] A. Cook and M. Franz, "Majorana fermions in a topological-insulator nanowire proximity-coupled to an s-wave superconductor," Phys. Rev. B **84**, 201105(R) (2011).

[28] T.-P. Choy, J. M. Edge, A. R. Akhmerov, and C. W. J. Beenakker, "Majorana fermions emerging from magnetic nanoparticles on a superconductor without spin-orbit coupling," Phys. Rev. B **84**, 195442 (2011).

[29] M. M. Vazifeh and M. Franz, "Self-Organized Topological State with Majorana Fermions," Phys. Rev. Lett. **111**, 206802 (2013).

[30] Jelena Klinovaja, Peter Stano, Ali Yazdani, and Daniel Loss, "Topological Superconductivity and Majorana Fermions in RKKY Systems," Phys. Rev. Lett. **111**, 186805 (2013).

[31] C. W. J. Beenakker, "Search for Majorana Fermions in Superconductors," Annu. Rev. Condens. Matter Phys. **4**, 113–136 (2013).

[32] Stevan Nadj-Perge, Ilya K. Drozdov, Jian Li, Hua Chen, Sangjun Jeon, Jungpil Seo, Allan H. MacDonald, B. Andrei Bernevig, and Ali Yazdani, "Observation of Majorana fermions in ferromagnetic atomic chains on a superconductor," Science **346**, 602–607 (2014).

[33] Steven R. Elliott and Marcel Franz, "Colloquium: Majorana fermions in nuclear, particle, and solid-state physics," Rev. Mod. Phys. **87**, 137–163 (2015).

[34] R. M. Lutchyn, E. P. A. M. Bakkers, L. P. Kouwenhoven, P. Krogstrup, C. M. Marcus, and Y. Oreg, "Majorana zero modes in superconductor–semiconductor heterostructures," Nat. Rev. Mater. **3**, 52–68 (2018).

[35] Antonio Fornieri, Alexander M. Whiticar, F. Setiawan, Elías Portolés, Asbjørn C. C. Drachmann, Anna Keselman, Sergei Gronin, Candice Thomas, Tian Wang, Ray Kallaher, Geoffrey C. Gardner, Erez Berg, Michael J. Manfra, Ady Stern, Charles M. Marcus, and Fabrizio Nichele, "Evidence of topological superconductivity in planar Josephson junctions," Nature **569**, 89–92 (2019).

[36] V. Mourik, K. Zuo, S. M. Frolov, S. R. Plissard, E. P. A. M. Bakkers, and L. P. Kouwenhoven, "Signatures of Majorana Fermions in Hybrid Superconductor-Semiconductor Nanowire Devices," Science **336**, 1003–1007 (2012).

[37] M. T. Deng, C. L. Yu, G. Y. Huang, M. Larsson, P. Caroff, and H. Q. Xu, "Anomalous Zero-Bias Conductance Peak in a Nb–InSb Nanowire–Nb Hybrid Device," Nano Lett. **12**, 6414–6419 (2012).

[38] Jie Liu, Andrew C. Potter, K. T. Law, and Patrick A. Lee, "Zero-Bias Peaks in the Tunneling Conductance of Spin-Orbit-Coupled Superconducting Wires with and without Majorana End-States," Phys. Rev. Lett. **109**, 267002 (2012).

[39] A. P. Higginbotham, S. M. Albrecht, G. Kiršanskas, W. Chang, F. Kuemmeth, P. Krogstrup, T. S. Jespersen, J. Nygård, K. Flensberg, and C. M. Marcus, "Parity lifetime of bound states in a proximitized semiconductor nanowire," Nat. Phys. **11**, 1017–1021 (2015).

[40] S. M. Albrecht, A. P. Higginbotham, M. Madsen, F. Kuemmeth, T. S. Jespersen, J. Nygård, P. Krogstrup, and C. M. Marcus, "Exponential protection of zero modes in Majorana islands," Nature **531**, 206–209 (2016).

[41] M. T. Deng, S. Vaitiekėnas, E. B. Hansen, J. Danon, M. Leijnse, K. Flensberg, J. Nygård, P. Krogstrup, and C. M. Marcus, "Majorana bound state in a coupled quantum-dot hybrid-nanowire system," Science **354**, 1557–1562 (2016).

[42] Fabrizio Nichele, Asbjørn C. C. Drachmann, Alexander M. Whiticar, Eoin C. T. O'Farrell, Henri J. Suominen, Antonio Fornieri, Tian Wang, Geoffrey C. Gardner, Candice Thomas, Anthony T. Hatke, Peter Krogstrup, Michael J. Manfra, Karsten Flensberg, and Charles M. Marcus, "Scaling of Majorana Zero-Bias Conductance Peaks," Phys. Rev. Lett. **119**, 136803 (2017).

[43] Hao Zhang, Chun-Xiao Liu, Sasa Gazibegovic, Di Xu, John A. Logan, Guanzhong Wang, Nick van Loo, Jouri D. S. Bommer, Michiel W. A. de Moor, Diana Car, Roy L. M. Op het Veld, Petrus J. van Veldhoven, Sebastian Koelling, Marcel A. Verheijen, Mihir Pendharkar, Daniel J. Pennachio, Borzoyeh Shojaei, Joon Sue Lee, Chris J. Palmstrøm, Erik P. A. M. Bakkers, S. Das Sarma, and Leo P. Kouwenhoven, "Quantized Majorana conductance," Nature **556**, 74–79 (2018).

[44] Leonid P. Rokhinson, Xinyu Liu, and Jacek K. Furdyna, "The fractional a.c. Josephson effect in a semiconductor–superconductor nanowire as a signature of Majorana particles," Nat. Phys. **8**, 795–799 (2012).

[45] J. Wiedenmann, E. Bocquillon, R. S. Deacon, S. Hartinger, O. Herrmann, T. M. Klapwijk, L. Maier, C. Ames, C. Brüne, C. Gould, A. Oiwa, K. Ishibashi, S. Tarucha, H. Buhmann, and L. W. Molenkamp, "4π-periodic Josephson supercurrent in HgTe-based topological Josephson junctions," Nat. Commun. **7**, 10303 (2016).

[46] Dominique Laroche, Daniël Bouman, David J. van Woerkom, Alex Proutski, Chaitanya Murthy, Dmitry I. Pikulin, Chetan Nayak, Ruben J. J. van Gulik, Jesper Nygård, Peter Krogstrup, Leo P. Kouwenhoven, and Attila Geresdi, "Observation of the 4π-periodic Josephson effect in indium arsenide nanowires," Nat. Commun. **10**, 1–7 (2019).

[47] A. Yu Kitaev, "Unpaired Majorana fermions in quantum wires," Phys. Usp. **44**, 131–136 (2001).

[48] H.-J. Kwon, K. Sengupta, and V. M. Yakovenko, "Fractional ac Josephson effect in p- and d-wave superconductors," Eur. Phys. J. B **37**, 349–361 (2004).

[49] Piotr Stefański, "Transport properties of a quantum dot-mediated fractional Josephson junction," J. Phys.: Condens. Matter **28**, 505301 (2016).

[50] A. M. Whiticar, A. Fornieri, E. C. T. O'Farrell, A. C. C. Drachmann, T. Wang, C. Thomas, S. Gronin, R. Kallaher, G. C. Gardner, M. J. Manfra, C. M. Marcus, and F. Nichele, "Interferometry and coherent single-electron transport through hybrid superconductor-semiconductor Coulomb islands," arXiv (2019), 1902.07085.

[51] A. R. Akhmerov, J. P. Dahlhaus, F. Hassler, M. Wimmer, and C. W. J. Beenakker, "Quantized Conductance at the Majorana Phase Transition in a Disordered Superconducting Wire," Phys. Rev. Lett. **106**, 057001 (2011).

[52] Anindya Das, Yuval Ronen, Yonatan Most, Yuval Oreg, Moty Heiblum, and Hadas Shtrikman, "Zero-bias peaks and splitting in an Al–InAs nanowire topological superconductor as a signature of Majorana fermions," Nat. Phys. **8**, 887–895 (2012).

[53] Eduardo J. H. Lee, Xiaocheng Jiang, Manuel Houzet, Ramón Aguado, Charles M. Lieber, and Silvano De Franceschi, "Spin-resolved Andreev levels and parity crossings in hybrid superconductor–semiconductor nanostructures," Nat. Nanotechnol. **9**, 79–84 (2013).

[54] Jorge Cayao, Elsa Prada, Pablo San-Jose, and Ramón Aguado, "SNS junctions in nanowires with spin-orbit coupling: Role of confinement and helicity on the subgap spectrum," Phys. Rev. B **91**, 024514 (2015).

[55] Pablo San-Jose, Jorge Cayao, Elsa Prada, and Ramón Aguado, "Majorana bound states from exceptional points in non-topological superconductors," Sci. Rep. **6**, 21427 (2016).

[56] Chun-Xiao Liu, Jay D. Sau, Tudor D. Stanescu, and S. Das Sarma, "Andreev bound states versus Majorana bound states in quantum dot-nanowire-superconductor hybrid structures: Trivial versus topological zero-bias conductance peaks," Phys. Rev. B **96**, 075161 (2017).

[57] Chun-Xiao Liu, Jay D. Sau, and S. Das Sarma, "Distinguishing topological Majorana bound states from trivial Andreev bound states: Proposed tests through differential tunneling conductance spectroscopy," Phys. Rev. B **97**, 214502 (2018).

[58] Michael Hell, Karsten Flensberg, and Martin Leijnse, "Distinguishing Majorana bound states from localized Andreev bound states by interferometry," Phys. Rev. B **97**, 161401(R) (2018).

[59] Ching-Kai Chiu and S. Das Sarma, "Fractional Josephson effect with and without Majorana zero modes," Phys. Rev. B **99**, 035312 (2019).

[60] Adriaan Vuik, Bas Nijholt, Anton Akhmerov, and Michael Wimmer, "Reproducing topological properties with quasi-Majorana states," SciPost Physics **7**, 061 (2019).

[61] J. Schulenborg and K. Flensberg, "Absence of supercurrent sign reversal in a topological junction with a quantum dot," Phys. Rev. B **101**, 014512 (2020).

[62] J. Manousakis, C. Wille, A. Altland, R. Egger, K. Flensberg, and F. Hassler, "Weak Measurement Protocols for Majorana Bound State Identification," Phys. Rev. Lett. **124**, 096801 (2020).

[63] Bela Bauer, Torsten Karzig, Ryan Mishmash, Andrey Antipov, and Jason Alicea, "Dynamics of Majorana-based qubits operated with an array of tunable gates,"

[64] Parsa Bonderson, Michael Freedman, and Chetan Nayak, "Measurement-Only Topological Quantum Computation," Phys. Rev. Lett. **101**, 010501 (2008).

[65] Sagar Vijay and Liang Fu, "Teleportation-based quantum information processing with Majorana zero modes," Phys. Rev. B **94**, 235446 (2016).

[66] Christina Knapp, Jukka I. Väyrynen, and Roman M. Lutchyn, "Number-conserving analysis of measurement-based braiding with Majorana zero modes," Phys. Rev. B **101**, 125108 (2020).

[67] Gábor Széchenyi and András Pályi, "Parity-to-charge conversion for readout of topological Majorana qubits," arXiv (2019), 1909.02326.

[68] J. Manousakis, A. Altland, D. Bagrets, R. Egger, and Yoichi Ando, "Majorana qubits in a topological insulator nanoribbon architecture," Phys. Rev. B **95**, 165424 (2017).

[69] Tommy Li, William A. Coish, Michael Hell, Karsten Flensberg, and Martin Leijnse, "Four-Majorana qubit with charge readout: Dynamics and decoherence," Phys. Rev. B **98**, 205403 (2018).

[70] Lupei Qin, Xin-Qi Li, Alexander Shnirman, and Gerd Schön, "Transport signatures of a Majorana qubit and read-out-induced dephasing," New J. Phys. **21**, 043027 (2019).

[71] Morten I. K. Munk, Reinhold Egger, and Karsten Flensberg, "Fidelity and visibility loss in Majorana qubits by entanglement with environmental modes," Phys. Rev. B **99**, 155419 (2019).

[72] Ryan V. Mishmash, Bela rer, Felix von Oppen, and Jason Alicea, "Dephasing and leakage dynamics of noisy Majorana-based qubits: Topological versus Andreev," Phys. Rev. B **101**, 075404 (2020).

[73] A. A. Clerk, M. H. Devoret, S. M. Girvin, Florian Marquardt, and R. J. Schoelkopf, "Introduction to quantum noise, measurement, and amplification," Rev. Mod. Phys. **82**, 1155–1208 (2010).

[74] F. Bloch, "Nuclear Induction," Phys. Rev. **70**, 460–474 (1946).

[75] A. G. Redfield, "The Theory of Relaxation Processes," Adv. Magn. Opt. Reson. **1**, 1–32 (1965).

[76] Vittorio Gorini, Andrzej Kossakowski, and E. C. G. Sudarshan, "Completely positive dynamical semigroups of N-level systems," J. Math. Phys. **17**, 821–825 (1976).

[77] G. Lindblad, "On the generators of quantum dynamical semigroups," Commun. Math. Phys. **48**, 119–130 (1976).

[78] Heinz-Peter Breuer and Francesco Petruccione, *The Theory of Open Quantum Systems* (Oxford University Press, 2002).

[79] Crispin Gardiner and Peter Zoller, *Quantum Noise* (Springer-Verlag Berlin Heidelberg, 2004).

[80] Eric Kleinherbers, Nikodem Szpak, Jürgen König, and Ralf Schützhold, "Relaxation dynamics in a Hubbard dimer coupled to fermionic baths: Phenomenological description and its microscopic foundation," Phys. Rev. B **101**, 125131 (2020).

[81] R. K. Wangsness and F. Bloch, "The Dynamical Theory of Nuclear Induction," Phys. Rev. **89**, 728–739 (1953).

[82] A. O. Caldeira and A. J. Leggett, "Quantum tunnelling in a dissipative system," Ann. Phys. **149**, 374–456 (1983).

[83] Ulrich Weiss, *Quantum Dissipative Systems* (World Scientific Publishing Company, 2011).

[84] M. Field, C. G. Smith, M. Pepper, D. A. Ritchie, J. E. F. Frost, G. A. C. Jones, and D. G. Hasko, "Measurements of Coulomb blockade with a noninvasive voltage probe," Phys. Rev. Lett. **70**, 1311–1314 (1993).

[85] J. M. Elzerman, R. Hanson, J. S. Greidanus, L. H. Willems van Beveren, S. De Franceschi, L. M. K. Vandersypen, S. Tarucha, and L. P. Kouwenhoven, "Few-electron quantum dot circuit with integrated charge read out," Phys. Rev. B **67**, 161308(R) (2003).

[86] Thomas Ihn, Simon Gustavsson, Urszula Gasser, Bruno Küng, Thomas Müller, Roland Schleser, Martin Sigrist, Ivan Shorubalko, Renaud Leturcq, and Klaus Ensslin, "Quantum dots investigated with charge detection techniques," Solid State Commun. **149**, 1419–1426 (2009).

[87] Christopher Bäuerle, D. Christian Glattli, Tristan Meunier, Fabien Portier, Patrice Roche, Preden Roulleau, Shintaro Takada, and Xavier Waintal, "Coherent control of single electrons: a review of current progress," Rep. Prog. Phys. **81**, 056503 (2018).

[88] Reinhold Egger and C. H. Mak, "Low-temperature dynamical simulation of spin-boson systems," Phys. Rev. B **50**, 15210–15220 (1994).

[89] Milena Grifoni and Peter Hänggi, "Driven quantum tunneling," Phys. Rep. **304**, 229–354 (1998).

[90] David P. DiVincenzo and Daniel Loss, "Rigorous Born approximation and beyond for the spin-boson model," Phys. Rev. B **71**, 035318 (2005).

[91] Carsten J. Lindner and Herbert Schoeller, "Dissipative quantum mechanics beyond the Bloch-Redfield approximation: A consistent weak-coupling expansion of the Ohmic spin boson model at arbitrary bias," Phys. Rev. B **98**, 115425 (2018).

[92] G. C. Wick, A. S. Wightman, and E. P. Wigner, "The Intrinsic Parity of Elementary Particles," Phys. Rev. **88**, 101–105 (1952).

[93] Yakir Aharonov and Leonard Susskind, "Charge Superselection Rule," Phys. Rev. **155**, 1428–1431 (1967).

[94] Raymond F. Streater and Arthur S. Wightman, *PCT, Spin and Statistics, and All That* (Princeton University Press, 2000).

[95] Tameem Albash, Sergio Boixo, Daniel A. Lidar, and Paolo Zanardi, "Quantum adiabatic Markovian master equations," New J. Phys. **14**, 123016 (2012).

[96] Alexander Altland and Reinhold Egger, "Nonequilibrium Dephasing in Coulomb Blockaded Quantum Dots," Phys. Rev. Lett. **102**, 026805 (2009).

[97] Pavel P. Aseev, Jelena Klinovaja, and Daniel Loss, "Lifetime of Majorana qubits in Rashba nanowires with nonuniform chemical potential," Phys. Rev. B **98**, 155414 (2018).

[98] Arne L. Grimsmo and Thomas B. Smith, "Majorana qubit readout using longitudinal qubit-resonator interaction," Phys. Rev. B **99**, 235420 (2019).

[99] Christina Knapp, Torsten Karzig, Roman M. Lutchyn, and Chetan Nayak, "Dephasing of Majorana-based qubits," Phys. Rev. B **97**, 125404 (2018).

[100] P. Lafarge, P. Joyez, D. Esteve, C. Urbina, and M. H. Devoret, "Measurement of the even-odd free-energy difference of an isolated superconductor," Phys. Rev. Lett. **70**, 994–997 (1993).

[101] M. T. Tuominen, J. M. Hergenrother, T. S. Tighe, and M. Tinkham, "Even-odd electron number effects in a small superconducting island: Magnetic-field dependence," Phys. Rev. B **47**, 11599–11602(R) (1993).

[102] Diego Rainis and Daniel Loss, "Majorana qubit decoherence by quasiparticle poisoning," Phys. Rev. B **85**, 174533 (2012).

[103] Manuel J. Schmidt, Diego Rainis, and Daniel Loss, "Decoherence of Majorana qubits by noisy gates," Phys. Rev. B **86**, 085414 (2012).

[104] Jacob F. Steiner and Felix von Oppen, "Readout of Majorana Qubits," arXiv (2020), 2004.02124.

[105] David J. Griffiths and Darrell F. Schroeter, *Introduction to Quantum Mechanics* (Cambridge University Press, 2018).

Chapter 3

Project B:
Dephasing of Majorana qubits due to classical noise

In this project we study the effects of local electromagnetic noise on the coherence of Majorana box qubits. The objective in particular is to understand how quickly information is lost in the most ideal situation where the Majoranas don't overlap, and there is no quasiparticle posioning from the outside. The electromagnetic fields are treated as classically fluctuating fields, and non-adiabatic corrections from the field fluctuations lead to transitions to excited states, which flip the ground-state parity. Such processes lead to potential errors in parity readouts. Since the fields are treated classically, the results are only valid when the temperature is much larger than some characteristic energy scale ω_0 in the environment.

The resulting dephasing rate is not found to be exponentially suppressed in the ratio between temperature T and the superconducting energy gap Δ. A partial summation of higher-order terms suggests that a small part of the coherence decays with a much faster rate, independent of temperature. This additional fast loss of coherence scales linearly with temperature. These suprising conclusions may be taken as an indication of model breakdown for temperatures much lower than the superconducting gap.

The technique of finding the instantaneous Majorana zero-energy modes and the non-adiabatic corrections may prove useful for future studies of Majorana readouts, including the slow coupling of the measurement apparatus. Our approach was inspired by the work of Karzig *et al.* [45] and Scheurer *et al.* [68] who studied the effect of moving around Majorana modes in topological nanowires by tuning local chemical potentials. Our technique could expand upon theirs by including statistical averaging of the noise in the time dependent potentials.

The work of this chapter is adapted from my master's thesis *Dephasing of Majorana Box Qubits*, which was defended August 30th 2017, as part of my integrated master's and PhD programme.

1 Introduction

The crux of quantum computation is developing an architecture which is resilient to decoherence. To this end, topological states of matter provide a conceptually promising direction, since they are inherently protected against local interactions. Majorana modes offer a viable implementation as they are thought to have already been experimentally found through zero-bias conductance measurements in proximitized nanowires with large Zeeman splitting and spin-orbit coupling. Although it remains to be proven that the measured zero-bias conductance peaks correspond to topological modes, the discoveries have still sparked excitement for the prospect of scalable, and inherently fault tolerant quantum computation.

One of the suggested architectures for building a quantum computer is based on the so-called Majorana box qubit [63]. This system is in essence a minimal qubit made of Majorana zero-energy modes. It consists of two topologically superconducting 1D nanowires, hosting Majorana zero-energy edge modes γ_1, γ_2, γ_3 and γ_4. The wires are connected by a superconducting backbone, and the system is well isolated from the environment, with a charging energy term

$$E_C(\hat{N} - n_g)^2, \tag{1.1}$$

where $\hat{N}$ is the electron number operator on the island, E_C is very large compared to all other energy scales, and n_g is controlled by a gate voltage. n_g is tuned to be very close to an integer, so the system is *Coulomb blockaded* and the total fermionic parity $P = (-1)^N$, in the system is conserved. In the absence of charging energy, the ground states consist of the states $|n_{12}, n_{34}\rangle$, where $n_{ij} = f_{ij}^\dagger f_{ij}$ is the occupancy of the fermionic mode spanned by the Majorana operators γ_i and γ_j, with the corresponding annihilation operator $f_{ij} = (\gamma_i + i\gamma_j)/2$. Adding the charging energy, the ground-state manifold consists only of linear combinations of $|n_{12}, n_{34}\rangle$, which obey the constraint $-\gamma_1\gamma_2\gamma_3\gamma_4 = P$.

Since quantum information is encoded in the fermionic parities, there are three types of errors that can occur. The first is when transitions between the ground states are caused without changing the overall fermionic parity. The topological nature of the Majorana modes implies that this can only happen using non-local operations, for instance by coupling two Majorana modes directly, by interacting with a non-zero overlap between the two modes or by exciting a quasiparticle in one end of the system and letting it relax at another. The second type of error is when an outside electron enters the system, flipping the total fermionic parity of the island. This is called quasiparticle poisoning, and is suppressed by the large charging energy E_C. The third type of error is when a quasiparticle inside the system is excited, flipping the ground-state parity.

In this project, we investigate a source of the third type of errors. We consider an ideal Majorana qubit, with zero overlap of the Majorana wavefunctions and no external quasiparticle poisoning. Furthermore, we assume that excited quasiparticles do not propagate between the Majorana modes of the system. Our question is then how a Majorana qubit under such idealized assumptions dephases, or phrased in another way, how little dephasing it is theoretically possible to have in a Majorana qubit.

Specifically, we consider electromagnetic noise in the system, and model this as a time-dependent classically fluctuating field $\phi(t)$. If the field fluctuates very slowly, the adiabatic theorem would imply that no quasiparticles are excited, and hence no errors occur. One could then diagonalize the system and find the *instantaneous zero-energy modes* that diagonalize the system at later times, and the quantum information would be perfectly stored by these. By including non-adiabatic corrections however, measurements may lead to quasiparticle excitations and a resulting flip of the ground-state parity. Since $\phi(t)$ is not known, we functionally average over it, using the classical limit for the correlation function $\langle\phi(t)\phi(t')\rangle$ calculated by linear response theory and the fluctuation-dissipation theorem.

2 The model and our measure of dephasing

Consider the setup sketched in Figure 10. The Majorana box qubit is coupled capacitively to an environment impedance Z_0, which for simplicity is taken to be frequency independent. The capacitance gives rise to a classical electric potential energy drop $\phi(t)$, which shifts the chemical potential in the Majorana system. Letting $\phi(0) = 0$, the zero-energy- and continuum modes are shifted over time. We denote the time-dependent instantaneous Majorana zero-energy modes by $\tilde{\gamma}_{i,t}$, and set out to address the following question: If we initialize the system in a particular eigenstate of, say, $i\tilde{\gamma}_{i,t=0}\tilde{\gamma}_{j,t=0}$, what
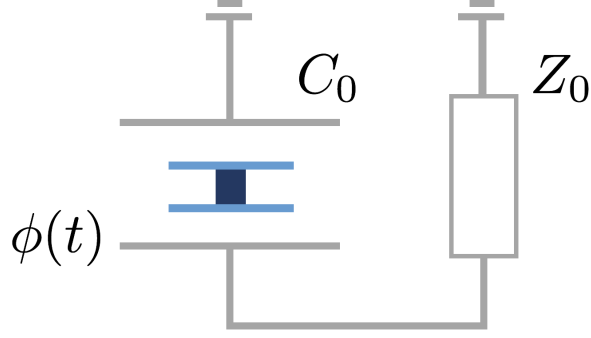
Figure 10: A Majorana box qubit, subjected to a classical potential $\phi(t)/e$, which arises from fluctuations in the electric circuit depicted in the figure. $\phi(t)/e$ is the voltage drop over a capacitance C, which models the coupling to the environment. The environment is represented by a frequency-independent impedance Z_0.

then is the expectation value of $i\tilde{\gamma}_{i,t}\tilde{\gamma}_{j,t}$? In order to make sense of this question, we will assume that it is possible to measure $i\tilde{\gamma}_{i,t}\tilde{\gamma}_{j,t}$ much quicker than the time scale on which $\phi(t)$ fluctuates.

We are interested in the decoherence effects from this which are independent of finite-size effects. Thus, we consider the Hamiltonian $H_{\text{pw},t}$ for a single half-infinite, spinless p-wave superconductor with the addition of the time-dependent potential energy fluctuations $\phi(t)$. This enters the Hamiltonian as a time-dependent linear shift of the energy gap Δ, so we write the BdG Hamiltonian H_t as

$$H_{\text{pw},t} = H_{\text{pw}} - \phi(t)\tau_z, \tag{2.1}$$

$$H_{\text{pw}} = \begin{pmatrix} \frac{p^2}{2m} - \Delta & vp \\ vp & -\frac{p^2}{2m} + \Delta \end{pmatrix}, \quad \tau_z = \begin{pmatrix} 1 & 0 \\ 0 & -1 \end{pmatrix}, \tag{2.2}$$

where the Hilbert space is defined only on the non-negative real axis $x \geq 0$. We need to impose $\phi(t) \ll \Delta$ at all times, to ensure that we are not pushed out of the topological regime. Furthermore, we will impose $\dot{\phi}(t)/\Delta \ll \Delta$, so non-adiabatic effects don't dominate. We denote the zero-energy eigenstate of (2.1) at time $t = 0$ by $|\psi_0\rangle$, and the eigenstate corresponding to the excited state with wavenumber k at time $t = 0$, as $|\psi_k\rangle$. We denote the matrix element between the zero energy state and the continuum by

$$\langle\psi_0|\phi(t)\tau_z|\psi_k\rangle = \phi(t)W_k, \tag{2.3}$$

With this, we may write Eq. (2.1) in second quantization as

$$H_{\text{pw},t} = \sum_k E_k \alpha_k^\dagger \alpha_k + \sum_k \left(V_{kt}\alpha_k^\dagger - V_{kt}^*\alpha_k\right)\gamma + \dots, \tag{2.4}$$

where we defined

$$V_{kt} = -\phi(t)W_k^*. \tag{2.5}$$

In Eq. (2.4), α_k is the annihilation operator associated with the state $|\psi_k\rangle$ and γ is the Hermitian Majorana operator associated with the state $|\psi_0\rangle$. Since the pairing is odd in momentum, it is effectively spinless. So to be precise, if $\Psi(x)$ is the (spinless) electron annihilation operator at position x, then in BdG space, γ and α_k are given by

$$\gamma = \int_0^\infty dx\langle x|\psi_0\rangle^T \begin{pmatrix} \Psi(x) \\ \Psi^\dagger(x) \end{pmatrix}, \tag{2.6}$$

$$\alpha_k = \int_0^\infty dx\langle x|\psi_k\rangle^T \begin{pmatrix} \Psi(x) \\ \Psi^\dagger(x) \end{pmatrix}, \tag{2.7}$$
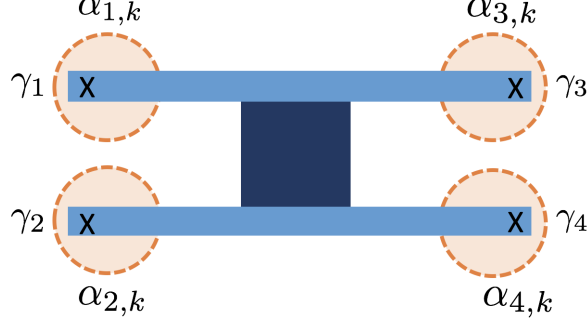
Figure 11: In view of the big system size, the Majoranas γ_i are modeled as only interacting with a set of local continuum states $\alpha_{i,k}$.

where we emphasize the BdG vector structure of the wave functions $\langle x|\psi_{0,k}\rangle$. The term that has been left out in (2.4) has the form $\sum_{k,k'}\langle\psi_k|\phi(t)\tau_z|\psi_{k'}\rangle\alpha_k^\dagger\alpha_{k'}$. This term renormalizes the continuum wave functions, causing transitions within the continuum, and we will neglect this terms, since they only contribute to a higher order in ϕ/Δ.

For the full Majorana box qubit, we assume that it is describable as four copies of (2.4), meaning that here is no overlap between the Majorana wave functions, that each end of the system is subjected to the same potential $\phi(t)$ and that the Majoranas interact only with localized quasiparticle continua, as sketched in Figure 11. This is a conservative approximation, as including the propagation of quasiparticles throughout the system would lead to non-trivial logical errors in the logical ground state space. It is a good approximation on time scales much shorter than the time it takes for quasiparticle wave packets to travel from one end of the system to the other. We denote the local continuum operators $\alpha_{i,k}$ and the Majorana operators γ_i, and impose the anticommutation relations

$$\{\alpha_{i,k},\alpha_{j,k'}^\dagger\}=\delta_{i,j}\delta_{k,k'} \tag{2.8}$$

$$\{\gamma_i,\gamma_j\}=2\delta_{i,j}. \tag{2.9}$$

With this, the Hamiltonian H_t for the Majorana box qubit with the potential fluctuations becomes

$$H_t=\sum_{i=1,4}\sum_k E_k\alpha_{i,k}^\dagger\alpha_{i,k}+\sum_{i=1,4}\sum_k\left(V_{kt}\alpha_{i,k}^\dagger-V_{kt}^*\alpha_{i,k}\right)\gamma_i. \tag{2.10}$$

The initial logical space is the span of the eigenvectors of the Pauli operator $\sigma_z\equiv i\gamma_1\gamma_2$, subject to the parity constraint

$$\gamma_1\gamma_2\gamma_3\gamma_4=s_0, \tag{2.11}$$

where $s_0=\pm1$. We denote the projection onto the subspace of the ground-state manifold satisfying Eq. (2.11) by Π_{s_0}, such that for general parities

$$\Pi_s=\frac{1}{2}(1+s\gamma_1\gamma_2\gamma_3\gamma_4). \tag{2.12}$$

Thus, we label the states of the initial logical space by $|p,s_0\rangle$, where $p=\pm1$ is the eigenvalue of σ_z.

At a later time t, the logical space has changed, since $[\gamma_i,H_t]\neq0$. The instantaneous logical space is instead given by the span of the eigenvectors of the instantaneous Pauli operator

$$\tilde{\sigma}_{z,t}\equiv i\tilde{\gamma}_{i,t}\tilde{\gamma}_{j,t}, \tag{2.13}$$

where the instantaneous Majorana operators $\tilde{\gamma}_{i,t}$ satisfy

$$[\tilde{\gamma}_{i,t},H_t]=0,\quad\tilde{\gamma}_{i,t=0}=\gamma_i, \tag{2.14}$$

and instantaneous logical space is subject to the parity constraints $\tilde{\gamma}_{1,t}\tilde{\gamma}_{2,t}\tilde{\gamma}_{3,t}\tilde{\gamma}_{4,t}=s_0$. Since non-adiabatic time evolution will tend to make the system leave the instantaneous logical space, we must be

careful when defining our error probability. If the system is prepared in an initial logical state $|p, s_0\rangle$, we will define it as the probability of measuring $\tilde{\sigma}_{z,t} = -p$; that is, we define it as the probability of detecting an error if the measurement can be carried out instantly. Realistically, measurements take a finite amount of time, which means that it is maybe more realistic to read out in the initial basis, since this is also the average instantaneous basis because $\langle \phi(t) \rangle = 0$. Our dephasing measure is therefore conservative, since a realistic measurement could also be affected by the mismatch of bases.

For initial states that are not eigenstates of σ_z, it is not possible to detect whether an error has occurred purely by measuring the parities of the ground state manifold. By also measuring $i\tilde{\gamma}_{3,t}\tilde{\gamma}_{4,t}$, it is possible, however, to check if the state has left the logical space. Note that the symmetry of the system means that we do not lose generality when we choose to initialize in the eigenbasis of σ_z.

We assume that the system is initialized perfectly, so the Majorana states are completely disentangled from the continua, whose density matrix is denoted by ρ_c. We assume the continuum density matrix to be a product state between the four continua,

$$\rho_c = \bigotimes_{i=1}^{4} \rho_{c,i}, \tag{2.15}$$

where $\rho_{c,i}$ contains only the degrees of freedom corresponding to the $\alpha_{i,k}$ operators. The initial logical state $|p = +, s_0\rangle$ may then be written

$$\rho(0) = \frac{1}{2}(\mathbb{1} + \sigma_z)\Pi_{s_0} \otimes \rho_c, \tag{2.16}$$

with $|\boldsymbol{r}| \leq 1$. Time evolving the initial state (2.16), using the Hamiltonian in (2.10), gives us a state entangled with the continuum, which at time t is

$$\rho(t) = \frac{1}{2}U(t)\big(\mathbb{1} + \sigma_z\big)\Pi_{s_0}\rho_c U^\dagger(t), \tag{2.17a}$$

$$U(t) = \mathcal{T}_t e^{-i \int_0^t dt' H_{t'}}, \tag{2.17b}$$

where $\mathcal{T}_t$ denotes the time ordering operator, placing terms at later times to the left. Given the state $\rho(t)$, we want to calculate the probability of measuring $\tilde{\sigma}_{z,t} = +1$, which is an operator only on a part of the instantaneous ground-state manifold. We denote this by $\mathcal{H}_{\tilde{p}} \equiv \mathrm{tr}_{\tilde{c},\tilde{s}} \mathcal{H}$, where $\mathcal{H}$ is the full Hilbert space, $\mathrm{tr}_{\tilde{c}}$ denotes trace over the instantaneous continuum states, and $\mathrm{tr}_{\tilde{s}}$ is trace over the instantaneous ground state's total fermionic parity. In general, the probability $P_{\psi,\rho}$ of measuring a pure state $|\psi\rangle$, when the initial state is given by a density matrix ρ, is

$$P_{\psi,\rho} = \langle \psi | \rho | \psi \rangle = \mathrm{tr}\Big(|\psi\rangle\langle\psi|\rho\Big), \tag{2.18}$$

and hence, when we denote trace over the eigenstates of $\tilde{\sigma}_{z,t}$ by $\mathrm{tr}_{\tilde{z}}$, the probability $P_{\tilde{z},z}$ of measuring $\tilde{\sigma}_{z,t} = +$ at time t, when the initial state is given by Eq. (2.17), is

$$
\begin{aligned}
P_{\tilde{z},z} &= \mathrm{tr}_{\tilde{z}}\left(\frac{1}{2}(\mathbb{1} + \tilde{\sigma}_{z,t})\,\mathrm{tr}_{\tilde{c},\tilde{s}}\left(U(t)\frac{1}{2}(\mathbb{1} + \sigma_z)\Pi_{s_0}\rho_c U^\dagger(t)\right)\right) \\
&= \frac{1}{4}\mathrm{tr}\left(U^\dagger(t)\big(\mathbb{1} + \tilde{\sigma}_{z,t}\big)U(t)\big(\mathbb{1} + \bar{\sigma}_z\big)\Pi_{s_0}\rho_c\right) \\
&= \frac{1}{4}\mathrm{tr}(\Pi_{s_0}\rho_c) + \frac{1}{4}\mathrm{tr}\left(U^\dagger(t)\tilde{\sigma}_{z,t}U(t)\sigma_z\Pi_{s_0}\rho_c\right) + 0 \\
&= \frac{1}{2} - \frac{1}{4}\left\langle U^\dagger(t)\tilde{\gamma}_{1,t}\tilde{\gamma}_{2,t}U(t)\gamma_1\gamma_2\Pi_{s_0}\right\rangle_c,
\end{aligned} \tag{2.19}
$$

where the subscript c indicates that the average is just with respect to the density matrix ρ_c. In the above we have made use of the fact that trace is basis independent, as well as the fact that terms containing only either σ_z or $\tilde{\sigma}_z$ have vanishing trace. The time evolution operator factorises, and we write $U(t) = \bigotimes_i U_i(t)$, stressing that $[U_i(t), \gamma_j] = 0$ when $i \neq j$. This implies that the average in (2.19)

becomes

$$
\begin{aligned}
&\left\langle U^\dagger(t)\tilde\gamma_{1,t}\tilde\gamma_{2,t}U(t)\gamma_1\gamma_2\Pi_{s_0}\right\rangle_c \\
&= \mathrm{tr}\left(\prod_{i=1}^4\left(U_i^\dagger(t)\right)\tilde\gamma_{1,t}\tilde\gamma_{2,t}\prod_{i=1}^4\left(U_i(t)\right)\gamma_1\gamma_2\prod_{i=1}^4\left(\rho_{c,i}\right)\Pi_{s_0}\right) \\
&= -\sum_{p,s}\langle p,s|\left(\mathrm{tr}_{c,1}\left(U_1^\dagger(t)\tilde\gamma_{1,t}U_1(t)\gamma_1\rho_{c,1}\right)\mathrm{tr}_{c,2}\left(U_2^\dagger(t)\tilde\gamma_{2,t}U_2(t)\gamma_2\rho_{c,2}\right)\right)\Pi_{s_0}|p,s\rangle \\
&= -\sum_{p,p',s'}\langle p,s_0|\,\mathrm{tr}_{c,1}\left(U_1^\dagger(t)\tilde\gamma_{1,t}U_1(t)\gamma_1\rho_{c,1}\right)|p',s'\rangle\langle p',s'|\,\mathrm{tr}_{c,2}\left(U_2^\dagger(t)\tilde\gamma_{2,t}U_2(t)\gamma_2\rho_{c,2}\right)|p,s_0\rangle,
\end{aligned}
\tag{2.20}
$$

where $\mathrm{tr}_{c,i}$ denotes trace over just the degrees of freedom corresponding to the $\alpha_{i,k}$, and we reiterate that the state $|p,s\rangle$ is the eigenstate of $i\gamma_1\gamma_2$ and $\gamma_1\gamma_2\gamma_3\gamma_4$ with eigenvalues p and s, respectively. We introduce the instantaneous Majorana propagator

$$
G_{\tilde\gamma_i}(t;p,s;p',s')\equiv\langle p,s_0|\,\mathrm{tr}_{c,i}\left(U_i^\dagger(t)\tilde\gamma_{i,t}U_i(t)\gamma_i\rho_{c,i}\right)|p',s'\rangle,
\tag{2.21}
$$

which satisfies the initial condition

$$
G_{\tilde\gamma_i}(t=0;p,s;p',s')=\delta_{p,p'}\delta_{s,s'}.
\tag{2.22}
$$

In the next section we will use an equations of motion analysis to derive an expression for the instantaneous Majorana propagator. Because the Hamiltonian is quadratic, we will find that the matrix structure of $G_{\tilde\gamma_i}(t;p,s;p',s')$ seen in Eq. (2.22) extends to finite times, $G_{\tilde\gamma_i}(t;p,s;p',s')\propto\delta_{p,p'}\delta_{s,s'}$, motivating the notation

$$
G_{\tilde\gamma_i}(t;p,s;p,s)\equiv G_{\tilde\gamma_i}(t).
\tag{2.23}
$$

Along with this fact, which we will verify in the end of the next section, the conclusion of this section is

$$
P_{\tilde z,z}(t)=\frac{1}{2}+\frac{1}{2}G_{\tilde\gamma_1}(t)G_{\tilde\gamma_2}(t).
\tag{2.24}
$$

$G_{\tilde\gamma_i}(t)$ depends on the field $\phi(t)$, which is stochastically fluctuating, and thus, we should average Eq. (2.24) over $\phi(t)$. To do this, we return to the setup in Fig. 10. The impedance $Z(\omega)$ of the circuit is

$$
Z(\omega)=\frac{1}{C}\frac{1}{i\omega+\omega_0}.
\tag{2.25}
$$

We assume that the circuit is in thermal equilibrium at temperature $k_BT=\frac{1}{\beta}$, which causes the potential energy drop $\phi(t)$ over the capacitor to fluctuate. We will initially treat ϕ as a quantum mechanically fluctuating operator and calculate the correlation function

$$
G_{\phi\phi}(t-t')=\frac{1}{2}\left\langle\{\phi(t),\phi(t')\}\right\rangle.
\tag{2.26}
$$

We equate this with the correlation function for the classically oscillating fields by taking the classical limit of large temperatures. The Kubo formula relates the conductance to the retarded current-current correlation function $G_{II}^R(t))-i\theta(t)\left\langle[I(t),I]\right\rangle$ in frequency space:

$$
\mathrm{Re}\,\frac{1}{Z(\omega)}=-\frac{1}{\omega}\mathrm{Im}\,G_{II}^R\omega=-\frac{1}{e^2\omega}\left|Z(\omega)\right|^{-2}\mathrm{Im}\,G_{\phi\phi}^R(\omega),
\tag{2.27}
$$

using $\phi(\omega)=\frac{1}{e}Z(\omega)I(\omega)$. This can be related to $G_{\phi\phi}(t)$ by the fluctuation-dissipation theorem,

$$
\mathrm{Im}\,G_{\phi\phi}^R(\omega)=-\tanh\left(\frac{\beta\omega}{2}\right)G_{\phi\phi}(\omega),
\tag{2.28}
$$

so

$$G_{\phi\phi}(\omega) = e^2\omega \operatorname{Re} \frac{1}{Z(\omega)} |Z(\omega)|^2 \coth\left(\frac{\beta\omega}{2}\right) =$$
$$= \frac{e^2}{C} \frac{\omega_0\omega}{\omega^2 + \omega_0^2} \coth\left(\frac{\beta\omega}{2}\right). \tag{2.29}$$

In the next section, when we set out to calculate $G_{\tilde{\gamma}_i}(t)$, we will change to the instantaneous eigenbasis and keep track of the non-adiabatic contributions. This means that in practice we will have to average over $\dot{\phi}(t)$ rather than $\phi(t)$. Eq. (2.29) implies

$$G_{\dot{\phi}\dot{\phi}}(\omega) = \frac{e^2}{C} \frac{\omega_0\omega^3}{\omega^2 + \omega_0^2} \coth\left(\frac{\beta\omega}{2}\right). \tag{2.30}$$

For large temperatures, $k_B T \gg \omega_0$, the quantum mechanically fluctuating operator ϕ becomes a classical object. From (2.30) the high-temperature limit of the propagator $G_{\dot{\phi}\dot{\phi}}(\omega)$ becomes

$$G_{\dot{\phi}\dot{\phi}}(\omega) \approx \frac{2e^2}{C} \frac{\omega_0\omega^2}{\omega^2 + \omega_0^2} k_B T. \tag{2.31}$$

The Fourier transform of (2.31) is

$$\begin{aligned}
G_{\dot{\phi}\dot{\phi}}(t) &= \frac{1}{2\pi} \int_{-\infty}^{\infty} d\omega\, e^{-i\omega t} G_{\dot{\phi}\dot{\phi}}(\omega) = \frac{e^2}{\pi C} \omega_0 k_B T \int_{-\infty}^{\infty} d\omega\, e^{-i\omega t} \frac{\omega^2}{\omega^2 + \omega_0^2} \\
&= \frac{e^2\omega_0 k_B T}{\pi C} \int_{-\infty}^{\infty} d\omega\, e^{-i\omega t} \left(1 - \frac{\omega_0^2}{\omega_2 + \omega_0^2}\right) \\
&= \frac{e^2\omega_0 k_B T}{\pi C} \left(2\pi\delta(t) - \omega_0^2 \int d\omega \frac{e^{-i\omega t}}{(\omega + i\omega_0)(\omega - i\omega_0)}\right) \\
&= \frac{e^2\omega_0 k_B T}{\pi C} \left(2\pi\delta(t) - \pi\omega_0 e^{-\omega_0|t|}\right) \\
&= \frac{2e^2\omega_0 k_B T}{C} \left(\delta(t) - \frac{\omega_0}{2} e^{-\omega_0|t|}\right). \tag{2.32}
\end{aligned}$$

If we denote average over ϕ by $\langle\cdot\rangle_\phi$ and $\langle G_{\tilde{\gamma}_i}(t)\rangle_\phi = \overline{G}_{\tilde{\gamma}_i}(t)$, we need to assume $\langle G_{\tilde{\gamma}_1}(t) G_{\tilde{\gamma}_2}(t)\rangle_\phi = \overline{G}_{\tilde{\gamma}_1}(t)\overline{G}_{\tilde{\gamma}_2}(t)$ in order to evaluate (2.24). This assumption means that the electromagnetic fields don't correlate the wavefunctions for the distant Majoranas γ_1 and γ_2. If, for example, $\overline{G}_{\tilde{\gamma}_i}(t)$ then decays to zero for large times, then $P_{\tilde{z},z}(t)$ is initially 1, and decays to $\frac{1}{2}$, corresponding to complete randomness.

In order to estimate the effect of dephasing due to the potential fluctuations, we ultimately want to derive an expression for the averaged propagator $\overline{G}_{\tilde{\gamma}_i}(t)$. In the next section, we will derive an expression for the instantaneous Majorana operators $\tilde{\gamma}_{i,t}$, and then calculate its propagator $G_{\tilde{\gamma}_i}(t)$.

3 Instantaneous Majorana operators

In this section we will derive expressions for all the ingredients related to the Majorana modes that are needed in order to calculate the decoherence. We start by deriving an expression for the instantaneous Majorana mode $\tilde{\gamma}_{i,t}$, which can then be used for deriving an expression for the instantaneous Majorana propagator $G_{\tilde{\gamma}_i}(t; p, s; p', s')$ by evaluating its equations of motion. The Hamiltonian in Eq. (2.10) may be simplified by introducing the following operator

$$\Omega_{i,t} \equiv \sum_k (V_{kt} \alpha_{i,k}^\dagger - V_{kt}^* \alpha_{i,k}), \tag{3.1}$$

in order to write

$$H_t = \sum_{i=1}^4 \Big(\sum_k E_k \alpha_{i,k}^\dagger \alpha_{i,k} + \Omega_{i,t} \gamma_i \Big). \tag{3.2}$$

Since we assume that the fluctuations $\phi(t)$ are small compared to the gap Δ, the topological protection of the zero-energy modes implies that there must be unitary operators S_t, allowing us to write $\tilde{\gamma}_{i,t}$ as

$$\tilde{\gamma}_{t,i} = S_t^\dagger \gamma_i S_t. \tag{3.3}$$

Note that (2.14) is equivalent to

$$[\tilde{H}_t, \gamma_i] = 0, \tag{3.4a}$$

$$\tilde{H}_t \equiv S_t H_t S_t^\dagger, \tag{3.4b}$$

which suggests the more convenient problem of unitarily transforming the Hamiltonian to a form that commutes with γ_i. We start with the ansatz

$$S_t = \prod_{i=1}^4 S_{i,t} \equiv \prod_{i=1}^4 e^{\Gamma_{i,t} \gamma_i}, \tag{3.5a}$$

$$\Gamma_{i,t} = \sum_k (F_{kt} \alpha_{i,k}^\dagger + F_{kt}^* \alpha_{i,k}). \tag{3.5b}$$

The operator $\Gamma_{i,t}$ satisfies

$$\begin{aligned}
\Gamma_{i,t}^2 &= \sum_{k,k'} \Big(F_{kt} F_{k't} \alpha_{i,k}^\dagger \alpha_{i,k'}^\dagger + F_{kt}^* F_{k't}^* \alpha_{i,k} \alpha_{i,k'} + F_{kt} F_{k't}^* \{\alpha_{i,k}^\dagger, \alpha_{i,k'}\} \Big) \\
&= \sum_{k,k'} \Big(\frac{1}{2} F_{kt} F_{k't} \{\alpha_{i,k}^\dagger, \alpha_{i,k'}^\dagger\} + \frac{1}{2} F_{kt}^* F_{k't}^* \{\alpha_{i,k}, \alpha_{i,k'}\} + F_{kt} F_{k't}^* \delta_{k,k'} \Big) \\
&= \sum_k |F_{kt}|^2 \equiv a_t^2, \tag{3.6}
\end{aligned}$$

which implies that $(\Gamma_{i,t} \gamma_i)^2 = -\Gamma_{i,t}^2 = -a_t^2$. Thus, we may write

$$\begin{aligned}
S_{i,t} &= \sum_{n=0}^\infty \frac{1}{n!} (\Gamma_{i,t} \gamma_i)^n = \sum_{n \text{ even}} \frac{1}{n!} (-1)^{n/2} a_t^n + \sum_{n \text{ odd}} \frac{1}{n!} (-1)^{(n-1)/2} a_t^{n-1} \Gamma_{i,t} \gamma_i \\
&= \cos a_t + \frac{\sin a_t}{a_t} \Gamma_{i,t} \gamma_i. \tag{3.7}
\end{aligned}$$

Transforming the second term in (3.2) gives

$$\begin{aligned}
S_t \Omega_{i,t} \gamma_i S_t^\dagger &= S_{i,t} \Omega_{i,t} \gamma_i S_{i,t}^\dagger = \Big(\cos a_t + \frac{\sin a_t}{a_t} \Gamma_{i,t} \gamma_i \Big) \Omega_{i,t} \gamma_i \Big(\cos a_t - \frac{\sin a_t}{a_t} \Gamma_{i,t} \gamma_i \Big) \\
&= \cos^2(a_t) \Omega_{i,t} \gamma_i + \frac{\sin^2(a_t)}{a_t^2} \Gamma_{i,t} \Omega_{i,t} \Gamma_{i,t} \gamma_i - \frac{\sin(2a_t)}{2a_t} [\Gamma_{i,t}, \Omega_{i,t}]. \tag{3.8}
\end{aligned}$$

The second term in (3.8) may be simplified by noticing that

$$\Gamma_{i,t}\Omega_{i,t}\Gamma_{i,t} = \Gamma_{i,t}\Omega_{i,t}\Gamma_{i,t} + \Gamma_{i,t}^2\Omega_{i,t} - a_t^2\Omega_{i,t} = \Gamma_{i,t}\{\Omega_{i,t},\Gamma_{i,t}\} - a_t^2\Omega_{i,t}, \tag{3.9}$$

and that

$$\{\Omega_{i,t},\Gamma_{i,t}\} = \sum_{k,k'}\{F_{kt}\alpha_{i,k}^\dagger + F_{kt}^*\alpha_{i,k}, V_{k't}\alpha_{i,k'}^\dagger - V_{k't}^*\alpha_{i,k'}\} = \sum_k(F_{kt}^*V_{kt} - F_{kt}V_{kt}^*). \tag{3.10}$$

We impose that F_{kt} and V_{kt} have the same complex phase, so that the expression (3.10) vanishes. We will later find this to be self-consistent. With this, Eq. (3.9) becomes

$$\Gamma_{i,t}\Omega_{i,t}\Gamma_{i,t} = -a_t^2\Omega_{i,t}. \tag{3.11}$$

Using $[\alpha_{i,k}^\dagger,\alpha_{i,k'}] = 2\alpha_{i,k}^\dagger\alpha_{i,k'} - \delta_{k,k'}$, the commutator in Eq. (3.8) may be evaluated:

$$\begin{aligned}
[\Gamma_{i,t},\Omega_{i,t}] &= \sum_{k,k'}\left[(F_{kt}\alpha_{i,k}^\dagger + F_{kt}^*\alpha_{i,k}),(V_{k't}\alpha_{i,k'}^\dagger - V_{k't}^*\alpha_{i,k'})\right] \\
&= \sum_{k,k'}\left(2F_{kt}V_{k't}\alpha_{i,k}^\dagger\alpha_{i,k'}^\dagger - 2F_{kt}^*V_{k't}^*\alpha_{i,k}\alpha_{i,k'} - F_{kt}V_{kt}^*[\alpha_{i,k}^\dagger,\alpha_{i,k'}] + F_{kt}^*V_{kt}[\alpha_{i,k},\alpha_{i,k'}^\dagger]\right) \\
&= \sum_{k,k'}\left(2F_{kt}V_{k't}\alpha_{i,k}^\dagger\alpha_{i,k'}^\dagger - 2F_{kt}^*V_{k't}^*\alpha_{i,k}\alpha_{i,k'} - 2F_{kt}V_{kt}^*\alpha_{i,k}^\dagger\alpha_{i,k'} + 2F_{kt}^*V_{kt}\alpha_{i,k}\alpha_{i,k'}^\dagger\right. \\
&\qquad\left. - \delta_{k,k'}(F_{kt}^*V_{kt} - F_{kt}V_{kt}^*)\right) \\
&= 2\Gamma_{i,t}\Omega_{i,t}, \tag{3.12}
\end{aligned}$$

where we used that the last term in the third line is again zero from the assumption that F_{kt} and V_{kt} have the same phase. Using (3.11) and (3.12), we finally get

$$S_t\Omega_{i,t}\gamma_i S_t^\dagger = \cos 2a_t\Omega_{i,t}\gamma_i - \frac{\sin 2a_t}{a_t}\Gamma_{i,t}\Omega_{i,t}. \tag{3.13}$$

Next, we define $n_{i,k} \equiv \alpha_{i,k}^\dagger\alpha_{i,k}$ and transform the first term in (3.2), obtaining

$$\begin{aligned}
S_t n_{i,k} S_t^\dagger = S_{i,t} n_{i,k} S_{i,t}^\dagger &= \left(\cos(a_t) + \frac{\sin(a_t)}{a_t}\Gamma_{i,t}\gamma_i\right)n_{i,k}\left(\cos(a_t) - \frac{\sin(a_t)}{a_t}\Gamma_{i,t}\gamma_i\right) \\
&= \cos^2(a_t)n_{i,k} + \frac{\sin^2(a_t)}{a_t^2}\Gamma_{i,t}n_{i,k}\Gamma_{i,t} + \frac{\sin(2a_t)}{2a_t}\gamma_i[n_{i,k},\Gamma_{i,t}] \\
&= \cos^2(a_t)n_{i,k} + \frac{\sin^2(a_t)}{a_t^2}\left(\Gamma_{i,t}[n_{i,k},\Gamma_{i,t}] + \Gamma_{i,t}^2 n_{i,k}\right) + \frac{\sin(2a_{i,t})}{2a_{i,t}}\gamma_i[n_{i,k},\Gamma_{i,t}] \\
&= n_{i,k} + \left(\frac{\sin^2(a_t)}{a_t^2}\Gamma_{i,t} + \frac{\sin(2a_t)}{2a_t}\gamma_i\right)[n_{i,k},\Gamma_{i,t}] \\
&= n_{i,k} + \left(\frac{\sin^2 a_t}{a_t^2}\Gamma_{i,t} + \frac{\sin 2a_t}{2a_t}\gamma_i\right)\left(F_{kt}\alpha_{i,k}^\dagger - F_{kt}^*\alpha_{i,k}\right). \tag{3.14}
\end{aligned}$$

Putting together (3.13) and (3.14), the transformed Hamiltonian $\tilde{H}_t$ defined in Eq. (3.4b) becomes

$$\begin{aligned}
\tilde{H}_t = \sum_i\Bigg[&-\frac{\sin 2a_t}{a_t}\Gamma_{i,t}\Omega_{i,t} + \sum_k E_k\left(n_{i,k} + \frac{\sin^2 a_t}{a_t^2}\Gamma_{i,t}\left(F_{kt}\alpha_{i,k}^\dagger - F_{kt}^*\alpha_{i,k}\right)\right) \\
&+ \sum_k\left(\cos 2a_t\Omega_{i,t} - \frac{\sin 2a_t}{2a_t}E_k\left(F_{kt}\alpha_{i,k}^\dagger - F_{kt}^*\alpha_{i,k}\right)\right)\gamma_i\Bigg]. \tag{3.15}
\end{aligned}$$

Equation (3.4a) is satisfied when the second term vanishes, so we choose

$$\cos 2a_t\left(V_{kt}\alpha_{i,k}^\dagger - V_{kt}^*\alpha_{i,k}\right) - \frac{\sin 2a_t}{2a_t}E_k\left(F_{kt}\alpha_{i,k}^\dagger - F_{kt}^*\alpha_{i,k}\right) = 0, \tag{3.16}$$

which is satisfied when

$$\cos(2a_t)V_{kt} = \frac{\sin 2a_t}{2a_t}E_k F_{kt}, \tag{3.17}$$

which finally gives us the expression for F_{kt}:

$$F_{kt} = 2a_t \frac{V_{kt}}{E_k}\cot 2a_t. \tag{3.18}$$

Eq. (3.18) verifies the self-consistency of choosing V_{kt} F_{kt} to have the same phase, and together with Eq. (3.6) it implies

$$a_t^2 = 4a_t^2 \sum_k \left(\frac{|V_{kt}|}{E_k}\right)^2 \cot^2 2a_t, \tag{3.19}$$

which gives us an expression for a_t:

$$\tan^2 2a_t = 4\sum_k \left(\frac{|V_{kt}|}{E_k}\right)^2. \tag{3.20}$$

Using (3.18), we can write the remaining terms left in the Hamiltonian as

$$\tilde{H}_t = S_t H_t S_t^\dagger = \sum_{i,k} E_k n_{i,k} + \sum_i \left(-\frac{\sin 2a_t}{a_t}\Gamma_{i,t}\Omega_{i,t} + \sum_k E_k \frac{\sin^2 a_t}{a_t^2}\Gamma_{i,t} 2a_t \frac{1}{E_k}\cot 2a_t\big(V_{kt}\alpha_{i,k}^\dagger - V_{kt}^*\alpha_{i,k}\big)\right)$$

$$= \sum_{i,k} E_k n_{i,k} + \sum_i \frac{1}{a_t}\Big(2\sin^2 a_t \cot 2a_t - \sin 2a_t\Big)\Gamma_{i,t}\Omega_{i,t}. \tag{3.21}$$

This could in principle now be diagonalized, so that but we won't need that level of detail. The instantaneous zero-energy mode is

$$\tilde{\gamma}_{i,t} = S_t^\dagger \gamma_i S_t = S_{i,t}^\dagger \gamma_i S_{i,t}$$

$$= \big(\cos(a_t) + \frac{\sin(a_t)}{a_t}\Gamma_{i,t}\gamma_i\big)\gamma_i\big(\cos(a_t) - \frac{\sin(a_t)}{a_t}\Gamma_{i,t}\gamma_i\big)$$

$$= \cos^2(a_t)\gamma_i - \frac{\sin^2(a_t)}{a_t^2}\Gamma_{i,t}\gamma_i\gamma_i\Gamma_{i,t}\gamma_i + \frac{\sin(2a_t)}{2a_t}[\Gamma_{i,t}\gamma_i,\gamma_i]$$

$$= \cos^2(a_t)\gamma_i - \sin^2(a_t)\gamma_i + \frac{\sin(2a_t)}{2a_t}(\Gamma_{i,t}\gamma_i\gamma_i - \gamma_i\Gamma_{i,t}\gamma_i)$$

$$= \cos(2a_t)\gamma_i + \frac{\sin(2a_t)}{a_t}\Gamma_{i,t}. \tag{3.22}$$

In order to evaluate $G_{\tilde{\gamma}_i}(t; p, s; p', s')$, it turns out to be much more useful to stay in the original basis, and instead transform the time-evolution operator, defining

$$\tilde{U}_i(t) \equiv S_{i,t}U_i(t)S_{i,t=0} = S_{i,t}U_i(t), \tag{3.23}$$

which corresponds to time-evolution, followed by changing to the basis of the instantaneous modes. Using this, we can rewrite

$$U_i^\dagger(t)\tilde{\gamma}_{i,t}U_i(t)\gamma_i = \tilde{U}_i^\dagger(t)\gamma_i\tilde{U}_i(t)\gamma_i, \tag{3.24}$$

which is a simpler starting point for writing the equations of motion for $G_{\tilde{\gamma}_i}(t; p, s; p', s')$. The time-evolution operator may be split into infinitesimal time slices of size Δt. By transforming H_t at each time step into the basis of the instantaneous modes, we write

$$U(t) = \mathcal{T}_t e^{-i\int_0^t dt' H_{t'}} = e^{-i\Delta t H_t}e^{-i\Delta t H_{t-\Delta t}}\ldots e^{-i\Delta t H_0} + \mathcal{O}(\Delta t^2)$$

$$= S_t^\dagger e^{-i\Delta t \tilde{H}_t}S_t S_{t-\Delta t}^\dagger e^{-i\Delta t \tilde{H}_{t-\Delta t}}\ldots e^{-i\Delta t \tilde{H}_0}. \tag{3.25}$$

This is as far as we can get exactly. We need to evaluate $S_t S_{t-\Delta t}^\dagger$, but it is very complicated in its full generality. The Baker-Campbell-Hausdorff formula lets us write

$$S_t \ S_{t-\Delta t}^\dagger = \prod_i e^{\Gamma_{i,t}\gamma_i} e^{-\Gamma_{i,t-\Delta t}\gamma_i} = \prod_i e^{(\Gamma_{it}-\Gamma_{i,t-\Delta t})\gamma_i + \cdots}$$
$$= \prod_i e^{\Delta t \dot{\Gamma}_{i,t}\gamma_i + \cdots}. \tag{3.26}$$

The terms left out in (3.26) are also proportional to $\frac{d}{dt}\phi(t)$. For the equations of motion analysis to close, we can only include up to the second order term

$$-\frac{1}{2}[\Gamma_{i,t}, \Gamma_{i,t-\Delta t}] = \Delta t[\Gamma_{i,t}, \dot{\Gamma}_{i,t}] + \mathcal{O}(\Delta t^2). \tag{3.27}$$

The contribution from this term to the equations of motion of $G_{\tilde{\gamma}_i}(t; p, s; p', s')$, however, can be shown to exactly cancel. Higher orders are all proportional to $a_t^2 \dot{a}_t$, and we neglect these terms in (3.26). Using the identity

$$e^{-i\Delta t \tilde{H}_t} e^{\Delta t \dot{\Gamma}_{i,t}\gamma_i} = e^{-i\Delta t(\tilde{H}_t + i\dot{\Gamma}_{i,t}\gamma_i) + \mathcal{O}(\Delta t^2)}, \tag{3.28}$$

we find the following expression for the rotated time-evolution operator

$$\tilde{U}(t) = S_t \ U_i(t) = S_t S_t^\dagger \mathcal{T}_t e^{-i\int_0^t dt'(\tilde{H}_{t'} + i\sum_{i=1}^4 \dot{\Gamma}_{i,t'}\gamma_i)}. \tag{3.29}$$

Now we are all set to calculate the instantaneous Majorana propagator. For now, we will suppress the p- and s-indices of $G_{\tilde{\gamma}_i}(t; p, s; p', s')$, and we use Eq. (3.24) to write

$$G_{\tilde{\gamma}_i}(t) = \left\langle \tilde{U}^\dagger(t)\gamma_i \tilde{U}(t)\gamma_i \right\rangle. \tag{3.30}$$

The Heisenberg equation of motion gives

$$i\partial_t G_{\tilde{\gamma}_i} = -\left\langle \tilde{U}^\dagger(t)[\tilde{H}_t + i\dot{\Gamma}_{i,t}\gamma_i, \gamma_i]\tilde{U}(t)\gamma_i \right\rangle$$
$$= -i\left\langle \tilde{U}^\dagger(t)[\dot{\Gamma}_{i,t}\gamma_i, \gamma_i]\tilde{U}(t)\gamma_i \right\rangle = -2i\left\langle \tilde{U}^\dagger(t)\dot{\Gamma}_{i,t}\tilde{U}(t)\gamma_i \right\rangle. \tag{3.31}$$

To be consistent, we should only evaluate (3.31) to order $\mathcal{O}(a_t^2)$. Equation (3.20) tells us that

$$\dot{\Gamma}_{i,t} = \frac{d}{dt}\sum_k \left(2a_t \cot(2a_t)\frac{V_{kt}}{E_k}\alpha_{i,k}^\dagger + 2a_t \cot(2a_t)\frac{V_{kt}^*}{E_k}\alpha_{i,k} \right)$$
$$= \sum_k \left(\frac{\dot{V}_{kt}}{E_k}\alpha_{i,k}^\dagger + \frac{\dot{V}_{kt}^*}{E_k}\alpha_{i,k} \right) + \mathcal{O}(a_t^2 \dot{a}_t). \tag{3.32}$$

Using this, (3.31) becomes

$$i\partial_t G_{\tilde{\gamma}_i} = -2i\sum_k \left(\frac{\dot{V}_{kt}}{E_k}G_{\alpha_{i,k}^\dagger, \gamma_i}(t) + \frac{\dot{V}_{kt}^*}{E_k}G_{\alpha_{i,k}, \gamma_i}(t) \right), \tag{3.33}$$

where we have defined the propagator

$$G_{\tilde{\alpha}_{i,k}^{(\dagger)}, \gamma_i} \equiv \left\langle \tilde{U}^\dagger(t)\alpha_{i,k}^{(\dagger)}\tilde{U}(t)\gamma_i \right\rangle. \tag{3.34}$$

The Heisenberg equation of motion for $G_{\alpha_{i,k}, \gamma_i}$ gives[1]

$$i\partial_t G_{\alpha_{i,k}, \gamma_i} = -\left\langle \tilde{U}^\dagger(t)[\tilde{H}_t + i\dot{\Gamma}_{i,t}\gamma_i, \alpha_k]\tilde{U}(t)\gamma_i \right\rangle$$
$$= -\left\langle \tilde{U}^\dagger(t)[\tilde{H}_t, \alpha_k]\tilde{U}(t)\gamma_i \right\rangle + i\left\langle \tilde{U}^\dagger(t)\{\dot{\Gamma}_{i,t}, \alpha_k\}\gamma_i \tilde{U}(t)\gamma_i \right\rangle. \tag{3.35}$$

---

[1]In this step, the inclusion of the term in Eq. (3.27) would cancel.

The first term may be evaluated using (3.21), and we see

$$[\tilde{H}_t, \alpha_{i,k}] = -E_k \alpha_{i,k} + \mathcal{O}(a_t^2 \cdot \Delta), \tag{3.36}$$

while the second term simplifies, thanks to Eq. (3.32), giving

$$\{\dot{\Gamma}_{i,t}, \alpha_{i,k}\} = \frac{\dot{V}_{kt}}{E_k} + \mathcal{O}(a_t^2 \cdot \dot{a}_t). \tag{3.37}$$

Thus, Eq. (3.35) becomes

$$(i\partial_t - E_k)G_{\alpha_{i,k},\gamma_i} = i\frac{\dot{V}_{kt}}{E_k}G_{\tilde{\gamma}_i}. \tag{3.38}$$

The solution to this differential equation, with the boundary condition $G_{\alpha_{i,k},\gamma_i}(0) = 0$, is

$$G_{\alpha_{i,k},\gamma_i}(t) = \int_0^t ds\, e^{-iE_k(t-s)}\frac{\dot{V}_{ks}}{E_k}G_{\tilde{\gamma}_i}(s). \tag{3.39}$$

Going through the same calculation for $G_{\alpha_{i,k}^\dagger,\gamma_i}$ leads to

$$G_{\alpha_{i,k}^\dagger,\gamma_i}(t) = \int_0^t ds\, e^{iE_k(t-s)}\frac{\dot{V}_{ks}^*}{E_k}G_{\tilde{\gamma}_i}(s), \tag{3.40}$$

and plugging (3.39) and (3.40) into (3.33), we get

$$i\partial_t G_{\tilde{\gamma}_i} = -2i\sum_k \int_0^t ds' \left(\frac{\dot{V}_{kt}}{E_k}e^{iE_k(t-s')}\frac{\dot{V}_{ks'}^*}{E_k} + \frac{\dot{V}_{kt}^*}{E_k}e^{-iE_k(t-s')}\frac{\dot{V}_{ks'}}{E_k}\right)G_{\tilde{\gamma}_i}(s'). \tag{3.41}$$

We can solve this by integration, using the boundary conditions in Eq. (2.22), and we obtain

$$G_{\tilde{\gamma}_i}(t;p,s;p',s') = \delta_{p,p'}\delta_{s,s'} - 2\sum_k \int_0^t ds \int_0^s ds' \left(\frac{\dot{V}_{ks}}{E_k}e^{iE_k(s-s')}\frac{\dot{V}_{ks'}^*}{E_k} + \frac{\dot{V}_{ks}^*}{E_k}e^{-iE_k(s-s')}\frac{\dot{V}_{ks'}}{E_k}\right)G_{\tilde{\gamma}_i}(s'), \tag{3.42}$$

which may be solved iteratively, by repeatedly inserting the left-hand side into the right-hand side. As long as $\left|\dot{V}_{kt}\right| \ll E_k^2$, then the series converges. When $p \neq p'$ or $s \neq s'$, $G_{\tilde{\gamma}_i}(t;p,s;p',s')$ becomes zero, and so we are justified in the simplified notation we have used in the previous section, writing $G_{\tilde{\gamma}_i}(t;p,s;p',s') = \delta_{p,p'}\delta_{s,s'}G_{\tilde{\gamma}_i}(t)$. In conclusion,

$$G_{\tilde{\gamma}_i}(t) = 1 + \int_0^t ds \int_0^s ds'\, K(s,s')G_{\tilde{\gamma}_i}(s') \tag{3.43a}$$

$$K(s,s') = -4\sum_k \frac{|W_k|^2}{E_k^2}\cos(E_k(s-s'))\dot{\phi}(s)\dot{\phi}(s') = -4\int_\Delta^\infty dE \frac{|W_E|^2}{E^2}\nu(E)\cos(E(s-s'))\dot{\phi}(s)\dot{\phi}(s'), \tag{3.43b}$$

where L is the system size which we take to be infinite in the end, and $\nu(E) = \frac{L}{2\pi}\frac{dk}{dE}$ is the density of states.

Let us reiterate the approximations we needed to arrive at the result in Eq. (3.43a). We assumed that $\phi(t) \ll \Delta$, and $\dot{\phi}(t)/\Delta \ll \Delta$, and included only contributions to second order in either of these. Averaging over ϕ, and using the correlation function in Eq. (2.32), the precise statement is that $\frac{e^2}{C}k_BT\omega_0^2 \ll \Delta^4$. This can be seen from Eq. (3.43), since the integral kernel $K(t,t')$ rapidly oscillates with frequency $E \geq \Delta$, which implies that the dimensionless second term in (3.43a) scales as $\sim \frac{e^2}{C}k_BT\omega_0^2/\Delta^4$.

Since we use the high-temperature result for the propagator in Eq. (2.32), we should have $\omega_0 \ll k_BT \lesssim \Delta$. The ratio $\frac{e^2}{C\Delta}$ defines how well isolated the Majorana box qubit is from the environment and should therefore be small. If we furthermore assume $\omega_0 \ll \Delta$, the analysis is simplified to the point where we can derive analytical expressions for the decay rates. Doing this is the objective of the next section.

82

4 Evaluating the Majorana propagator

With the work of the last sections, we are at last in position to calculate the instantaneous Majorana propagator $G_{\tilde{\gamma}_i}(t)$. Introducing the functions

$$A(t) = -4 \int_\Delta^\infty dE \, m(E) \cos Et, \tag{4.1}$$

$$m(E) = \frac{|W_E|^2 \nu(E)}{E^2}, \tag{4.2}$$

Eq. (3.43a) takes the form

$$G_{\tilde{\gamma}_i}(t) = 1 + \int_0^t ds \int_0^s ds' \dot{\phi}(s) \dot{\phi}(s') A(s - s') G_{\tilde{\gamma}_i}(s'). \tag{4.3}$$

Repeated insertion of the left-hand side of (4.3) into the right-hand side yields

$$
G_{\tilde{\gamma}_i}(t) = 1 + \int_0^t ds_1 \int_0^{s_1} ds_2 \dot{\phi}(s_1) \dot{\phi}(s_2) A(s_1 - s_2)
$$
$$
+ \int_0^t ds_1 \int_0^{s_1} ds_2 \int_0^{s_2} ds_3 \int_0^{s_3} ds_4 \dot{\phi}(s_1) \dot{\phi}(s_2) \dot{\phi}(s_3) \dot{\phi}(s_4) A(s_1 - s_2) A(s_3 - s_4) + \dots \tag{4.4}
$$

At this stage, we average over $\dot{\phi}(t)$, using the correlation function in Eq. (2.32), and we get

$$
\overline{G}_{\tilde{\gamma}_i}(t) = 1 + \int_0^t ds_1 \int_0^{s_1} ds_2 G_{\dot{\phi}\dot{\phi}}(s_1 - s_2) A(s_1 - s_2)
$$
$$
+ \int_0^t ds_1 \int_0^{s_1} ds_2 \int_0^{s_2} ds_3 \int_0^{s_3} ds_4 \Big(G_{\dot{\phi}\dot{\phi}}(s_1 - s_2) G_{\dot{\phi}\dot{\phi}}(s_3 - s_4) + G_{\dot{\phi}\dot{\phi}}(s_1 - s_3) G_{\dot{\phi}\dot{\phi}}(s_2 - s_4)
$$
$$
+ G_{\dot{\phi}\dot{\phi}}(s_1 - s_4) G_{\dot{\phi}\dot{\phi}}(s_2 - s_3) \Big) A(s_1 - s_2) A(s_3 - s_4)
$$
$$
+ \dots, \tag{4.5}
$$

which we represent diagrammatically by introducing

$$
\begin{aligned}
t_i \,\text{———}\, t_j &= 1, \\
t_i \,\text{———}\, t_j &= G_{\dot{\phi}\dot{\phi}}(t_j - t_i), \\
t_i \,\text{\wedge\wedge\wedge}\, t_j &= A(t_j - t_i).
\end{aligned} \tag{4.6}
$$

We will suppress the time variables for notational clarity, since the external times are always 0 and t. At every vertex there is a new time variable, and the whole diagram should be time-ordered, so intermediate times are latest to the right. A sample diagram is

$$
= 0 \,\text{——}\, t_4 \,\text{\wedge\wedge\wedge}\, t_3 \,\text{——}\, t_2 \,\text{\wedge\wedge\wedge}\, t_1 \,\text{——}\, t
$$
$$
= \int_0^t dt_1 \int_0^{t_1} dt_2 \int_0^{t_2} dt_3 \int_0^{t_3} dt_4 A(t_3 - t_4) A(t_1 - t_2) G_{\dot{\phi}\dot{\phi}}(t_1 - t_4) G_{\dot{\phi}\dot{\phi}}(t_2 - t_3). \tag{4.7}
$$

Using this, Eq. (4.5) becomes

$$ \tag{4.8} $$

The constraint that the time variables are nested implies that the three fourth order diagrams in (4.8) are distinct.

We cannot analytically solve Eq. (4.8) as it is. If $\omega_0 \ll \Delta$, then, as detailed below, we may discard all crossing diagrams to leading order in ω_0/Δ, and the resulting Dyson series may be solved in the usual way [16]. Subleading orders contain crossing diagrams, complicating the analysis. Let us unpack these statements by introducing the following new propagator lines

$$t_i \;\rule[0.5ex]{1.2em}{0.8pt}\; t_j \;\equiv\; t_i \;\text{-{}-{}-}\; t_j \;+\; t_i \;\wwbar\; t_j \;, \tag{4.9a}$$

$$t_i \;\text{-{}-{}-}\; t_j \;=\; \frac{2e^2\omega_0 k_B T}{C}\delta(t_j - t_i), \tag{4.9b}$$

$$t_i \;\wwbar\; t_j \;=\; -\frac{2e^2\omega_0 k_B T}{C}\frac{\omega_0}{2}e^{-\omega_0(t_j - t_i)}, \tag{4.9c}$$

corresponding to the two terms in Eq. (2.30). First note that diagrams vanish if they contain a dotted-line propagator and it crosses any other line. This is because of the nesting of the time variables; when the dotted-line connects to time which is not adjacent to its own, it collapses the integration range of the intermediate integral to a measure 0 set. Secondly, terms containing the curly propagator in Eq. (4.9c) are suppressed by $(\omega_0/\Delta)^2$, since those diagrams contain at least one more time integral. So at each order in $e^2/(C\Delta)$, corresponding to the half the number of vertices in the diagram, to the lowest order in ω_0/Δ we may neglect the curly-line propagators and only keep the diagrams with the dotted lines, which we will refer to as *delta diagrams*. Thus, at this order the crossing diagrams vanish.

If curly-line propagators are included, only some of the crossing diagrams may be dropped. These diagrams consist of a single curly-line propagator, crossing over any number of dotted-line propagators. An example is the following diagram:

$$\tag{4.10}$$

Here, because the dotted-line propagator is not aligned with the oscillating wavy-line propagator, after time integration a $\cos(\Delta\xi t)$ survives to the lowest order in ω_0/Δ. After integrating over ξ, this brings out another factor of $1/\Delta$, making it supressed compared to, for example, the related non-crossing diagram

$$\tag{4.11}$$

which appears to the same order in $e^2/(C\Delta)$. We will refer to the non-crossing diagram with a single curly-line propagator as a *sheep*. Keeping the curly-line propagator and only the non-crossing diagrams means retaining the sheep diagrams. However, diagrams where only curly-line propagators cross, like the following

$$\tag{4.12}$$

are not suppressed. In Section 4.1, we calculate the leading order terms of $G_{\tilde{\gamma}_i}(t)$ in ω_0/Δ by only summing the delta diagrams. In Section 4.2, we will sum all non-crossing sheep- and delta diagrams to get a flavor of what this qualitatively changes in the result for $G_{\tilde{\gamma}_i}(t)$.

Dropping the crossing diagrams in 4.8, we have

$$\overline{G}_{\tilde{\gamma}_i}(t) \approx \rule[0.5ex]{2em}{0.8pt} + \cdots + \cdots$$
$$+ \cdots + \ldots$$
$$= \rule[0.5ex]{2em}{0.8pt} + \cdots \left(\rule[0.5ex]{2em}{0.8pt} + \cdots + \ldots \right)$$
$$= 1 + \int_0^t ds_1 \int_0^{s_1} ds_2\, G_{\dot{\phi}\dot{\phi}}(s_1 - s_2)A(s_1 - s_2)\overline{G}_{\tilde{\gamma}_i}(s_2), \tag{4.13}$$

84

which means that

$$\partial_t \overline{G}_{\tilde{\gamma}_i}(t) = \int_0^t ds\, G_{\dot{\phi}\dot{\phi}}(t-s)A(t-s)\overline{G}_{\tilde{\gamma}_i}(s). \tag{4.14}$$

Since the right-hand side of Eq. (4.14) is a convolution, it may be solved by Laplace transformation. We denote the Laplace transformed propagator $\mathcal{G}_i(z) = \mathcal{L}[\overline{G}_{\tilde{\gamma}_i}](z)$. Using the boundary condition $\overline{G}_{\tilde{\gamma}_i}(0) = 1$, we find

$$\mathcal{G}_i(z) = \frac{1}{z - R(z)}, \tag{4.15a}$$

$$R(z) = \mathcal{L}[G_{\dot{\phi}\dot{\phi}}(t)A(t)]. \tag{4.15b}$$

4.1 Leading order in ω_0/Δ

To leading order in ω_0/Δ, we keep only the first term of $G_{\dot{\phi}\dot{\phi}}(t)$ in Eq. (2.32). Evaluating Eq. (4.15b), we find

$$R(z) = -8\frac{e^2\omega_0 k_B T}{C}\int_\Delta^\infty dE\, m(E)\int_0^\infty dt\cos(Et)\delta(t)e^{-tz} = -4\frac{e^2\omega_0 k_B T}{C}\int_\Delta^\infty dE\, m(E), \tag{4.16}$$

Let us simplify this with a bit of dimensional analysis. The matrix element W_E and density of states $\nu(E)$ are calculated in Appendix 6. In terms of the dimensionless energy $\xi = E/\Delta$ and wavenumber $\tilde{k} = k/mv$, we write

$$W_E = \frac{1}{\sqrt{mvL}}\delta\tilde{H}_{0,\xi}, \tag{4.17a}$$

$$\nu(E) = \frac{Lmv}{\Delta}\frac{1}{2\pi}\frac{d\tilde{k}}{d\xi} = \frac{Lmv}{2\pi\Delta}\tilde{\nu}(\xi), \tag{4.17b}$$

where the notation $\delta\tilde{H}_{0,\xi}$ and $\tilde{\nu}(\xi)$ is used to indicate that only the dimensionless part is included, and the factor of $\frac{1}{2\pi}$ has been taken out of the density of states. With this notation, we may write

$$m(E) = \frac{1}{2\pi\Delta^3}\tilde{m}(\xi), \tag{4.18a}$$

$$\tilde{m}(\xi) = \frac{|W_\xi|^2}{\xi^2}\nu(\xi). \tag{4.18b}$$

Using this, we rewrite Eq. (4.16) to

$$R(z) = -pD\omega_0, \tag{4.19}$$

where we introduced the quantities

$$p = 2\frac{e^2 k_B T}{\pi C\Delta^2}, \tag{4.20a}$$

$$D = \int_1^\infty d\xi\,\tilde{m}(\xi). \tag{4.20b}$$

From Eq. (4.15a), the Laplace transformed propagator is

$$\mathcal{G}_i(z) = \frac{1}{z + 4p}. \tag{4.21}$$

Picking a real $\lambda > -4p$, then the inverse Laplace transform is given by the Bromwich integral

$$\overline{G}_{\tilde{\gamma}_i}(t) = \frac{1}{2\pi i}\lim_{A\to\infty}\int_{\lambda-iA}^{\lambda+iA} dz\, e^{zt}\frac{1}{z + pD\omega_0}, \tag{4.22}$$

from which we have

$$\overline{G}_{\tilde{\gamma}_i}(t) = e^{-pD\omega_0 t}. \tag{4.23}$$

Going back to Eq. (2.24), if we denote the Majorana box qubit lifetime by τ, we arrive at the main result

85

$$\tau^{-1} = 2pD\omega_0 = \frac{4e^2 k_B T \omega_0}{\pi C \Delta^2} \int_1^\infty d\xi \tilde{m}(\xi). \tag{4.24}$$

Note that the expression depends on the energy mv^2, which is hiding inside $m(\xi)$.

4.2 Partial summation for higher order terms

Next, let us try to get a feeling for what happens if we include some higher order terms and keep the full form of $G_{\dot\phi\dot\phi}(t)$. We still only keep the non-crossing diagrams, so it amounts to summing the delta diagrams of the previous section along with all sheep diagrams. As explained above, this is an uncontrolled approximation since we are missing some diagrams of the same order. Still, we may obtain a qualitative understanding of how $\overline{G}_{\tilde\gamma_i}(t)$ is modified by sheep diagrams.

We simplify $A(t)$ by using the saddle-point approximation. What this will accomplish is to pick out a single frequency component for $A(t)$. We write

$$A(t) \equiv I_+(t) + I_-(t), \tag{4.25a}$$

$$I_\pm = -\frac{1}{\pi\Delta^2} \int_1^\infty d\xi e^{\pm i\Delta\xi t + \log(m(\xi))}. \tag{4.25b}$$

If we define the positive/negative Wick rotations $\mathcal{W}_\pm(f(t)) = f(\mp it)$, we can rewrite $A(t)$ as

$$A(t) = \mathcal{W}_+\Big(\mathcal{W}_-\big(I_+(t)\big)\Big) + \mathcal{W}_-\Big(\mathcal{W}_+\big(I_-(t)\big)\Big) = \mathcal{W}_+\Big(\mathcal{I}(t)\Big) + \mathcal{W}_-\Big(\mathcal{I}(t)\Big), \tag{4.26}$$

where

$$\mathcal{I}(t) = -\frac{1}{\pi\Delta^2} \int_1^\infty d\xi e^{-\Delta\xi t + \log(m(\xi))}. \tag{4.27}$$

At any time t, the exponent $-\Delta\xi t + \log(m(\xi))$ has a global maximum $\xi = \xi_0(t) > 1$. This is illustrated on Figure 12, where $-\Delta\xi t + \log(m(\xi))$ is plotted for a few different times and with $\frac{\Delta}{mv^2} = 0.3$. At later times, the maximum is sharper, which makes the saddle-point approximation more accurate. The saddle-point approximation gives [7]

$$\mathcal{I}(t) \approx -\frac{1}{\pi\Delta^2} \frac{e^{-\Delta\xi_0 t + \log(m(\xi_0))}}{\sqrt{-\frac{1}{2\pi}\frac{d^2}{d\xi^2}\Big|_{\xi=\xi_0}(-\Delta\xi t + \log m(\xi))}} = -\frac{1}{\pi\Delta^2} \frac{m(\xi_0)}{\sqrt{\frac{1}{2\pi}\left(\frac{m'(\xi_0)}{m^2(\xi_0)} - \frac{m''(\xi_0)}{m(\xi_0)}\right)}} e^{-\Delta\xi_0 t}$$

$$\equiv -\frac{1}{\pi\Delta^2} C_{\xi_0}(t) e^{-\Delta\xi_0 t}. \tag{4.28}$$

As can be numerically verified, $\lim_{t\to\infty} \xi_0(t) = 1$ and $\lim_{t\to\infty} C_{\xi_0}(t) = 0$. After the Wick rotation, this function will shift the frequency of $A(t)$. For simplicity, we will approximate it as an exponentially decaying function, and write

$$C_{\xi_0}(t) \approx D_{\xi_0} e^{-\omega_C t}. \tag{4.29}$$

Figure 13 shows a plot of $C_{\xi_0}(t)$ against a few exponentially decaying functions for $\Delta/mv^2 = 0.3$. As can be seen, $D_{\xi_0} = C_{\xi_0}(t=0) \approx 0.08$. The plot suggests that $C_{\xi_0}(t)$ decays polynomially. However, on the appropriate time scales, ω_C may be chosen conservatively, so the resulting decay rates are overestimated, and while a polynomial could be fitted better, we don't need that level of accuracy in this uncontrolled approximation. So we limit the accuracy of the model to times $t \lesssim 30/\Delta$, and take $\omega_C \approx 0.6\Delta$. With the saddle-point approximation, we therefore have

$$A(t) \approx -\frac{2}{\pi\Delta^2} D_{\xi_0} \cos(\omega_m t), \tag{4.30}$$

where $\omega_m = (\Delta + \omega_C)\xi_0$, and from the discussion above, we have $\omega_m \approx 2\Delta$.
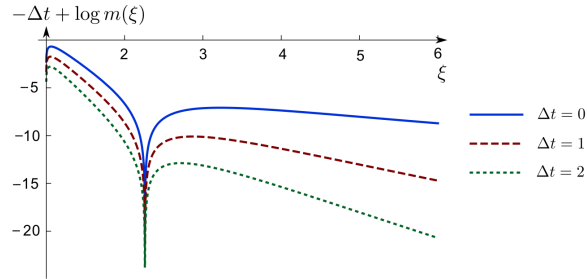
Figure 12: The exponent of the integrand in equation (4.27), evaluated for $\delta = 0.3$ at time $\Delta t = 0, 1, 2$, in solid blue, dashed red and dotted green, respectively. Qualitatively similar behaviour is observed for different values of δ.
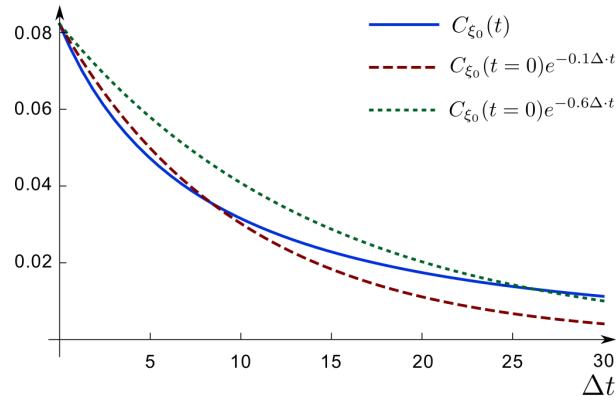
Figure 13: Plot of $C_{\xi_0}(t)$ in solid blue, along with two exponentially decaying functions in red dashed and green dotted. The true behaviour of $C_{\xi_0}(t)$ appears to be polynomial decay, but for the purpose of this section, we approximate the function by an exponential. This means that the decoherence is underestimated at late times.

With this, we can use (2.32) to calculate

$$R(z) = -\frac{2}{\pi\Delta^2}D_{\xi_0}\int_0^\infty dt e^{-tz}G_{\dot\phi\dot\phi}(t)\cos(\omega_m t) = -2pD_{\xi_0}\omega_0\int_0^\infty dt e^{-zt}\left(\delta(t) - \frac{\omega_0}{2}e^{-\omega_0 t}\right)\cos(\omega_m t)$$

$$= -pC_{\xi_0}\omega_0\left(1 - \frac{\omega_0}{2}\sum_{d=\pm}\int_0^\infty dt e^{-(z+\omega_0+id\omega_m)t}\right) = -pD_{\xi_0}\omega_0\left(1 - \frac{\omega_0}{2}\sum_{d=\pm}\frac{1}{z+\omega_0+id\omega_m}\right)$$

$$= -pD_{\xi_0}\omega_0\frac{z(z+\omega_0)+\omega_m^2}{(z+\omega_0)^2+\omega_m^2}, \tag{4.31}$$

where again we used the dimensionless parameter p, introduced in Eq. (4.20a). Using this, Eq.(4.15) becomes

$$\mathcal{G}_i(z) = \frac{1}{z + pD_{\xi_0}\omega_0\frac{z(z+\omega_0)+\omega_m^2}{(z+\omega_0)^2+\omega_m^2}} = \frac{(z+\omega_0)^2+\omega_m^2}{z(z+\omega_0)^2+\omega_m^2 z + pD_{\xi_0}\omega_0(z(z+\omega_0)+\omega_m^2)}$$

$$= \frac{(z+\omega_0)^2+\omega_m^2}{z^3 + \left(pD_{\xi_0}+2\right)\omega_0 z^2 + \left((1+pD_{\xi_0})\omega_0^2+\omega_m^2\right)z + pD_{\xi_0}\omega_0\omega_m^2}. \tag{4.32}$$

This may be written as

$$\mathcal{G}_i(z) = \frac{(z+\omega_0)^2+\omega_m^2}{(z-z_1)(z-z_2)(z-z_3)}, \tag{4.33}$$

where z_i are the solutions to the cubic equation

$$z^3 + (pD_{\xi_0}+2)\omega_0 z^2 + \left((1+pD_{\xi_0})\omega_0^2+\omega_m^2\right)z + pD_{\xi_0}\omega_0\omega_m^2 = 0. \tag{4.34}$$

To obtain the inverse Laplace transform, we now need to perform the Bromwich integral choosing a real $\lambda > \max\{\text{Re}(z_i)\}$. We then have

$$\overline{G}_{\tilde\gamma_i}(t) = \frac{1}{2\pi i}\lim_{A\to\infty}\int_{\lambda-iA}^{\lambda+iA}dz e^{zt}\frac{(z+\omega_0)^2+\omega_m^2}{(z-z_1)(z-z_2)(z-z_3)}, \tag{4.35}$$

from which we get

$$\overline{G}_{\tilde\gamma_i}(t) = \frac{(z_1+\omega_0)^2+\omega_m^2}{(z_1-z_2)(z_1-z_3)}e^{z_1 t} + \frac{(z_2+\omega_0)^2+\omega_m^2}{(z_2-z_1)(z_2-z_3)}e^{z_2 t} + \frac{(z_3+\omega_0)^2+\omega_m^2}{(z_3-z_1)(z_3-z_2)}e^{z_3 t}. \tag{4.36}$$

The expression (4.36) only makes sense for all times if all the roots z_i have non-positive real values. To figure out whether this condition holds, we introduce the dimensionless quantities $\zeta \equiv \frac{z}{\omega_0}$ and $\nu \equiv \frac{\omega_m}{\omega_0}$ and rewrite Eq. (4.34) as

$$f(\zeta) \equiv \zeta^3 + a\zeta^2 + b\zeta + c = 0, \tag{4.37a}$$
$$a = pD_{\xi_0} + 2, \tag{4.37b}$$
$$b = 1 + pC_{\xi_0} + \nu^2, \tag{4.37c}$$
$$c = pD_{\xi_0}\nu^2. \tag{4.37d}$$

Notice that all coefficients a, b, c are positive in the third-degree polynomial (4.37). This means that $f(\zeta) > 0$ for all $\zeta \geq 0$. We also have $f'(\zeta) = 3\zeta^2 + 2a\zeta + b > 0$ when $\zeta \geq 0$. Because of this, all real roots need to be negative or equal to 0. In particular it means that there is always at least one negative real root ζ_0. The discriminant d_f of f is given by

$$d_f = a^2 b^2 - 4b^3 - 4a^3 c - 27c^2 - 18abc. \tag{4.38}$$

When $d_f > 0$, all roots are real, distinct and non-positive, and $\overline{G}_{\tilde\gamma_i}(t)$ thus always decays without oscillating.

In the marginal case $d_f = 0$, there is the negative real root ζ_0, as well as a non-positive real double root. Equation (4.36) doesn't hold in this case since $\mathcal{G}_i(z)$ then has a second order pole. This is not a
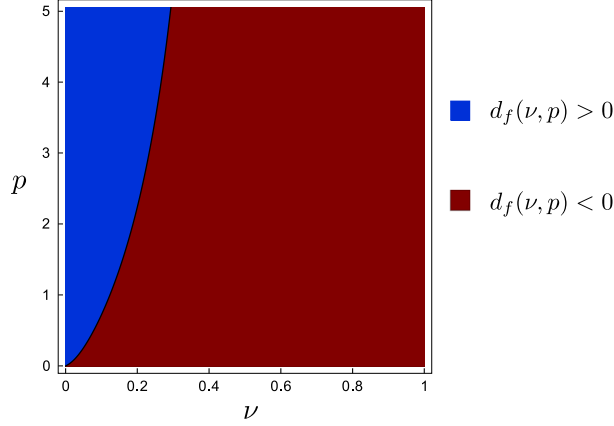
Figure 14: Plot of the sign of the discriminant d_f for the polynomial defined in Eq. (4.37). When $d_f > 0$, all the rates are real and non-positive. In most of the parameter space where $d_f < 0$, the rates are complex with non-positive real part, implying an oscillating decay.

computational problem, but this case will be excluded since it only matters in a measure 0 part of the parameter space.

In the last case, when $d_f < 0$, there is a negative real solution $\zeta_0 < 0$ as well as two complex conjugate solutions $\zeta_\pm = r \pm is$. We need to check when $r \leq 0$. Factoring Eq. (4.37a), we write

$$f(\zeta) = (\zeta - \zeta_0)(\zeta - r - is)(\zeta - r + is)$$
$$= \zeta^3 + \zeta^2(-\zeta_0 - 2r) + \zeta(r^2 + s^2 + 2r\zeta_0) - (r^2 + s^2)\zeta_0. \tag{4.39}$$

Comparing this to Eq. (4.37) gives $r = \frac{-\zeta_0 - a}{2}$, which is negative when $-a < \zeta_0$. This can be numerically verified to always hold. Figure 14 shows a plot of the sign of d_f, as a function of ν and p. Since ν is assumed to be large, d_f will tend to be negative, and we thus expect an oscillatory decay of $\overline{G}_{\tilde{\gamma}_i}(t)$.

Now that we have checked the consistency of Eq. (4.36), let us see what the addition of the sheep diagrams have changed. Taylor expanding the exact solutions of Eq. (4.37a) in ν^{-1}, the solutions are

$$\zeta_0 = -pD_{\xi_0} + \mathcal{O}\left(\frac{p}{\nu^2}\right), \tag{4.40a}$$

$$\zeta_\pm = -1 \pm i\left(\nu - \frac{1}{2\nu}pD_{\xi_0}\right) + \mathcal{O}\left(\frac{p}{\nu^2}\right). \tag{4.40b}$$

Substituting these solutions into Eq. (4.35), we get

$$\overline{G}_{\tilde{\gamma}_i}(t) = \left[1 + (1 - 2pD_{\xi_0})\frac{\omega_0^2}{\omega_m^2}\right]e^{-pD_{\xi_0}\omega_0 t} - \frac{\omega_0^2}{\omega_m^2}pD_{\xi_0}e^{-\omega_0 t}\cos(\omega_m t). \tag{4.41}$$

The partial summation by including all non-crossing diagrams leads to a slowly decaying part, just like we found in the previous section, as well as a faster decaying and oscillating part. This suggests that the decoherence has a fast initial time scale τ_1, given by

$$\tau_1 = \omega_0^{-1}, \tag{4.42}$$

on which a fraction of the coherence quickly dies. This fraction is controlled by the system parameters, and is suppressed by the large energy gap. After this initial quick decay, the rest of the coherence dies on a time scale τ_2 given by

$$\tau_2 = pD_{\xi_0}\omega_0, \tag{4.43}$$

which has a similar structure to what we found in the previous section in Eq. (4.24). Figure 15 shows a plot of both D and D_{ξ_0} as a function of $\Delta/(mv^2)$, and we see $D_{\xi_0} < D$, so the partial summation predicts a slower decay rate. This is probably partly an artifact of the saddle-point approximation, since this picks out only a frequency close to the gap, when there should actually be larger contributions.
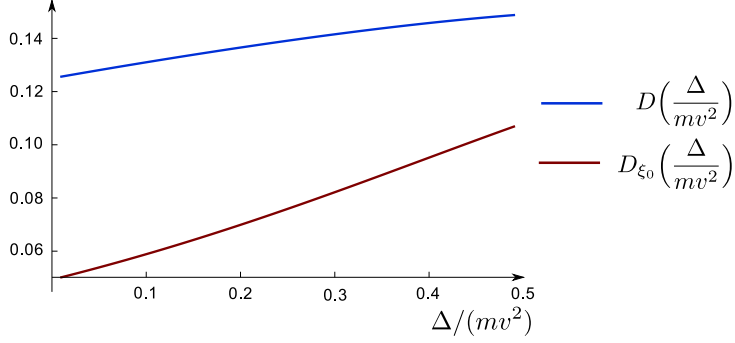
89

Figure 15: Plot of dimensionless factors D and $D_{\xi_0} = C_{\xi_0}(t = 0)$, defined in Eq. (4.20b) and Eq. (4.29), respectively, against $\Delta/(mv^2)$. The partial summation with the saddle-point approximation apparently predicts a slower decay.

5   Conclusions

We have calculated the decoherence times for a Majorana box qubit under the influence of electromagnetic noise from fluctuations in a capacitively coupled circuit. The noise was modeled as a classically fluctuating electric potential, and the time-dependency shifts the eigenstates of the system, lead to time-dependent instantaneous Majorana zero-energy modes.

The error probability $P_{\tilde{i},i}(t) = \frac{1}{2} + \frac{1}{2}\overline{G}^2_{\tilde{\gamma}_i}(t)$ was defined through a correlation function $\overline{G}_{\tilde{\gamma}_i}(t)$ of the instantaneous Majorana modes, and it captures the probability of measuring the parity of the instantaneous zero-energy modes at time t to be identical to the parity of Majorana pair at initialization. After statistically averaging over the potential fluctuations, an equations of motion analysis lead us to a diagrammatic expansion of $\overline{G}_{\tilde{\gamma}_i}(t)$. The order of the diagramatic expansion is controlled by the small parameter $e^2/(C\Delta)$.

If the environment frequency is much smaller than the gap $\omega_0 \ll \Delta$, the decoherence could be calculated by a partial summation of diagrams to leading order in ω_0/Δ. From this we concluded $\overline{G}^2_{\tilde{\gamma}_i}(t) = e^{-2t/\tau}$, where $\tau \propto \frac{\Delta}{e^2/C}\frac{\Delta}{k_B T}\omega_0^{-1}$. This result requires the parameters to obey $e^2/C, \omega_0 \ll k_B T \lesssim \Delta$. The eventual decay to a completely mixed state is thus expected because of the high temperature, and from the tendency of driven systems to heat up.

A partial summation of the diagrams to next-leading order in ω_0/Δ suggested an additional much shorter time scale $\tau_i = \omega_0^{-1}$, set purely by the circuit frequency, on which $\overline{G}_{\tilde{\gamma}_i}(t)$ is reduced by an amount proportional to $\omega_0^2 e^2 k_B T/(C\Delta^4)$. If true, this fast decay could be important in practical implementation of quantum computation, since this needs a low error rate to be practical.

Notably, the dephasing times are not found to be exponentially suppressed in temperature, which is a clear qualitative difference from what we will conclude by a Markovian treatment in the next chapter. This could be taken as an indication of a model breakdown for temperatures much smaller than the gap. In that case, the model has dubious applicability, since such temperatures would also imply substantial errors from quasiparticle poisoning [67].

Similar techniques to those we have used in this project have been used to study the problem of moving Majorana bound states by tuning local chemical potentials [45, 68]. Such studies could possibly be complemented by our models ability to handle additional random fluctuations from noisy gates.

6 Appendix: Deriving the matrix element

In this appendix we will calculate the matrix element in Eq. (2.3) in order to obtain an expression for the matrix element $W_E = W_{E(k)} = \langle \psi_0 | \tau_z | \psi_{E(k)} \rangle$, as defined in Eq. (2.5). We use the Hamiltonian H_{pw} from Eq. (2.2) for a single 1-dimensional p-wave superconductor in Eq. (2.2). We take the system to be half-infinite, with the position coordinate x constrained to $x \in [0, \infty)$, and impose $\Delta > 0$, which, as we shall see, corresponds with having the system in the topological phase. This means that we expect H_{pw} to have a single eigenstate $\psi_0(x)$ with zero energy, exponentially localized at $x = 0$. For computational simplicity we calculate W_E under the assumption $0 < \mu < \frac{m\Delta^2}{2}$. It will be useful to write H_{pw} in the form

$$H_{\mathrm{pw}} = \Delta \begin{pmatrix} \frac{\tilde{p}^2}{2\delta} - 1 & \tilde{p}/\delta \\ \tilde{p}/\delta & -\frac{\tilde{p}^2}{2\delta} + 1 \end{pmatrix}, \tag{6.1a}$$

$$\delta = \frac{\Delta}{mv^2}, \quad \tilde{p} = \frac{p}{mv}, \tag{6.1b}$$

in order to explicitly keep track of the dimensions. First, we calculate $\psi_0(x)$. The eigenvalue equation at zero energy reads

$$\begin{pmatrix} \frac{\tilde{p}^2}{2\delta} - 1 & \tilde{p}/\delta \\ \tilde{p}/\delta & -\frac{\tilde{p}^2}{2\delta} + 1 \end{pmatrix} \psi_0 = 0. \tag{6.2}$$

The solution has the form $\psi_0(x) = \sum_q \psi_{0,q}(x) = \sum_q \begin{pmatrix} u_{1,q} \\ u_{2,q} \end{pmatrix} e^{iqx} = \sum_q \chi_{0,q}^{iqx}$, and we impose the Dirichlet boundary conditions that $\psi(0) = \lim_{x\to\infty} \psi(x) = 0$. Each $\psi_{0,q}(x)$ satisfies Eq. (6.2) and are linearly independent. This gives us

$$\begin{pmatrix} \frac{\tilde{q}^2}{2\delta} - 1 & \tilde{q}/\delta \\ \tilde{q}/\delta & -\frac{\tilde{q}^2}{2\delta} + 1 \end{pmatrix} \chi_{0,q} = 0, \tag{6.3}$$

with $\tilde{q} = q/mv$. Eq. (6.3) implies

$$\tilde{q} = i\left(s_1 + s_2\sqrt{1 - 2\delta}\right), \tag{6.4}$$

where $s_1, s_2 = \pm 1$. In order to have a normalizable solution, the imaginary part of $\tilde{q}$ must be positive. With the assumption $0 < \delta < \frac{1}{2}$, we have $1 > \sqrt{1 - 2\delta}$, and so

$$\tilde{q} = \tilde{q}_\pm = i\left(1 \pm \sqrt{1 - 2\delta}\right). \tag{6.5}$$

The boundary condition $\psi(0) = 0$ implies that $\chi_{0,q_+} = -\chi_{0,q_-} \equiv \chi_0$. Noting that both components of χ_0 must be non-zero for a non-trivial solution, we write $\chi_0 = \frac{1}{\mathcal{N}_0} \begin{pmatrix} 1 \\ b \end{pmatrix}$. With this, we can solve Eq. (6.3), and find

$$\psi_0(x) = \frac{\sqrt{mv}}{\mathcal{N}_0} \begin{pmatrix} 1 \\ -i \end{pmatrix} \left(e^{-mv\left(1+\sqrt{1-2\delta}\right)x} - e^{-mv\left(1-\sqrt{1-2\delta}\right)x}\right), \tag{6.6}$$

where the normalization $\mathcal{N}_0$ is

$$\mathcal{N}_0 = \sqrt{\frac{1 - 2\delta}{\delta}}. \tag{6.7}$$

Note, that in the case with $\delta < 0$, corresponding to negative Δ, there is no normalizable solution at zero energy compatible with the boundary conditions, since that would imply $\mathrm{Im}\,\tilde{q}_- < 0$. This underlines the fact that the topological phase transition happens at $\Delta = 0$, where the gap also closes.

Above the energy gap, the wavefunctions $\psi_E(x)$ have a similar form $\psi_E(x) = \sum_k \chi_k e^{ikx}$, where $k = k(E)$ is a continuous function of the energy E. The Schrödinger equation for each term is now

$$\begin{pmatrix} \frac{\tilde{k}^2}{2\delta} - 1 & \tilde{k}/\delta \\ \tilde{k}/\delta & -\frac{\tilde{k}^2}{2\delta} + 1 \end{pmatrix} \chi_k = \xi\chi_k, \tag{6.8}$$

where $\xi = E/\Delta$ and $\tilde{k} = k(E)/mv$. The eigenvalue equation (6.8) leads to the following relation

$$\tilde{k} = s_1 \sqrt{2} \sqrt{-1 + \delta + s_2 \sqrt{1 - 2\delta + \delta^2 \xi^2}} \equiv s_1 \tilde{k}_{s_2}, \tag{6.9}$$

where $s_1, s_2 = \pm 1$. Since $\xi \geq 1$ we see $\tilde{k}_+$ is real. Furthermore, $(1 - \delta)^2 + \delta^2(\xi^2 - 1) > 0$, so the assumption that $\delta < \frac{1}{2}$ implies that $\tilde{k}_-$ is purely imaginary. For the wave number k_+, the corresponding normalizable wave functions are found from (6.8):

$$\psi_{\pm k_+}(x) \propto e^{\pm i k_+ x} \begin{pmatrix} \pm \tilde{k}_+/\delta \\ \xi - \frac{\tilde{k}_+^2}{2\delta} + 1 \end{pmatrix}. \tag{6.10}$$

Since $\tilde{k}_-$ is imaginary, the only normalizable solution with $\tilde{k}_-$ is

$$\psi_{+k_-}(x) = e^{i k_- x} \begin{pmatrix} \tilde{k}_-/\delta \\ \xi - \frac{\tilde{k}_-^2}{2\delta} + 1 \end{pmatrix}. \tag{6.11}$$

For convenience we rename $k_+ \equiv k$ and $k_- \equiv i\kappa$ and write the wave function at energy E as

$$\psi_E(x) = \frac{1}{\mathcal{N}_E} \left(e^{ikx} \begin{pmatrix} \tilde{k}/\delta \\ \xi - \frac{\tilde{k}^2}{2\delta} + 1 \end{pmatrix} + A e^{-ikx} \begin{pmatrix} -\tilde{k}/\delta \\ \xi - \frac{\tilde{k}^2}{2\delta} + 1 \end{pmatrix} + B e^{-\kappa x} \begin{pmatrix} i\tilde{\kappa}/\delta \\ \xi + \frac{\tilde{\kappa}^2}{2\delta} + 1 \end{pmatrix} \right). \tag{6.12}$$

We can use the continuity equation to simplify Eq. (6.12). Since the state $\psi_E(x)$ is stationary, the continuity equation imposes $\partial_x j_E(x) = 0$, where the probability current $j_E(x)$ is proportional to $\psi_E^*(x)\partial_x \psi_E(x) - \psi_E(x)\partial_x \psi_E^*(x)$. At positions far away from the left edge x, the last term in (6.12) has completely decayed. The probability current there is

$$j_E(x \gg \kappa^{-1}) \propto \frac{1}{|\mathcal{N}_E|^2} 2ik (1 - |A|^2) \left(\frac{\tilde{k}^2}{\delta^2} + \frac{\tilde{k}^4}{4\delta^2} \right), \tag{6.13}$$

The continuity equation demands $j_E(x_1) = j_E(x_2)$ for all x_1, x_2, and in particular, using that the wavefunction is zero for $x < 0$, we must have that Eq. (6.13) vanishes. This means $|A| = 1$, and so, we write $A = e^{i\theta_k}$. Imposing the Dirichlet boundary conditions $\psi_E(0) = 0$, we get two equations for B:

$$0 = \begin{pmatrix} \tilde{k}/\delta \\ \xi - \frac{\tilde{k}^2}{2\delta} + 1 \end{pmatrix} + e^{i\theta_k} \begin{pmatrix} -\tilde{k}/\delta \\ \xi - \frac{\tilde{k}^2}{2\delta} + 1 \end{pmatrix} + B \begin{pmatrix} i\tilde{\kappa}/\delta \\ \xi + \frac{\tilde{\kappa}^2}{2\delta} + 1 \end{pmatrix}. \tag{6.14}$$

These two equation yield the following

$$B = i\frac{k}{\kappa}(1 - e^{i\theta_k}), \tag{6.15a}$$

$$B = -\epsilon_k(1 + e^{i\theta_k}), \tag{6.15b}$$

where

$$\epsilon_k \equiv \frac{\xi - \frac{\tilde{k}^2}{2\delta} + 1}{\xi + \frac{\tilde{\kappa}^2}{2\delta} + 1}. \tag{6.16}$$

The Eqs. (6.15) imply

$$\tan \frac{\theta_k}{2} = \frac{\tilde{\kappa}}{\tilde{k}} \epsilon_k, \tag{6.17}$$

and so the wave function above the gap is

$$\psi_E(x) = \frac{1}{\sqrt{L}\mathcal{N}_E} \left(e^{ikx} \begin{pmatrix} \tilde{k}/\delta \\ \xi - \frac{\tilde{k}^2}{2\delta} + 1 \end{pmatrix} + e^{-ikx + i\theta_k} \begin{pmatrix} -\tilde{k}/\delta \\ \xi - \frac{\tilde{k}^2}{2\delta} + 1 \end{pmatrix} - \epsilon_k(1 + e^{i\theta_k})e^{-\kappa x} \begin{pmatrix} i\tilde{\kappa}/\delta \\ \xi + \frac{\tilde{\kappa}^2}{2\delta} + 1 \end{pmatrix} \right), \tag{6.18}$$

where we explicitly pulled the dimensionful factor $\sqrt{L}$, anticipating its emergence from the normalization. Next we need to determine the normalization $\mathcal{N}_E$. This is regularised by cutting off x at L, which we

will later take to infinity. Note, that when taking the norm of (6.18), the x-independent terms will be proportional to L after integration and thus will dominate all other terms. Thus, we approximate the normalization as

$$\mathcal{N}_E \approx \sqrt{2\frac{\tilde{k}^2}{\delta^2} + 2\left(\xi - \frac{\tilde{k}^2}{2\delta} + 1\right)^2}. \tag{6.19}$$

Now we are in position to calculate $W_E = \langle \psi_0 | \tau_z | \psi_E \rangle$. The algebra is lengthy, and we will omit the steps here. Keeping only the terms to order $1/\sqrt{L}$ we find

$$W_E = \frac{4ie^{-i\theta_k/2}}{\sqrt{mvL}\mathcal{N}} \left[\frac{1}{(2\delta - \tilde{k}^2)^2 + 4\tilde{k}^2} \left[(2\tilde{k}^2/\delta - a_k(2\delta - \tilde{k}^2)) \cos\left(\frac{\theta_k}{2}\right) - (2a_k\tilde{k} + 2\tilde{k} - \tilde{k}^3/\delta) \sin\left(\frac{\theta_k}{2}\right) \right] \right.$$
$$\left. - \epsilon_k \cos\left(\frac{\theta_k}{2}\right) \frac{\tilde{\kappa}/\delta - b_k}{\tilde{\kappa}^2 + 2(\tilde{\kappa} + \delta)}, \right. \tag{6.20}$$

where

$$a_k = \xi - \frac{\tilde{k}^2}{2\delta} + 1, \tag{6.21a}$$

$$b_k = \xi + \frac{\tilde{\kappa}^2}{2\delta} + 1, \tag{6.21b}$$

$$\mathcal{N} = \sqrt{\frac{2}{\delta}\left(\frac{\tilde{k}^2}{\delta^2} + a_k^2\right)}. \tag{6.21c}$$

Chapter 4

Project C:
Fidelity and visibility loss in Majorana qubits by entanglement with environmental modes

Inspired by the previous project, we set out to understand the coherence properties of ideal Majorana qubits better and to overcome some of the restrictions presented by the classical treatment. The central model of this paper is very similar to that studied in the previous chapter, with electromagnetic fluctuations in the environment causing quasiparticle excitations which result in parity flips of the Majorana modes. Like we saw in the previous chapter, the zero-energy modes get shifted by the electromagnetic fluctuations, but in this project, we treat the full quantum mechanical problem, which implies that the exact zero-energy modes are dressed by gapless bosonic modes in the environment. Using a Markovian approximation, we calculate the decay rates at finite temperatures. In contrast with the results of Project B, we find that the decay rates are exponentially suppressed in the ratio between the energy gap and temperature.

Even at zero temperature, the dressing of the zero-energy mode has consequences for the visibility of parity readouts that rely on quantum dots coupled to the bare Majorana modes. Intuitively, if the bosonic modes are heavily populated, energy can be extracted from them and excite a quasiparticle. This can lead to errors in readouts, but in the most optimistic cases it only leads to a drop of visibility in the readout. By including the full non-Markovian dynamics at zero temperature, we explicitly calculate the decoherence at late times, in the extreme case where the parity of the bare Majorana modes is projectively measured. We find a potentially significant loss of coherence in this case.

Our calculation demonstrates that the coupling and decoupling of measurement apparatus must be carefully implemented: Not only is there a risk of exciting quasiparticles directly, but also bosons, which can lead to a higher risk of errors and a lower readout visibility. Since the bosonic modes are gapless, some level of visibility loss is unavoidable.

Fidelity and visibility loss in Majorana qubits by entanglement with environmental modes

Morten I. K. Munk,[1] Reinhold Egger,[2] and Karsten Flensberg[1]

[1]*Center for Quantum Devices, Niels Bohr Institute, University of Copenhagen, 2100 Copenhagen, Denmark*
[2]*Institut für Theoretische Physik, Heinrich-Heine-Universität, 40225 Düsseldorf, Germany*

We study the dynamics and readout of topological qubits encoded by zero-energy Majorana bound states in a topological superconductor. We take into account bosonic modes due to the electromagnetic environment which couple the Majorana manifold to above-gap continuum quasiparticles. This coupling causes the degenerate ground state of the topological superconductor to be dressed in a polaronlike manner by quasiparticle states and bosons, and the system to become gapless. Topological protection and hence full coherence is only maintained if the qubit is operated and read out within the low-energy spectrum of the dressed states. We discuss reduction of fidelity and/or visibility if this condition is violated by a quantum-dot readout that couples to the bare (undressed) Majorana modes. For a projective measurement of the bare Majorana basis, we formulate a Bloch-Redfield approach that is valid for weak Majorana-environment coupling and takes into account constraints imposed by fermion-number-parity conservation. Within the Markovian approximation, our results essentially confirm earlier theories of finite-temperature decoherence based on Fermi's golden rule. However, the full non-Markovian dynamics reveals, in addition, the fidelity reduction by a projective measurement. Using a spinless nanowire model with *p*-wave pairing, we provide quantitative results characterizing these effects.

I. INTRODUCTION

Currently, there is a large interest in topological phases with defects that can nonlocally store quantum information and thus possibly offer avenues to topologically protected quantum information processing [1,2]. One such example is a topological superconductor (TS) wire which supports Majorana bound states (MBSs) at its ends [3]. Because it takes two MBSs to form a fermionic level, the occupancy of this level is stored nonlocally when the MBSs are spatially well separated. As a consequence, under ideal conditions, the quantum information can neither be retrieved by a local measurement nor be destroyed by local noise sources. The search for MBSs has intensified since the appearance of theoretical proposals in hybrid systems made of superconductors and semiconductors [4–10] or topological insulators [11]. Several tunneling spectroscopy experiments have already been published and appear to be consistent with the existence of MBSs [12–17].

The prospect of robust MBS realizations in solid-state systems has spurred many proposals for Majorana-based qubits [18–22] and for error-correction schemes [23–29]. The latter can correct errors due to, e.g., quasiparticle poisoning caused by spurious fermionic excitations. Majorana-based architectures do not have a universal set of topologically protected gates and are limited to Clifford gates only. The above-mentioned schemes must therefore be augmented by nonprotected gates in order to achieve universal quantum computation [18,21,27,30–32]. More complex anyon excitations, e.g., Fibonacci anyons, would allow to implement a universal set of topologically protected gates [2]. However, such systems are still far from experimental realization.

Majorana qubits are often argued to have long coherence times because of the underlying topological protection.

The usual reasoning is that because no local operator can split the topological ground-state degeneracy, the quantum information is protected against local perturbations as long as the MBSs are nonoverlapping. For finite MBS overlap, the protection of the ground-state degeneracy is lifted and protection is lost. This case has recently been analyzed in Ref. [33]. Even when direct MBS overlaps are negligibly small, as will be assumed in our work, boson-mediated couplings of MBSs to above-gap quasiparticles cause a coherence decay at finite temperatures [34–43]. The bosonic modes could represent, for instance, phonons or fluctuating charge degrees of freedom. This finite-temperature decoherence mechanism follows from a Markovian approximation, i.e., by assuming a negligible memory time of the environment. Available estimates of the corresponding decoherence rate Γ, obtained by assuming either uniform [36,37] or nonuniform [43] gate voltage fluctuations, suggest that coherent qubit operation may be hard to achieve on above-microsecond timescales even though the rate is exponentially small, $\Gamma \propto T \exp(-\Delta/k_{\mathrm{B}}T)$, with the TS gap Δ and temperature T (see, e.g., Ref. [37]). Recent work has also studied the fault tolerance threshold for Majorana qubits in a similar setting [44].

One of our goals is to address what happens in the non-Markovian case, both at $T = 0$ and finite T. We consider a specific encoding, which we denote a *bare-Majorana qubit* [Fig. 1(a)], where the qubit space is addressed by quantum dots that couple to the *uncoupled* and *undressed* MBSs, as schematically illustrated in Fig. 1(a). This setup has, for example, been proposed for measurement-based manipulations of a topological quantum computer [20,21]. In such setups, MBSs couple both to readout devices, e.g., the dot in Fig. 1(a), and to bosonic and quasiparticle environments.
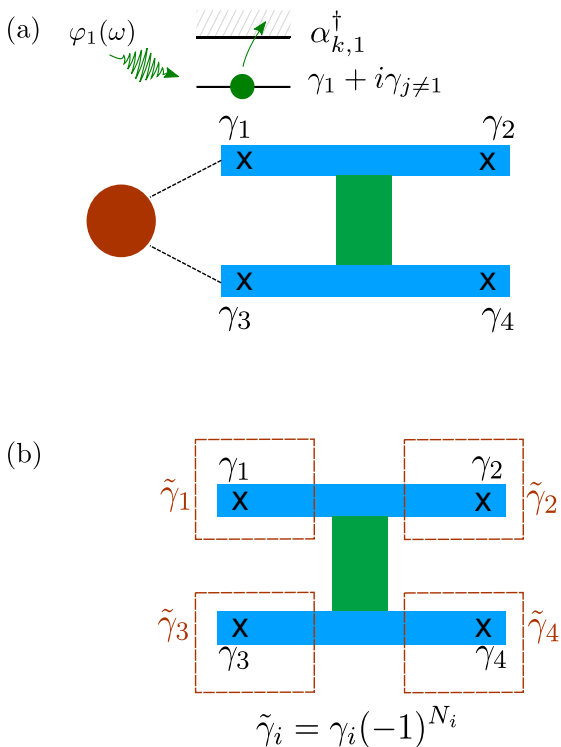
FIG. 1. Basic setup and two types of qubit readouts with $M = 4$ MBSs. Each MBS is coupled to independent local charge fluctuations. The blue horizontal bars represent TS wires which are connected by a conventional superconductor bridge (green vertical bar). The basic mechanism for decoherence is also illustrated for bosons representing voltage fluctuations $\varphi_1(\omega)$, which cause coupling between the MBS sector and the gapped quasiparticle sector. (a) *Bare Majorana readout*. With a tunnel-coupled quantum dot (red circle), one can read out $i\gamma_1\gamma_3$ [20,21,31]. (b) *Total fermion-parity encoding* where the qubit information is stored in the combined parity of the MBS plus the local quasiparticle continua, mathematically represented by the modified Majorana operators $\tilde{\gamma}_i$. In principle, this qubit is immune to local charge fluctuations. However, manipulation and readout by, e.g., control of total charge in each arm is practically very difficult. In this paper, we focus on case (a).

In order to analyze the non-Markovian dynamics of the bare-Majorana qubit, we develop and apply a modified Bloch-Redfield master-equation approach [45] which is valid for weak Majorana-environment coupling. Moreover, we also analyze the readout protocol by using perturbation theory. Employing the Bloch-Redfield equations, we investigate the dynamics of bare-Majorana qubits formed from M nonoverlapping MBSs in the presence of local (quantum) charge fluctuations. The interaction between these fluctuations and the MBSs implies that eigenstates of the entire system exhibit entanglement between the MBS sector and the environment. (The latter is formed by quasiparticles and the bosonic modes describing charge fluctuations.) Because of this entanglement, topological protection is only preserved for a combined fermion-parity degree of freedom (combined continua and MBSs) [cf. Fig. 1(b) and Sec. II B below] and not for the isolated MBS manifold.

The entanglement of MBSs and environmental modes can physically be understood as result of virtual (off-shell)

processes. As a consequence, all coherences of the bare (undressed) Majorana system will be reduced by a factor $1/(1 + \eta)$ at long times. For the ground state, the reduction factor corresponds to the squared overlap between the true polaronlike ground state and the bare ground state and it is relevant for a *projective* measurement of the state of the bare MBS. We discuss qualitatively how this theory can be adapted to the case of slow turn-on of the measurement circuit. Even though the system is gapless, it should still be possible to minimize the effect of quasiparticle generation if one effectively reads out the entangled (polaronlike) states by carefully timing the readout device. Moreover, by engineering of the electromagnetic environment, it would be possible to improve on the adiabaticity condition, for example by creating a gapped or reduced low-energy environment spectrum.

The minimal setup with $M = 4$ is illustrated in Fig. 1(a), where the MBSs forming the qubit are individually coupled to independent local charge fluctuations. The qubit state can then be read out, for example, by coupling a MBS pair to a nearby quantum dot [20,21,31]. We emphasize that the four edge regions of the qubit are not coupled in our analysis. Therefore, the effects we consider all result from a system which in principle has topological protection. Effects beyond this model, for example, finite overlap of the MBSs or the quasiparticle states, come on top of our analysis. The topological protection here means that if one operates and reads out the qubit in a total-parity basis, coherence is fully maintained. This could, for example, be done by a charge readout after disconnecting sections of the Majorana system as suggested by Aasen *et al.* [19].

The paper is organized as follows. In Sec. II, we define the bare-Majorana qubit encoding and discuss an alternative fermion-parity qubit encoding [46], which would be free from decoherence but seems difficult to realize in practice. In Sec. III, we then explain the physics of the Majorana-environment coupling. In Sec. IV, we give a simple physical argument for the reduction of fidelity based on first-order perturbation theory. In Sec. V, we consider projective readout of the bare MBS. For this purpose, we develop in Sec. V B a Bloch-Redfield master-equation approach for studying the dynamics of a bare-Majorana qubit. The Markovian limit is discussed in Sec. V C, followed by a study of non-Markovian effects Sec. V D. In Sec. V E, we apply this theory to a specific case where MBSs and quasiparticles originate from a spinless TS wire with p-wave pairing symmetry [7]. In Sec. V E 1, we address the finite-T case, and in Sec. V E 2 our $T = 0$ results are presented. The paper closes in Sec. VI with a summary and concluding remarks. Technical details have been delegated to several appendices.

II. QUBIT READOUT

In this section, we discuss how the quantum information is addressed in Majorana-based qubits and we distinguish between two different principles. The first relies directly on the zero modes such that coupling to MBSs, for example, via quantum dots [20,21], is used to read out or initialize the qubit state. We refer to this setup as a *bare-Majorana qubit*. The second method represents a *total-parity qubit*. The latter requires measurements of total parities which in

turn necessitate tunable Josephson junctions as, e.g., in the proposal of Ref. [19]. The difficulty is therefore in choosing the right timescales for switching on and off the coupling between the various segments of the qubit, a problem analyzed in Ref. [47]. In this paper, we investigate the decoherence dynamics of a bare-Majorana qubit.

A. Bare-Majorana qubit

Consider a Majorana island as the one depicted in Fig. 1(a), where MBSs correspond to self-adjoint Majorana operators $\gamma_j = \gamma_j^\dagger$, with $j = 1, \ldots, M$ and anticommutation relations $\{\gamma_j, \gamma_{j'}\} = 2\delta_{jj'}$. For more detailed device layouts and measurement schemes, see Refs. [20,21]. A quantum dot is tunnel coupled to two MBSs for the purpose of reading out the joint MBS parity. The qubit with attached readout device is described by the Hamiltonian

$$H = \varepsilon_d c_d^\dagger c_d + \sum_i (t_i^* c_d^\dagger \Psi(r_i) + \text{H.c.})$$
$$+ H_{\text{qubit}} + E_C(N_{\text{qubit}} - N_g)^2, \quad (1)$$

where c_d is the fermionic dot-level annihilation operator, $\Psi(r_i)$ is the electron operator in the TS taken at the position of the tunnel coupling to MBS i, t_i is the corresponding tunneling amplitude, H_{qubit} describes the qubit with its coupling to other environments (see Sec. III), N_{qubit} is the qubit total electron-number operator, N_g is a dimensionless gate potential, and, finally, E_C is the charging energy of the Majorana island. If the readout is done measuring the quantum charge by a charge sensor, the readout device is effectively distinguishing the derivative of the energy:

$$\langle n_d \rangle = \frac{d\langle H \rangle}{d\varepsilon_d}. \quad (2)$$

Similarly, if instead the capacitance of a circuit is measured, the readout device effectively reads out the second derivatives $d^2\langle H \rangle/d\varepsilon_d^2$ [21].

We assume the system is tuned so that the charge configuration (n_d, N_{qubit}) is near $(0,0)$ and $(1, -1)$. In this case, the Hamiltonian (1) becomes (up to a constant)

$$H = \tilde{\varepsilon}_d c_d^\dagger c_d + \sum_i (t_i^* c_d^\dagger \Psi(r_i) + \text{H.c.}) + H_{\text{qubit}}, \quad (3)$$

where $\tilde{\varepsilon}_d = \varepsilon_d + E_C(1 + 2N_g)$.

When projecting the qubit to its low-energy subspace, we replace the electron operator by the respective Majorana operator $\Psi(r_i) \approx a_i \gamma_i$, where a_i is the value of the electron component of the MBS wave function at r_i. We then include the a_i in the definition of the tunnel couplings t_i.

We can only solve for the energy in the case where $H_{\text{qubit}} = 0$, i.e., for the ideal situation without environmental degrees of freedom. In this case, assuming that the quantum dot is tunnel coupled to γ_1 and γ_3 only, the energies $E_{s=\pm}$ of the split ground-state manifold are given by

$$E_s = \frac{\tilde{\varepsilon}_d}{2} - \sqrt{\left(\frac{\tilde{\varepsilon}_d}{2}\right)^2 + |t_1|^2 + |t_3|^2 - 2s\,\text{Im}[t_1 t_3^*]}, \quad (4)$$

where the combined parity $s = (-1)^{(i\gamma_1\gamma_3-1)/2+n_d}$ is a good quantum number.

When the qubit Hamiltonian is nonzero, we need to study the tunneling Hamiltonian perturbatively. For small t_i, and assuming that N_g is tuned to a value where the quantum dot is empty ($c_d^\dagger c_d = 0$) without tunneling, second-order perturbation theory gives the effective Hamiltonian [21]

$$H^{(2)} = \sum_{i,j} \frac{2i\gamma_i\,\gamma_j\,\text{Im}[t_i\,t_j^*] - |t_i|^2 - |t_j|^2}{2\tilde{\varepsilon}_d} + H_{\text{qubit}}. \quad (5)$$

The expression (5) is perturbative in the tunneling coupling and valid away from the charge-degeneracy point. Evidently, in this regime, when the dot is only coupled to γ_1 and γ_3, then $i\gamma_1\gamma_3 = \pm 1$ is a good quantum number.

To summarize, in this section we have discussed various readout schemes of Majorana qubits. When reading out the parity of two MBSs using a quantum dot, the readout device couples (for $M = 4$) to the Pauli operators

$$\sigma_x = i\gamma_1\gamma_2, \quad \sigma_y = i\gamma_2\gamma_3, \quad \sigma_z = i\gamma_1\gamma_3. \quad (6)$$

However, when the Majorana qubit is coupled to other degrees of freedom, the qubit as defined in Eq. (6) is no longer well defined (because the Pauli operators σ_i do not necessarily commute with H_{qubit}) and one needs to discuss the influence on the readout fidelity and/or readout visibility. This is the main purpose of this paper. In Sec. III, we set up our model for the qubit (6) in the presence of environmental modes. In the subsequent sections, we then study the influence of qubit-environment entanglement on the qubit dynamics.

B. Total-parity qubit

As an alternative to the bare-Majorana readout discussed above, one can define a set of Pauli operators based on the total number parity of each region which is fully protected against decoherence. This approach was pointed out by Akhmerov [46] who showed that topological protection is maintained as long as different MBSs do not interact directly or via continuum states. Instead of Eq. (6), one defines Pauli operators by taking into account the total number of fermions in each spatial region,

$$\tilde{\sigma}_x = \sigma_x(-1)^{N_1+N_2}, \quad \tilde{\sigma}_y = \sigma_y(-1)^{N_2+N_3},$$
$$\tilde{\sigma}_z = \sigma_z(-1)^{N_1+N_3}, \quad N_i = \sum_k \alpha_{k,i}^\dagger \alpha_{k,i}, \quad (7)$$

where the operator N_i counts the number of above-gap quasiparticles in the respective region (cf. Sec. III). It is easy to check that the $\tilde{\sigma}_{x,y,z}$ satisfy the Pauli algebra, e.g.,

$$\tilde{\sigma}_x\tilde{\sigma}_y = i\sigma_z(-1)^{N_1+2N_2+N_3} = i\tilde{\sigma}_z. \quad (8)$$

In addition, all $\tilde{\sigma}$ matrices commute with the full Hamiltonian H (including the environmental degrees of freedom), which in turn conserves all parities associated with pairs of regions,

$$P_{ij} = [(i\gamma_i\gamma_j - 1)/2 + N_i + N_j]\text{mod}2. \quad (9)$$

Another way to understand this fact is to verify that the modified Majorana operators

$$\tilde{\gamma}_j = \gamma_j(-1)^{N_j} \quad (10)$$

commute with H. We refer to Fig. 1(b) for an illustration of the total-parity Majorana operators.

The new Pauli operators (7) represent quantum information that is topologically protected and can only be corrupted by finite-size effects, causing MBS wave-function overlap or transfer of quasiparticles between different MBS regions. However, in practice this protection can only be employed if one is able to manipulate and read out in this basis. This could in principle be performed by using the charging energy to fuse two MBSs [18,19] which would require tunable Josephson junctions that can be tuned to the closed regime, thereby limiting the allowed timescales [47]. However, the coupling to environmental bosons imposes further restrictions because of the absence of a gap.

III. COUPLING OF MAJORANA STATES TO ENVIRONMENT

We now describe a general model for studying how the dynamics of a Majorana-based qubit is affected by the coupling between MBSs and environmental degrees of freedom. By environmental modes, we here mean above-gap TS quasiparticles and bosonic modes corresponding to electric potential fluctuations. Let us begin with the unperturbed superconducting system in the absence of charge fluctuations. It is governed by the Hamiltonian

$$H_0 = \frac{1}{2} \int d\mathbf{r} \, \Psi^\dagger(\mathbf{r}) \mathcal{H}_{\text{BdG}} \Psi(\mathbf{r}), \qquad (11)$$

where we define 4-spinors

$$\Psi(\mathbf{r}) = (\Psi_\uparrow(\mathbf{r}), \Psi_\downarrow(\mathbf{r}), \Psi_\downarrow^\dagger(\mathbf{r}), -\Psi_\uparrow^\dagger(\mathbf{r}))^T, \qquad (12)$$

with the electron annihilation operator $\Psi_\sigma(\mathbf{r})$ for spin $\sigma = \uparrow, \downarrow$ and position $\mathbf{r}$. We use Pauli matrices $\tau_{x,y,z}$ in Nambu (particle-hole) space. The Bogoliubov–de Gennes (BdG) Hamiltonian appearing in Eq. (11) corresponds to the Nambu matrix

$$\mathcal{H}_{\text{BdG}} = \begin{pmatrix} \mathcal{H}_0 & \Delta \\ \Delta^\dagger & -\mathcal{T}\mathcal{H}_0\mathcal{T}^{-1} \end{pmatrix}, \qquad (13)$$

where $\mathcal{H}_0$ is the spinful single-electron Hamiltonian in the absence of pairing (and, of course, without charge fluctuations), Δ is the pairing potential in BCS mean-field approximation, and $\mathcal{T}$ is the time-reversal operator. After diagonalizing the BdG Hamiltonian, the Hamiltonian (11) can be written in terms of BdG quasiparticle eigenmodes corresponding to a set of annihilation operators α_k. The α_k operators describe fermionic eigenstates with energy $E_k \geqslant \Delta$, where quantum numbers k label different eigenmodes. Consequently, Eq. (11) takes the form

$$H_0 = \sum_k E_k \alpha_k^\dagger \alpha_k + \text{constant}. \qquad (14)$$

In the topological phase, an even number M of localized zero-energy MBSs can be present in addition. In particular, for one-dimensional (1D) TS wires, MBSs exist at each end of a topological wire segment. As the Majorana operators γ_j describe zero-energy modes, they do not appear in H_0 and thus also commute with the unperturbed Hamiltonian $[H_0, \gamma_j] = 0$ [6–10].

We next note that H_0 implicitly includes the electric potential in the superconducting material. If this potential can

change due to fluctuations mediated by other (bosonic) degrees of freedom, it must be included in the model. The full Hamiltonian $H = H_{\text{qubit}}$ is then given by

$$H = H_0 + H_\varphi + H_{\text{int}}, \quad H_{\text{int}} = \int d\mathbf{r} \, \rho_e(\mathbf{r})\varphi(\mathbf{r}), \qquad (15)$$

where $\varphi(\mathbf{r})$ is an operator that describes the electric potential fluctuations caused by a set of bosonic modes. The potential fluctuations occur, in principle, on all length scales. For simplicity, we here focus on the most important components, namely, the potential fluctuations with length scales of order the coherence length. Hence, we replace $\varphi(\mathbf{r})$ by M-independent fluctuating potentials φ_j, one for each region $j = 1, \ldots, M$. The bare dynamics of these fluctuations is governed by a noninteracting bosonic Hamiltonian H_φ. In principle, one could also include fields describing fluctuations of the magnetic field, but for simplicity we focus on electrical fluctuations below.

Expressing the electron density $\rho_e(\mathbf{r})$ in Eq. (15) in terms of BdG quasiparticle operators, we get two contributions $H_{\text{int}} = H_1 + H_2$, with

$$H_1 = \sum_{j=1}^M \gamma_j \Gamma_j \varphi_j, \quad \Gamma_j = \sum_k (W_{k,j} \alpha_{k,j}^\dagger - W_{k,j}^* \alpha_{k,j}) \qquad (16)$$

and

$$H_2 = \sum_{k,k',j} \left(V_{kk'j}^{(1)} \alpha_{k,j}^\dagger \alpha_{k',j} + V_{kk'j}^{(2)} \alpha_{k,j}^\dagger \alpha_{k',j}^\dagger \right) \varphi_j + \text{H.c.} \qquad (17)$$

We here define the W matrix elements as

$$W_{k,j} = \langle k, j | \tau_z | \text{MBS}, j \rangle, \qquad (18)$$

where $|k, j\rangle$ ($|\text{MBS}, j\rangle$) denotes a BdG quasiparticle (MBS) spinor wave function in the jth region. For concrete results, one has to consider a specific model for the TS nanowire. In Sec. V E (see also Appendix B), we discuss the matrix elements (18) for a semi-infinite spinless TS wire model with p-wave pairing.

To recapitulate, the above model Hamiltonian describes coupling between a TS and bosonic potential fluctuations. To emphasize the important physics studied in this paper, we have made the following key simplifications: (i) All MBSs are treated as nonoverlapping zero-energy states. (ii) Quasiparticle modes described by the fermionic operators $\alpha_{k,j}$ are assumed to have no significant support in spatial regions where other MBSs reside, and hence no MBS-MBS interactions are mediated through continuum states either. (iii) The charge density $\rho_e(\mathbf{r})$ in the region near the jth MBS couples to an operator φ_j describing the long-wavelength component of the field in that region. Given the typically small size of these regions, we neglect the spatial dependence of φ_j. (iv) We assume that different φ_j operators are uncorrelated, i.e., each MBS is independently coupled to its own fluctuating electric field. (v) The $V^{(1,2)}$ matrix elements in Eq. (17) are not important for the Bloch-Redfield approach used below, and we will assume that the main effect of H_2 is to contribute to the fast quasiparticle relaxation processes.

Finally, the Gaussian Hamiltonian H_φ is fully determined by first noting that $\langle\varphi_j\rangle_{H_\varphi} = 0$ and then specifying the two-point bath correlation function [45]. For simplicity, we here
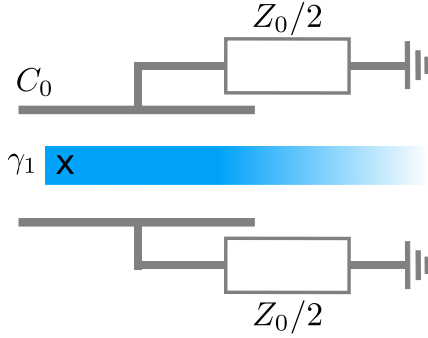
FIG. 2. Equivalent circuit for the electromagnetic environment coupled to the Majorana operator γ_1. The environments near the other MBSs are not shown.

assume that the different environments in the various regions ($j = 1, \ldots, M$) can be characterized by the same spectral density $J(\omega)$. By assumption (iv) above, the only nonvanishing correlator is given by

$$
\begin{aligned}
B(t) &= \langle \varphi_j(t) \varphi_j(0) \rangle_{H_\varphi} \\
&= \int_0^\infty \frac{d\omega}{2\pi} J(\omega) \{ e^{-i\omega t}[1 + n_B(\omega)] + e^{i\omega t} n_B(\omega) \}, \quad (19)
\end{aligned}
$$

where $n_B(\omega) = 1/(e^{\beta\omega} - 1)$ with $\beta = 1/k_B T$ is the Bose-Einstein function. The spectral density $J(\omega)$ of the electromagnetic environment is taken for the equivalent circuit in Fig. 2, where fermions couple through the capacitance C_0 to the electromagnetic environment with resistance Z_0. We note that other spectral densities, for example, containing a $1/f$ component could be more relevant, but here we focus on the so-called Ohmic case for simplicity. Using linear response theory, $B(t)$ in Eq. (19) can be related to the impedance of the circuit [45]. We thereby obtain the spectral density

$$
J(\omega) = \frac{2e^2 \omega_0}{C_0} \frac{\omega}{\omega^2 + \omega_0^2}, \quad \omega_0 = \frac{1}{C_0 Z_0}. \quad (20)
$$

The linear low-frequency dependence is characteristic of an Ohmic environment. It is of course possible to engineer the environment spectral function, such that it is has low-energy modes suppressed. This would be relevant if one wants to improve on the adiabaticity conditions for the qubit operations.

IV. READOUT OF THE MAJORANA QUBIT WITH ENVIRONMENTAL COUPLING

A. General remarks

In this section, we discuss on a general level the principles of Majorana-qubit readout when the qubit Hamiltonian does not commute with the degree of freedom that is being measured. As we saw above, the qubit in principle still has topological protection in the sense that the total-parity qubit operators $\tilde{\sigma}_i$ in Eq. (7) are conserved and cannot be measured by any local operator (when the readout device is detached). However, when attached to the readout device, the topological protection is of course broken and care must be taken if the measurement device should not give the wrong readout yielding a loss of fidelity.

We define a basis $|p, \tilde{\sigma}\rangle$ using eigenstates of the Pauli operator $\tilde{\sigma}_z = i\tilde{\gamma}_1 \tilde{\gamma}_3$ which is the basis natural for the quantum-dot coupling in Fig. 1,

$$
i\tilde{\gamma}_1 \tilde{\gamma}_3 |p, \tilde{\sigma}\rangle = \tilde{\sigma} |p, \tilde{\sigma}\rangle, \quad (21)
$$

where p refers to environmental quantum numbers (see below for a concrete calculation to first order). The states $\{|p, \tilde{\sigma}\rangle\}$ are also eigenstates of the Hamiltonian

$$
H_{\text{qubit}} = \sum_{p, \tilde{\sigma} = \pm 1} \Omega_p |p, \tilde{\sigma}\rangle \langle p, \tilde{\sigma}|, \quad (22)
$$

where Ω_p are the eigenenergies. The even and odd eigenstate sectors are related by

$$
|p, -1\rangle = \tilde{\gamma}_1 |p, 1\rangle. \quad (23)
$$

Next, we wish to express the operator $\sigma_z = i\gamma_1 \gamma_3$, which couples to the quantum dot see Eq. (4) in the eigenbasis of the topological qubit. First, we note that

$$
\langle p, -1|i\gamma_1\gamma_3|p', -1\rangle = -\langle p, 1|i\gamma_1\gamma_3|p', 1\rangle, \quad (24a)
$$

$$
\langle p, -1|i\gamma_1\gamma_3|p', 1\rangle = 0. \quad (24b)
$$

The first relation follows from Eq. (23) and the definition of $\tilde{\gamma}_1$ in Eq. (10), while the second one follows from parity conservation. These relations now allow us to write the operator $i\gamma_1\gamma_3$ as

$$
\sigma_z = i\gamma_1\gamma_3 = \sum_{pp'} A_{pp'}[|p, 1\rangle\langle p', 1| - |p, -1\rangle\langle p', -1|]. \quad (25)
$$

For an example of $A_{pp'}$, see below where we calculate it in perturbation theory.

Let us now discuss the readout procedure using a quantum dot that effectively couples to the operator in Eq. (25). Clearly the bare-Majorana Pauli operator σ_z does in general not commute with the Hamiltonian of the qubit H_{qubit} in Eq. (22). However, if we consider the situation where the energy scales of the quantum dot, the inverse timescales for switching on the readout circuit τ^{-1} and temperature $k_B T$, all are well within the gap of the topological superconductor ($\varepsilon_d, t_1, t_2, \tau^{-1}, k_B T) \ll \Delta$, we should project Eq. (25) to the low-energy sector determined by these energy scales. Moreover, for the case without splitting of the topological qubit, the initial density matrix of the qubit is assumed to be in a thermal (low-temperature) state of the form

$$
\rho_{\text{qubit}} = \sum_p (\alpha|p, 1\rangle + \beta|p, -1\rangle)(\alpha^* \langle p, 1| + \beta^* \langle p, -1|)P_p, \quad (26)
$$

which has full coherence in the topologically protected sector. Here, $P_p \propto \exp(-\Omega_p/k_B T)$ is the thermal distribution.

When adding the measurement circuit, the Hamiltonian has additional terms. For example, for weak dot tunneling and $\tilde{\varepsilon}_d > 0$, the Hamiltonian is given by Eq. (5), which in the qubit eigenbasis follows from Eqs. (22) and (25):

$$
H^{(2)} = \sum_{pp', \tilde{\sigma}} (\Omega_p \delta_{pp'} + \tilde{\sigma} A_{pp'} \Lambda)|p, \tilde{\sigma}\rangle\langle p', \tilde{\sigma}| - \frac{|t_1|^2 + |t_3|^2}{\tilde{\varepsilon}_d}, \quad (27)
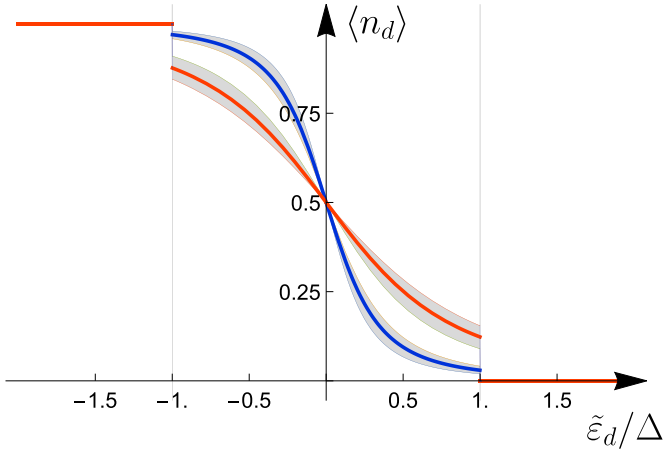$$

FIG. 3. The measured dot occupation $\langle n_d \rangle$ as a function of the dot potential $\tilde{\varepsilon}_d$ for the readout protocol shown in Fig. 1. The outcomes for the two parity states are illustrated with the blue and red curves. The full lines show the result without environmental coupling, while the shaded areas illustrate the possible outcomes for when the bare-Majorana parity $i\gamma_1\gamma_3$ does not commute with the qubit Hamiltonian. If the shaded regions do not overlap, the coupling to environments gives rise to a visibility reduction, while when they do overlap the fidelity is reduced. Note that $|\tilde{\varepsilon}_d|$ must be smaller than the gap (vertical lines) for the readout to be valid.

where we defined the energy scale that splits the topological degeneracy

$$\Lambda = \frac{2 \, \text{Im}[t_1 t_3^*]}{\tilde{\varepsilon}_d}. \tag{28}$$

The sensor measures the charge on the dot, which is given by the operator $n_d = dH^{(2)}/d\tilde{\varepsilon}_d$.

After the quantum-dot readout circuit has been switched on, the population of the energy spectrum is not necessarily a thermal population of the eigenstates as in Eq. (27), but depends on the protocol for attaching the dot. The readout fidelity then depends on both this population and on the structure of the matrix **A**.

For small dot-qubit coupling (which means that Λ is small compared to $k_B T$ and $\hbar \tau^{-1}$), one can treat the parity-dependent term in Eq. (27) as a perturbation. Therefore, if the diagonal elements A_{pp} for the relevant energies have a definite sign, the total-parity degree of freedom η can in principle be read out with perfect fidelity. This corresponds to the situation depicted in Fig. 3 where the possible outcomes for the two parity states do not overlap. In this situation, the environmental coupling only leads to a reduction of visibility. However, if the sign of A_{pp} varies for the populated energies, the two distribution functions of possible readouts overlap and, as a result, the fidelity is reduced.

For stronger Λ, the full matrix $A_{pp'}$ is important for determining the eigensystem of the Hamiltonian (27). Again, if the signs of the diagonal elements of A in this new basis are not unique for the energies that are populated, the fidelity of the readout procedure is reduced.

B. Perturbative treatment of the entangled environment-qubit basis

In this section, we present a perturbative analysis of the entanglement between the MBS manifold and the environment and discuss the consequences for the readout visibility/fidelity. For concreteness, we discuss the case $M = 4$ and use the basis $|n_{13}, n_{24}\rangle \otimes |\{k, j\}, \{q, j\}\rangle_{\text{env}}$, where $\{k, j\}, \{q, j\}$ label states in the quasiparticle and boson environments, respectively. On the other hand, n_{13} and n_{24} refer to the fermion level occupations corresponding to the respective fermion operators

$$d_{13} = (\gamma_1 + i\gamma_3)/2, \quad d_{24} = (\gamma_2 + i\gamma_4)/2, \tag{29}$$

where the number states $|n_{13}, n_{24}\rangle$ follow from the empty state $|00\rangle$ as

$$d_{13}^\dagger|00\rangle = |10\rangle, \quad d_{24}^\dagger|00\rangle = |01\rangle, \quad d_{24}^\dagger d_{13}^\dagger|00\rangle = |11\rangle. \tag{30}$$

The bosonic environment is in diagonal form written as

$$H_\varphi = \sum_{q,j} \omega_{q,j} b_{q,j}^\dagger b_{q,j}, \tag{31}$$

where $b_{q,j}$ are boson annihilation operators. The potential fields φ_j are given in terms of the bosons as

$$\varphi_j = \sum_q (M_{q,j}^* b_{q,j} + M_{q,j} b_{q,j}^\dagger). \tag{32}$$

For the arguments in this section, we do not need the explicit form of the matrix elements $M_{q,j}$.

We take the case of even total fermion-number parity. The two degenerate even-parity unperturbed ground states are $|00\rangle \otimes |0\rangle_{\text{env}}$ and $|11\rangle \otimes |0\rangle_{\text{env}}$. First-order perturbation theory then gives that the ground states of the interacting system are

$$|G_0\rangle = \frac{1}{\sqrt{C}} \left(|00\rangle|0\rangle_{\text{env}} - \sum_{ikq} \frac{W_{k,i}M_{q,i}}{E_k + \omega_q} \gamma_i |00\rangle \alpha_{k,i}^\dagger b_{q,i}^\dagger |0\rangle_{\text{env}} \right),$$

$$|G_1\rangle = \frac{1}{\sqrt{C}} \left(|11\rangle|0\rangle_{\text{env}} - \sum_{ikq} \frac{W_{k,i}M_{q,i}}{E_k + \omega_q} \gamma_i |11\rangle \alpha_{k,i}^\dagger b_{q,i}^\dagger |0\rangle_{\text{env}} \right), \tag{33}$$

with

$$C = 1 + \sum_{ikq} \frac{|W_{k,i}M_{q,i}|^2}{(E_k + \omega_q)^2} \equiv 1 + \eta. \tag{34}$$

For simplicity, we here assume that the energies E_k and ω_q are identical in different regions $j = 1, \ldots, 4$.

The excited states can be written in a similar way. For example, let us consider the unperturbed excited states $b_{q,j}^\dagger |ss\rangle \otimes |0\rangle_{\text{env}}$ (with $s = 0, 1$), where the corresponding entangled

excited states are to first order given by

$$
|E_{qjs}\rangle = \frac{1}{\sqrt{B_{q,j}}} \left(b_{q,j}^{\dagger}|ss\rangle|0\rangle_{\text{env}} - \sum_{ikq'} \frac{W_{k,i}M_{q',i}}{E_k + \omega_{q'}} \gamma_i|ss\rangle \right.
$$
$$
\left. \times \alpha_{k,i}^{\dagger}b_{q',i}^{\dagger}b_{q,j}^{\dagger}|0\rangle_{\text{env}} - \sum_{k} \frac{W_{k,j}M_{q,j}^{*}}{E_k - \omega_q} \gamma_j|ss\rangle\alpha_{k,j}^{\dagger}|0\rangle_{\text{env}} \right),
$$
$$(35)$$

with the normalization factor

$$
B_{q,j} = 1 + \sum_{ikq'} \frac{|W_{k,i}M_{q',i}|^2}{(E_k + \omega_{q'})^2} + \sum_{k,z=\pm 1} \frac{|W_{k,j}M_{q,j}|^2}{(E_k + z\omega_q)^2}. \quad (36)
$$

Similarly, one can generate the corrections to the unperturbed two-boson excited states: $b_{q,j}^{\dagger}b_{q',j'}^{\dagger}|ss\rangle \otimes |0\rangle_{\text{env}}$, etc.

With the above perturbative results for the eigenstates, one can now construct the corresponding matrix elements of the matrix **A**. As we saw in Eq. (25), the matrix elements are identical for the two topologically degenerate sectors. For example, we have for the diagonal elements

$$
A_{G_0,G_0} = A_{G_1,G_1} = \langle G_0|i\gamma_1\gamma_3|G_0\rangle, \quad (37)
$$

$$
A_{q10,q10} = A_{q11,q11} = \langle E_{q10}|i\gamma_1\gamma_3|E_{q10}\rangle, \quad (38)
$$

that

$$
A_{G_0,G_0} = \frac{2-C}{1+C} = \frac{1-\eta}{2+\eta}, \quad A_{q10,q10} = \frac{2-B_{q,1}}{1+B_{q,1}}. \quad (39)
$$

Off-diagonal elements between the excited states in Eq. (35) are

$$
A_{q10,q'10} = - \sum_{k,z=\pm 1} \frac{|W_{k,1}|^2 M_{q,1}M_{q',1}^{*}}{(E_k + z\omega_q)(E_k + z\omega_{q'})} \quad (40)
$$

for $q \neq q'$.

From the above, we conclude that for weak measurements and weak coupling to the environment, there is no loss of fidelity (only visibility) as long as the diagonal elements remain positive, whereas for strong measurement one has to investigate the structure of the eigenvalue spectrum of **A** more carefully. However, it is not well understood when the assumption of weak measurements is valid. It depends on both the strength of Λ and the timescale τ, and it is an interesting topic for further studies. Here, we focus on establishing the result for the limit of an instantaneous and projective measurement of the bare MBSs, i.e., the bare Pauli operator σ. This is the topic of the next section.

V. READOUT OF A MAJORANA BASIS IN THE SUDDEN APPROXIMATION

In this section, we discuss the limit where the operator $\sigma_z = i\gamma_1\gamma_2$ is measured projectively. This is relevant when the energy scale Λ in Eq. (27) is larger than temperature and the timescale τ for turning on the measurement device is short compared to all scales, including Δ. As discussed above, this therefore constitutes a worst case scenario and slower turn-on would reduce the fidelity loss even though full adiabaticity is

never possible because the combined fermion-boson system is gapless.

A. Perturbative estimate

Let us start by assuming that the system has been initialized in a linear superposition of the two dressed ground states (33) (at $T = 0$),

$$
|\psi\rangle = \alpha|G_0\rangle + \beta|G_1\rangle. \quad (41)
$$

A projective measurement of σ_z then yields the outcome $+1$ with probability

$$
P(\sigma_z = 1) = \text{Tr}(\Pi_1|\psi\rangle\langle\psi|), \quad (42)
$$

where the projection operator Π_1 is

$$
\Pi_1 = \sum_{n_{24}=0,1} |0, n_{24}\rangle\langle 0, n_{24}| \otimes \mathbb{1}_{\text{env}}, \quad (43)
$$

and $\mathbb{1}_{\text{env}}$ denotes the identity operator in the Hilbert space of the environment. The probability in Eq. (42) thus becomes

$$
P(\sigma_z = 1) = \frac{|\alpha|^2}{1+\eta} + \frac{|\beta|^2\eta}{1+\eta}, \quad (44)
$$

and similarly for the probability to measure $\sigma_z = -1$,

$$
P(\sigma_z = -1) = \frac{|\beta|^2}{1+\eta} + \frac{|\alpha|^2\eta}{1+\eta}, \quad (45)
$$

where the decoherence parameter η has been defined in Eq. (34). Equations (44) and (45) show that the readout error is of order η. Moreover, because there is no value of α for which $P(\sigma_z = 1) = 1$, they also demonstrate that reading out σ_z does not simply correspond to reading out the qubit defined by the basis states $\{|G_0\rangle, |G_1\rangle\}$ in some other direction.

At finite temperature, we have instead of Eq. (41) a mixed state with contributions from excited states as in Eq. (35). The resulting density matrix is still coherent within the topologically protected set of degenerate states because no local perturbation (say, for region $j = 1$) mixes the two sectors $\{|00, \text{even}\rangle, |10, \text{odd}\rangle\}$ and $\{|11, \text{even}\rangle, |01, \text{odd}\rangle\}$, where odd and even refer to the parity of the quasiparticle continua. However, even though coherence in the topologically protected subspace is maintained, the coefficients α and β can again not be read out truthfully using the projection (43) because the projection operators $\Pi_{\pm 1}$ do not commute with the interacting Hamiltonian.

To summarize this section, the reduction factors in Eqs. (44) and (45) are caused by reading out in the bare (undressed) basis $\{|00\rangle, |11\rangle\}$ instead of using the true (dressed) states (33). The factor $1/(1 + \eta)$, which here was determined by first-order perturbation theory, will appear in the non-Markovian Bloch-Redfield approach below (see Sec. V D). We note that a similar dressing of the ground state by environmental modes has been studied in detail for the related but simpler spin-boson model [45,48], where the coherence reduction is well established even at zero temperature.

B. Bloch-Redfield approach to sudden readout of a bare-Majorana qubit

We now study the decoherence dynamics of Majorana qubits in terms of a modified Bloch-Redfield approach. The main difference between our approach and standard quantum master equations for, e.g., a qubit coupled to a bosonic bath [45,49], arises from the fact that the fermion numbers in the Majorana sector and in the environment are not independent since the total fermion-number parity of each spatial region ($j = 1, \ldots, M$) is conserved by the full Hamiltonian H. In this section, we discuss the Bloch-Redfield approach for the general class of models in Sec. III. In Sec. V E, we will then apply these results to a specific TS wire model.

By adopting the standard derivation of quantum master equations [49] to the case of our Hamiltonian H, we obtain the equation of motion for the reduced density matrix $\rho_M(t)$, describing the MBS sector

$$\frac{d}{dt}\rho_M(t) = -\int_0^t dt' \, \mathrm{Tr}_{\mathrm{env}}[H_{\mathrm{int}}(t), [H_{\mathrm{int}}(t'), \rho(t')]]. \quad (46)$$

For $M = 4$, the space spanned by the MBSs is equivalent to two fermions and ρ_M can be represented by a 4×4 matrix. In Eq. (46), $H_{\mathrm{int}}(t)$ is the MBS-environment coupling Hamiltonian in the interaction picture, with $H_0 + H_\varphi$ as unperturbed

part, $\rho(t)$ is the full density matrix of the entire system, and $\mathrm{Tr}_{\mathrm{env}}$ indicates a trace over environmental degrees of freedom. In Eq. (46), we assume the weak MBS-environment coupling limit such that the standard Born approximation applies [45,49].

If relaxation processes in the environment are much faster than the timescale for changes in the reduced density matrix ρ_M, the density matrix $\rho(t')$ appearing in Eq. (46) effectively separates into $\rho_M(t')$ and an environmental part, and we can neglect MBS-environment entanglement in $\rho(t')$. Assuming that above-gap quasiparticles quickly decohere because of H_2 in Eq. (17), $\rho(t')$ will therefore factorize into $\rho_M(t')$ and an *equilibrium* environmental density matrix ρ_{env}. Since the main role of H_2 is to decohere quasiparticles, we also replace $H_{\mathrm{int}}(t) \to H_1(t)$ [see Eq. (16)] in Eq. (46).

However, there is an important catch: the parities of the Majorana subsystem and of the environmental sector are not independent because of total-parity conservation. In what follows, we always take the conserved fermion-number parity of the entire system as even such that

$$\rho(t') = \rho_M^e(t') \otimes \rho_{\mathrm{env}}^e + \rho_M^o(t') \otimes \rho_{\mathrm{env}}^o, \quad (47)$$

where the superscripts e/o refer to even–plx-sol-plxodd-parity sectors of the respective subsystem. Next, we insert Eq. (47) into Eq. (46). Noting that coherent contributions with different parities in the Majorana sector are absent, we obtain

$$\frac{d}{dt}\rho_M^{e/o}(t) = -\sum_{i,j}\int_0^t dt' \big[g_{ij}^{e/o}(t-t')\gamma_i\gamma_j\rho_M^{e/o}(t') + g_{ij}^{e/o}(t'-t)\rho_M^{e/o}(t')\gamma_i\gamma_j - \big(g_{ij}^{o/e}(t-t') + g_{ij}^{o/e}(t'-t)\big)\gamma_i\rho_M^{e/o}(t')\gamma_j\big] \quad (48)$$

with the functions ($i, j = 1, \ldots, M$)

$$g_{ij}^{e/o}(t-t') = -\langle\Gamma_i(t)\varphi_i(t)\Gamma_j(t')\varphi_j(t')\rangle_{e/o}, \quad (49)$$

where $\langle\ldots\rangle_{e/o} = \mathrm{Tr}_{\mathrm{env}}(\rho_{\mathrm{env}}^{e/o}\ldots)$ and $\Gamma_i(t)$ has been defined in Eq. (16).

We now use two properties of the environment which follow from the conditions specified after Eq. (17). First, all MBSs are assumed to be so far away from each other that there is no phase coherence between quasiparticles in different regions. As a consequence, $g_{ij} \propto \delta_{ij}$. (Nonetheless, quasiparticles may incoherently diffuse throughout the device.) Second, quasiparticles and bosonic modes are taken to be uncorrelated, implying that the expectation value (49) can be factorized. This assumption is equivalent to disregarding the Hamiltonian H_2 when evaluating $g_{ij}^{e/o}(t)$. (As discussed above, the main role of H_2 is to induce quasiparticle relaxation.) After those steps, we obtain

$$g_{ij}^{e/o}(t-t') = F_i^{e/o}(t-t')B(t-t')\delta_{ij}, \quad (50)$$

with the boson correlation function $B(t)$ in Eq. (19) and the quasiparticle correlator

$$F_i^{e/o}(t) = -\langle\Gamma_i(t)\Gamma_i(0)\rangle_{e/o} = \int_\Delta^\infty dE \, \nu(E)|W_i(E)|^2$$

$$\times \big[e^{-iEt}\big[1 - n_F^{e/o}(E)\big] + e^{iEt}n_F^{e/o}(E)\big]. \quad (51)$$

Here, $\nu(E) = \sum_k \delta(E - E_k)$ is the quasiparticle density of states. From Eq. (18), we then obtain

$$\nu(E)|W_i(E)|^2 = \sum_k \delta(E - E_k)|W_{k,i}|^2. \quad (52)$$

The Fermi-Dirac functions in Eq. (51) are given by

$$n_F^{e/o}(E) = \frac{1}{e^{\beta(E \pm \delta F)} + 1}, \quad (53)$$

where δF is the free-energy difference between the even- and odd-parity cases, $\delta F = F_{\mathrm{odd}} - F_{\mathrm{even}}$. The thermodynamics of a superconducting island with fixed total parity has been considered in Refs. [50–52]. At low temperatures, one can parametrize δF by the number N_{eff} of quasiparticle states on the island,

$$\delta F = \Delta - k_{\mathrm{B}}T\ln N_{\mathrm{eff}}, \quad N_{\mathrm{eff}} \simeq \int_\Delta^\infty dE \, \nu(E)e^{-\beta(E-\Delta)}. \quad (54)$$

Assuming a BCS form for $\nu(E)$, one obtains the estimate

$$N_{\mathrm{eff}} \approx d_{\mathrm{S}}V_{\mathrm{S}}\sqrt{2\pi k_{\mathrm{B}}T\Delta}, \quad (55)$$

where d_{S} is the normal density of states and V_{S} the volume of the superconductor. We note that N_{eff} determines the temperature T^* at which the probability of having the first quasiparticle in the system approaches unity, $T^* \approx \Delta/(k_{\mathrm{B}}N_{\mathrm{eff}})$. Recent

experiments have reported the value $T^* \approx 0.3$ K for a single nanowire [52].

C. Markovian approximation

The integrodifferential equation (48) includes memory effects because the change of $\boldsymbol{\rho}_M(t)$ depends on $\boldsymbol{\rho}_M(t')$ at earlier times $t' < t$. One can in principle solve this equation, but in order to have simple results (and to reproduce results obtained by earlier studies), we first turn to the Markovian approximation. The standard Markovian approximation for the Bloch-Redfield master equation (48) involves two steps [45,49]. First, the density matrix $\boldsymbol{\rho}_M(t')$ under the integral is replaced by $\boldsymbol{\rho}_M(t)$. Second, the upper limit in the time integral is replaced by infinity. In addition, to simplify notation, we again take identical but uncorrelated environments for different MBSs. With these steps, the master equation (48) is given in Lindblad form

$$\frac{d}{dt} \boldsymbol{\rho}_M^{e/o} = -\Gamma^{e/o} \boldsymbol{\rho}_M^{e/o} + \frac{\Gamma^{o/e}}{M} \sum_i \gamma_i \, \boldsymbol{\rho}_M^{o/e} \gamma_i \,, \qquad (56)$$

with the rates [cf. Eq. (50)]

$$\Gamma^{e/o} = M \int_{-\infty}^{\infty} dt \, g^{e/o}(t) = M \int_{\Delta}^{\infty} dE \, f^{e/o}(E). \qquad (57)$$

We here define the auxiliary functions

$$f^{e/o}(E) = \nu(E) |W(E)|^2 J(E) \big(n_B(E) + n_F^{e/o}(E) \big). \qquad (58)$$

For low temperatures $T \ll T^*$, we now have

$$n_B(E) + n_F^{e/o}(E) \simeq \begin{cases} e^{-\beta E}, & \text{even} \\ N_{\text{eff}}^{-1} e^{-\beta(E-\Delta)}, & \text{odd}. \end{cases} \qquad (59)$$

From Eq. (57), we thus obtain the asymptotic low-temperature expressions

$$\Gamma^o \approx k_B T N_{\text{eff}}^{-1} \mathcal{S}(\Delta), \quad \Gamma^e \approx k_B T \mathcal{S}(\Delta) e^{-\Delta/k_B T}, \quad (60)$$

with $\mathcal{S}(\Delta) = M \nu(\Delta) |W(\Delta)|^2 J(\Delta)$. We observe that in general, $\Gamma^o \gg \Gamma^e$ due to the absence of the exponential suppression factor in Γ^o. To understand this result, note that for even total parity, the odd-parity Majorana sector must come with at least one quasiparticle excitation. For $T > 0$, this above-gap excitation can now quickly relax and thereby bring the Majorana subsystem to the energetically favorable even-parity sector.

To explicitly obtain the decoherence dynamics from the Lindblad equation (56), we take $M = 4$ and parametrize $\boldsymbol{\rho}_M^{e/o}$ in the basis introduced in Eqs. (29) and (30). With real coefficients $a_\pm^{e/o}$ and complex numbers $b^{e/o}$,

$$\boldsymbol{\rho}_M^{e/o} = \begin{pmatrix} a_+^{e/o} & b^{e/o} \\ (b^{e/o})^* & a_-^{e/o} \end{pmatrix}, \qquad (61)$$

where $p^{e/o} = a_+^{e/o} + a_-^{e/o}$ is the probability for the Majorana sector having even/odd parity, respectively. We next note that the last term in Eq. (56) can be written as

$$\sum_i \gamma_i \, \boldsymbol{\rho}_M^{e/o} \gamma_i = 2 p^{e/o} P_{o/e}, \qquad (62)$$

where $P_{o/e}$ is the projector onto the odd–plx-sol-plxeven-parity Majorana subspace. The identity (62) follows directly by using the basis defined in Eq. (30) along with the definition of d_{13} and d_{24} in Eq. (29). We will see below that for $t \to \infty$ and $T > 0$, Eq. (62) implies that the bare-Majorana qubit will fully decohere. The simple form of Eq. (62) is a consequence of our assumption that different environments are identical and uncorrelated. If they have different spectral functions, the long-time limit of $\boldsymbol{\rho}_M(t)$ is also affected.

Let us now assume that at time $t = 0$, we start from the even-parity Majorana sector, i.e., $\boldsymbol{\rho}_M^o(0) = 0$. The off-diagonal components of $\boldsymbol{\rho}_M^e$ will then show an exponential decay with rate Γ^e:

$$b^e(t) = e^{-\Gamma^e t} b^e(0). \qquad (63)$$

Using the normalization condition $p^e + p^o = 1$, the dynamics of the diagonal elements $a_\pm^e$ follows from

$$\dot{a}_\pm^e = -\Gamma^e a_\pm^e + \frac{\Gamma^o}{2}(1 - a_+^e - a_-^e). \qquad (64)$$

By adding those equations, we obtain

$$\dot{p}^e = -\Gamma^e p^e + \Gamma^o(1 - p^e), \qquad (65)$$

with the solution

$$p^e(t) = e^{-(\Gamma^e + \Gamma^o)t}(1 - p_{\text{eq}}) + p_{\text{eq}}, \qquad (66)$$

where the equilibrium probability reached for $t \to \infty$ is

$$p_{\text{eq}} = \frac{1}{1 + \Gamma^e/\Gamma^o}. \qquad (67)$$

Inserting Eq. (66) back into Eq. (64) one easily finds $a_+^e(t)$ and $a_-^e(t)$, given their initial values at $t = 0$. Equation (66) shows that the decay toward equilibrium involves two separate contributions. One is due to the rate Γ^e which is exponentially small at low temperatures. The other is due to Γ^o which does not contain the exponential suppression factor and thus implies a faster decay (for $T > 0$). In addition, we observe from Eq. (67) that for $k_B T \ll \Delta$, the probability for remaining in the even-parity sector at $t \to \infty$ is very close to unity, $p_{\text{eq}} \simeq 1 - N_{\text{eff}} e^{-\Delta/k_B T}$ [see Eq. (60)]. In particular, at $T = 0$ the bare-Majorana qubit does not decohere at all within the Markovian approximation. This conclusion and some of the above results have been reported before (see, e.g., Refs. [34,37]).

D. Non-Markovian case

1. $T = 0$ case

We next turn to the $T = 0$ qubit dynamics and take into account non-Markovian memory effects. In Sec. IV B, we have presented a fidelity reduction mechanism for the bare-Majorana qubit state due to entanglement of the MBS sector with environmental degrees of freedom. Within the Markovian approximation, this effect is exponentially suppressed at low temperatures due to the energy difference Δ between both sectors. For our system, this conclusion equivalently follows under a Fermi golden rule approach with on-shell scattering between the two parity sectors. However, we will show below that the fidelity of the bare-Majorana qubit is affected even

at $T = 0$ due to *virtual off-shell* processes which give rise to non-Markovian dynamics.

Our starting point is Eq. (48), where we again assume that the environments coupled to different MBS are identical but uncorrelated. Setting $M = 4$, we parametrize $\boldsymbol{\rho}_M^{e/o}$ using the real Bloch vector components $d_\alpha^{e/o}$ and population factors $p^{e/o}$,

$$\boldsymbol{\rho}_M^{e/o}(t) = \sum_{\alpha = x,y,z} d_\alpha^{e/o}(t)\sigma_\alpha^{e/o} + \frac{1}{2}p^{e/o}(t)P_{e/o}, \quad (68)$$

where the Pauli matrices $\sigma_\alpha^{e/o}$ act in the even/odd 2×2 spaces defined in Eq. (61) and $P_{e/o}$ projects to the even/odd Majorana sector. From Eq. (48), we then obtain the non-Markovian $T = 0$ master equation

$$\frac{d}{dt}\boldsymbol{\rho}_M^{e/o}(t) = -4\int_0^t dt'\, g(t-t')\left(\boldsymbol{\rho}_M^{e/o}(t') - \frac{p^{e/o}(t')}{2}P_{o/e}\right). \quad (69)$$

The function $g(t) = g^{e/o}(t) + g^{e/o}(-t)$ follows from Eq. (50), where we notice that $g^{e/o}(t)$ does not depend on parity (e/o) for $T = 0$:

$$g(t) = \frac{1}{\pi}\int_0^\infty d\omega \int_\Delta^\infty dE\, \nu(E)|W(E)|^2 J(\omega)\cos[(\omega + E)t]. \quad (70)$$

Let us first consider the dynamics of $d_\alpha(t)$. The equations of motion are obtained by multiplying Eq. (69) with $\sigma_\alpha^{e/o}$ and taking the trace

$$\dot{d}_\alpha^{e/o}(t) = -4\int_0^t dt'\, g(t-t')d_\alpha^{e/o}(t'). \quad (71)$$

The solution follows by Laplace transformation

$$\tilde{d}_\alpha^{e/o}(s) = \frac{1}{s + 4\tilde{g}(s)}d_\alpha^{e/o}(t=0), \quad (72)$$

where $\tilde{h}(s)$ denotes the Laplace transform of a function $h(t)$. For the asymptotic long-time behavior, we thereby find

$$d_\alpha^{e/o}(t \to \infty) = \frac{1}{1+\eta}d_\alpha^{e/o}(t=0), \quad (73)$$

with the dimensionless decoherence parameter

$$\eta = \frac{4}{\pi}\int_0^\infty d\omega \int_\Delta^\infty dE\, \frac{J(\omega)\nu(E)|W(E)|^2}{(\omega + E)^2}. \quad (74)$$

The coherences encoded by $d_\alpha^{e/o}(t)$ are thus reduced for $t \to \infty$ due to the coupling of MBS to quantum fluctuations of the environment, even at zero temperature. Quantitatively, this effect is described by the number η as explained in Sec. IV B. Although $d_\alpha^{e/o}(t)$ does not decay all the way down to zero for $t \to \infty$, it is reduced by a finite amount. Note that this result equally applies to both parity sectors.

Likewise, the equations of motion for the population factors follow as

$$\dot{p}^{e/o}(t) = -4\int_0^t dt'\, g(t-t')[p^{e/o}(t') - p^{o/e}(t')]. \quad (75)$$

After Laplace transformation, we have

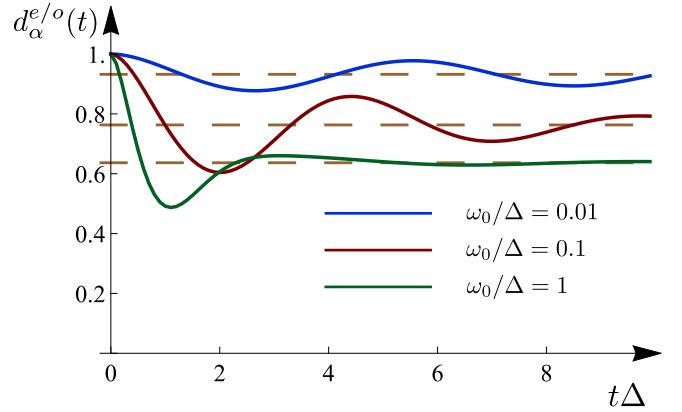$$s\tilde{p}^{e/o}(s) - p^{e/o}(t=0) = -4\tilde{g}(s)[\tilde{p}^{e/o}(s) - \tilde{p}^{o/e}(s)]. \quad (76)$$

FIG. 4. Time dependence of the coherences $d_\alpha^{e/o}(t)/d_\alpha^{e/o}(0)$, at $T = 0$, where results are independent of the parity (e/o) sector and of the component ($\alpha = x, y, z$). For three values of ω_0/Δ [cf. Eq. (20)], the curves have been obtained numerically by inverse Laplace transformation of Eq. (72), with $B = 1$ in Eq. (C5). Dashed lines show the respective long-time asymptotic value $1/(1 + \eta)$.

Noting that $\tilde{p}^{e/o}(s) + \tilde{p}^{o/e}(s) = 1/s$ because of $p^{e/o}(t) + p^{o/e}(t) = 1$, Eq. (76) yields

$$\tilde{p}^{e/o}(s) = \frac{p^{e/o}(t=0) + 4\tilde{g}(s)/s}{s + 8\tilde{g}(s)}. \quad (77)$$

From this expression, the asymptotic long-time behavior follows in the form

$$p^{e/o}(t \to \infty) = \frac{p^{e/o}(t=0) + \eta}{1 + 2\eta}. \quad (78)$$

Starting, say, from the even-parity sector, the probability to end up with odd parity is given by $p^o(\infty) = \eta/(1 + 2\eta) \leqslant 1/2$. For $\eta \to \infty$, the full parity mixing limit with $p^e(\infty) = p^o(\infty) = 1/2$ is realized. In that case, also all coherences die out, $d_\alpha^{e/o}(\infty) \to 0$. Importantly, these predictions are in marked contrast to the corresponding $T = 0$ Markovian results in Sec. V C.

In order to obtain the full time dependence of the $T = 0$ coherences in the non-Markovian case, the inverse Laplace transformation of Eq. (72) has been performed numerically by using a simplifying assumption for the E integral in Eq. (70), replacing $E \to \Delta$ in the cosine. The rationale behind this approximation is that for the *p*-wave nanowire model in Sec. V E, the function $\nu(E)|W(E)|^2$ has a clear peak at E slightly above Δ (see Fig. 10 in Appendix B). Using Eq. (20), the ω integral can then be performed (see Appenidx C for details). The corresponding numerical results are shown in Fig. 4 and illustrate how Eq. (73) is approached at long times. We observe that the coherences oscillate and decay on timescales corresponding to fractions of Δ^{-1}. For smaller η, we find that both the oscillations and the decay become slower.

We conclude that at $T = 0$, non-Markovian effects can be very important. In particular, they induce a coherence reduction and cause parity mixing between the bare-Majorana qubit and the environment, especially for large η in Eq. (74).

2. Finite T

For finite T, we have to distinguish $g^e(t)$ and $g^o(t)$. In the Laplace domain, this parity-dependent correlation function can be calculated for $\text{Re}(s) > 0$ and subsequently be analytically continued to $\text{Re}(s) < 0$. From Eq. (50), we then find

$$\tilde{g}^{e/o}(s) = \frac{s}{\pi} \int_0^\infty d\omega \int_\Delta^\infty dE \, \nu(E) |W(E)|^2 J(\omega)$$
$$\times \left(\frac{n_B(\omega) + n_F^{e/o}(E)}{s^2 + (E - \omega)^2} + \frac{1 + n_B(\omega) - n_F^{e/o}(E)}{s^2 + (E + \omega)^2} \right).$$
(79)

Keeping track of the differences between g^e and g^o leads to modifications of Eqs. (72) and (77). We find

$$\tilde{d}_\alpha^{e/o}(s) = \frac{1}{s + 4\tilde{g}^{e/o}(s)} d_\alpha^{e/o}(t = 0),$$
(80)

$$\tilde{p}^{e/o}(s) = \frac{p^{e/o}(t = 0) + 4\tilde{g}^{o/e}(s)/s}{s + 4[\tilde{g}^{e/o}(s) + \tilde{g}^{o/e}(s)]}.$$
(81)

We now observe that $\tilde{d}_\alpha^{e/o}(s)$ has a pole at $s = 0$, and that the first term within the brackets in Eq. (79) is divergent for $\omega = E$ when $\text{Re}(s) = 0$ and $T > 0$. As shown in Appendix A, this implies $d_\alpha^{e/o}(t \to \infty) = 0$ for all finite T, in accordance with the Markovian results discussed in Sec. V C. For asymptotically long times, $t \to \infty$, the decay law follows by expanding $\tilde{g}^{e/o}(s)$ for $s \to 0$, as we show in detail in Appendix A. All coherences then die out exponentially,

$$d_\alpha^{e/o}(t) \propto e^{-\Gamma^{e/o}t},$$
(82)

where we obtain the same decay rates $\Gamma^{e/o}$ as from the Markovian approach [see Eq. (57)]. As expected intuitively, environmental memory effects are thus erased at very long times.

Finally, we discuss the long-time behavior of $p^{e/o}(t)$ which illustrates the equilibration of the system. Again, the result follows by expanding $\tilde{p}^{e/o}(s)$ in Eq. (81) for small s (see Appendix A for details). We find that at $T = 0$, Eq. (78) is recovered. However, for $T > 0$, we get

$$p^{e/o}(t \to \infty) = \frac{\int_\Delta^\infty dE \, f^{o/e}(E)}{\int_\Delta^\infty dE [f^{e/o}(E) + f^{o/e}(E)]}$$
$$= \frac{\Gamma^{o/e}}{\Gamma^{e/o} + \Gamma^{o/e}},$$
(83)

with the function $f^{e/o}(E)$ in Eq. (58). Equation (83) also matches the corresponding result in the Markovian limit [see Eq. (67)].

E. Case study

Here, we provide concrete estimates to illustrate the above results for a specific TS nanowire model. To that end, we use a spinless model for a TS wire with p-wave pairing symmetry. One can write the corresponding BdG Hamiltonian in the form [7]

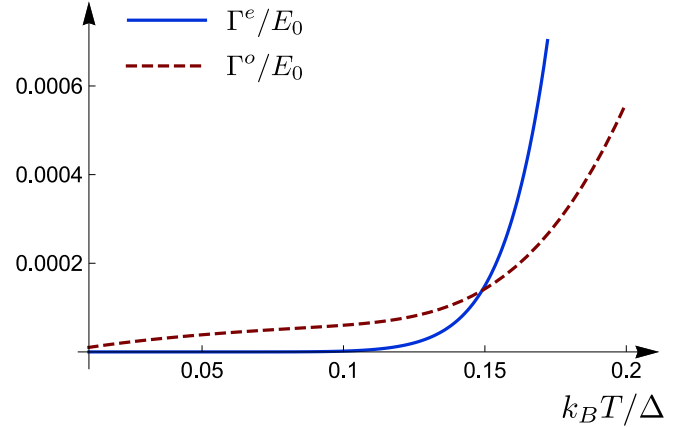$$\mathcal{H}_{\text{BdG}} = \frac{p^2}{2m}\tau_z - \Delta\tau_z + vp\tau_x.$$
(84)

FIG. 5. Decay rates $\Gamma^{e/o}$ vs temperature T obtained from Eq. (57) for the spinless p-wave TS wire model in Eq. (84). We use $\omega_0 = \Delta$, $\Delta/(mv^2) = 0.2$, $d_S V_S \Delta_{\text{Al}} = 850$, and $E_0 = e^2/C_0$ [see Eq. (20)].

We focus on a semi-infinite wire in order to obtain the zero-energy MBS wave function $|\text{MBS}\rangle$, as well as the above-gap quasiparticle wave functions $|k\rangle$. Given these wave functions, we then compute the W matrix elements needed in Eqs. (18) and (52). The result can be found in Appendix B, where Fig. 10 shows a plot of $\nu(E)|W(E)|^2$. In order to evaluate δF from Eqs. (54) and (55), we assume the dimensionless parameter $d_S V_S \Delta_{\text{Al}} = 850$. To obtain this value, we employed the Fermi energy for Al (11.7 eV) and the volume V_S as for the experimental setup in Ref. [14]. The nanowires in the latter experiment were fairly short, but since we are interested in describing the states at just one nanowire end, such a reduced volume should be appropriate. We use the gap value for Al, $\Delta_{\text{Al}} = 2 \times 10^{-4}$ eV, and throughout focus on the topological parameter regime $\Delta > 0$. For simplicity, we will consider the case of relatively small TS gap, $\Delta/(mv^2) \leqslant 1/2$, since the solution described in Appendix B otherwise becomes slightly more involved. Finally, the electromagnetic environment is fully characterized by specifying the frequency ω_0 and the energy scale $E_0 = e^2/C_0$ [see Eq. (20)].

1. Finite-T decay rates

In Fig. 5, we show the temperature dependence of the decay rates $\Gamma^{e/o}$ [Eq. (57)] when using the BdG Hamiltonian in Eq. (84). For $k_B T < 0.1\Delta$, we observe that $\Gamma^e(T)$ remains exponentially small, in contrast to what is found for the rate Γ^o in the odd-parity sector. We thus expect that in this low-temperature regime, the $T = 0$ results presented in Sec. V D should also apply for the even-parity sector at intermediate times. In particular, for long times but subject to the condition $t \ll \Gamma^{-1}$, where $\Gamma = (\Gamma^e + \Gamma^o)/2$, the off-diagonal entries of $\rho_M^e(t)$ are expected to remain approximately constant $d_\alpha^e(t) \simeq R_\alpha^e$ (with $\alpha = x, y, z$). Neglecting the effects of early-time transients, R_α^e is given by the residue of $\tilde{d}_\alpha^e(s)$ [Eq. (80)] at the pole $s = -\Gamma^e$. Keeping for the moment both parity sectors, we have

$$R_\alpha^{e/o} = \lim_{s \to -\Gamma^{e/o}} \frac{s + \Gamma^{e/o}}{s + 4\tilde{g}^{e/o}(s)} d_\alpha^{e/o}(t = 0).$$
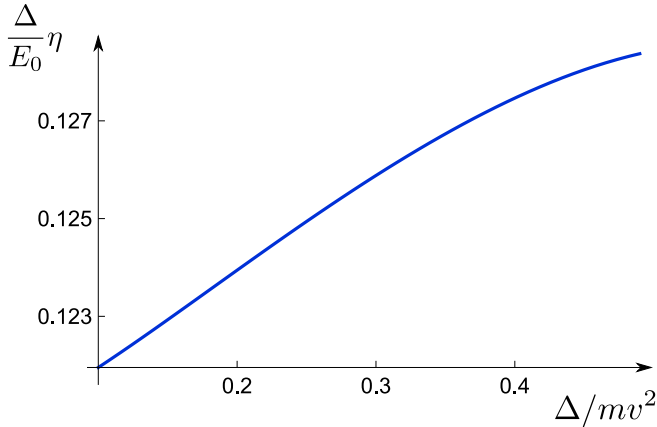(85)

FIG. 6. Decoherence parameter η [see Eq. (74)] vs $\Delta/(mv^2)$ for the p-wave TS nanowire model in Eq. (84). We assume an environmental frequency $\omega_0 = \Delta$, other parameters are described in the text. All coherences are reduced by a factor $1/(1+\eta)$ at long times. Since we have rescaled η by E_0/Δ in the plot, the shown results hold for arbitrary ratio E_0/Δ.

Using the fact that $\Gamma^{e/o} \ll \Delta$, Eq. (85) can be simplified to

$$R_\alpha^{e/o} = \frac{d_\alpha^{e/o}(t=0)}{1+\zeta^{e/o}(T)}, \tag{86}$$

with

$$\zeta^{e/o}(T) = \frac{4}{\pi} \int_\Delta^\infty dE \int_0^\infty d\omega \, \nu(E) |W(E)|^2 J(\omega)$$
$$\times \left(\frac{1 + n_B(\omega) - n_F^{e/o}(E)}{(E+\omega)^2} + \frac{n_B(\omega) + n_F^{e/o}(E)}{(\Gamma^{e/o})^2 + (E-\omega)^2} \right). \tag{87}$$

Noting that $\zeta^{e/o}(T=0) = \eta$ [see Eq. (74)], we first confirm that Eq. (86) correctly recovers the $T=0$ result (73). For finite but low T and focusing on the even-parity sector, the coherence reduction saturates at the value R_α^e in Eq. (86) for intermediate-to-long times, $\Delta^{-1} \ll t < \Gamma^{-1}$. However, for $t > \Gamma^{-1}$, all coherences will ultimately decay to zero.

2. Zero-temperature fidelity reduction

We found in Sec. V D that even at zero temperature, quantum fluctuations in the electrodynamic environment can generate virtual (off-shell) processes that, on the non-Markovian level, cause a fidelity reduction in the readout of the bare-Majorana qubit. The efficiency of this process is encoded by the dimensionless parameter η in Eq. (74), where all long-time coherences $d_\alpha^{e/o}(t \to \infty)$ are reduced by a common factor $1/(1+\eta)$ with respect to their initial value [see Eq. (73)] and the qualitative discussion in Sec. IV B. In Figs. 6 and 7, we show the dependence of η on the dimensionless parameters $\Delta/(mv^2)$ and ω_0/Δ, respectively. Since η has been rescaled by E_0/Δ in both figures, these results are valid for arbitrary E_0/Δ. In fact, for large values of E_0/Δ, one gets large values of η and hence a strong suppression of the coherences. To minimize the reduction, one should thus minimize $E_0 = e^2/C_0$.
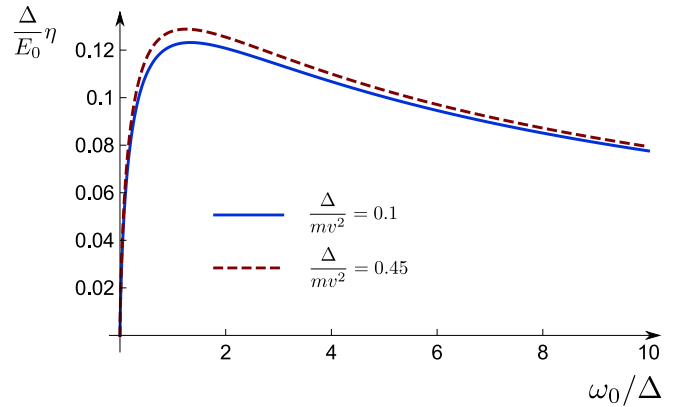

FIG. 7. Decoherence parameter η vs ω_0/Δ for $\Delta/(mv^2) = 0.1$ and $\Delta/(mv^2) = 0.45$ (cf. the caption of Fig. 6).

Apart from its significance for quantum information processing applications, the $T=0$ fidelity reduction for bare-Majorana qubits is also of importance from a theoretical point of view. Figure 7 indicates that this effect is most pronounced for $\omega_0 \approx \Delta$, where quantum fluctuations of the Ohmic electromagnetic environment can almost resonantly match the TS gap. In addition, Fig. 6 shows that η grows with decreasing TS gap. This can be rationalized by noting that the Ohmic spectral function (20) includes gapless low-energy bosons that can participate in the coherence reduction (see Sec. IV B). In Fig. 8, we illustrate the value of $d_\alpha^{e/o}(t)$ reached at long times in the $T=0$ limit. We observe that especially for large E_0/Δ and $\omega_0 \approx \Delta$, the coherence reduction is quite significant. Finally, Fig. 9 depicts the ω_0/Δ dependence of the $T=0$ probability for staying in the even-parity Majorana sector at very long times, $p^e(t \to \infty)$, provided that one has started out from this sector, $p^e(0) = 1$. The analytical prediction for this quantity is given by $(1+\eta)/(1+2\eta) \geqslant 1/2$ [see Eq. (78)]. We find that for large E_0/Δ, the parity reduction can be rather large. Taking, say, $E_0/\Delta = 10$ and $\omega_0 \approx \Delta$, a parity leakage of ≈ 0.35 from the even- into the odd-parity Majorana sector is observed in Fig. 9.
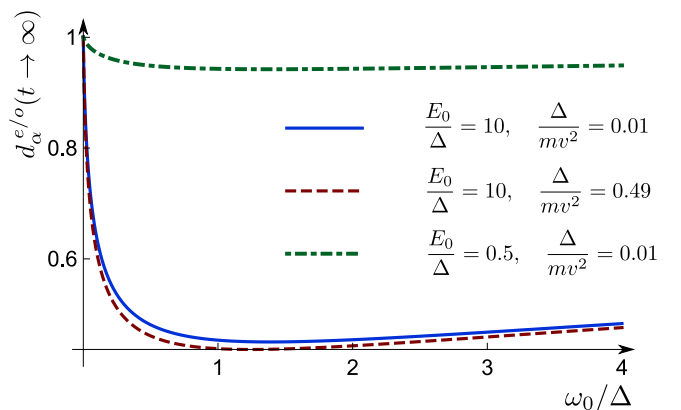

FIG. 8. Asymptotic $T=0$ long-time coherences $d_\alpha^{e/o}(t \to \infty)$ [in units of $d_\alpha^{e/o}(0)$] vs ω_0/Δ. Results are shown for several parameter sets $(E_0/\Delta, \Delta/mv^2)$ [cf. Eq. (73)], and neither depend on $\alpha(=x,y,z)$ nor on the parity (e/o) index.
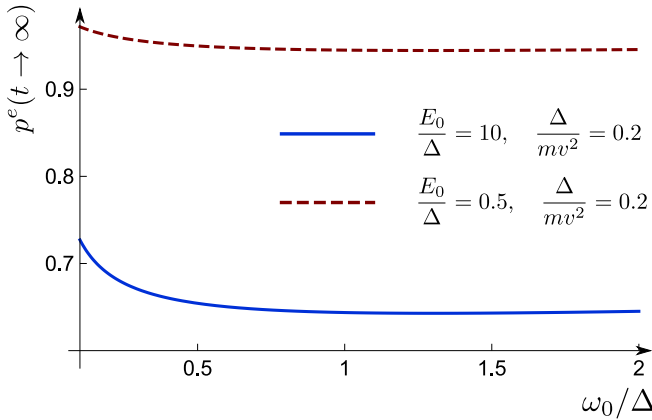
FIG. 9. Long-time $T = 0$ probability for staying in the even-parity sector $p^e(t \to \infty)$ in Eq. (78) vs ω_0/Δ, for $p^e(0) = 1$, $\Delta/mv^2 = 0.2$, and two different values for E_0/Δ.

VI. CONCLUSIONS

We have reexamined the issue of decoherence of qubits formed by zero-energy Majorana bound states when coupled to an electromagnetic environment that causes transition matrix elements between the qubit and the above-gap states. The environment is described by a Caldeira-Leggett bath of noninteracting bosons with an Ohmic spectral density [45]. Concrete estimates have been provided in Sec. V E for a specific microscopic superconductor model, where the topological superconductor corresponds to a spinless nanowire with p-wave pairing.

We have pointed that if the MBSs do not overlap, there is still in principle full topological protection, but the parity is not shared between the MBS and the quasiparticle continuum. Therefore, in order to take advantage of the protection, it is necessary that the readout couples to the dressed states, i.e., the MBS dressed by bosons and continuum quasiparticles. Related proposals for the operation of topological qubits in this basis were discussed in Refs. [19,46], and we have here pointed out that there are limitations when using quantum-dot readout because of lack of adiabaticity. The timescale of switching on the quantum dot will be extremely important for the fidelity of the readout.

We have studied in detail the situation for a projective measurement of the bare (undressed) MBS. Our theoretical approach is based on a modified Bloch-Redfield quantum master equation for the reduced density matrix of the bare-Majorana qubit, and it holds for weak coupling between the Majorana sector and the environment. In formulating this theory, we have carefully accounted for the fact that total fermion-number parity is conserved (within our model) and we have emphasized that it is necessary to keep track of the entanglement between the Majorana subsystem and environmental degrees of freedom. For a quantitative description, the virtual off-shell scattering processes behind this physics require a full non-Markovian master-equation approach. From this approach, we find that the off-diagonal elements of the reduced density matrix of the isolated Majorana subsystem (the *bare-Majorana qubit*), taken at $T = 0$, become suppressed

by a factor $1/(1 + \eta)$ at long times, where η is defined in Eq. (74). The fidelity therefore saturates at a reduced but finite value at $T = 0$. On a qualitative level, this conclusion already follows from a simple perturbative consideration (see Sec. IV B). Likewise, the probability to remain in a given parity sector of the Majorana subsystem will be reduced by a finite amount. With minor modifications, our $T = 0$ results also describe the case of very low but finite temperatures when considering the decoherence dynamics on intermediate-to-long timescales $\Delta^{-1} \ll t < \Gamma^{-1}$ (see Sec. V E 1). At finite temperatures, the asymptotic long-time behavior of the decoherence dynamics is well described by the Markovian approximation which has also been used in most previous theories [34–43].

The important fidelity-reduction parameter η in Eq. (74) depends on the spectral density of the electromagnetic environment, on the quasiparticle density of states, and on a function $W(E)$ which encodes the transition matrix elements between Majorana and quasiparticle states. Physical conditions for when η becomes significant have been specified in detail in Sec. V E.

We conclude by noting that fluctuating gate charges are ubiquitous in candidate devices for realizing Majorana qubits. For that reason, the fidelity reduction discussed in this paper may constitute an important limitation for the coherent operation of Majorana qubits. However, our theory also shows the fidelity-reduction parameter η could be minimized by proper parameter choices and we point out that it would be extremely interesting for future studies to determine how one can minimize the fidelity reduction by careful timing of the readout protocol.

APPENDIX A: ON THE FINITE-T NON-MARKOVIAN CASE

We here provide additional details concerning Sec. V D 2. We first give a detailed derivation of Eq. (82) describing the long-time dephasing dynamics. In general, the long-time limit is dominated by small-s contributions in the Laplace transformed picture. We start by examining the small-s form of the Laplace transformed functions $\tilde{g}^{e/o}(s)$ in Eq. (79). To lowest order in s, the second term of Eq. (79) equals $2sA^{e/o}$ with

$$A^{e/o} = \int_0^\infty \frac{d\omega}{2\pi} \int_\Delta^\infty dE \, \frac{J(\omega)\nu(E)|W(E)|^2}{(\omega + E)^2}$$
$$\times \left[1 + n_{\mathrm{B}}(\omega) - n_{\mathrm{F}}^{e/o}(E) \right]. \tag{A1}$$

For the first term of Eq. (79), we change variables to $\omega_\pm = (\omega \pm E)/2$, with integral limits $\omega_+ \in [\Delta/2, \infty)$ and $\omega_- \in [-\omega_+, \omega_+ - \Delta]$. For $s = 0$, the integrand in Eq. (79) diverges

as $\omega_- \to 0$. This divergence happens outside the integration limits when $\omega_+ < \Delta$. The contribution from $\omega_+ \in [\Delta/2, \Delta)$ can thus safely be evaluated by putting $s = 0$ in the integrand. The result is written as $sK^{e/o}/4$ with

$$K^{e/o} = \frac{2}{\pi} \int_{\Delta/2}^{\Delta} d\omega_+ \int_{-\omega_+}^{\omega_+ - \Delta} \frac{d\omega_-}{\omega_-^2} \nu(\omega_+ - \omega_-)$$
$$\times |W(\omega_+ - \omega_-)|^2 J(\omega_+ + \omega_-)$$
$$\times [n_B(\omega_+ + \omega_-) + n_F^{e/o}(\omega_+ - \omega_-)]. \quad (A2)$$

In the remaining part of $\tilde{g}^{e/o}(s)$, the dominant contribution from the ω_- integral is picked up around $\omega_- = 0$, and so we approximate the integrand by evaluating all terms except for the $1/(s^2 + \omega_-^2)$ factor at $\omega_- = 0$. With $f^{e/o}(\omega)$ in Eq. (58), this results in a third contribution to $\tilde{g}^{e/o}(s)$ of the form

$$\frac{s}{2\pi} \int_{\Delta}^{\infty} d\omega_+ \, f^{e/o}(\omega_+) \int_{-\omega_+}^{\omega_+ - \Delta} \frac{d\omega_-}{s^2 + 4\omega_-^2}.$$

Performing the ω_- integration, renaming $\omega_+ \to E$, and collecting all terms, we arrive at the small-s expansion

$$\tilde{g}^{e/o}(s) = 2sA^{e/o} + \frac{sK^{e/o}}{4} + \frac{1}{4} \int_{\Delta}^{\infty} dE \, f^{e/o}(E)$$
$$- \frac{s}{8\pi} \int_{\Delta}^{\infty} dE \, f^{e/o}(E) \frac{2E - \Delta}{E(E - \Delta)} + \mathcal{O}(s^2). \quad (A3)$$

From Eq. (80), we then find a pole for the Laplace transform of the coherences $\tilde{d}_\alpha^{e/o}(s)$. This pole dictates the long-time behavior of $d_\alpha^{e/o}(t)$. For $t \to \infty$, we thereby arrive at Eq. (82) where the rates are given by

$$\Gamma^{e/o} = \frac{M \int_{\Delta}^{\infty} dE \, f^{e/o}(E)}{1 + 8A^{e/o} + K^{e/o} - \int_{\Delta}^{\infty} \frac{dE}{2\pi} f^{e/o}(E) \frac{2E - \Delta}{E(E - \Delta)}}$$
$$\simeq M \int_{\Delta}^{\infty} dE \, f^{e/o}(E). \quad (A4)$$

In the last step, we have used that the coupling between the Majorana system and the environment is weak. The final result for these rates coincides with the corresponding Markovian result (57).

Next, we address the asymptotic values $p^{e/o}(t \to \infty)$, which follow by inserting the small-s expansion of $\tilde{g}^{e/o}(s)$ in Eq. (A3) into Eq. (81). We then find that $\tilde{p}^{e/o}(s)$ has a pole at $s = 0$. At finite T, only the s-independent term in Eq. (A3) contributes to the residue of $\tilde{p}^{e/o}(s)$ at $s = 0$, and thus Eq. (83) follows. On the other hand, the $T = 0$ result for $p^{e/o}(t \to \infty)$ [see Eq. (78)] is recovered by noting that the only nonvanishing $T = 0$ term in Eq. (A3) comes from $A^{e/o}$. Some algebra then leads to Eq. (78).

APPENDIX B: SOLUTION OF TS NANOWIRE MODEL

In what follows, we discuss the solution of the specific TS nanowire model in Eq. (84) and determine the W matrix elements which encode the energy-dependent transition matrix elements between the MBS subsystem and the quasiparticle sector. These results have been used for generating the numerical data shown in Secs. V B and V E. We consider the BdG Hamiltonian (84) for a spinless semi-infinite TS

nanowire with 1D coordinate $x \geqslant 0$. We first write Eq. (84) in the equivalent form

$$\mathcal{H}_{BdG} = \Delta \left[\left(\frac{\tilde{p}^2}{2\delta} - 1 \right) \tau_z + \frac{\tilde{p}}{\delta} \tau_x \right], \quad (B1)$$

where we define

$$\tilde{p} = \frac{p}{mv}, \quad \delta = \frac{\Delta}{mv^2}. \quad (B2)$$

Similarly, we use the notation $\tilde{k} = k/(mv)$ below. The zero-energy MBS wave function is denoted by $\psi_0(x) = \langle x|\text{MBS}\rangle$, and quasiparticle wave functions by $\psi_k(x) = \langle x|k\rangle$. With the ansatz $\psi_0(x) = \chi_0 e^{ik_0 x}$, normalizable MBS solutions are found for k_0 with positive imaginary values $k_0 = i\kappa_0^{\pm}$, where

$$\kappa_0^{\pm} = mv(1 \pm \sqrt{1 - 2\delta}). \quad (B3)$$

We only consider the regime $0 \leqslant \delta \leqslant 1/2$ here and in Sec. V E.

Taking a linear superposition of the two states corresponding to Eq. (B3), and imposing Dirichlet boundary conditions $\psi_0(0) = 0$, we obtain the Nambu spinor wave function for the MBS

$$\psi_0(x) = \frac{1}{\mathcal{N}_0} (e^{-\kappa_0^+ x} - e^{-\kappa_0^- x}) \begin{pmatrix} 1 \\ -i \end{pmatrix}, \quad \mathcal{N}_0 = \sqrt{\frac{1 - 2\delta}{mv\delta}}. \quad (B4)$$

As expected, this wave function is exponentially localized near the boundary at $x = 0$. Similarly, quasiparticle wave functions follow from the ansatz $\psi_k(x) = \chi_k e^{ikx}$, with $E_k \geqslant \Delta$ given by

$$E_k = \Delta \left[\left(\frac{\tilde{k}^2}{2\delta} - 1 \right)^2 + \frac{\tilde{k}^2}{\delta^2} \right]^{1/2}. \quad (B5)$$

We then find four solutions $k = \pm k_s$ (with $s = \pm$),

$$k_s = \sqrt{2} mv \sqrt{\delta - 1 + s\sqrt{1 - 2\delta + \delta^2 \xi^2}}, \quad (B6)$$

with $\xi_k = E_k/\Delta$. For $0 \leqslant \delta \leqslant 1/2$, we observe that $k_- = i\kappa$ (with $\kappa > 0$) is purely imaginary while k_+ is purely real. Dropping the non-normalizable states with $k = -i\kappa$, we write $k_+ = k$. We now impose Dirichlet boundary conditions at $x = 0$. Exploiting the continuity equation at large x, we find

$$\mathcal{N}_k \psi_k(x) = \begin{pmatrix} \tilde{k}/\delta \\ a_k \end{pmatrix} e^{ikx} + \begin{pmatrix} -\tilde{k}/\delta \\ a_k \end{pmatrix} e^{-ikx + i\theta_k}$$
$$- \varepsilon_k \begin{pmatrix} i\tilde{\kappa}/\delta \\ b_k \end{pmatrix} (1 + e^{i\theta_k}) e^{-\kappa x}, \quad (B7)$$

with

$$a_k = 1 + \xi_k - \tilde{k}^2/(2\delta), \quad (B8a)$$
$$b_k = 1 + \xi_k + \tilde{\kappa}^2/(2\delta), \quad (B8b)$$

and

$$\varepsilon_k = \frac{a_k}{b_k}, \quad \tan \frac{\theta_k}{2} = \frac{\kappa}{k} \varepsilon_k. \quad (B9)$$
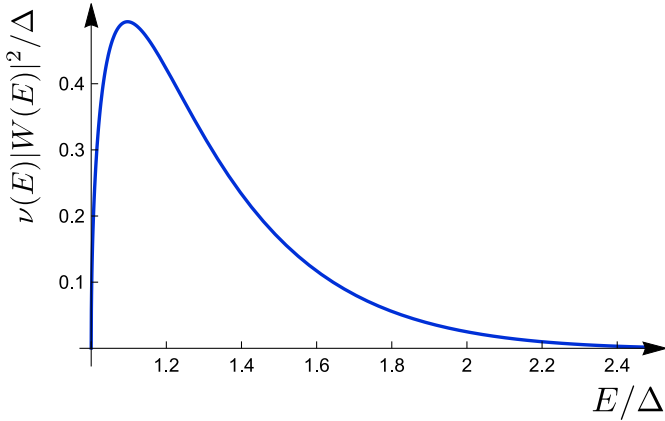
FIG. 10. Transition matrix element $\nu(E)|W(E)|^2$ vs energy E for the TS nanowire model (84) with $\Delta/(mv^2) = 0.2$.

The normalization constant follows from

$$\mathcal{N}_k^2 = 2L\tilde{k}^2/\delta^2 + 2La_k^2. \tag{B10}$$

Here, L is wire length, where we let $L \to \infty$ in the end. Equation (18) then yields

$$
\begin{aligned}
W_k = \frac{4ie^{-i\theta_k/2}}{\tilde{\mathcal{N}}\sqrt{mvL}} &\left[\frac{1}{(2\delta - \tilde{k}^2)^2 + 4\tilde{k}^2} \left[(2\tilde{k}^2/\delta - a_k(2\delta - \tilde{k}^2)) \right.\right. \\
&\times \cos\left(\frac{\theta_k}{2}\right) - (2a_k\tilde{k} + 2\tilde{k} - \tilde{k}^3/\delta)\sin\left(\frac{\theta_k}{2}\right) \bigg] \\
&\left. - \varepsilon_k \cos\left(\frac{\theta_k}{2}\right) \frac{\tilde{\kappa}/\delta - b_k}{\tilde{\kappa}^2 + 2(\tilde{\kappa} + \delta)} \right],
\end{aligned}
\tag{B11}
$$

where

$$\tilde{\mathcal{N}} = \sqrt{\frac{2}{\delta}\left(\frac{\tilde{k}^2}{\delta^2} + a_k^2\right)}. \tag{B12}$$

Finally, $\nu(E)|W(E)|^2$ follows from Eq. (52) by observing that the density of states is with $k = k_+(E)$ in Eq. (B6) given by

$$\nu(E) = \sum_k \delta(E - E_k) = \frac{L}{2\pi}\frac{dk}{dE}. \tag{B13}$$

Note that the L-dependent prefactors in $|W(E)|^2$ are canceled by those in $\nu(E)$. Figure 10 shows a plot of the resulting product $\nu(E)|W(E)|^2$.

APPENDIX C: APPROXIMATE LAPLACE TRANSFORM

We here provide details about the numerical inverse Laplace transformation used for generating Fig. 4. We start with the Laplace transformed function $\tilde{g}^{e/o}(s)$ in Eq. (79), which at $T = 0$ becomes parity independent and given by

$$\tilde{g}_0(s) = \frac{s}{\pi}\int_0^\infty d\omega \int_\Delta^\infty dE \frac{\nu(E)|W(E)|^2 J(\omega)}{s^2 + (E + \omega)^2}. \tag{C1}$$

Since $\nu(E)|W(E)|^2$ is peaked at $E = \Delta_p$, where Δ_p is slightly above Δ (see Fig. 10), we write

$$\tilde{g}_0(s) \approx \frac{s}{\pi}\int_0^\infty d\omega \frac{J(\omega)}{s^2 + (\Delta_p + \omega)^2}\int_\Delta^\infty dE\, \nu(E)|W(E)|^2. \tag{C2}$$

Inserting $J(\omega)$ from Eq. (20), we encounter the auxiliary function

$$\tilde{h}_0(s) = 2s\int_0^\infty d\omega \frac{\omega}{\omega^2 + \omega_0^2}\frac{1}{s^2 + (\Delta_p + \omega)^2}. \tag{C3}$$

For $\mathrm{Re}(s) > 0$, this yields

$$\tilde{h}_0(s) = \omega_0 \frac{-\pi\Delta_p\big[\Delta_p^2 + (s + \omega_0)^2\big] + 2\Delta_p\big[\Delta_p^2 + s^2 + \omega_0^2\big]\tan^{-1}(\Delta_p/s) + s\big(\Delta_p^2 - \omega_0^2 + s^2\big)\ln\big[(s^2 + \Delta_p^2)/\omega_0^2\big]}{\big[\Delta_p^2 + (s - \omega_0)^2\big]\big[\Delta_p^2 + (s + \omega_0)^2\big]}. \tag{C4}$$

For the Laplace transformed coherences in Eq. (72), we then obtain

$$\tilde{d}_\alpha^{e/o}(s) = \frac{d_\alpha^{e/o}(t=0)}{s + B\tilde{h}_0(s)}, \quad B = \frac{E_0}{\pi}\int_\Delta^\infty dE\, \nu(E)|W(E)|^2. \tag{C5}$$

At this stage, the inverse Laplace transform can be performed numerically in an efficient manner (see Fig. 4).

For finite but very low temperatures, $k_B T \ll \Delta$, we should keep the Bose function $n_B(\omega)$ in Eq. (79). The function $\tilde{h}_0(s)$

should then be replaced by $\tilde{h}(s) = \tilde{h}_0(s) + \tilde{h}_1(s)$, where

$$\tilde{h}_1(s) = 2s\int_0^\infty d\omega \frac{\omega n_B(\omega)}{\omega^2 + \omega_0^2}\left(\frac{1}{s^2 + (\Delta_p + \omega)^2} + \frac{1}{s^2 + (\Delta_p - \omega)^2}\right). \tag{C6}$$

We see that the saturation value $d_\alpha^{e/o}(t \to \infty)$, which follows by setting $s = 0$, now vanishes because $\tilde{h}_1(0)$ diverges. This feature is a general result of the exponential decay of all coherences in the Markovian case with $T > 0$. Finally, we remark that finite temperature also gives only minor modifications to the dynamics shown in Fig. 4.

[1] A. Y. Kitaev, Ann. Phys. (N.Y.) **303**, 2 (2003).

[2] C. Nayak, S. H. Simon, A. Stern, M. Freedman, and S. Das Sarma, Rev. Mod. Phys. **80**, 1083 (2008).

[3] A. Y. Kitaev, Phys. Usp. **44**, 131 (2001).

[4] R. M. Lutchyn, J. D. Sau, and S. Das Sarma, Phys. Rev. Lett. **105**, 077001 (2010).

[5] Y. Oreg, G. Refael, and F. von Oppen, Phys. Rev. Lett. **105**, 177002 (2010).

[6] C. W. J. Beenakker, Annu. Rev. Condens. Matter Phys. **4**, 113 (2013).

[7] J. Alicea, Rep. Prog. Phys. **75**, 076501 (2012).

[8] R. Aguado, La Rivista del Nuovo Cimento **40**, 523 (2017).

[9] M. Leijnse and K. Flensberg, Semicond. Sci. Technol. **27**, 124003 (2012).

[10] R. M. Lutchyn, E. P. A. M. Bakkers, L. P. Kouwenhoven, P. Krogstrup, C. M. Marcus, and Y. Oreg, Nat. Rev. Mater. **3**, 52 (2018).

[11] L. Fu and C. L. Kane, Phys. Rev. Lett. **100**, 096407 (2008).

[12] V. Mourik, K. Zuo, S. M. Frolov, S. R. Plissard, E. P. A. M. Bakkers, and L. P. Kouwenhoven, Science **336**, 1003 (2012).

[13] M. T. Deng, S. Vaitiek, E. B. Hansen, J. Danon, M. Leijnse, K. Flensberg, P. Krogstrup, and C. M. Marcus, Science **354**, 1557 (2016).

[14] S. M. Albrecht, A. P. Higginbotham, M. Madsen, F. Kuemmeth, T. S. Jespersen, J. Nygård, P. Krogstrup, and C. M. Marcus, Nature (London) **531**, 206 (2016).

[15] H. J. Suominen, M. Kjaergaard, A. R. Hamilton, J. Shabani, C. J. Palmstrøm, C. M. Marcus, and F. Nichele, Phys. Rev. Lett. **119**, 176805 (2017).

[16] F. Nichele, A. C. C. Drachmann, A. M. Whiticar, E. C. T. O'Farrell, H. J. Suominen, A. Fornieri, T. Wang, G. C. Gardner, C. Thomas, A. T. Hatke, P. Krogstrup, M. J. Manfra, K. Flensberg, and C. M. Marcus, Phys. Rev. Lett. **119**, 136803 (2017).

[17] H. Zhang, C.-X. Liu, S. Gazibegovic, D. Xu, J. A. Logan, G. Wang, N. van Loo, J. D. S. Bommer, M. W. A. de Moor, D. Car, R. L. M. O. het Veld, P. J. van Veldhoven, S. Koelling, M. A. Verheijen, M. Pendharkar, D. J. Pennachio, B. Shojaei, J. S. Lee, C. J. Palmstrom, E. P. A. M. Bakkers *et al.*, Nature (London) **556**, 74 (2018).

[18] T. Hyart, B. van Heck, I. C. Fulga, M. Burrello, A. R. Akhmerov, and C. W. J. Beenakker, Phys. Rev. B **88**, 035121 (2013).

[19] D. Aasen, M. Hell, R. V. Mishmash, A. Higginbotham, J. Danon, M. Leijnse, T. S. Jespersen, J. A. Folk, C. M. Marcus, K. Flensberg, and J. Alicea, Phys. Rev. X **6**, 031016 (2016).

[20] S. Plugge, A. Rasmussen, R. Egger, and K. Flensberg, New J. Phys. **19**, 012001 (2017).

[21] T. Karzig, C. Knapp, R. M. Lutchyn, P. Bonderson, M. B. Hastings, C. Nayak, J. Alicea, K. Flensberg, S. Plugge, Y. Oreg, C. M. Marcus, and M. H. Freedman, Phys. Rev. B **95**, 235305 (2017).

[22] J. Manousakis, A. Altland, D. Bagrets, R. Egger, and Y. Ando, Phys. Rev. B **95**, 165424 (2017).

[23] B. M. Terhal, F. Hassler, and D. P. DiVincenzo, Phys. Rev. Lett. **108**, 260504 (2012).

[24] L. A. Landau, S. Plugge, E. Sela, A. Altland, S. M. Albrecht, and R. Egger, Phys. Rev. Lett. **116**, 050501 (2016).

[25] C. G. Brell, S. Burton, G. Dauphinais, S. T. Flammia, and D. Poulin, Phys. Rev. X **4**, 031058 (2014).

[26] S. Vijay, T. H. Hsieh, and L. Fu, Phys. Rev. X **5**, 041038 (2015).

[27] S. Plugge, L. A. Landau, E. Sela, A. Altland, K. Flensberg, and R. Egger, Phys. Rev. B **94**, 174514 (2016).

[28] D. Litinski, M. S. Kesselring, J. Eisert, and F. von Oppen, Phys. Rev. X **7**, 031048 (2017).

[29] D. Litinski and F. von Oppen, Phys. Rev. B **97**, 205404 (2018).

[30] S. Bravyi, Phys. Rev. A **73**, 042313 (2006).

[31] K. Flensberg, Phys. Rev. Lett. **106**, 090503 (2011).

[32] T. Karzig, Y. Oreg, G. Refael, and M. H. Freedman, Phys. Rev. X **6**, 031019 (2016).

[33] C. Knapp, T. Karzig, R. M. Lutchyn, and C. Nayak, Phys. Rev. B **97**, 125404 (2018).

[34] G. Goldstein and C. Chamon, Phys. Rev. B **84**, 205109 (2011).

[35] M. Cheng, R. M. Lutchyn, and S. Das Sarma, Phys. Rev. B **85**, 165124 (2012).

[36] D. Rainis and D. Loss, Phys. Rev. B **85**, 174533 (2012).

[37] M. J. Schmidt, D. Rainis, and D. Loss, Phys. Rev. B **86**, 085414 (2012).

[38] G. Yang and D. E. Feldman, Phys. Rev. B **89**, 035136 (2014).

[39] H.-L. Lai, P.-Y. Yang, Y.-W. Huang, and W.-M. Zhang, Phys. Rev. B **97**, 054508 (2018).

[40] Y. Song and S. Das Sarma, Phys. Rev. B **98**, 075159 (2018).

[41] T. Li, W. A. Coish, M. Hell, K. Flensberg, and M. Leijnse, Phys. Rev. B **98**, 205403 (2018).

[42] A. Nag and J. D. Sau, arXiv:1808.09939.

[43] P. P. Aseev, J. Klinovaja, and D. Loss, Phys. Rev. B **98**, 155414 (2018).

[44] C. Knapp, M. Beverland, D. I. Pikulin, and T. Karzig, Quantum **2**, 88 (2018).

[45] U. Weiss, *Quantum Dissipative Systems*, 4th ed. (World Scientific, Singapore, 2012).

[46] A. R. Akhmerov, Phys. Rev. B **82**, 020509(R) (2010).

[47] M. Hell, J. Danon, K. Flensberg, and M. Leijnse, Phys. Rev. B **94**, 035424 (2016).

[48] K. Le Hur, Ann. Phys. (N.Y.) **323**, 2208 (2008).

[49] H.-P. Breuer and F. Petruccione, *The Theory of Open Quantum Systems* (Oxford University Press, Oxford, 2007).

[50] P. Lafarge, P. Joyez, D. Esteve, C. Urbina, and M. H. Devoret, Phys. Rev. Lett. **70**, 994 (1993).

[51] M. T. Tuominen, J. M. Hergenrother, T. S. Tighe, and M. Tinkham, Phys. Rev. B **47**, 11599 (1993).

[52] A. P. Higginbotham, S. Albrecht, G. Kiršanskas, W. Chang, F. Kuemmeth, P. Krogstrup, T. Jespersen, J. Nygård, K. Flensberg, and C. Marcus, Nat. Phys. **11**, 1017 (2015).

111

Chapter 5

Project D:
Dyonic zero-energy modes

In this project we seek to further generalize Majorana zero-energy modes. The approach is based on the mathematical fact that the Ising model is isomorphic to the Kitaev chain through the Jordan-Wigner transformation. This relationship is generalized by the so-called Potts chiral clock model, which is isomorphic to a parafermionic model with a topological phase featuring zero-energy $\mathbb{Z}_N$ parafermionic edge modes. This generalization serves as the inspiration for the work in this project.

The generalization we propose in this paper provides a Jordan-Wigner-like mapping from a bosonic model with a global gauge symmetry given by an arbitrary finite group G, to a one-dimensional lattice model of dyonic modes. Crucially, G is allowed to be non-abelian. That the modes are dyonic means they carry both a "magnetic charge", that is a group element, and an "electric charge", which means an index corresponding to an irreducible representation of G. Our model has a topological phase with zero-energy edge modes, which are also dyonic. We show that this phase has a topologically ordered ground state when specific conditions are met.

The fusion rules of the dyonic zero-energy modes are discussed, although a full understanding of the braiding rules remains an open problem, since standard arguments relying on the spin-statistics theorem are ruled out, owing to the fact that our model is not inherently build out of fermions or bosons.

The zero-energy modes are in general weak, meaning that the degeneracy corresponding to the modes does not continue indefinitely into the excited states. Numerical evidence is provided for the smallest non-abelian group S_3, which agrees with our theoretical conclusions.

Dyonic zero-energy modes

Morten I. K. Munk,[1] Asbjørn Rasmussen,[2] and Michele Burrello[1,3]

[1]*Center for Quantum Devices, Niels Bohr Institute, University of Copenhagen, Juliane Maries Vej 30, 2100 Copenhagen, Denmark*
[2]*Center for Atomic-scale Materials Design, Department of Physics, Technical University of Denmark, 2800 Kongens Lyngby, Denmark*
[3]*Niels Bohr International Academy, Niels Bohr Institute, University of Copenhagen, Juliane Maries Vej 30, 2100 Copenhagen, Denmark*

One-dimensional systems with topological order are intimately related to the appearance of zero-energy modes localized on their boundaries. The most common example is the Kitaev chain, which displays Majorana zero-energy modes and it is characterized by a twofold ground-state degeneracy related to the global $\mathbb{Z}_2$ symmetry associated with fermionic parity. By extending the symmetry to the $\mathbb{Z}_N$ group, it is possible to engineer systems hosting topological parafermionic modes. In this work, we address one-dimensional systems with a generic discrete symmetry group G. We define a ladder model of gauge fluxes that generalizes the Ising and Potts models and displays a symmetry broken phase. Through a non-Abelian Jordan-Wigner transformation, we map this flux ladder into a model of dyonic operators, defined by the group elements and irreducible representations of G. We show that the so-obtained dyonic model has topological order, with zero-energy modes localized at its boundary. These dyonic zero-energy modes are in general weak topological modes, but strong dyonic zero modes appear when suitable position-dependent couplings are considered.

I. INTRODUCTION

With his seminal work [1], Kitaev gave life to the study of one-dimensional models with topological order. These are models displaying degenerate ground states, without any local order parameter able to distinguish them. Their prototypical example is, indeed, the Kitaev chain, a fermionic model characterized by the presence of zero-energy Majorana modes localized at its edges. These modes commute with the Hamiltonian but anticommute with each other, thus enforcing a twofold degeneracy of the energy spectrum up to exponential corrections in the system size.

The unpaired Majorana modes in Kitaev's model are protected by a global $\mathbb{Z}_2$ symmetry, which corresponds to the conservation of the fermionic parity; once embedded in a two-dimensional system, these zero-energy modes behave like non-Abelian anyons, thus opening an invaluable scenario for topological quantum computation [2–4].

In the search for richer kinds of non-Abelian anyons, the Kitaev chain has been generalized to a family of models with global $\mathbb{Z}_N$ symmetries [5]. These models can be build from a nonlocal representation of the chiral $\mathbb{Z}_N$ Potts model in terms of parafermions, which are a generalization of the Majorana modes to the $\mathbb{Z}_N$ case. Through an iterative procedure, Fendley argued that these $\mathbb{Z}_N$-symmetric chains are characterized by localized zero-energy parafermionic modes [5] and, consequently, their ground states are N-fold degenerate, up to exponential corrections due to finite size effects [6–8] (see also Ref. [9]).

Is it possible to generalize further these systems and build one-dimensional topological models characterized by an underlying non-Abelian symmetry group? What are the corresponding zero-energy modes?

These are the questions addressed in this paper. We will define one-dimensional topological models whose Hamiltonian is invariant under the action of a discrete non-Abelian symmetry group G and, based on an iterative expansion, we will show the presence of localized zero-energy modes. These zero-energy modes can be characterized based on their transformation rules under the action of the global symmetry group G; similarly to anyons in a two-dimensional quantum double model [10], they will be labeled by both a group element g and an irreducible representation K of G. For this reason we call them *dyonic zero-energy modes*.

Our strategy to build these exotic 1D models with topological order is inspired by the duality between the Ising and Kitaev chains and its generalization to the Potts and parafermionic models: it is known that the Kitaev chain can be described in terms of the Ising model through a Jordan-Wigner transformation mapping spins into fermions; in the same way, the parafermionic chains are equivalent to $\mathbb{Z}_N$ clock models based on a generalized Jordan-Wigner (JW) transformation [11,12]. In both situations, the JW transformation maps a bosonic (spin or clock) model, characterized by spontaneous symmetry breaking in an ordered phase, into a model with topological order built from operators (fermionic or parafermionic), which do not commute when spatially separated. The JW transformation is nonlocal and it maps the degeneracy of the ground states in the ordered (ferromagnetic) phase of the bosonic models into a degeneracy caused by localized zero-energy modes in the topological models.

Our construction will be based on an analogous mapping: we will begin from the "bosonic" side and we will first define a G-symmetric ladder model, inspired by quantum double models [10] and lattice gauge theories. G will be a global non-Abelian gauge symmetry, which will be spontaneously broken, thus resulting in an ordered phase. In this ladder model, the ground states are $|G|$-fold degenerate, where $|G|$ is the order of the symmetry group, and they can be locally distinguished. We will argue that, for chiral models,

TABLE I. The table represents the relation between the topological models by Kitaev and Fendley and their nontopological counterparts given by the Ising and Potts models. The related Jordan-Wigner mapping preserves the corresponding global symmetries. The scope of this paper is to define analogous models with a non-Abelian symmetry and verify the existence of localized zero-energy modes.

Global symmetry	Bosonic model	Mapping	Topological model	Zero modes
$\mathbb{Z}_2$	Ising	$\xleftrightarrow{\text{JW}}$	Kitaev [1]	Majorana modes
$\mathbb{Z}_N$	Chiral Potts	$\xleftrightarrow{\mathbb{Z}_N\text{ JW}}$	Fendley [5]	Parafermionic modes
Non-Abelian G	Chiral gauge flux ladder	$\xleftrightarrow{\text{Non-Abelian JW}}$	Chiral dyonic model	Dyonic modes

the ground-state degeneracy is preserved up to corrections exponentially suppressed in the system size. Then we will proceed by defining a non-Abelian JW transformation, which maps the bosonic "gauge" degrees of freedom into dyonic operators labeled by an element $g \in G$ and transforming under the symmetry group G based on its fundamental (standard) irreducible representation F.

Based on both a quasiadiabatic continuation and an iterative construction, we will show that localized dyonic zero-energy modes emerge in the system and we will investigate their fusion rules, which can be understood in terms of the effect of the symmetry transformations and are consistent with the $|G|$-fold degeneracy of the ground state.

Let us summarize the content of this paper. Section II is devoted to the introduction and analysis of the "bosonic" gauge-flux ladder model. In Sec. II A, we interpret the Ising and Potts models in terms of flux ladder models to set the stage for the more complicated non-Abelian case; Sec. II B introduces the building blocks for the non-Abelian flux ladder Hamiltonian, which is built and analyzed in Secs. II C and II D; Sec. II E finally deals with the example provided by the smallest non-Abelian group, S_3. Section III is dedicated to the construction of the dyonic model; in Sec. III A, we introduce the JW transformation for discrete non-Abelian groups and the resulting dyonic operators which allow us to build the dyonic Hamiltonian; in Sec. III B, we define the notion of topological order for one-dimensional systems with a non-Abelian global symmetry. Section IV is devoted to the analysis of the zero-energy modes of the dyonic model; in Sec. IV A, we show that the dyonic model fulfills the criteria for topological order and presents protected weak zero-energy edge modes; in Secs. IV B–IV E, we present the construction of strong topological zero-energy modes and we discuss divergences that hinder their appearance and the conditions the Hamiltonian must fulfill to avoid these divergences; Sec. IV F analyzes the fusion properties of the topological modes. Section V discusses further properties of the family of models we introduced and the appearance of additional holographic and local symmetries in the dyonic Hamiltonian. Section VI presents a numerical analysis of the lowest energy excitations of the model for $G = S_3$ in the single-flux approximation. Finally, in Sec. VII, we summarize our results and Appendices provide additional analyses of some technical aspects.

II. NON-ABELIAN GAUGE FLUX LADDERS

A. Ising and Potts models as gauge-flux ladders

Before beginning the construction of models with non-Abelian symmetries, it is useful to provide a description of

the Ising and Potts models in terms of gauge-flux ladders for the Abelian gauge groups and summarize some of their properties. This construction is based on associating each site of the Ising or Potts models with a rung in a ladder and interpreting its states in terms of a gauge degree of freedom related to the $\mathbb{Z}_2$ or $\mathbb{Z}_N$ group. In particular, let us consider the Ising model:

$$H = -J \sum_{r=1}^{L} \sigma_{z,r}\sigma_{z,r+1} - h \sum_{r=1}^{L} \sigma_{x,r}. \tag{1}$$

For each site r, we can consider the state $|\uparrow\rangle$ as representing the identity element $e \in \mathbb{Z}_2$ and the state $|\downarrow\rangle$ as the nontrivial element $-1 \in \mathbb{Z}_2$. Under this point of view, the term $-J\sigma_{z,r}\sigma_{z,r+1}$ is minimized if the gauge degrees of freedom in neighboring sites are equal. Therefore, by interpreting the ladder as a set of plaquettes in a gauge theory, we can state that this term is minimized if no gauge flux is present in the plaquette r, such that a hypothetical particle coupled to this gauge degrees of freedom undergoes a trivial gauge transformation when moving around the plaquette: a gauge flux thus corresponds to a domain wall in the usual ferromagnetic description. The effect of the h term, instead, is to allow for transitions between the $|\uparrow\rangle$ and $|\downarrow\rangle$ states. This can be interpreted as an electric field term in the $\mathbb{Z}_2$ gauge theory and it amounts to a local gauge transformation acting on a single gauge degree of freedom. In this work, we will mostly be interested in the ordered phase $J > h$ of these models. In such a phase, the term J provides a mass for the $\mathbb{Z}_2$ gauge fluxes, whereas the term h nucleates pairs of these fluxes and

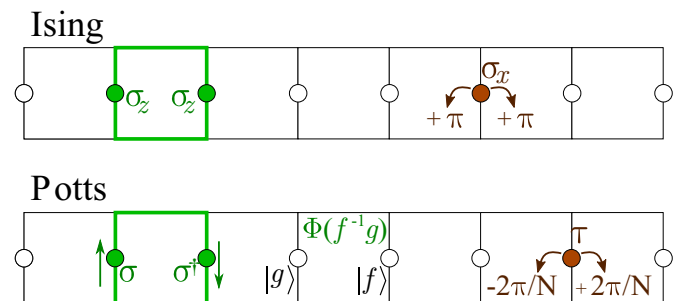FIG. 1. The Ising (first row) and Potts (second row) models are interpreted as $\mathbb{Z}_N$ gauge-flux ladders. The nearest-neighbor (green) terms assign a mass to the nontrivial gauge fluxes Φ and can be interpreted as plaquette operators. The on-site h terms have the effect of adding a pair flux-antiflux to the neighboring plaquettes; π fluxes in the Ising case, a pair of $\pm 2\pi/N$ fluxes in the Potts case.

constitutes their kinetic energy (see Fig. 1). The related global gauge symmetry is given by the string operator $\mathcal{Q} = \prod_r \sigma_{x,r}$.

An alternative interpretation of the Ising model / $\mathbb{Z}_2$ gauge-flux ladder is provided by the toric code [10]. The gauge-flux ladder is a row of the toric code in which all the horizontal degrees of freedom have been frozen into the $|\uparrow\rangle$ state (corresponding to the identity transformation in G) and do not appear in the Hamiltonian. Only the rung degrees of freedom are dynamical and describe the dynamics of the $\mathbb{Z}_2$ magnetic fluxes moving along the ladder.

The same flux-ladder description can be applied to the Potts model:

$$H = -J \sum_{r=1}^{L} (e^{i\phi} \sigma_{r+1}^{\dagger} \sigma_r + \text{H.c.}) - h \sum_{n=1}^{N-1} \sum_{r=1}^{L} \tau_r^n, \quad (2)$$

where we introduced the $\mathbb{Z}_N$ clock operators σ and τ obeying the commutation rule $\sigma_r \tau_{r'} = e^{i \frac{2\pi}{N} \delta_{r,r'}} \tau_{r'} \sigma_r$ and the relations $\sigma^N = \tau^N = 1$. This model is symmetric under the global $\mathbb{Z}_N$ transformations $\mathcal{Q}_k = \prod_r \tau_r^k$ and can be interpreted as a $\mathbb{Z}_N$ flux-ladder model with the magnetic fluxes taking N different values. In the Potts model, we can associate the N eigenstates $|g\rangle$ of the operator σ, such that $\sigma|g\rangle = e^{i 2\pi n_g / N}|g\rangle$, with the N elements g of the group $\mathbb{Z}_N$; also in this case, we can interpret the states of each site as gauge degrees of freedom lying on the rungs of a ladder. For $\phi = 0$, the J term of the Hamiltonian is minimized if the gauge degrees of freedom of neighboring rungs coincide, thus no domain walls are present. This corresponds to a situation in which all the plaquettes host a trivial gauge flux. As in the Ising case, the gauge fluxes correspond to the domain walls of the system and they belong to N inequivalent kinds, one for each element of the group $\mathbb{Z}_N$.

Let us consider a single plaquette (see Fig. 1). For a generic product state $|g\rangle_r |f\rangle_{r+1}$, the operator $\sigma_{r+1}^{\dagger} \sigma_r$ has eigenvalue $e^{i 2\pi (n_g - n_f) / N}$. Therefore this state corresponds to a $\mathbb{Z}_N$ gauge flux $\Phi(f^{-1} g) = 2\pi (n_g - n_f)/N$ and the J term of the Hamiltonian returns an energy $-2J \cos[2\pi (n_g - n_f)/N + \phi]$ which determines its mass. By embedding the model in a lattice gauge theory, this gauge flux would correspond to the transformation in $\mathbb{Z}_N$ of a hypothetical matter particle moving clockwise around the ladder plaquette.

Generalizing the Ising case, the h term in the Hamiltonian corresponds to the sum of the nontrivial local $\mathbb{Z}_N$ gauge transformations that can be applied to each local gauge degree of freedom. In the gauge theory interpretation it is an energy term associated to the electric field in the rung. In particular we have $\tau_r^{n_h} |g\rangle_r = |hg\rangle_r$. The Potts model can thus be interpreted as a ladder of $\mathbb{Z}_N$ magnetic fluxes in the spirit of the $\mathbb{Z}_N$ toric code [13] (see also [14] for an analogous stripe model).

In the case $\phi = 0$ the system is invariant under both the time-reversal symmetry $\tau \to \tau^{\dagger}$, $\sigma \to \sigma^{\dagger}$ and the space inversion symmetry $\tau_r \to \tau_{L-r}$, $\sigma_r \to \sigma_{L-r}$, where L is the system size. This implies that the fluxes $\Phi(g)$ and $\Phi(g^{-1})$ have the same mass. When introducing $\phi \neq 0$, both the symmetries are violated and the model becomes chiral. In general, for $\phi \neq 0$, the global $\mathbb{Z}_N$ transformations are the only nonspatial symmetries preserved and it was showed that only in this chiral case zero-energy modes can be stable

in the corresponding parafermionic theory [5]. Therefore, to extend the $\mathbb{Z}_N$ theory to a non-Abelian group, we will adopt a similar approach and consider Hamiltonians violating the time-reversal and space-inversion symmetries.

For both the Ising and Potts models, the phase diagram includes an ordered ferromagnetic phase when $h \ll J$ and a disordered paramagnetic phase for $J \ll h$ (the $\mathbb{Z}_N$ symmetric models include additional gapless phases for $N > 4$). The related symmetries are unbroken in the paramagnetic phase and become spontaneously broken for the ferromagnetic phases such that the eigenstates of the models are, in general, not invariant under the gauge group $\mathbb{Z}_N$. The disorder operator introduces a domain wall in the system, which corresponds with the gauge flux in the ladder [11]. We define the disorder operators as the product of local gauge symmetries from the left edge of the system to the position of the flux: $\mathcal{L}_g(r) = \prod_{j<r} \tau_j^{n_g}$. These disorder operators are dual to the order operators σ_r and, from their product, it is possible to build the Abelian Jordan-Wigner transformations mapping the clock into the parafermionic models [5].

B. The rung Hilbert space and operators

The construction of the flux-ladder model is based on lattice gauge theories and quantum double models [10] (see also Ref. [15]). In particular, we will exploit the formalism adopted for the quantum simulations of lattice gauge theories (see, for example, the reviews [16,17]) and we will adopt the notation developed in Refs. [18,19] for their tensor-network study.

Our aim is to define a chiral flux-ladder model invariant under a global gauge group G, with G being a discrete group. In analogy with the previous section, we consider degrees of freedom associated with the rungs of the ladder. Each of these rung degrees of freedom spans a local Hilbert space of dimension $|G|$, the order of the group G, and a basis for the local states in each rung is given by $\{|g\rangle, g \in G\}$. This is the group element basis which allows us to easily define the gauge-fluxes populating the plaquettes of the ladder.

For the construction of our model, we want to generalize both the τ and the σ operators from $\mathbb{Z}_N$ to a generic non-Abelian G. These are extended by defining, for each rung: (i) local operators θ_g and $\tilde{\theta}_g$ that implement left and right local gauge transformations and play the role of the τ operators; (ii) local matrices U_{mn} of operators which constitute gauge-connection operators and are associated to the fundamental irreducible representation F of G; the operators U generalize the σ operators in the Potts model.

Based on the group element basis, the previous operators are defined in the following way:

$$\theta_g |h\rangle = |gh\rangle, \quad \theta_g^{\dagger} |h\rangle = |g^{-1} h\rangle, \quad (3)$$

$$\tilde{\theta}_g |h\rangle = |hg\rangle, \quad \tilde{\theta}_g^{\dagger} |h\rangle = |hg^{-1}\rangle, \quad (4)$$

$$U_{mn} |h\rangle = D_{mn}(h)|h\rangle, \quad U_{mn}^{\dagger} |h\rangle = D_{mn}^{\dagger}(h)|h\rangle \quad (5)$$

for any $g, h \in G$. In Eq. (5), the matrix $D_{mn}(h)$ is the unitary matrix which represents the element $h \in G$ in the fundamental representation F of the group. More generally, $D_{mn}^K(g)$ will label the $\dim(K) \times \dim(K)$ unitary matrix representing the element g in the representation K of the group; these matrices

generalize the Wigner matrices of SU(2). For any irreducible representation K, we define operators

$$U_{mn}^K |h\rangle = D_{mn}^K(h)|h\rangle, \quad U_{mn}^{K\dagger}|h\rangle = D_{mn}^{K\dagger}(h)|h\rangle. \quad (6)$$

When the irrep index is not specified, the fundamental representation is assumed.

We observe that all the connection operators U are diagonal in the group element basis, consistently with our previous description of the $\mathbb{Z}_N$ models; furthermore, we emphasize that $U_{lm}U_{mn}^\dagger = \delta_{ln}\mathbb{1}$, where $\mathbb{1}$ is the identity operator. Hereafter the Einstein summation convention (summation on repeated indices) is used for the matrix indices.

The operators θ_g and $\tilde{\theta}_g$ are unitary operators, which transform the state $|h\rangle$ based on the group composition rules. In particular, they fulfill $\theta_g = \theta_{g^{-1}}^\dagger$ and $\tilde{\theta}_g = \tilde{\theta}_{g^{-1}}^\dagger$.

From the previous relations, it is easy to calculate the commutators of these operators:

$$U_{mn}\theta_g = \theta_g[D(g)U]_{mn}, \quad (7)$$

$$U_{mn}\tilde{\theta}_g = \tilde{\theta}_g[UD(g)]_{mn}, \quad (8)$$

$$\theta_g\tilde{\theta}_h = \tilde{\theta}_h\theta_g. \quad (9)$$

Following the convention in Ref. [18], we finally point out that the matrices $D_{mn}^K(g)$ allow us to define a Fourier transformation that changes the basis for the rung Hilbert space from the group to the irreducible representation basis, and, in particular, from the eigenstates of U to the eigenstates of θ and $\tilde{\theta}$. This unitary transformation is given by

$$|Kmn\rangle = \sum_{g\in G}\sqrt{\frac{\dim K}{|G|}}D_{mn}^K(g)|g\rangle. \quad (10)$$

For the states $|Kmn\rangle$ of this basis, we have

$$\theta_g|Kmn\rangle = D_{ml}^K(g^{-1})|Kln\rangle, \quad (11)$$

$$\tilde{\theta}_g|Kmn\rangle = D_{ln}^K(g^{-1})|Kml\rangle. \quad (12)$$

To describe the flux ladder model, we label the connection operator by $U(r)$ and the gauge transformations acting locally on the rung r by $\theta_g(r)$ and $\tilde{\theta}_g(r)$. In particular, the global left and right gauge transformations assume the form

$$\mathcal{Q}_g = \prod_r \theta_g(r), \quad \tilde{\mathcal{Q}}_g = \prod_r \tilde{\theta}_g(r), \quad (13)$$

for any nontrivial group element $g \neq e \in G$, with $e \in G$ labeling the identity element.

Besides the U and θ operators, we introduce for later convenience the family of "dressed" gauge operators, acting on a single rung:

$$\Theta_{g,\mathsf{ac}}^K = U_{\mathsf{ab}}^{K\dagger}\theta_g U_{\mathsf{bc}}^K = \theta_g U_{\mathsf{am}}^{K\dagger}D_{\mathsf{mn}}^{K\dagger}(g)U_{\mathsf{nb}}^K. \quad (14)$$

Hereafter we will use different fonts for the matrix indices associated to the dressed gauge operators. The operators Θ appear in the study of bond-algebraic dualities for non-Abelian symmetric models developed by Cobanera *et al.* [20], and obey the same group composition rules of the gauge operators

θ_g. In particular, it is easy to verify that

$$\Theta_{g,\mathsf{ab}}^K\Theta_{h,\mathsf{bc}}^K = U_{\mathsf{am}}^{K\dagger}\theta_g U_{\mathsf{mb}}^K U_{\mathsf{bn}}^{K\dagger}\theta_h U_{\mathsf{nc}}^K = \Theta_{gh,\mathsf{ac}}^K, \quad (15)$$

for any irreducible representation K, and

$$\Theta_{g,\mathsf{ab}}^K\Theta_{g,\mathsf{bc}}^{K\dagger} = \delta_{\mathsf{ac}}\mathbb{1}; \quad (16)$$

from these relations we get, in particular $\Theta_g^\dagger = \Theta_{g^{-1}}$. From the definition (14), it is easy to derive that the behavior of the Θ operators under the global left transformations matches the behavior of the gauge operators θ:

$$\mathcal{Q}_h^\dagger\Theta_g^K(r)\mathcal{Q}_h = \Theta_{h^{-1}gh}^K(r). \quad (17)$$

For Abelian representations K, Θ_g is reduced to $\theta_g D^K(g^{-1})$.

C. The flux Hamiltonian and its symmetries

By exploiting the operators introduced above, we define the flux-ladder model through the Hamiltonian:

$$H = -J\left(\sum_r \text{Tr}[U(r+1)CU^\dagger(r)] + \text{H.c.}\right) - \mu\sum_r\sum_{g\neq e\in G}\chi^A(g^{-1})\theta_g(r), \quad (18)$$

where J and μ are real coupling constants and C is a unitary matrix responsible for the chiral nature of the system. In this expression,

$$\chi^A(g^{-1}) = \text{Tr}\,D^A(g^{-1}) \quad (19)$$

labels the character of an auxiliary irreducible representation A of the group element g. Its role will be important in the definition of the dyonic topological model and it will be discussed in detail in Section V.

In the following, we label the first term in the Hamiltonian (18) by H_J and the second term by H_μ. In this work we are mostly interested in the ordered regime $J \gg \mu$ where H_J dominates and the system presents degenerate ground states in the thermodynamic limit.

In the following, we discuss the main features of H_J and H_μ, the role of the C matrix and the symmetries of the Hamiltonian H. A pictorial representation of the system is provided in Fig. 2.

1. H_J and the flux masses

The first term in the Hamiltonian (18) is responsible for the definition of the mass spectrum of the fluxes in the ladder and it generalizes the J term in the chiral Potts model (2). Each operator acts on neighboring degrees of freedom, therefore, it is useful to consider the two-rung state $|g_r\rangle_r|g_{r+1}\rangle_{r+1}$: such a state defines a flux $\Phi(r)$ in the rth plaquette which corresponds to the element $g_r^{-1}g_{r+1}$ of the group G. In our model, the fluxes are indeed in one-to-one correspondence with the group elements, thus, to define their mass, we exploit the connection operators U, which are diagonal in the group element basis. Analogously to the Kogut and Susskind formulation of lattice gauge theories [21], we consider the trace of these operators as a building block for the masses m_g associated to the fluxes. In the simple case of $C = \mathbb{1}$, the operator $\text{Tr}[U(r+1)U^\dagger(r)]$
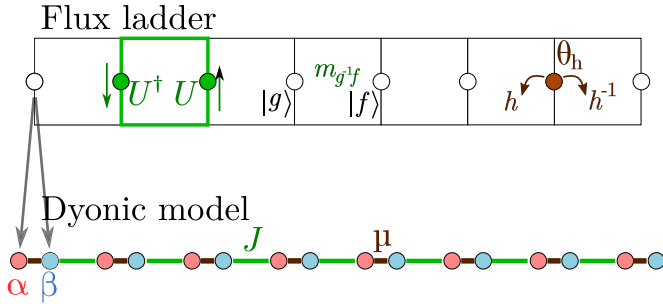
Flux ladder

Dyonic model

FIG. 2. (Top) Graphical representation of the operators in the flux-ladder Hamiltonian. The nearest-neighbor (green) terms define H_J and assign a mass to the gauge fluxes: these terms are plaquette operators built from the connection operators U. The rung θ_h terms in H_μ modify the fluxes in the two neighboring plaquettes. Bottom: the dyonic model is obtained by redefining each rung based on two kinds of operators, α and β. The Hamiltonians H_J and H_μ act on different pairs of dyonic operators.

returns the character $\chi^F(\Phi(r))$ of the group element $\Phi(r) = g_r^{-1} g_{r+1}$ associated to the fundamental representation F. The character is maximized by the identity, thus the trivial flux, but it cannot distinguish between group elements in the same conjugacy class, leading to degeneracies in the mass spectrum. To avoid these degeneracies, we introduce the unitary C matrix, of dimension given by $\dim(F) \times \dim(F)$, such that, in general, we can define nondegenerate flux masses:

$$m_g = -J(\text{Tr}[D(g)C] + \text{Tr}[C^\dagger D^\dagger(g)]).\tag{20}$$

For our analysis, it will be important to consider the following conditions on the mass spectrum.

$\mathcal{C}1$: For the sake of simplicity, we impose that the mass of the trivial flux $e \in G$ is the lowest. This means that the ground states of H_J are states with no fluxes, thus no domain walls in the group element basis. This condition is not necessary for our results, but it simplifies our analysis because it implies that the ordered phase is ferromagnetic-like rather than helical-like. This is analogous to choosing $|\theta| < \pi/3$ in the $\mathbb{Z}_3$ chiral Potts model.

$\mathcal{C}2$: We impose the mass spectrum to be nondegenerate. As we will discuss in the next sections, this is a necessary but not sufficient requirement for the definition of strong zero-energy modes in the corresponding topological models. This condition implies that we must choose a C matrix such that

$$\text{Re}\,(\text{Tr}[CD(g)]) \neq \text{Re}\,(\text{Tr}[CD(h)]),\tag{21}$$

for any $g \neq h \in G$.

It is now important to define the left and right global gauge transformations of the operators in H_J based on Eqs. (7) and (8):

$$\mathcal{Q}_g^\dagger \text{Tr}[U(r+1)CU^\dagger(r)]\mathcal{Q}_g$$
$$= \text{Tr}[D(g)U(r+1)CU^\dagger(r)D^\dagger(g)] = \text{Tr}[U(r+1)CU^\dagger(r)],\tag{22}$$

$$\tilde{\mathcal{Q}}_g^\dagger \text{Tr}[U(r+1)CU^\dagger(r)]\tilde{\mathcal{Q}}_g$$
$$= \text{Tr}[U(r+1)D(g)CD^\dagger(g)U^\dagger(r)] \neq \text{Tr}[U(r+1)CU^\dagger(r)].\tag{23}$$

From these equations, we see that, in general, H_J is invariant under left global transformation but it is not invariant under right transformations. This is true if C is not a multiple of the identity, since the matrices $D(g)$ are an irreducible representation of the group. The matrix C breaks the global right gauge symmetry, and this is a manifestation of the chiral nature of the model. We observe that, by exchanging the order of C and $U(r+1)$ in the Hamiltonian, we would get a corresponding model with right rather than left gauge symmetry.

2. About the C matrix

The C matrix is a unitary $\dim(F) \times \dim(F)$ matrix that generalizes the role of the phase $e^{i\theta}$ in the chiral Potts model (2) to the non-Abelian case. By expressing the matrix $C = e^{-i\gamma_j T_j}$ as a function of the generators T_j of $U(\dim(F))$, we see that C is a collection of $\dim(F)^2$ parameters. C must be chosen to fulfill the condition (21) and, *a priori*, it is not evident that such a matrix exists for all G. In the following, we provide a geometrical interpretation of C aimed at showing its existence for groups whose fundamental representation has dimension 2. These include, for example, the group S_3, which is the smallest non-Abelian group. In this case, any matrix $D(g)$ can be parametrized as a function of four parameters:

$$D(g) = e^{i\eta_{g,0}\sigma_0 + i\vec{\eta}_g\vec{\sigma}} = e^{i\eta_{g,0}}(\cos|\vec{\eta}_g|\sigma_0 + i\sin|\vec{\eta}_g|\hat{\eta}_g\vec{\sigma}),\tag{24}$$

where σ_0 is the 2×2 identity, $\vec{\sigma}$ is the vector of the Pauli matrices, and $\hat{\eta}_g$ is the three-dimensional unit vector in the direction of $\vec{\eta}_g$. A similar decomposition holds for $C = e^{-i\gamma_0\sigma_0 - i\vec{\gamma}\vec{\sigma}}$. We define four-component vectors in the unitary S^3 sphere:

$$\mathcal{D}(g) = \begin{pmatrix} \cos|\vec{\eta}_g| \\ \sin|\vec{\eta}_g|\hat{\eta}_g \end{pmatrix}, \quad \mathcal{C} = \begin{pmatrix} \cos|\vec{\gamma}| \\ \sin|\vec{\gamma}|\hat{\gamma} \end{pmatrix}.\tag{25}$$

Based on this parametrization, the mass of the g flux is

$$m_g = -4J\cos(\eta_{0,g} - \gamma_0)\mathcal{D}(g) \cdot \mathcal{C}.\tag{26}$$

Hence the condition (21), for any $g \neq h$, becomes

$$[\cos(\eta_{0,g} - \gamma_0)\mathcal{D}(g) - \cos(\eta_{0,h} - \gamma_0)\mathcal{D}(h)] \cdot \mathcal{C} \neq 0.\tag{27}$$

We fix a value of γ_0 such that $\cos(\eta_{0,g} - \gamma_0) \neq 0$ for every g and we define a set of rescaled vectors $\mathcal{D}'_g = \cos(\eta_{0,g} - \gamma_0)\mathcal{D}(g)$. In particular, if F is orthogonal (as in the $G = S_3$ case, or any dihedral group), $\eta_{0,g} = 0, \pi/2$, and we can choose $\gamma_0 = \pi/4$ such that all the cosines become $1/\sqrt{2}$. The equations (27) fix $|G|(|G| - 1)/2$ conditions that the vector $\mathcal{C}$ must fulfill: the unit vector $\mathcal{C}$ cannot be orthogonal to any of the vectors defined by the differences $\mathcal{D}'_g - \mathcal{D}'_h$ in (27). Each of these $|G|(|G| - 1)/2$ vectors define a great circle on the S^3 sphere of orthogonal vector. Therefore we conclude that we can choose any C matrix corresponding to a $\mathcal{C}$ vectors on the S^3 sphere that does not belong to any of these great circles. When $\mathcal{C}$ approaches one of these great circles, one of the mass gap closes, thus violating (21). A similar geometric interpretation can be build for any irreducible representation in $U(N)$ (see Appendix A).

3. The H_μ term

The H_μ term of the Hamiltonian is meant to provide a dynamics to the fluxes in the ladder, it does not commute with H_J and, differently from H_J is diagonalized in the irreducible representation basis of the rung degrees of freedom, based on Eq. (11).

We observe that, since $\theta_g = \theta_{g^{-1}}^\dagger$, H_μ is Hermitian. Furthermore, for $g = e$, the gauge transformation is just an identity and it provides only an overall energy shift. Therefore we can choose to include or not this term in the Hamiltonian.

H_μ is meant to generalize the h term in the Potts model (2): for A corresponding to the trivial irreducible representation, H_μ is the sum of all the possible gauge transformation operators over all the degrees of freedom and it directly generalizes (2). For a different representation A, the resulting Hamiltonian is instead related to a more general form of $\mathbb{Z}_N$ symmetric models studied in Ref. [5].

The H_μ term in the Hamiltonian (18) corresponds to a projector over the subspace of the states of the rung r corresponding to the irreducible representation A. We recall that the projector over a generic irreducible representation K is given by

$$\Pi^K = \frac{\dim(K)}{|G|} \sum_{g \in G} \chi^K(g^{-1}) \theta_g = \sum_{mn} |Kmn\rangle\langle Kmn|. \quad (28)$$

Such expression is invariant under both left and right gauge transformations, and H_μ is thus symmetric under both global transformations. Therefore the (left) set of transformation $\mathcal{Q}_g$ corresponds in general to the global symmetry group for the whole Hamiltonian H when $C \neq \mathbb{1}$.

The form of H_μ we have chosen in (18) is not the most general preserving such gauge symmetry. We could extend H_μ to

$$H_\mu' = -\mu \sum_{r, C_l} f_{C_l} \sum_{g \in C_l} \theta_g(r) = -\mu \sum_{r, A} f_A' \Pi^A(r), \quad (29)$$

where C_l runs over the conjugacy classes of G, and A runs over the irreducible representations. For the purpose of defining a model with topological order, it is sufficient to consider a single non-Abelian irreducible representation A as in (18).

4. The symmetries of the system

We have already emphasized that the Hamiltonian (18) is invariant under the action of the global left gauge transformation for arbitrary C, whereas the right transformations do not constitute a symmetry of the system. Analogously to the Potts case, the matrix C breaks also the time-reversal and space-inversion symmetries. The time reversal T transforms the connection and local gauge operators in the following way:

$$T^\dagger U(r) T = U^\dagger(r), \quad T^\dagger \theta_g(r) T = \theta_g(r). \quad (30)$$

Therefore H_μ is time-reversal invariant, whereas it is easy to verify that H_J is not for any $C \neq \mathbb{1}$, due to the representation F being irreducible. Space inversion P can be defined by

$$P^\dagger U(r) P = U(L - r), \quad P^\dagger \theta_g(r) P = \theta_g(L - r). \quad (31)$$

with L being the system size. H_μ is invariant also for the inversion transformation, whereas $P^\dagger H_J(C) P = H_J(C^\dagger)$; therefore H is symmetric under P only if C is Hermitian. For generic unitary C matrices, the system is invariant neither under P and T, nor under PT. Therefore we do not expect exact degeneracies in the spectrum besides the ones dictated by the global symmetries $\mathcal{Q}_g$.

Concerning the exact degeneracies of the system caused by the global gauge group G, each eigenstate of H must transform under G following one of its irreducible representations. Therefore, in general, the spectrum will present exact degeneracies given by the dimensions $\dim(K)$ of the group's irreducible representations.

D. The ordered phase

Let us consider first a system with $\mu = 0$. In this case, the gauge fluxes have no dynamics and we can associate each state to a collection of fluxes $\{\Phi\}$. In a ladder of length L, the spectrum of H_J is given by the energy levels:

$$E(\{\Phi\}) = \sum_{g \in G} n_g m_g, \quad (32)$$

where n_g counts how many times the flux g appears in the set $\{\Phi\}$ for a given state of the ladder, and $\sum_g n_g = L - 1$. This is analogous to the analysis of the $\mathbb{Z}_N$ symmetric case in [9].

When the identity flux is the flux with the lowest mass (condition $\mathcal{C}1$), H_J presents $|G|$ ground states corresponding to ferromagnetic states, i.e., without domain walls, in the group element basis. We label these ground states as

$$||g\rangle\rangle = \bigotimes_r |g\rangle_r. \quad (33)$$

To emphasize the transformation properties of the ground states under the global symmetries $\mathcal{Q}_g$ it is convenient to introduce also a representation basis, analogous to (10), for the ground states,

$$||Kmn\rangle\rangle = \sum_{g \in G} \sqrt{\frac{\dim K}{|G|}} D_{mn}^K(g) ||g\rangle\rangle \quad (34)$$

such that

$$\mathcal{Q}_h^\dagger ||Kmn\rangle\rangle = D_{mm'}^K(h) ||Km'n\rangle\rangle. \quad (35)$$

When we introduce a weak H_μ perturbation, the exact degeneracy of the ground states is split: the $|G|$ ground states are perturbed and separate into a set of families; if C is not a multiple of the identity, the right gauge symmetry is broken and there are $\dim K$ families for each irreducible representation K. Each of these families has dimension $\dim K$. On the other hand, for a trivial C matrix, the right gauge symmetry is restored and there is one family of ground states per irreducible representation, with dimension $(\dim K)^2$.

The states within each family maintain their exact degeneracy due to the global symmetry, but, for finite-size systems, small energy gaps are introduced between different ground-state families. Similarly to the $\mathbb{Z}_N$ systems, this splitting of the energies of the ground-state manifold is exponentially suppressed in the system size and it is roughly proportional to μ^L/J^{L-1}. This can be deduced by a perturbative approach:

in order for the H_μ perturbation to turn one ground state into another, it must be applied L times. In this way a flux can be introduced into the system and can propagate from one edge to the other similarly to the domain walls in the $\mathbb{Z}_N$ case [6]. Other terms that introduce multiple fluxes are suppressed by their higher energy. Quantitatively, we find that the ground-state splitting is given by the effective Hamiltonian:

$$
\begin{aligned}
&\langle\langle gh||H'||h\rangle\rangle \\
&= -\left[\frac{(\chi^A(g^{-1})\mu)^L}{(m_{h^{-1}gh} - m_e)^{L-1}} + \frac{(\chi^A(g^{-1})\mu)^L}{(m_{h^{-1}g^{-1}h} - m_e)^{L-1}}\right],
\end{aligned}
\tag{36}
$$

where the masses m_g are defined in Eq. (20) and are proportional to J.

The situation is more complicated for the excited states, in which processes of order lower than L can cause transitions between different flux configurations, thus opening gaps that potentially may depend on the specific states involved and break the $|G|$ quasidegeneracy of the spectrum.

In particular, this may happen between degenerate flux configurations, which are states with different flux multiplicities n_g and n'_g, but the same energy. In Ref. [9], it has been shown that, in the presence of these resonances among excited states of H_J, there may be perturbation processes of low order (namely with an order that does not scale with the system size), which may split these degeneracies in the $\mathbb{Z}_N$ symmetric model (2). Similar processes can imply that the energy splitting of the excited states is not exponentially suppressed with the system size in the non-Abelian model as well.

E. The S_3 flux ladder

To exemplify the flux ladder models in Eq. (18) and verify our analysis of the spectrum of the ordered phase, we consider the smallest non-Abelian group, namely the symmetric group S_3 of all the permutations of three elements (s_1, s_2, s_3). S_3 has six elements and can also be considered the group of transformations that leave an equilateral triangle invariant. It is generated by two elements, b and c, which satisfy the relations $b^2 = c^3 = e$, where e is the identity element, and $bc = c^2 b$.

Using the latter relation, one can write every element of S_3 in "normal form": $g = b^n c^m$. In particular, we choose b to permute the first two elements, $b : (s_1, s_2, s_3) \mapsto (s_2, s_1, s_3)$, and c to cyclically permute the three elements, $c : (s_1, s_2, s_3) \mapsto (s_3, s_1, s_2)$. We denote the representations of this group by I and write the representation matrices as D^I. There are three irreducible representations of S_3. The trivial representation, where each element is represented by the number 1, the parity representation, where elements $g = b^n c^m$ are represented by $(-1)^n$, and the two-dimensional (fundamental) irreducible representation, which is defined below. We denote these representations by $I = 1, -1, 2$, respectively. To construct the Hamiltonian, we use the fundamental representation $I = 2$ for the definition of the operators U. This representation is

a subgroup of $O(2)$ and we have

$$
D^{(2)}(b) = \begin{pmatrix} 1 & 0 \\ 0 & -1 \end{pmatrix}, \quad D^{(2)}(c) = \frac{1}{2}\begin{pmatrix} -1 & -\sqrt{3} \\ \sqrt{3} & -1 \end{pmatrix}. \tag{37}
$$

One can think of $D^{(2)}(c)$ as the rotation matrix for a $2\pi/3$ rotation about the z axis, and $D^{(2)}(b)$ as a two-dimensional mirror symmetry about the x axis.

The terms of the Hamiltonian H_J are diagonal in the group element basis. We decide to work in this basis and to use, for each rung, the following ordering of the group elements: $\{|e\rangle, |c\rangle, |c^2\rangle, |b\rangle, |bc\rangle, |bc^2\rangle\}$. The states may be conveniently expressed in the tensor product structure $|n\rangle \otimes |m\rangle \equiv |b^n c^m\rangle$, with $n = 0, 1$ and $m = 0, 1, 2$. From the point of view of the transformations of the equilateral triangle in itself, the states with $n = 0$ correspond to the orientation-preserving transformations (rotations), whereas $n = 1$ labels the transformation inverting the orientation of the vertices (inversions). In the basis $|n\rangle \otimes |m\rangle$, we may write the local gauge transformations as

$$
\theta_b = \begin{pmatrix} 0 & 1 \\ 1 & 0 \end{pmatrix} \otimes \mathbb{1}, \tag{38}
$$

$$
\theta_c = \begin{pmatrix} 1 & 0 \\ 0 & 0 \end{pmatrix} \otimes \begin{pmatrix} 0 & 0 & 1 \\ 1 & 0 & 0 \\ 0 & 1 & 0 \end{pmatrix} + \begin{pmatrix} 0 & 0 \\ 0 & 1 \end{pmatrix} \otimes \begin{pmatrix} 0 & 1 & 0 \\ 0 & 0 & 1 \\ 1 & 0 & 0 \end{pmatrix}. \tag{39}
$$

All other gauge transformations can be found by compositions of these.

To illustrate the energy features of the ground-state manifold, we consider the cases $C = \mathbb{1}$ and $C = C_0$, with

$$
C_0 \equiv \frac{e^{-i\pi/4}}{\sqrt{2}}\left(\mathbb{1} + \frac{i}{\sqrt{3}}\sigma_x + \frac{i}{\sqrt{3}}\sigma_y - \frac{i}{\sqrt{3}}\sigma_z\right). \tag{40}
$$

The choice $C = \mathbb{1}$ is the trivial case with fluxes in the same conjugacy class being degenerate, while $C = C_0$ is a choice that satisfies conditions $\mathcal{C}1$ and $\mathcal{C}2$, and presents the following mass spectrum in units of J, using the same ordering of the group elements as above: $\{-2, 0, 2, 2/\sqrt{3}, 1 - 1/\sqrt{3}, -1 - 1/\sqrt{3}\}$.

We calculated the ground-state energies via exact diagonalization as a function of the system size and μ, for $C = \mathbb{1}, C_0$ and the auxiliary representations $A = 1, 2$. Due to the global symmetries, for generic values of the matrix C and $\mu \ll J$, the six ground states present a degeneracy pattern 1,1,2,2 corresponding to the nondegenerate states $||K = 1, 11\rangle\rangle$, $||K = -1, 11\rangle\rangle$, $||K = 2, j1\rangle\rangle$, and $||K = 2, j2\rangle\rangle$ based on their behavior under the symmetry group expressed in Eq. (35). For $C = \mathbb{1}$, when the right gauge symmetry is restored, the four ground states with $K = 2$ become exactly degenerate.

We define the ground-state splitting ΔE as the difference between the energies of the highest and lowest state in the ground-state manifold. Based on the perturbative result in Eq. (36), the dominant contribution in this splitting must scale as $\Delta E \propto \mu(\gamma\mu/J)^{L-1}$ for a suitable numerical coefficient γ. The ground-state splitting ΔE as a function of L is shown in Fig. 3 for $\mu = 0.03J$. For all the analyzed cases, we numerically find the expected exponential suppression of
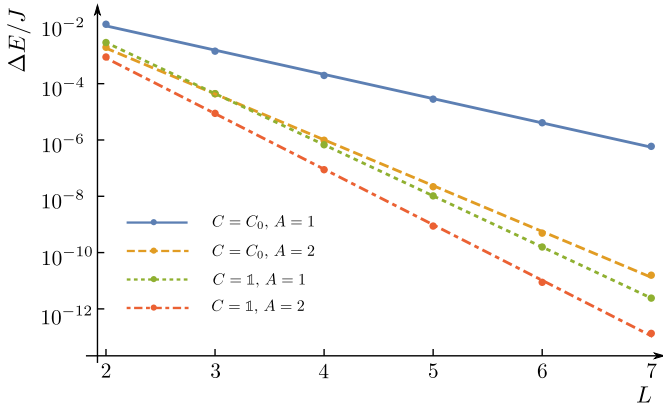
FIG. 3. Maximal splitting of the six ground states in units of J of the model with $G = S_3$ and $\mu/J = 0.03$, shown on a semilogarithmic plot. There are four different cases, depending on the matrix C [see Eq. (40) for the matrix C_0] and the irreducible representation A. In all cases, the exponential decay of the energy splitting with the system size is evident.

the ground-state splitting with the system size. In Fig. 4, we illustrate instead the ground-state splittings as a function of μ for $L = 7$. The power law behavior for small μ is clearly evident. For all the analyzed cases, the energy splitting approximately behaves like $\delta E \propto \mu^\alpha$ with the exponent α in the range between 7 and 9, compatible with the dominant contribution in Eq. (36). For larger values of μ and $C \neq \mathbb{1}$, our numerics suggest a change in the exponent, signaling a transition into a different phase.

The study of the full phase diagram as a function of the matrix C and the auxiliary irreducible representation A is an interesting and highly nontrivial problem, which goes beyond the scope of this paper. We observe, however, that for $\mu \to \infty$, H_μ projects each site on the subspace spanned by the states $|Amn\rangle$. For A Abelian, this implies the existence of a paramagnetic phase for $\mu \gg J$ with a nondegenerate ground state. For A non-Abelian, instead, H_μ presents a ground-state
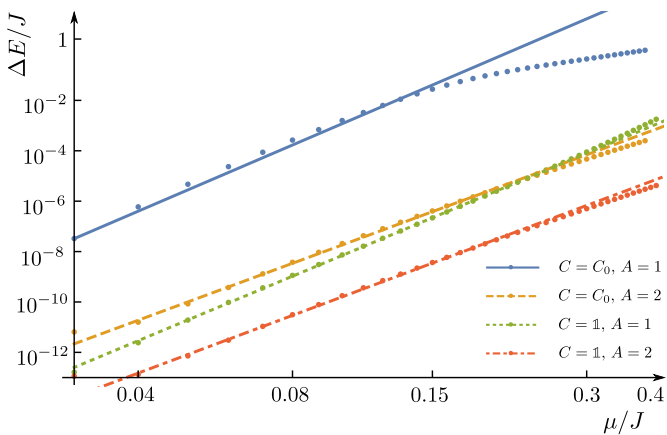

FIG. 4. The ground-state splitting in units of J, as a function of μ/J for seven sites, shown on a logarithmic plot, in the same cases as Fig. 3. The lines are linear fits based on the points with lowest μ, and the change of slope for larger values of μ is a possible signature of phase transitions.

degeneracy, which grows as $(\dim(A))^{2L}$; these ground states are then split by the introduction of a weak H_J. Between the regimes dominated by H_μ and H_J, other phases may be present. For example, in analogy with the $\mathbb{Z}_n$ case, we expect that, for suitable choices of C, critical incommensurate phases (see, for instance, Refs. [22–25]) and phase transitions with dynamical critical exponent $z \neq 1$ [25,26] may appear.

III. NON-ABELIAN MODELS WITH TOPOLOGICAL ORDER

A. The non-Abelian Jordan-Wigner transformation and the dyonic modes

A model with topological order can be defined by a nonlocal transformation which maps the flux-ladder operators into dyonic operators, characterized by a group element g and by the fundamental representation F. These dyonic operators display nontrivial commutation relations even when spatially separated, thus they are nonlocal in the original degrees of freedom of the ladder Hamiltonian. In this respect, they constitute a generalization of the parafermionic operators from $\mathbb{Z}_N$ to non-Abelian groups. In the $\mathbb{Z}_N$ model [5], the definition of the parafermionic operators is based on a $\mathbb{Z}_N$ JW transformation that amounts to the multiplication of order and disorder operators [11]. The definition of disorder operators, in turn, can be rigorously based on a bond-algebraic duality transformation [27]. Inspired by the bond-algebraic dualities for non-Abelian models [20], we introduce the following disorder operators for the non-Abelian flux-ladder, which is defined in terms of the dressed gauge operators (14):

$$\mathcal{L}^A_{g,\mathsf{a}_1\mathsf{a}_{r+1}}(r)$$
$$= \Theta^{A\dagger}_{g,\mathsf{a}_1\mathsf{a}_2}(1)\Theta^{A\dagger}_{g,\mathsf{a}_2\mathsf{a}_3}(2)\dots\Theta^{A\dagger}_{g,\mathsf{a}_r\mathsf{a}_{r+1}}(r)$$
$$= \left[\prod_{x=1}^r \theta^\dagger_g(x)\right] U^\dagger(1)D(g)U(1)U^\dagger(2)\dots U^\dagger(r)D(g)U(r),$$
(41)

where we omitted the representation superscript A in the second row. The string operator $\mathcal{L}$ introduces a flux g in the rth plaquette of the system and returns the matrix $D(h_1^{-1}gh_1h_2^{-1}gh_2\dots h_r^{-1}gh_r)$ in the auxiliary representation A when applied to any state $|h_1\rangle_1\dots|h_r\rangle_r$. These operators $\mathcal{L}_g$ fulfill the following properties for any A:

$$\mathcal{L}_{g,\mathsf{ab}}(r)\mathcal{L}^\dagger_{g,\mathsf{bc}}(r) = \mathcal{L}^\dagger_{g,\mathsf{ab}}(r)\mathcal{L}_{g,\mathsf{bc}}(r) = \delta_{\mathsf{ac}}\mathbb{1}, \quad (42)$$

$$\mathcal{Q}^\dagger_h\mathcal{L}_g(r)\mathcal{Q}_h = \mathcal{L}_{h^{-1}gh}(r), \quad (43)$$

$$\mathcal{L}_{g,\mathsf{a}_1\mathsf{a}_2}\mathcal{L}_{g,\mathsf{a}_2\mathsf{a}_3}\dots\mathcal{L}_{g,\mathsf{a}_{|G|}\mathsf{a}_{|G|+1}} \equiv \left(\mathcal{L}^{|G|}_g\right)_{\mathsf{a}_1\mathsf{a}_{|G|+1}} = \delta_{\mathsf{a}_1\mathsf{a}_{|G|+1}}\mathbb{1}.$$
(44)

The last equation is easily proved by considering that, in the third row of Eq. (41), the gauge operator string $[\prod_{x=1}^r \theta^\dagger_g(x)]$ commutes with the string of matrix operators.

We are now ready to define the dyonic operators through a generalized JW transformation obtained by the product of

order operators $U^\dagger$ and disorder operators $\mathcal{L}$. In full generality, we express the dyonic operators as

$$\alpha^{K,A}_{g,mn,\mathsf{ab}}(2r-1) = \mathcal{L}^A_{g,\mathsf{ab}}(r-1)U^{K\dagger}_{mn}(r), \qquad (45)$$

$$\beta^{K,A}_{g,mn,\mathsf{ab}}(2r) = \mathcal{L}^A_{g,\mathsf{ab}}(r)U^{K\dagger}_{mn}(r), \qquad (46)$$

for every $g \neq e$. These operators carry two pairs of matrix indices, (mn) and (ab), which are associated with the two irreducible representations K and A respectively. If we do not specify otherwise, we will consider $K = A = F$ and we will not specify the irreducible representation superscripts. However, it is necessary to keep the two representation distinguished: we adopt different fonts for their matrix indices and we will label by $\mathrm{Tr}_{K/A}$ the trace over the matrix indices of the two irreducible representations, respectively.

In analogy with the Kitaev and parafermionic chains, each site r of the flux ladder hosts two kinds of operators, U and θ, and it is decomposed in this dyonic description into a pair of sites, $2r-1$ and $2r$, each hosting the tensors of operators α and β, living in the odd and even sublattice respectively (see Fig. 2). In the Abelian case, however, all the irreducible representations are one-dimensional, and no tensor structure of this kind appear.

We call these modes *dyonic* because their transformation relations under the global gauge symmetries are similar to the ones of the irreducible representations of the Drienfield quantum double of G [10], as can be derived from Eqs. (7) and (43):

$$\mathcal{Q}^\dagger_h \alpha_{g,mn,\mathsf{ab}} \mathcal{Q}_h = \alpha_{h^{-1}gh,ml,\mathsf{ab}} D^\dagger_{ln}(h), \qquad (47)$$

$$\mathcal{Q}^\dagger_h \beta_{g,mn,\mathsf{ab}} \mathcal{Q}_h = \beta_{h^{-1}gh,ml,\mathsf{ab}} D^\dagger_{ln}(h), \qquad (48)$$

for any site r. These relations are obtained by considering that the disorder operators $\mathcal{L}$ are conjugated by the global symmetry, whereas the operators U transform following the fundamental irreducible representation F (or a different irreducible representation K in the most general case). We also observe that the first operator $\alpha(1) = U^\dagger(1)$ does not have a dependence on any group element, differently from all the other operators.

Similarly to parafermionic modes, the following relations hold:

$$\alpha_{g,lm,\mathsf{ab}} \alpha^\dagger_{g,mn,\mathsf{bc}} = \alpha^\dagger_{g,lm,\mathsf{ab}} \alpha_{g,mn,\mathsf{bc}} = \delta_{ln}\delta_{\mathsf{ac}}\mathbb{1}, \qquad (49)$$

$$\beta_{g,lm,\mathsf{ab}} \beta^\dagger_{g,mn,\mathsf{bc}} = \beta^\dagger_{g,lm,\mathsf{ab}} \beta_{g,mn,\mathsf{bc}} = \delta_{ln}\delta_{\mathsf{ac}}\mathbb{1}. \qquad (50)$$

The commutation relations between α and β operators can be obtained from the commutations between $\mathcal{L}(r)$ and $U^\dagger(r')$ and the non-Abelian JW transformations, but, for general auxiliary representations A, they do not assume a simple form. In the following, we report the results for the special case of Abelian auxiliary representations, which offers the possibility of comparing the dyonic modes to $\mathbb{Z}_N$ parafermionic modes. When A is Abelian, we can omit its trivial indices. Collectively denoting $\alpha(x)$ and $\beta(x)$ by $\gamma(x)$ for odd and even x

respectively, we get for $y > x$:

$$\gamma_{g,mn}(x)\gamma_{h,pq}(y) = \gamma_{h,pq}(y)\gamma_{hgh^{-1},ml}(x)D_{ln}(h), \qquad (51)$$

$$\gamma_{g,mn}(x)\gamma^\dagger_{h,pq}(y) = \gamma^\dagger_{h,pq}(y)\gamma_{h^{-1}gh,ml}(x)D^\dagger_{ln}(h), \qquad (52)$$

$$\gamma^\dagger_{g,mn}(x)\gamma_{h,pq}(y) = \gamma_{h,pq}(y)D^\dagger_{ml}(h)\gamma^\dagger_{hgh^{-1},ln}(x), \qquad (53)$$

$$\gamma^\dagger_{g,mn}(x)\gamma^\dagger_{h,pq}(y) = \gamma^\dagger_{h,pq}(y)D_{ml}(h)\gamma^\dagger_{h^{-1}gh,ln}(x), \qquad (54)$$

where only the l indices are summed over. The commutation relations for $y < x$ can be derived by conjugation. The relations for $x = y$ and $g \neq h$, instead, differ for α and β operators:

$$\alpha_{g,mn}(r)\alpha_{h,pq}(r) = \alpha_{h,pq}(r)\alpha_{hgh^{-1},mn}(r)$$
$$= \alpha_{g^{-1}hg,pq}(r)\alpha_{g,mn}(r), \qquad (55)$$

$$\beta_{g,mn}(r)\beta_{h,pq}(r) = \beta_{h,ps}(r)D^\dagger_{sq}(g)\beta_{hgh^{-1},ml}(r)D_{ln}(h)$$
$$= \beta_{g^{-1}hg,ps}(r)D^\dagger_{sq}(g)\beta_{g,ml}(r)D_{ln}(h). \qquad (56)$$

These commutation rules can be seen as a non-Abelian extension of the parafermionic commutation relations. For non-Abelian A representations, the algebra of the dyonic modes is more complicated. Furthermore, differently from their Abelian counterpart, the dyonic operators α and β present different algebraic properties. In particular, for any choice of A, we observe that

$$\alpha_{g,m_1m_2,\mathsf{a_1a_2}}\alpha_{g,m_2m_3,\mathsf{a_2a_3}}\cdots\alpha_{g,m_{|G|}m_{|G|+1},\mathsf{a_{|G|}a_{|G|+1}}}$$
$$= \left(\alpha^{|G|}_g\right)_{m_1m_{|G|+1},\mathsf{a_1a_{|G|+1}}} = \delta_{m_1m_{|G|+1}}\delta_{\mathsf{a_1a_{|G|+1}}}\mathbb{1}, \qquad (57)$$

$$\beta_{g,m_1m_2,\mathsf{a_1a_2}}\beta_{g,m_2m_3,\mathsf{a_2a_3}}\cdots\beta_{g,m_{|G|^2}m_{|G|^2+1},\mathsf{a_{|G|^2}a_{|G|^2+1}}}$$
$$= \left(\beta^{|G|^2}_g\right)_{m_1m_{|G|^2+1},\mathsf{a_1a_{|G|^2+1}}} = \delta_{m_1m_{|G|^2+1}}\delta_{\mathsf{a_1a_{|G|^2+1}}}\mathbb{1}. \qquad (58)$$

The tensor of operators $\beta^{|G|}$ is not proportional to the identity in general, due to the nontrivial commutation relations between $\mathcal{L}(r)$ and $U^\dagger(r)$.

The definitions of the α and β modes allow us to express the Hamiltonian H as a local Hamiltonian of the dyonic operators. In particular, the following relation hold for any $h \in G$:

$$\mathrm{Tr}_A[\alpha^\dagger_{h,mn,\mathsf{ab}}(2r+1)C_{no}\beta_{h,op,\mathsf{bc}}(2r)]$$
$$= U_{mn}(r+1)C_{no}U^\dagger_{op}(r)\dim(A). \qquad (59)$$

Here we are tracing only over the indices of the auxiliary representation A characterizing the disorder operators and the effect of this trace is indeed to cancel out the operators $\mathcal{L}$ based on Eq. (42). The product with the C matrix instead affects the indices of the K representation. The mapping from the dyonic to the θ operators instead is based on the following relation:

$$\beta^\dagger_{g,lm,\mathsf{ab}}(2r)\alpha_{g,mn,\mathsf{bc}}(2r-1)$$
$$= U^K_{lm}(r)\Theta^A_{g,\mathsf{ac}}(r)U^{K\dagger}_{mn}(r)$$
$$= U^{A\dagger}_{\mathsf{ab}}(r)\theta_g(r)U^A_{\mathsf{bc}}(r)D^K_{ln}(g)$$
$$= \theta_g(r)U^{A\dagger}_{\mathsf{ab'}}(r)D^{A\dagger}_{\mathsf{bb'}}(g)U^A_{\mathsf{b'c}}(r)D^K_{ln}(g), \qquad (60)$$

where we applied (7). By taking the trace over A, we get

$$\text{Tr}_A[\beta^\dagger_{g,lm}(2r)\alpha_{g,mn}(2r-1)] = \theta_g(r)\chi^A(g^{-1})D^K_{ln}(g). \tag{61}$$

Therefore, by taking $A = K = F$, we can re-express the Hamiltonian (18) as

$$H = -\frac{J}{\dim(F)}\left(\sum_r \text{Tr}_K \text{Tr}_A[\alpha^\dagger_h(2r+1)C\beta_h(2r)] + \text{H.c.}\right) \\ -\frac{\mu}{\dim(F)}\sum_r \sum_{g\neq e\in G} \text{Tr}_K \text{Tr}_A[\beta^\dagger_g(2r)\alpha_g(2r-1)D^{K\dagger}(g)], \tag{62}$$

where, in the first term, we can choose any $h \in G$ and, in the second, the dimension of F appears because we have chosen to adopt a trace to sum over the matrix indices of the representation $K = F$ in (61). Both H_J and H_μ are the sum of local commuting operators in terms of the dyonic modes α and β. See Fig. 2 for a graphical representation of the Hamiltonian.

We observe that Eq. (60) implies that the operator Θ_g is a local operator in the dyonic modes. The operators θ_g, instead, can be obtained as a linear function of $\beta^\dagger_g(2r)\alpha_g(2r-1)$ only if $\chi^A(g^{-1}) \neq 0$, as evident from Eq. (61). Therefore, for a generic choice of the group G and the auxiliary irreducible representation A, it is possible that some of the operators θ_g cannot be defined as local functions of the dyonic modes. We will discuss in detail the role of the auxiliary representation A in Sec. V.

B. Topological order

The nonlocal mapping [(45) and (46)] transforms the quasidegenerate ground states in the spontaneously symmetry-broken phase of the flux ladder Hamiltonian (18) into topologically protected ground states of the dyonic Hamiltonian (62). To clarify this point it is useful to introduce a formal definition of topological order for the dyonic system, which is able to generalize the notion of topological order of the Kitaev and parafermionic chains. We consider a gapped one-dimensional system defined on an open chain of length L, with a set of orthogonal quasidegenerate ground states $\{|\psi_q\rangle\}$ whose energy splitting decays superpolynomially in the system size. We define the system topologically ordered if it fulfills the following conditions.

$\mathcal{T}1$: For any bounded and local operator $V(r)$, and for any pair of ground states $|\psi_{q_1}\rangle, |\psi_{q_2}\rangle$:

$$\langle\psi_{q_1}|V(r)\psi_{q_2}\rangle = \bar{V}\delta_{q_1,q_2} + c(r,q_1,q_2), \tag{63}$$

where r specifies the position of the support of V, the constant $\bar{V}$ does not depend on the ground states, and $c(r,q_1,q_2)$ is a function, which decays superpolynomially with the distance of r from the boundary of the system (thus with the minimum between r and $L - r$).

This condition imposes that no local operator in the bulk of the system can cause transitions between the ground states, up to corrections c that are strongly suppressed with the distance with the boundary. A typical example may be given

by considering the Kitaev chain in the topological phase and the annihilation operator of a fermion in the system: if such operator is applied close to the boundary, with a considerable overlap with the zero-energy Majorana modes, then it can cause a transition between the two ground states; if instead it is applied in the bulk, with a negligible overlap with the exponentially localized zero-energy modes, then this transition is exponentially suppressed with the distance with the edges.

$\mathcal{T}2$: Any local observable cannot distinguish the ground states. To formalize this local indistinguishability requirement, we must carefully define what is the set of operators that constitute legitimate observables in the presence of a non-Abelian symmetry. In the case of fermionic systems, the observables are Hermitian operators that commute with the fermionic number; thus they have vanishing matrix elements between states with different fermionic parities. This property is maintained in the parafermionic $\mathbb{Z}_N$ generalization, where the set of observables is restricted to the set of operators commuting with the conserved $\mathbb{Z}_N$ charge and, in general, with the symmetry transformations [7]. In the case of a non-Abelian symmetry, the requirement of commuting with the whole symmetry group is very strong, because the group transformations themselves do not fulfill it. Therefore it is useful to weaken this requirement to the purpose of defining a broader set of observables. Instead of considering a set of operators which commute with the conserved charges, we demand that the observables do not allow for transitions between states transforming under different irreducible representations. For our purposes, the irreducible representations play indeed the role of the conserved charges. In particular, we define two distinct sets of operators we label with $\mathcal{C}$ and $\tilde{\mathcal{C}}$.

The set $\mathcal{C}$ includes the rank-2 tensor operators O_L that are block diagonal in the irreducible representation basis and transform under the group symmetry by conjugation, such that

$$\mathcal{Q}_h O_L \mathcal{Q}^\dagger_h = \bigoplus_I D^I(h)O^I_L D^{I\dagger}(h) \tag{64}$$

and

$$\tilde{\mathcal{Q}}_h O_L \tilde{\mathcal{Q}}^\dagger_h = O_L, \tag{65}$$

for a suitable decomposition $O_L = \sum_I O^I_L$ into components $O^I_L = \Pi^I O_L \Pi^I$, where I labels the irreducible representations and the projectors Π^I are defined in (28). As a particular case, we observe that the elements $\mathcal{Q}_g$ of the symmetry group belong to $\mathcal{C}$ since they fulfill the transformation relations (64) and (65).

The set $\tilde{\mathcal{C}}$ is the right counterpart of $\mathcal{C}$ and it includes the operators transforming as $\tilde{\mathcal{Q}}_g$. Namely, $\tilde{\mathcal{C}}$ is the set of the rank-2 tensor operators O_R transforming by conjugation as

$$\tilde{\mathcal{Q}}_h O_R \tilde{\mathcal{Q}}^\dagger_h = \bigoplus_I D^{I\dagger}(h)O^I_R D^I(h) \tag{66}$$

and

$$\mathcal{Q}_h O_R \mathcal{Q}^\dagger_h = O_R. \tag{67}$$

We observe that, for both sets, these operators reduce to the set of observables invariant under the symmetry group in the Abelian case. The non-Abelian structure of the symmetry group provides in this case an additional richness to the

system since it is not possible to define a single conserved charge in the G-invariant models.

Finally, we can define the following condition for the local indistinguishability of the ground states in systems with a non-Abelian symmetry group: for any local observable $O(r)$, belonging to either $\mathcal{C}$ or $\tilde{\mathcal{C}}$, and any pair of ground states, the following equation must be satisfied:

$$\langle \psi_{q_1} | O(r) \psi_{q_2} \rangle = \bar{O} \delta_{q_1, q_2} + o(L, q_1, q_2), \qquad (68)$$

where the parameter $\bar{O}$ does not depend on the ground states, and the function $o(L, q_1, q_2)$ decays superpolinomially in the system size L.

This condition properly generalizes the requirement of the local indistinguishability of the ground states under symmetric observables for the Abelian symmetric systems [7] to the non-Abelian case.

Both the conditions $\mathcal{T}1$ and $\mathcal{T}2$ are related to the notion of locality and, for the dyonic model, we will consider an operator local if it can be defined as a function of the α and β modes in a small (nonextensive) domain.

In the dyonic model, analogously to the flux ladder model with $J \gg \mu$, we can label the quasidegenerate ground states as $||Imn\rangle$ based on their transformations (35) under the global symmetry group. This is indeed a property that does not depend on the definition of locality and it is not affected by the nonlocal nature of the JW transformation. In this basis, the matrix $\langle \psi_{q_1} | \tilde{V} \psi_{q_2} \rangle$ in Eq. (63) is diagonal for any operator W which preserves the symmetry under G, such that $[W, \mathcal{Q}_g] = [W, \tilde{\mathcal{Q}}_g] = 0$ for any $g \in G$:

$$\langle\langle Imn || W || Rpq \rangle\rangle \propto W_I \delta_{RI} \delta_{mp} \delta_{nq}. \qquad (69)$$

This is analogous to the effect of operators preserving the fermionic parity in the Kitaev chain and operators preserving the $\mathbb{Z}_N$ symmetry in the parafermionic chains [7]. For the same reason, any observable O that is invariant under the action of the symmetry group, presents all the off-diagonal terms in (68) equal to zero if we choose the ground-state basis $\{||Imn\rangle\}$. For any observable O in the set $\mathcal{C}$ (or in its right counterpart $\tilde{\mathcal{C}}$), instead, the matrix $\langle\langle Imn || O || I'm'n' \rangle\rangle$ in Eq. (68) has vanishing entries for $I \neq I'$ but the elements of $\mathcal{C}$ and $\tilde{\mathcal{C}}$ enable transitions between m and m', and between n and n', respectively. We conclude that, under this point of view, the condition $\mathcal{T}2$ can be considered a stronger condition than its Abelian counterpart [7].

Both the conditions $\mathcal{T}1$ and $\mathcal{T}2$ are intimately related to the existence of a set of topologically protected zero-energy modes, localized on the boundaries (or, more accurately, on the interface between gapped topological and nontopological regions), which transform nontrivially under the symmetry group G. The transitions between ground states driven by all the local operators V must be understood in terms of the overlap with these zero-energy modes, and the local indistinguishability of the ground states is justified by the fact that these states differ only by the application of these boundary modes. In the next section, we will discuss the properties of these boundary modes and we will show that the dyonic model fulfills the previous criteria for topological order.

IV. THE TOPOLOGICAL ZERO-ENERGY MODES

A. Weak zero-energy modes

The condition $\mathcal{T}1$ for the system to be topologically ordered is the most immediately related to the existence of zero-energy modes localized on the boundary of the system. In general, it is necessary to distinguish two kinds of topologically protected zero modes and, consequently, two kinds of one-dimensional topological order [6,7]. A system enjoys weak topological order, and it possesses weak zero-energy modes, if the ground-state manifold is $|G|$-degenerate up to an energy splitting which is exponentially suppressed in the system size, whereas we speak of strong topological order when the whole energy spectrum is $|G|$-degenerate up to exponentially small corrections in the system size.

Therefore the weak topological order is a property only of the ground states. The excited states may present no specific regularity in their energy. In the $\mathbb{Z}_3$ parafermionic model in proximity of the nonchiral point in parameter space, for example, it is known that excited states labeled by different eigenvalues of the symmetries have relevant energy differences which decay only algebraically with the system size [6]. The strong topological order is instead a property of the whole spectrum.

The strong or weak kind of topological order are related to the presence of a strong or weak kind of localized zero-energy modes. Both these kind of modes must fulfill the following properties.

(1) To cause transitions between the quasidegenerate ground states, these modes must transform nontrivially under the global symmetries of the Hamiltonian. We denote these modes with Γ; in the simplest case, they can be associated to a (nontrivial) irreducible representation K of the symmetry group G in such a way that

$$\mathcal{Q}_h \Gamma^K \mathcal{Q}_h^\dagger = \Gamma^K D^K(h), \qquad (70)$$

or more general nontrivial transformation relations. In the $\mathbb{Z}_N$ Abelian case, this requirement reduces to the condition $\mathcal{Q}_1 \Gamma^K = e^{\frac{i 2\pi K}{N}} \Gamma^K \mathcal{Q}_1$, where K, for an Abelian group, can be interpreted simply as a power, $\mathcal{Q}_1$ is the $\mathbb{Z}_N$ charge of the system and $D^K = e^{\frac{i 2\pi K}{N}}$ [5].

(2) The zero-energy modes must be bounded operators, localized on the edge of the system (or at an interface between different gapped phases).

Besides these common requirements, weak and strong zero-energy modes must, respectively, satisfy the following conditions.

(1) Weak topological modes Γ_W must satisfy

$$[\Gamma_W, P_0 H P_0] \leqslant \gamma e^{-L/\xi}, \qquad (71)$$

where P_0 is the projector operator over the ground-state manifold, γ is a generic (bounded) operator acting on the ground-state manifold, L is the system size, and ξ is a suitable length scale. This requirement imposes that the weak zero modes quasicommute with the Hamiltonian projected on the ground-state manifold. Therefore, when we consider the subspace of the ground states, the projected Hamiltonian commutes with the symmetries $\mathcal{Q}$ and quasicommutes with the mode Γ_W, but Γ_W and $\mathcal{Q}$ do not commute with each-other due

to the condition (70). This implies the quasidegeneracy of the ground-state manifold.

(2) Strong topological modes Γ_S must satisfy the stronger requirement

$$[\Gamma_S, H] \leqslant \gamma e^{-L/\xi}. \tag{72}$$

This requirement, together with (70), implies the $|G|$-degeneracy of the whole spectrum up to exponentially suppressed corrections.

Let us discuss how the notion of topological order and weak zero-energy modes apply to the dyonic system. The topological order of the model can be easily verified for the Hamiltonian H_J: the Hamiltonian H_J is a sum of commuting terms and its $|G|$ ground states $||Imn\rangle\rangle$ are determined by imposing that

$$\mathrm{Tr}_A[\alpha_{h,m_2m_3}^{\dagger}(2r+1)\beta_{h,m_1m_2}(2r)]||Imn\rangle\rangle$$
$$= \delta_{m_1m_3}\dim(A)||Imn\rangle\rangle, \tag{73}$$

for every r and $h \neq e$. This implies that the bulk properties of all the ground states are the same. Like in the parafermionic case, the operators $\alpha(1)$ and $\beta_g(2L)$ do not appear in H_J and commute with it: this can be derived by the definitions in (45) and (46). Therefore $\alpha(1)$ and $\beta_g(2L)$ constitute localized zero-energy modes. Specifically for the case of H_J, they satisfy the requirements of strong topological modes, but, analogously to the $\mathbb{Z}_N$ case, their strong behavior is not stable against the addition of a small term H_μ in the Hamiltonian, and in general they must be considered weak zero modes.

Let us first analyze what happens for the unperturbed Hamiltonian H_J. The bulk operators by definition are independent of $\alpha(1)$ and $\beta_g(2L)$, and a generic bulk operator therefore is either composed only by terms independent of the operators Θ_g^A, like the ones in Eq. (73), or includes terms which are functions of some of the operators Θ_g^A. In the first case, the operator is proportional to the identity when projected on the ground-state manifold; in the second, instead, the operators Θ_g^A introduce domain walls in the corresponding flux-ladder model, thus completely driving any ground state into excited states. We conclude in both cases that bulk operators do not violate the condition $\mathcal{T}1$ for topological order.

The ground states cannot be distinguished by observables that do not involve either $\alpha(1)$ or the operators $\beta_g(2L)$. Taken singularly, $\alpha(1)$ and $\beta_g(2L)$ do not allow us to build nontrivial observables that belong to the set $\mathcal{C}$ [see Eqs. (64) and (65)] or to its right counterpart $\tilde{\mathcal{C}}$. Therefore operators, which are a function of $\alpha(1)$ or $\beta_g(2L)$ only, do not violate condition $\mathcal{T}2$.

Hence, the only possible way to build observables in $\mathcal{C}$ or $\tilde{\mathcal{C}}$ that distinguish the ground states is to multiply either $\alpha(1)$ or $\beta_g(2L)$ with suitable bulk dyonic modes. These additional modes, however, necessarily introduce domain walls in the model, as it can be seen from the action of their JW strings in Eqs. (45) and (46) on the ground states of H_J. Therefore, under the action of these operators, the ground states are fully transformed in excited states and the expectation values of the kind (68) vanish.

The only observables which can distinguish the ground states and belong to $\mathcal{C}$ are the ones build by products of the form $\alpha(1)\beta^{\dagger}(2L)$. In particular, for $\mu = 0$, it is convenient to define the operators

$$\Upsilon_g = \mathrm{Tr}_K\,\mathrm{Tr}_A[\alpha(1)\beta_g^{\dagger}(2L)] = \chi^A(g^L)\mathcal{Q}_g, \tag{74}$$

where the last equality can be derived from Eq. (41). Υ_g transforms as $\mathcal{Q}_h\Upsilon_g\mathcal{Q}_h^{\dagger} = \Upsilon_{hgh^{-1}}$ and it belongs to $\mathcal{C}$. From these operators it is possible to build observables that generalize the conserved $\mathbb{Z}_N$ charge in the Abelian systems and allow us to distinguish the ground states. All these observables, though, are crucially nonlocal. We conclude therefore that also the condition $\mathcal{T}2$ is fulfilled by H_J. Hence H_J fulfills the criteria to be topologically ordered.

We additionally remark that in the flux-ladder model the symmetry breaking order parameter is provided by the operators $U(r)$. Such operators are nonlocal in the dyonic model if and only if the auxiliary irreducible representation A is non-Abelian. In the following, we restrict to this condition, which is necessary to fulfill the criteria $\mathcal{T}1$ and $\mathcal{T}2$, thus to have topological order. We will discuss the nontopological system defined by A being the trivial representation in Sec. V.

The existence of weak zero-energy modes for the full Hamiltonian H for $\mu \ll J$ can be inferred by a quasiadiabatic continuation [28] by following the same procedure presented in [7] for the $\mathbb{Z}_N$ symmetric models. In particular, in the presence of a gap $\Delta(\mu)$ separating the ground-state manifold from the excited states, it is possible to define a quasiadiabatic continuation $\mathcal{V}(\mu)$, which is a unitary mapping preserving locality and symmetry under the group G that maps the ground states of H_J into the ground states of H: $||Imn\rangle\rangle_\mu = V(\mu)||Imn\rangle\rangle_{\mu=0}$. Therefore the continuation $\mathcal{V}(\mu)$ allows us to map the projector $P(0)$ over the ground states of H_J into the projector $P(\mu) = \mathcal{V}(\mu)P(0)\mathcal{V}^{\dagger}(\mu)$ over the ground-state manifold at finite μ. Through the continuation $\mathcal{V}(\mu)$ it is possible to define the new weak zero-energy modes $\mathcal{V}(\mu)\alpha(1)\mathcal{V}^{\dagger}(\mu)$ and $\mathcal{V}(\mu)\beta_g(2L)\mathcal{V}^{\dagger}(\mu)$ and verify that the conditions for topological order hold also for H as long as the energy gap $\Delta(\mu)$ does not close. The arguments presented in Ref. [7] extend straightforwardly to the non-Abelian case and show the persistence of topological order for the dyonic mode at finite μ.

By following the approach in Ref. [7], we obtain the following first-order expression in μ/J for the left weak zero-energy modes in the case $C = \mathbb{1}$:

$$\mathcal{V}(\mu)\alpha(1)\mathcal{V}^{\dagger}(\mu) = \alpha(1) + \mu\sum_{h\neq e}\frac{\mathrm{Tr}_{K,A}[\beta_h^{\dagger}(2)\alpha_h(1)D^{K\dagger}(h)]}{m_h - m_e}$$

$$\times \alpha(1)(\mathbb{1} - D^{K\dagger}(h)) + O\left(\frac{\mu^2}{J^2}\right), \tag{75}$$

and an analogous expression holds for the right edge modes (see Appendix B for more detail). These weak zero modes depend on the ratio of μ and the energy gaps $m_h - m_e$ between the ground states and the first excited states at $\mu = 0$. For $\mu \ll \min[m_h - m_e]$, this result suggests that the weak zero modes survive and maintain their localization when introducing the H_μ perturbation, in analogy with the Abelian models [7]. This is consistent with the perturbative result in Eq. (36).

We notice that the left weak zero-energy mode, originating from $\alpha(1)$, does not carry a group index, differently from the right modes, which originate from $\beta_g(2L)$. This apparent discrepancy is due to the open boundary conditions we are using in the analysis of our system. However, we can generalize our investigation by embedding the topological

phase in a larger nontopological system: in this case, also the weak left zero-energy modes would acquire a nontrivial JW string, thus acquiring a full dyonic character like the right modes. In Appendix C we present the first-order calculation of the left zero-energy mode at the interface between a non-topological and a topological region and we verify that the introduction of this different kind of boundary does not spoil the localization of the mode.

B. Strong zero-energy modes

So far, we considered only the existence of weak zero-energy modes. In the following, we will investigate under which conditions it is possible to define strong zero-energy modes. In particular, inspired by the approach in Ref. [5], we will present a constructive iterative technique for $\mu \ll J$ to build strong zero modes. Such approach will in general result in unbounded operators that, consequently, do not satisfy the criteria for the definition of topological modes. We will show however that by modifying the Hamiltonian (62) and introducing additional constraints, it is possible to find strong topological modes on the edges of the system.

Our goal is to derive zero modes of the form

$$\Gamma^{(r)} = \Gamma_0 + \Gamma_1 + \cdots + \Gamma_r \tag{76}$$

such that

(1) Γ_x has support on the first $2x + 1$ α and β dyonic modes starting from the edge. For the zero modes localized on the left edge, this implies that Γ_x is a function of $\alpha(1), \beta(2), \ldots \alpha(2x + 1)$. In the right case instead we search for a function of $\beta(2L), \alpha(2L - 1), \ldots \beta(2L - 2x)$.

(2) The mode $\Gamma^{(r)}$ must asymptotically fulfill

$$[\Gamma^{(r)}, H] < \mu \rho^r, \tag{77}$$

where $\rho < 1$ is a suitable parameter obtained in general as a function of μ, J, and C. In this way, the requirement (72) is satisfied for $r \to L$.

(3) The zero modes $\Gamma^{(r)}_{g,mn,\text{ab}}$ may be characterized by a group element g, and, analogously to α and β operators, they are tensors of operators defined by four matrix indices, which in general obey dyonic transformation rules with respect to the K irreducible representation:

$$\mathcal{Q}_h \Gamma^{(r)}_{g,mn,\text{ab}} \mathcal{Q}_h^\dagger = \Gamma^{(r)}_{hgh^{-1},mm',\text{ab}} D^K_{m'n}(h). \tag{78}$$

The indices ab of the auxiliary representation $\mathcal{A}$ are invariant under transformations of the symmetry group and, in the following, we will omit them.

The requirement (78), analogously to the condition (70), implies for $r \to L$ the quasidegeneracy of the whole energy spectrum. Furthermore, starting from the symmetry invariant ground state $||000\rangle\rangle$, we obtain

$$\Gamma^{(L)}_{g,mn} ||000\rangle\rangle \in \text{Span}\{||Kpq\rangle\rangle, \ p, q = 1, \ldots, \dim K\}. \tag{79}$$

This implies that the zero modes allow for transitions between ground states $||Rpq\rangle\rangle$ with different irreducible representations R. By applying the zero modes multiple times, the resulting ground states are defined by the Clebsch-Gordan series of the group G [29] and we will show that it is possible to span the whole ground-state manifold, thus extending the

behavior of zero-energy Majorana and parafermionic modes to the non-Abelian case.

In the following, we will use $\Lambda^{(r)}$ to label the strong zero-energy modes localized on the left boundary of the system, and $\Omega^{(r)}_g$ to label the ones on the right boundary. Analogously to their weak counterpart, only the strong right modes carry a group index. This is again due to the chosen boundary conditions (see Appendix C for more detail).

The first step of the iterative procedure is to impose the first term to be the zero-energy mode of H_J. Therefore we have $\Lambda_0 = \alpha(1)$ and $\Omega_{g,0} = \beta_g(2L)$ for the left and right boundaries, respectively. In this way, $[\Lambda_0, H_J] = [\Omega_{g,0}, H_J] = 0$.

Let us consider the right boundary as example. Following Ref. [5], we define the commutator

$$C_1(g) \equiv [\Omega_{g,0}, H] = [\Omega_{g,0}, H_\mu]. \tag{80}$$

C_1 is of order μ and it transforms under the symmetry group as $\Omega_{g,0} = \beta_g(2L)$, from which it inherits the dyonic character:

$$\begin{aligned} \mathcal{Q}_h C_1(g) \mathcal{Q}_h^\dagger &= [\mathcal{Q}_h \Omega_{g,0} \mathcal{Q}_h^\dagger, \mathcal{Q}_h H_\mu \mathcal{Q}_h^\dagger] \\ &= [\Omega_{0,hgh^{-1}} D(h), H_\mu] \\ &= C_1(hgh^{-1}) D(h). \end{aligned} \tag{81}$$

The next step is finding an operator $\Omega_{1,g}$ obeying the above conditions such that

$$[\Omega_{1,g}, H_J] = -C_1(g). \tag{82}$$

In this way, we get

$$[\Omega_{0,g} + \Omega_{1,g}, H] = C_1 - C_1 + [\Omega_{1,g}, H_\mu] \equiv C_2. \tag{83}$$

In general, $\Omega_{1,g}$ is of order μ/J and, due to the Hamiltonian being symmetric, it is always possible to define it in such a way that it obeys the same transformation rules of $\Omega_{0,g}$. In general, at each iteration step, we evaluate the commutator $C_r(g) = [\Omega^{(r-1)}_g, H]$ and we construct the corresponding operator $\Omega_{r,g}$ such that

$$[\Omega_{r,g}, H_J] = -C_r = -[\Omega_{r-1,g}, H_\mu]. \tag{84}$$

The resulting operators $\Omega_{r,g}$ are suppressed by a factor of order $(\mu/J)^r$.

This procedure guarantees the fulfillment of the constraints (77) and (78) and, as we will show in the following, of the localization constraint. In the following sections, we will express all the zero-energy modes in terms of the operators θ_g and U to exploit their commutation relations. It is important to stress, however, that the resulting modes Λ and Ω are localized based on the notion of locality obtained by the dyonic operators α and β.

C. Iterative procedure for strong modes on the left boundary

The starting point for the left strong zero mode is $\Lambda_0 = \alpha(1) = U^\dagger(1)$ and we have

$$\begin{aligned} C_1 &= [\Lambda_0, H_\mu] = \mu \sum_{h_1 \neq e} \chi^A(h_1^{-1}) [U^\dagger(1), \theta_{h_1}(1)] \\ &= -\mu \sum_{h_1 \neq e} \chi^A(h_1^{-1}) \theta_{h_1}(1) U^\dagger(1)(D^\dagger(h) - \mathbb{1}). \end{aligned} \tag{85}$$

We must identify an operator Λ_1 with support on $\alpha(1)$, $\beta(2)$, and $\alpha(3)$, such that its commutator with H_J cancels C_1. We observe that H_J commutes with any function of the operators U, therefore we may assume that Λ_1 inherits a factor $U^\dagger(1)(D^\dagger(h) - \mathbb{1})$ from C_1. Hence we adopt the following ansatz for Λ_1:

$$\Lambda_1 = \frac{\mu}{J} \sum_{h_1 \neq e} F_1(h_1) \chi^A(h_1^{-1}) \theta_{h_1}(1) U^\dagger(1)(D^\dagger(h_1) - \mathbb{1}), \tag{86}$$

where F_1 is a function only of the operators U(1) and U(2) and the matrices $D(h_1)$, in such a way that $[F_1, H_J] = 0$. The commutator $[\Lambda_1, H_J]$ gives

$$[\Lambda_1, H_J] = \mu \sum_{h_1 \neq e} F_1(h_1) \chi^A(h_1^{-1}) [\theta_{h_1}(1), \mathrm{Tr}[U(2)CU^\dagger(1)] + \mathrm{H.c.}] U^\dagger(1)(D^\dagger(h_1) - \mathbb{1})$$

$$= \mu \sum_{h_1 \neq e} F_1(h_1) \chi^A(h_1^{-1}) (\mathrm{Tr}[U(2)CU^\dagger(1)(D(h_1) - \mathbb{1})] + \mathrm{H.c.}) \theta_{h_1}(1) U^\dagger(1)(D^\dagger(h_1) - \mathbb{1}), \tag{87}$$

which is equal to the desired value $-C_1$ when we take

$$F_1(h_1) = (\mathrm{Tr}[U(2)CU^\dagger(1)(D(h_1) - \mathbb{1})] + \mathrm{H.c.})^{-1}. \tag{88}$$

In the group element basis, the operator F_1 always corresponds to the inverse of the difference of two different flux masses (20), since $h_1 \neq e$. Therefore in order to obtain a bounded operator Λ_1, it is necessary to choose a matrix C such that all the flux masses in the model are different [condition (21)]. Hence, similarly to the Abelian case [5], it is necessary to break the chiral symmetry in order to have strong zero-energy modes.

In the second iterative step, the commutator C_2 results

$$C_2 = -\mu \sum_{h_2 \neq e} \chi^A(h_2^{-1}) [\Lambda_1, \theta_{h_2}(1) + \theta_{h_2}(2)]. \tag{89}$$

It is convenient to split this commutator into two pieces, $C_2 = C_{\mathrm{in},2} + C_{\mathrm{out},2}$, representing the contributions given by the term in $\theta_{h_2}(1)$ and $\theta_{h_2}(2)$, respectively. These two terms of C_2 are defined on different supports: $C_{\mathrm{out},2}$ includes all the dyonic modes up to $\beta(4)$, whereas $C_{\mathrm{in},2}$ has support only up to $\alpha(3)$. Based on this difference, we can distinguish two contributions also for the operator $\Lambda_2 = \Lambda_{\mathrm{in},2} + \Lambda_{\mathrm{out},2}$, such that $[\Lambda_{\mathrm{in/out},2}, H_J] = -C_{\mathrm{in/out},2}$. The operator $\Lambda_{\mathrm{in},2}$ defines the inner part of Λ_2, with support up to $\alpha(3)$, thus with the

same support of Λ_1; $\Lambda_{\mathrm{out},2}$, instead, is the outer part and it includes all the terms of $\Lambda^{(2)}$ that extend its support to $\alpha(5)$.

This distinction between inner and outer contributions can be extended to all the iteration levels and, in general, we have

$$C_{\mathrm{out},n} = -\mu \sum_{h_n \neq e} \chi^A(h_n^{-1}) [\Lambda_{n-1}, \theta_{h_n}(n)], \tag{90}$$

$$C_{\mathrm{in},n} = -\mu \sum_{i < n} \sum_{h_i \neq e} \chi^A(h_i^{-1}) [\Lambda_{n-1}, \theta_{h_i}(i)]. \tag{91}$$

Correspondingly, we define $\Lambda_n = \Lambda_{\mathrm{in},n} + \Lambda_{\mathrm{out},n}$ such that

$$[\Lambda_{\mathrm{in/out},n}, H_J] = -C_{\mathrm{in/out},n}. \tag{92}$$

The operator $\Lambda_{\mathrm{out},n}$ includes all the *outer terms* with domain extending from $\alpha(1)$ to $\alpha(2n+1)$, whereas $\Lambda_{\mathrm{in},n}$ includes the *inner terms* with the same domain of Λ_{n-1}. At the nth level of iteration both $\Lambda_{\mathrm{out},n}$ and $\Lambda_{\mathrm{in},n}$ appear to be of order $(\mu/J)^n$, therefore only the outer modes define the spatial penetration of the zero-energy modes in the bulk.

Let us focus first on the calculation of the outer modes: in the second iteration step, $\Lambda_{\mathrm{out},2}$ is determined from the commutator $C_{\mathrm{out},2}$ in Eq. (90). The only part of Λ_1 that does not commute with $\theta_{h_2}(2)$ is F_1 [see Eq. (86)], and we denote $[F_1, \theta_{h_2}(2)] = \tilde{F}_1 \theta_{h_2}(2)$. Concretely,

$$\tilde{F}_1(h_1, h_2) = (\mathrm{Tr}[U(2)CU^\dagger(1)(D(h_1) - \mathbb{1}) + \mathrm{H.c.}])^{-1} - (\mathrm{Tr}[U(2)CU^\dagger(1)(D(h_1) - \mathbb{1})D^\dagger(h_2) + \mathrm{H.c.}])^{-1}, \tag{93}$$

which implies

$$C_{\mathrm{out},2} = -\frac{\mu^2}{J} \sum_{h_1, h_2 \neq e} \chi^A(h_1^{-1}) \chi^A(h_2^{-1}) \tilde{F}_1(h_1, h_2) \theta_{h_1}(1) \theta_{h_2}(2) U^\dagger(1)(D^\dagger(h_1) - \mathbb{1}). \tag{94}$$

Similarly to the first step, we assume that the outer mode $\Lambda_{\mathrm{out},2}$ takes the form

$$\Lambda_{\mathrm{out},2} = \left(\frac{\mu}{J}\right)^2 \sum_{h_1, h_2 \neq e} \chi^A(h_1^{-1}) \chi^A(h_2^{-1}) \tilde{F}_1(h_1, h_2) F_2(h_1, h_2, h_3) \theta_{h_1}(1) \theta_{h_2}(2) U^\dagger(1)(D^\dagger(h_1) - \mathbb{1}), \tag{95}$$

where we introduced a new function of the U operators $F_2(h_1, h_2, h_3)$. By taking

$$F_2 = \left(\mathrm{Tr}\left[U(2)CU^\dagger(1)\left(D(h_1 h_2^{-1}) - \mathbb{1}\right) + \mathrm{H.c.}\right] + \mathrm{Tr}[U(3)CU^\dagger(2)(D(h_2) - \mathbb{1}) + \mathrm{H.c.}]\right)^{-1}, \tag{96}$$

we ensure that $[\Lambda_{\mathrm{out},2}, H_J] = -C_{\mathrm{out},2}$.

From this expression we deduce that the condition (21) on C is not strong enough to guarantee the existence of the strong zero-energy modes. This condition only ensures that each term in (96) do not cancel individually, but they may still cross cancel. This happens when the action of h_1 and h_2 results in a swap of the gauge fluxes in the first two plaquettes of the ladder model. For instance, $F_2|g_1, g_2, g_3, \ldots\rangle$ is singular when $h_2 = g_2 g_1^{-1} g_2 g_3^{-1}$ and $h_1 h_2^{-1} = g_1 g_2^{-1} g_3 g_2^{-1}$. For a given group G, these two equations will be compatible with the requirement $h_1, h_2 \neq e$ for some state, thus causing a divergence of the operators F_2 and Λ_2. To avoid this problem, we can introduce a suitable position dependence in either the parameters J or C; we will discuss the problem of the possible divergences of the zero-energy modes in Sec. IV D, based on the final result for $\Lambda_{\text{out},n}$.

When calculating $C_{\text{out},3}$ by computing $[\Lambda_2, \theta_{h_3}(3)]$, only F_2 is modified by the action of $\theta_{h_3}(3)$, and we define a new function $\tilde{F}_2$ analogously to the previous term. In general, all the outer modes follow the same pattern and, at the nth iteration step, we can define

$$\Lambda_{\text{out},n} = \left(\frac{\mu}{J}\right)^n \sum_{h_1,\ldots,h_n \neq e} \chi^A\left(h_1^{-1}\right) \ldots \chi^A\left(h_n^{-1}\right) \tilde{F}_1$$
$$\ldots \tilde{F}_{n-1} F_n \theta_{h_1}(1) \ldots \theta_{h_n}(n) U^\dagger(1)(D^\dagger(h_1) - \mathbb{1}), \quad (97)$$

where

$$F_n(h_1, \ldots, h_n)$$
$$\equiv \left(\frac{1}{J}[H_J, \theta_{h_1}(1) \ldots \theta_{h_n}(n)]\theta_{h_1}^\dagger(1) \ldots \theta_{h_n}^\dagger(n)\right)^{-1}$$
$$= \left(\sum_{r=1}^n \text{Tr}[U(r+1)CU^\dagger(r)(D(h_r h_{r+1}^{-1}) - \mathbb{1}) + \text{H.c.}]\right)^{-1}, \quad (98)$$

with the constraint $h_{n+1} = e$. The function $\tilde{F}$ is defined in turn as

$$\tilde{F}_{n-1}(h_1, \ldots, h_n) = F_{n-1} - \theta_{h_n}(n)F_{n-1}\theta_{h_n}^\dagger(n). \quad (99)$$

From the following expression, it is easy to verify that the operator $\Lambda_{\text{out},n}$ is a function of the dyonic modes from $\alpha(1)$ to $\alpha(2n+1)$ based on the relations (59), (61), which map all the operators of the flux-ladder Hamiltonian into local combinations of the dyonic modes. A similar result is obtained for the inner modes (see Appendix D) which display similar terms with suitable modifications of the F and $\tilde{F}$ functions.

D. Divergences of the strong modes and space-dependent Hamiltonians

The previous expressions we derived for the strong zero-energy modes are ill-defined at all the iteration orders after the first. There are two kinds of divergences that affect the operators F_n and $\tilde{F}_n$ entering in the definition of $\Lambda_{\text{out},n}$. Let us analyze for simplicity the case of F_n defined in Eq. (98), since $\tilde{F}_n$ is given by the difference of two analogous operators, and the same conclusions hold for both. For ease of notation we adopt $J = 1$ and $\mu \ll 1$ in the following analysis.

Given a state of the flux ladder $|\psi\rangle = |h_1 \ldots h_n\rangle$, the denominator of F_n returns the difference of the H_J eigenenergies

of $|\psi\rangle$ and $|\psi'\rangle = \prod_{r=1}^{n-1} \theta_{h_r}^\dagger(r)|\psi\rangle$. This denominator can go to zero in two different cases: (i) ψ and ψ' are characterized by different sets of gauge fluxes $\{\Phi\}$ and $\{\Phi'\}$ but their energy is the same; (ii) ψ and ψ' are defined by two different permutations of the same gauge fluxes, thus $\{\Phi\} = \{\Phi'\}$.

The case (i) corresponds to resonances of the kind

$$\sum_g n_g m_g = \sum_g n'_g m_g. \quad (100)$$

with $\{n_g\} \neq \{n'_g\}$. This kind of resonance corresponds to the same divergences met in the Abelian $\mathbb{Z}_3$ model analyzed in Ref. [9] and, in general, it hinders the formation of strong modes for large system sizes, although their effects is usually relevant only at large energies. To avoid this kind of resonance, in principle, we could strengthen our requirement $\mathcal{C}2$ on the C matrix by imposing that the C matrix must be such that all the flux masses m_g are incommensurate with each other. In this case, the condition (100) can never be fulfilled, although the difference between the energies of the two fluxes configurations can be arbitrary small for sufficiently long systems. In particular, we can estimate that the energy splitting becomes smaller than a quantity ϵ at order $O(1/\epsilon f(|G|))$ of the iteration process, where f is a suitable function of the group order only. This kind of splitting implies that the norm of the strong mode contribution Λ_n behaves like $\sim nf(|G|)[(|G|-1)\mu/J]^n$, thus displaying an exponential decay for large n. Therefore we conclude that, under the previous incommensurability assumption for the flux masses, strong zero-energy modes are, in general, not critically affected by this kind of resonance.

The case (ii) is characteristic of the non-Abelian groups only. For the Abelian models, the requirements $h_1 \neq e$ and $h_{n+1} = e$ in Eq. (98) would imply that the sets of fluxes defining $|\psi\rangle$ and $|\psi'\rangle$ cannot be the same. This does not hold for non-Abelian groups because, by changing the order of the fluxes in the ladder, it is possible to modify the total flux $\Phi_{\text{tot}} = g_1^{-1} g_{n+1}$. Therefore there can be choices of $h_1, \ldots, h_n$ and of the state ψ such that ψ and ψ' share exactly the same fluxes, $\{\Phi\} = \{\Phi'\}$. We emphasize, however, that the resonances of kind (ii) require that ψ and ψ' present at least two nontrivial fluxes. If we assume that ψ and ψ' are both states with a single nontrivial flux of the kind $\Phi(g)$, a divergence would entail that $\Phi_{\text{tot}} = \Phi'_{\text{tot}} = \Phi(g)$, but this is impossible since Φ_{tot} and Φ'_{tot} differ by an overall multiplication of the nontrivial group element h_1. We conclude that, similarly to the ground states, also the single-flux states are protected against this kind of divergence.

For multiflux states, the resonances of the case (ii) are unavoidable in uniform systems. To obtain well-defined strong zero-energy modes is thus necessary to consider adding a position dependence to the Hamiltonian parameters. We decide, in particular, to focus on the case of a space-dependent J of the form $J_r = (1 + \eta_r)$ with $|\eta_r| \ll \min[|m_g - m_h|]$ for $g, h \in G$. To show that strong zero-energy modes can, indeed, exist in such a situation, we consider the fine-tuned case $\eta_r = \eta_0/2^r$. In this situation, the maximum value of F_n is

$$\max[F_n] = \frac{2^n}{2\Delta\eta_0}, \quad (101)$$

where we labeled the minimum of the absolute values of the differences between two flux masses with Δ. This value is reached when all the group elements h_k are the same for $k < n - 1$, such that the first $n - 2$ terms in Eq. (98) cancel, whereas h_{n-1} and h_n are chosen to exchange the last two fluxes. In a similar configuration, it is possible to check that all the denominators assumed by the operators $\tilde{F}_r$ with $r < n$ are out of resonance, thus bounded by $|\tilde{F}_r| < 2/\Delta$ without any dependence on the η coefficients. We conclude that

$$\sum_{h_1 \dots h_n \neq e} |\tilde{F}_1| \dots |\tilde{F}_{n-1}| |F_n| < \frac{1}{4\eta_0} \left(\frac{4}{\Delta} \right)^n. \tag{102}$$

Therefore, for $\mu/\Delta < (4(|G| - 1))^{-1}$, the strong zero-energy mode is exponentially suppressed in the bulk of the system.

This result is achieved through an exponential fine-tuning of the coupling constants, however, we expect that the zero-energy modes exist also for disordered setups, in which the parameters η_r become random variables with a suitable distribution. This corresponds to assigning a small random contribution to the flux masses which depends on the plaquettes of the model, thus avoiding the possibility of resonances of the second kind. The inner terms of the strong zero-energy modes do not introduce additional resonances and, therefore, do not qualitatively modify the general decay behavior of the modes we discussed (see Appendix D).

E. Iterative procedure for strong modes on the right boundary

The construction of the strong zero-energy mode Ω_g localized on the right boundary of the system is very similar to the left modes, except for the fact that it carries a JW string $\mathcal{L}_g^A$ and, consequently, a group index. The starting point is $\Omega_{g,0} = \beta_g(2L) = \mathcal{L}_g^A(L) U^{K\dagger}(L)$. It is important to notice

that the full JW string $\mathcal{L}_g^A(L)$ commutes with all terms in the Hamiltonian: it is easy to prove that $[\mathcal{L}_g^A(L), H_J] = 0$; concerning the commutator with H_μ, instead, it is useful to rewrite H_μ as a sum of projectors $\Pi^A(r)$ over the auxiliary representation [see Eq. (28)] and exploit the relation $[\Theta_g(r), \Pi^A(r)] = 0$. Therefore $\mathcal{L}_g^A(L)$ is a symmetry of the system, and the iterative definition of the right modes can proceed in the same way of the left modes. We define the commutators

$$C_1(g) = [\Omega_{g,0}, H_\mu]$$
$$= -\mu \mathcal{L}_g^A(L) U^\dagger(L) \sum_{h_1 \neq e} \chi^A(h_1^{-1}) \theta_{h_1}(L) (\mathbb{1} - D(h_1)), \tag{103}$$

and we build the first-order correction of the strong mode:

$$\Omega_{g,1} = -\frac{\mu}{J} \mathcal{L}_g^A(L) U^\dagger(L) \sum_{h_1 \neq e} \chi^A(h_1^{-1}) P_1 \theta_{h_1}(L) (\mathbb{1} - D(h_1)), \tag{104}$$

with

$$P_1 = (\mathrm{Tr}[U(L) C U^\dagger(L-1)(D^\dagger(h_1) - \mathbb{1})] + \mathrm{H.c.})^{-1}, \tag{105}$$

such that $[\Omega_{g,1}, H_J] = -C_1(g)$.

Also, in this case, it is convenient to distinguish inner and outer contributions of the operators, where the outer contributions are the ones defining the decay in the bulk of the system:

$$C_2(G) = [\Omega_{g,1}, H_\mu] = C_{\mathrm{in},2}(g) + C_{\mathrm{out},2}(g) \tag{106}$$

with

$$C_{\mathrm{out},2}(g) = -\mu \left[\Omega_{g,1}, \sum_{h_2} \chi^A(h_2) \theta_{h_2}(L-1) \right] = -\frac{\mu^2}{J} \mathcal{L}_g^A(L) U^\dagger(L) \sum_{h_1, h_2} \chi^A(h_1) \chi^A(h_2) \tilde{P}_1 \theta_{h_1}(L) \theta_{h_2}(L-1) (\mathbb{1} - D(h_1)), \tag{107}$$

where

$$\tilde{P}_1(h_1, h_2) = [P_1, \theta_{h_2}(L-1)] \theta_{h_2}^\dagger(L-1)$$
$$= (\mathrm{Tr}[U(L) C U^\dagger(L-1)(D^\dagger(h_1) - \mathbb{1})] + \mathrm{H.c.})^{-1} - (\mathrm{Tr}[U(L) C U^\dagger(L-1) D(h_2)(D^\dagger(h_1) - \mathbb{1})] + \mathrm{H.c.})^{-1}, \tag{108}$$

and the corresponding outermost term at second order is

$$\Omega_{g,\mathrm{out},2} = -\frac{\mu^2}{J^2} \mathcal{L}_g^A(L) U^\dagger(L) \sum_{h_1, h_2} \chi^A(h_1) \chi^A(h_2) \tilde{P}_1 P_2 \theta_{h_1}(L) \theta_{h_2}(L-1) (\mathbb{1} - D(h_1)). \tag{109}$$

The general construction of all the iterative terms in the right modes follows from the one for left modes with a suitable substitution of the functions F and $\tilde{F}$ with their right counterparts P and $\tilde{P}$:

$$\Omega_{g,\mathrm{out},n} = \left(\frac{\mu}{J} \right)^n \mathcal{L}_g^A(L) U^\dagger(L) \sum_{h_1, \dots, h_n \neq e} \chi^A(h_1^{-1}) \dots \chi^A(h_n^{-1}) \tilde{P}_1 \dots \tilde{P}_{n-1} P_n \theta_{h_1}(L) \dots \theta_{h_n}(L-n+1)(\mathbb{1} - D(h_1)), \tag{110}$$

where

$$P_n(h_1, \dots, h_n) \equiv J \left(H_J - \theta_{h_1}(L) \dots \theta_{h_n}(L-n+1) H_J \theta_{h_1}^\dagger(L) \dots \theta_{h_n}^\dagger(L-n+1) \right)^{-1} \tag{111}$$

and

$$\tilde{P}_n(h_1, \ldots, h_{n+1}) = P_n - \theta_{h_{n+1}}(L-n) P_n \theta_{h_{n+1}}^\dagger (L-n). \tag{112}$$

It is easy to observe that these operators are local in the dyonic modes: they all result proportional to $\beta_g(2L)$ and all the terms in the sum in Eq. (110) can be expressed as products of dyonic operators through Eqs. (59) and (61). The operators P and $\tilde{P}$ are subject to the same kind of divergences of their left counterparts and an analogous space dependence of the coupling constant J can be adopted to achieve the exponential suppression of the right modes in the bulk.

F. Properties of the dyonic zero-energy modes

The strong zero-energy dyonic modes are characterized in general by the irreducible representation K, which determines the transformation relation (78) through the matrices $D^K(h)$, and by the group index g, which appears in the right modes through the operator $\mathcal{L}_g^A$ in (110). A group index characterizes also the left modes at the interfaces with nontopological regions of the system (see Appendix C), however, for simplicity, we will restrict our analysis to the uniform case with open boundaries.

The commutation relation between left and right modes is given by

$$\Lambda_{m_1 m_2} \Omega_{g, m_3 m_4} = \Omega_{g, m_3 m_4} \Lambda_{m_1 m_2'} D_{m_2' m_2}^{K\dagger}(g), \tag{113}$$

up to corrections exponentially suppressed in the system size. Here and in the following we will explicitly write only the indices related to the representation K, since the auxiliary representation indices are left invariant under this commutation. The commutation relation (113) corresponds to the commutation relations between $\alpha(1)$ and $\beta_g(2L)$ and it generalizes the commutation relations of Majorana and parafermionic zero-energy modes to the non-Abelian case. It can be derived by observing that all the contributions of Λ and Ω are proportional to $\alpha(1)$ and $\beta_g(2L)$ respectively; thus, Eq. (113) results from the commutation between the factor $\alpha(1)$ and the JW string in the factor $\beta_g(2L)$. Other corrections may appear in the commutation relation due to the overlap of the zero modes for $\mu \neq 0$, but they are all of order $(\mu/J)^L$.

It is important to observe that the zero-energy modes $\Lambda_{m_1 m_2}$ and $\Omega_{g, m_1 m_2}$ do not exhaust all the possible localized zero modes of the model. Different localized zero-energy modes are generated by multiplying left or right modes with each other. This additional modes are associated, in general, with irreducible representations of the group G different from K, therefore, in the following, we will label left and right modes by $\Lambda_{m_1 m_2}(I)$ and $\Omega_{g, m_1 m_2}(I)$ with I belonging to the irreducible representations of G. The zero modes built in the previous section correspond to the case $I = K$.

The analogy with Majorana and parafermionic modes suggests that also the dyonic modes can be considered as extrinsic topological defects with projective non-Abelian anyonic statistics [30,31] and their algebra provides information about the corresponding fusion rules. Let us consider first the products obtained by multiplying different left modes:

$$\Lambda_{m_1 m_2}(K) \Lambda_{m_3 m_4}(K); \tag{114}$$

this is the product of two rank-2 operators which transforms following the irreducible representation K under global gauge symmetries:

$$\mathcal{Q}_h \Lambda_{m_1 m_2}(K) \Lambda_{m_3 m_4}(K) \mathcal{Q}_h^\dagger$$
$$= \Lambda_{m_1 m_2'}(K) \Lambda_{m_3 m_4'}(K) D_{m_2' m_2}^K(h) D_{m_4' m_4}^K(h). \tag{115}$$

To understand the nature of this operator, we exploit the Clebsch-Gordan series relation [29]:

$$D_{m_2' m_2}^{I_1}(h) D_{m_4' m_4}^{I_2}(h)$$
$$= \sum_{I, n, n'} \langle I_1 m_2' I_2 m_4' | In' \rangle \langle In | I_1 m_2 I_2 m_4 \rangle D_{n' n}^I(h). \tag{116}$$

Here, we introduced the notation $\langle I_1 m_2' I_2 m_4' | In' \rangle$ and $\langle In | I_1 m_2 I_2 m_4 \rangle$ for the Clebsch-Gordan coefficients of the group and their conjugate, respectively. By combining the previous two equations, we get

$$\mathcal{Q}_h \Lambda_{m_1 m_2}(K) \Lambda_{m_3 m_4}(K) \mathcal{Q}_h^\dagger$$
$$= \sum_{I, n, n', m_2', m_4'} \Lambda_{m_1 m_2'}(K) \Lambda_{m_3 m_4'}(K)$$
$$\times \langle K m_2' K m_4' | In' \rangle \langle In | K m_2 K m_4 \rangle D_{n' n}^I(h). \tag{117}$$

This demonstrates that the product of two zero-energy modes Λ is a linear superposition of operators transforming according to the irreducible representations I allowed by the Clebsch-Gordan series. Therefore, in general, we must define a family of zero-energy operators localized on the left edge, $\Lambda_{n_1 n_2}(I)$, such that

$$\Lambda_{m_1 m_2}(I_1) \Lambda_{m_3 m_4}(I_2)$$
$$= \sum_{I, n_1, n_2} \langle I_1 m_1 I_2 m_3 | In_1 \rangle \langle In_2 | I_1 m_2 I_2 m_4 \rangle \Lambda_{n_1 n_2}(I) \tag{118}$$

and

$$\mathcal{Q}_h \Lambda_{mn}(I) \mathcal{Q}_h^\dagger = \Lambda_{mn'}(I) D_{n' n}^I(h). \tag{119}$$

Based on this transformation relation, we obtain that, starting from the gauge-invariant ground state $||000\rangle$, the ground state $\Lambda_{mn}^\dagger(I)||000\rangle = ||Imn\rangle$ will transform as $\mathcal{Q}_h||Imn\rangle = D_{mm'}^{I\dagger}(h)||Im'n\rangle$.

From Eq. (119), it is also easy to show that $\Lambda^{|G|}(I)$ is invariant under the symmetries $\mathcal{Q}_h$. Therefore, for any irreducible representation I and any ground state $||Rmn\rangle$, we obtain $\Lambda^{|G|}(I)||Rmn\rangle \propto ||Rmn\rangle$. This suggests that the operators $\Lambda_{n_1 n_2}(I)$ behave like the dyonic operator $\alpha^{K=I}(1)$.

The situation is more complicated for the right modes: also in this case, we can consider modes associated with any irreducible representation I, but, with respect to the left modes, we must account also for the group element conjugation in (78) and the indices of the irreducible representation A:

$$\mathcal{Q}_h \Omega_{g, m_1 m_2, \mathsf{ab}}(I_1) \Omega_{k, m_3 m_4, \mathsf{cd}}(I_2) \mathcal{Q}_h^\dagger$$
$$= \sum_{I, n, n', m_2', m_4'} \Omega_{hgh^{-1}, m_1 m_2', \mathsf{ab}}(I_1) \Omega_{hkh^{-1}, m_3 m_4', \mathsf{cd}}(I_2)$$
$$\times \langle I_1 m_2' I_2 m_4' | In' \rangle \langle In | I_1 m_2 I_2 m_4 \rangle D_{n' n}^I(h). \tag{120}$$

From this relation, we deduce that $\Omega_g(I_1)\Omega_k(I_2)$ is indeed proportional to $\prod_r \theta_{kg}^\dagger(r)$ and can be decomposed into a linear superposition of dyonic operators associated to the irreducible representations I. For non-Abelian auxiliary representations, however, the set $\Omega_g(I)$ does not exhaust all the possible right zero-energy modes due to the nontrivial composition of the disorder operators $\mathcal{L}^A$. Moreover, given the previous composition rule for $g = k$, it is possible to show that the modes $\Omega_g(I)$ behave like the operators $\beta_g^{K=I}(2L)$, and, in particular $\Omega_g^{|G|^2}(I) \propto \mathbb{1}_I \mathbb{1}_A$ is a symmetric operator, similarly to Eq. (58).

The previous rules dictate how left modes fuse with left modes, and right modes with right modes. Concerning the fusion of a left with a right mode, it is convenient to introduce the operator

$$\Upsilon(g) \equiv \mathrm{Tr}_K[\Lambda(K)\Omega_g^\dagger(K)], \tag{121}$$

where the indices of the auxiliary representation do not play any fundamental role. These operators generalize (74) to the general case with $\mu \neq 0$. Their transformation under the symmetry group results in

$$\mathcal{Q}_h \Upsilon(g)\mathcal{Q}_h^\dagger = \mathcal{Q}_h \, \mathrm{Tr}_K[\Lambda(K)\Omega_g^\dagger(K)]\mathcal{Q}_h^\dagger$$
$$= \mathrm{Tr}_K[\Lambda(K)\Omega_{hgh^{-1}}^\dagger(K)] = \Upsilon(hgh^{-1}). \tag{122}$$

The operators $\Upsilon(g)$ extend the usual idea of $\mathbb{Z}_N$ parity from the Abelian to the non-Abelian case: in analogy with the gauge transformations $\mathcal{Q}_g$ themselves, they transform under conjugation and they belong to the class of operators $\mathcal{C}$ characterizing the condition $\mathcal{T}2$ for topological order. In particular, the operators Υ_g are block diagonal in the irreducible representation basis and can be decomposed in the following way:

$$\Upsilon(g) = \sum_{I,m,n} D_{mn}^{I*}(g)\tilde{\Upsilon}(I)_{m,n}, \tag{123}$$

with $\tilde{\Upsilon}(I)_{m,n} = \upsilon_I \sum_l |Iml\rangle\langle Inl|$ (where υ_I are suitable constants) and

$$\mathcal{Q}_h \tilde{\Upsilon}(I)\mathcal{Q}_h^\dagger = D^I(h^{-1})\tilde{\Upsilon}(I)D^I(h). \tag{124}$$

The decomposition (123) can be considered the fusion rule for left and right zero modes: $\Upsilon(g)$, which plays the role of their operator product, results in a set of *fusion channels* in one-to-one correspondence with the irreducible representations I of the group, which can be schematically represented as

$$\Lambda \times \Omega = \oplus_I \Xi_I. \tag{125}$$

Each channel Ξ_I has a quantum dimension given by $\dim(I)^2$, such that, in total, we can attribute the quantum dimension $\sqrt{|G|}$ to the zero-energy mode $\Lambda(K)$ and $\Omega(K)$. This is analogous to the case of Majorana and parafermionic zero modes.

We observe that the decomposition (123) holds true independently of our choice of the irreducible representation of the zero modes $\Lambda(I)$ and $\Omega(I)$: our definition of $\Upsilon(g)$ can indeed be extended to the operators $\Upsilon(I, g) \equiv \mathrm{Tr}_I[\Lambda(I)\Omega_g^\dagger(I)]$. These operators behave under gauge transformations in the

same way, and can be decomposed in terms of the same operators $\tilde{\Upsilon}(R)$.

It is possible to extend our analysis also to the case of a topological region embedded in a nontopological environment (see Appendix C). In this situation, the left modes acquire a group index too, and the operators $\Upsilon(g)$ must be defined by contracting Λ_g and $\Omega_g^\dagger$ taken with the same group index. In this way, the JW strings $\mathcal{L}_g^A$ cancel outside the topological region, and all the previous observations still hold.

This situation is analogous to the study of twist defects in symmetry-enriched phases with topological order [32–34]. Majorana and parafermionic modes behave like twist defects in the $\mathbb{Z}_2$ and $\mathbb{Z}_N$ toric codes, respectively [32,34]; this suggests that the dyonic modes in the system (62) may be interpreted as twist defects in a suitable two-dimensional topological system. The requirement of combining Λ_g and $\Omega_g^\dagger$ corresponds to having two twist defects with opposite flux which identify a g-defect branch line [32], and, in this scenario, the study of the topological and braiding properties of the dyonic zero-energy modes must be framed in a G-crossed braided tensor category theory [32].

V. THE ROLE OF THE AUXILIARY REPRESENTATION

The analysis of the topological models in Eq. (62) crucially relies on the choice of the group G and of the auxiliary irreducible representation A. The auxiliary representation A enters the definition of the disorder operators $\mathcal{L}^A$, which, in turn, define the dyonic modes (45) and (46). Because we define locality through the dyonic modes α and β, the selection of A directly determines which operators are local in the dyonic model.

The connection operators $\mathrm{U}(r)$ constitute order parameters able to distinguish the ground states of the flux-ladder Hamiltonian (18) in its ferromagnetic phase. Importantly, these operators are nonlocal in the dyonic modes if and only if the irreducible representation A is non-Abelian. This implies that, in case of an Abelian representation A, the topological order of the system (62) is lost.

The operators $\Theta_g(r)$, instead, are always local in terms of the dyonic modes [see Eq. (60)]. Furthermore, from Eq. (61), we obtain that also the operators $\theta_g(r)$ are local, provided that $\chi^A(g^{-1}) \neq 0$. For $\chi^A(g^{-1}) = 0$, instead, θ_g may be local or nonlocal depending on the group properties. This is related to certain additional symmetries which may appear in the flux-ladder Hamiltonian (18) for particular combinations of G and A, as for example, the choice $G = S_3$ with its non-Abelian irreducible representation $A = 2$.

In the following, we will first examine the features of the systems with a trivial auxiliary representation A, which exemplifies what happens for all the Abelian auxiliary representations, then we will consider in more detail the case of non-Abelian irreducible representations A with elements with vanishing character $\chi^A(g^{-1}) = 0$.

A. Trivial auxiliary representations: absence of topological order and appearance of holographic symmetries

In the case of an Abelian auxiliary representation A, the Hamiltonian (62) loses its topological order. This is due to the

properties of the Jordan-Wigner strings $\mathcal{L}^A$. For A Abelian and irreducible, the matrices D^A in (41) become just phases. The composition rules of the disorder operators then simplify, $\mathcal{L}^A_{g_1} \mathcal{L}^A_{g_2} = \mathcal{L}^A_{g_2 g_1}$, thus we obtain

$$U^\dagger(r) = \beta_{hg^{-1}}(2r) \beta^\dagger_h(2r) \beta_g(2r). \tag{126}$$

This relation is fulfilled because the Abelian JW strings in the β modes annihilate. Equation (126) proves that the operators $U^\dagger(r)$ are local in the dyonic operators, and, from these operators, it is possible to build local operators and observables that violate both the conditions $\mathcal{T}1$ and $\mathcal{T}2$ for topological order.

On the contrary, when A is non-Abelian, the only combinations of JW strings which allow for their annihilation are given by Eqs. (42) and (44) and it is impossible to find operators local in the dyonic modes that return $U^\dagger(r)$.

Let us focus on the trivial case $A = 1$ such that $\mathcal{L}^A_g(r) = \prod_{x=1}^r \theta^\dagger_g(x)$, without additional indices related to the auxiliary representation. In this case, we obtain the apparent inconsistency:

$$\beta_{kg^{-1}}(2r) \beta^\dagger_k(2r) = \prod_{j=1}^r \alpha_g(2j-1) \beta^\dagger_g(2j); \tag{127}$$

this relation is paradoxical because the left-hand-side is a local operator, expressed as a function of β's only, but it is equivalent to a nonlocal string operator when expressed in terms of both β's and α's. This contradiction is solved by taking into account that, for $A = 1$, the operators α and β are not independent from each other. In particular, it is possible to express any operator α as a function of the operators β:

$$\alpha(1) = \beta_{\tilde{k}\tilde{h}^{-1}}(2) \beta^\dagger_{\tilde{k}}(2) \beta_{\tilde{h}}(2), \tag{128}$$

$$\alpha_g(2r-1)$$
$$= \underbrace{\beta_k(2r-2) \beta^\dagger_{kg^{-1}}(2r-2)}_{\mathcal{L}_g(r-1)} \underbrace{\beta_{hg^{-1}}(2r) \beta^\dagger_h(2r) \beta_g(2r)}_{U^\dagger(r)}, \tag{129}$$

for $r > 1$ and any arbitrary choice of $\tilde{h}, \tilde{k}, h, k \neq e$ such that $\tilde{h} \neq \tilde{k}$ and $k, h \neq g$.

Equations (128) and (129) allow us to solve the apparent inconsistency of Eq. (127): for the sake of simplicity, we can take $k = h = \tilde{k}$ and $\tilde{h} = g$; in this case, it is easy to see that the right-hand side of Eq. (127) reduces telescopically to the left-hand side, thus verifying its local nature in terms of the β operators.

We conclude that, for the case $A = 1$, the notion of locality must be based on the β operators only: the α operators can be expressed as local combination of the β operators and all the Hamiltonian terms are local in turn. Based on this notion of locality, also the symmetry operators $\mathcal{Q}_g$ become localized:

$$\mathcal{Q}_g = \beta_{kg^{-1}}(2L) \beta^\dagger_k(2L), \tag{130}$$

for an arbitrary $k \neq g, e$. This relation establishes a mapping from the global (thus nonlocal) gauge symmetry in the flux-ladder Hamiltonian (18), to a set of symmetry operators localized on the last site of the system (62). This is an example of holographic symmetry [35].

As a result, all the operators of the form (130) are localized and exact zero-energy modes of the Hamiltonian (62), independently on the values of μ, J, or C. Therefore it is possible to identify the behavior of any eigenstate of the system under the symmetry group G just by considering expectation values of suitable observables localized on the last site, thanks to Eq. (130). This also implies that any local perturbation of the form $\mathcal{Q}_g$ can split the ground-state degeneracy of the system in the J-dominated phase. For example, by exploiting the projector (28), we can build the following symmetry-invariant operator, which separates in energy the gauge-invariant ground state $\| |000\rangle\rangle$ from the others:

$$\Pi^{(1)}_{\text{tot}} = -\sum_{g \in G} \mathcal{Q}_g. \tag{131}$$

This perturbation splits the ground-state degeneracy, despite preserving the group symmetry. We observe, however, that the holographic zero-energy modes can be used to build observables that determine only the global behavior under the symmetry transformation (as in the case of the total fermionic parity in the Kitaev chain); when considering a nonuniform system with alternating μ-dominated and J-dominated segments, the number of degenerate ground states scales with the number of interfaces and the holographic modes cannot distinguish all the ground states.

B. Non-Abelian auxiliary representations and additional symmetries

For a non-Abelian group G and a non-Abelian auxiliary representation A, in general, there will be a set of conjugacy classes such that the character χ^A vanishes for their elements. Let G_0 denote the set of group elements g with vanishing character $\chi^A(g^{-1})$:

$$G_0 = \{g \in G \quad \text{s. t.} \quad \chi^A(g^{-1}) = 0\}, \tag{132}$$

and by G_0^c its complement:

$$G_0^c = \{g \in G \quad \text{s. t.} \quad \chi^A(g^{-1}) \neq 0\}. \tag{133}$$

For all the elements $\tilde{g} \in G_0$, $\theta_{\tilde{g}}$ does not appear in the gauge-flux Hamiltonian (18). Furthermore, $\theta_{\tilde{g}}(r)$ cannot be expressed simply in terms of the trace over A of $\beta^\dagger_{\tilde{g}}(2r) \alpha_{\tilde{g}}(2r-1)$, because the right-hand side of Eq. (61) vanishes.

Depending on the choice of G and A, we must distinguish two cases: (i) G_0^c is not a proper subgroup of G and (ii) G_0^c is a proper subgroup of G.

An example of the kind (i) is the S_4 group, corresponding to the 24 orientation-preserving symmetries of the cube, associated with its fundamental representation $A = 3$ of dimension 3. When G_0^c is not a proper subgroup, the elements of G_0 can be generated by the products of elements of G_0^c. Therefore, in case (i), all the operators $\theta_g(r)$ can be expressed in a local form in terms of the dyonic modes: for $g \in G_0^c$, it is enough to apply Eq. (60); for $\tilde{g} \in G_0$, instead, we can express $\tilde{g} = g_1 \ldots g_l$ with all the g_i's belonging to G_0^c; in this way $\theta_{\tilde{g}}(r) = \theta_{g_1}(r) \ldots \theta_{g_l}(r)$ results from the product of the local terms θ_{g_i} and it is local in turn.

The case (ii) can be exemplified by the group S_3 with its fundamental representation $A = 2$ (and analogously by all the

groups D_n). In this case, the operators $\theta_{\tilde{g}}(r)$ with $\tilde{g} \in G_0$ cannot be obtained in this way because G_0^c is closed under composition. This implies that the operators $\theta_{\tilde{g}}(r)$ are not local operators as a function of the dyonic modes. Therefore, adding to the Hamiltonian small perturbations that include the operators $\theta_{\tilde{g}}(r)$ may in general destroy the topological order.

Furthermore, in case (ii), the system acquires additional local symmetries. To examine the appearance of these symmetries, it is useful to consider the flux-ladder Hamiltonian (18). The operators $\theta_{\tilde{g}}(r)$ (with $\tilde{g} \in G_0$) do not appear in the Hamiltonian and cannot be obtained as products of the other operators θ_g. Let us consider the unitary operator

$$V(r) = \exp\left[i \sum_{\tilde{g} \in G_0} \alpha(r) |\tilde{g}(r)\rangle\langle\tilde{g}(r)| \right]. \quad (134)$$

This is a U(1) local transformation that multiplies the wave function by a phase $e^{i\alpha(r)}$ if the rth rung is in a state belonging to G_0. It is easy to see that $V^\dagger(r)HV(r) = H$: $V(r)$ is diagonal in the group element basis, it trivially commutes with H_J and, in case (ii), there are no terms in the Hamiltonian mixing the states in G_0 and G_0^c due to G_0^c being closed under composition. Therefore there is an extensive set of conserved quantities $Q(r) = \sum_{\tilde{g} \in G_0} \alpha(r) |\tilde{g}(r)\rangle\langle\tilde{g}(r)|$, which split the Hilbert space in 2^L subspaces. In each of these subspaces, the Hamiltonian has a reduced global symmetry group G_0^c rather than the full symmetry group G.

In the case $G = S_3$ and $A = 2$, for example, the degrees of freedom $|m\rangle$ and $|n\rangle$ introduced in Sec. II E decouple: the conserved charges $Q(r)$ correspond to the $n = 0, 1$ degrees of freedom and the dynamics in each subspace is characterized by an Abelian $\mathbb{Z}_3$ symmetry generated by the global c transformations only. The global b transformations, instead, map a subspace into its complementary with charges $1 - Q(r)$.

In this case (in a system with open boundary conditions), the left zero-energy modes Λ and their weak counterpart do not include any of the operators $\theta_{\tilde{h}}(r)$ with $\tilde{h} \in G_0$ and act only within a single subspace. Their role becomes analogous to the $\mathbb{Z}_3$ parafermionic zero modes. The right zero modes $\Omega_{\tilde{g}}$ and their weak counterparts, instead, map a subspace into its complementary through the JW string in Eq. (110). In case (ii), therefore, it is possible to decompose the dyonic modes into the product of $\mathbb{Z}_3$ parafermionic zero modes with $\mathbb{Z}_2$ operators. An analogous situation is verified for any group D_n with $A = 2$. We conclude, therefore, that the groups D_n are unsuitable to study the genuine non-Abelian nature of the zero-energy dyonic modes. The groups with non-Abelian irreducible auxiliary representations of the kind (i), instead, offer the suitable playground to study the topological ordered phases of the dyonic models in their full extent.

VI. ANALYSIS OF THE SINGLE-FLUX SUBSPACE FOR THE GROUP S_3

In this section, we numerically investigate some of the features of the system for the specific case of the S_3 flux ladder introduced in Sec. II E: we discuss the roles of the matrix C and the auxiliary irreducible representation A in the spectrum

of the lowest excited states and in the definition of the strong zero-energy modes.

We follow the approach presented in Ref. [6] for Abelian symmetries, and we restrict our analysis to the subspace of the states with a single-flux excitation in the ladder. This is a strong limitation in the study of the overall system, but, despite that, it is useful to verify some of the analytical results of the previous sections and to investigate the onset of resonances in the first step of the iterative definition of the strong zero-energy modes in Eqs. (86) and (88).

For small values of μ/J, the energy spectrum of the single-flux excitations presents $|G| - 1$ energy bands, each associated with one of the nontrivial fluxes $g \in G$ of the model. Each energy band includes $(L - 1) \times 6$ states, corresponding to the choice of the plaquette r of the flux g and the background group element h, namely the state of the last rung of the ladder. We can represent a basis of the single-flux states based on the domain-wall picture:

$$|g, h, r\rangle = |hg\rangle_1 \ldots |hg\rangle_r |h\rangle_{r+1} \ldots |h\rangle_L, \quad (135)$$

with $g \neq e$.

The flux-ladder Hamiltonian, projected into the single-flux subspace, includes three contributions related to the masses of the fluxes (20), their kinetic energy, and the boundary terms of the system. We label these contributions by M, K, and B, respectively, such that

$$H_{\text{sf}} = M + K + B, \quad (136)$$

with

$$\langle g_1, h_1, r_1 | M | g_2, h_2, r_2 \rangle = \delta_{g_1, g_2} \delta_{h_1, h_2} \delta_{r_1, r_2} m_{g_2^{-1}}, \quad (137)$$

$$\langle g_1, h_1, r_1 | K | g_2, h_2, r_2 \rangle = \delta_{g_1, g_2} \delta_{h_1, h_2} \delta_{r_1 \pm 1, r_2} \big[-\mu \chi^A \big(g_2^{\pm 1} \big) \big], \quad (138)$$

$$\langle g_1, h_1, 1 | B | g_2, h_2, 1 \rangle = \delta_{h_1, h_2} \big(1 - \delta_{g_1, g_2} \big) \big[-\mu \chi^A \big(g_2 g_1^{-1} \big) \big], \quad (139)$$

$$\langle g_1, h_1, L - 1 | B | g_2, h_2, L - 1 \rangle = \delta_{h_1 g_1, h_2 g_2} \big(1 - \delta_{g_1, g_2} \big) \big[-\mu \chi^A \big(g_1 g_2^{-1} \big) \big]. \quad (140)$$

The resulting spectrum is characterized by three different energy scales. The largest energy scale is determined by the differences of the masses m_g in Eq. (20), which establish the gaps among the energy bands in the limit $\mu \to 0$. The second energy scale is related to the kinetic energy of the fluxes and is approximately proportional to μ/L; it defines the typical energy gaps appearing within each band in finite size system as effect of the dispersion of the fluxes. Finally, the smallest energy scale is given by the splitting of the quasidegenerate states corresponding to the same fluxes but different backgrounds and it is determined by the effect of the boundary terms.

The scaling of the smallest energy splitting is related to the onset of resonances that hinder the formation of the strong zero-energy modes. In a system with well-defined strong zero-energy modes, all the states must be $|G|$-fold degenerate up to exponentially suppressed corrections in the system size. If the splitting among quasidegenerate states decays in a slower way

with L, therefore, no strong zero-energy modes can be present in the system.

Analogously to the Abelian case [6], we expect in general a large splitting of the $|G|$-plets of quasidegenerate states in regions of the spectrum in which at least two different bands overlap. The most common scenario is that the related splitting may decay algebraically in the system size, as in the case of the nonchiral $\mathbb{Z}_3$ model [6]. This is due to the effect of the boundary terms: the term (140) allows for transitions between states with different fluxes and different backgrounds, whereas the term (139) allows for transitions between states with different fluxes and the same background. The combined action of the both of them, therefore, couples states with the same flux and different backgrounds, thus splitting the $|G|$-plets. This effect, though, is exponentially suppressed in the system size if there is an energy gap between the bands of different fluxes (as it can be derived through perturbation theory) and it becomes relevant only when two energy bands overlap. Stronger modifications of the spectrum may also occur in the presence of more overlapping band.

In the following, we analyze the case $G = S_3$ and we verify that, indeed, in the presence of overlapping bands, the splitting of the 6-plets of quasidegenerate single-flux states does not decay exponentially with the system size. On the contrary, for well-separated bands, such splitting decays exponentially. We observe that the exponential decay of the single-flux splitting is certainly not sufficient to assess the presence of strong zero-energy modes: It is only related to the absence of resonances between states with a single flux. This implies, for example, that the first order of the iterative procedure (86) is well-defined, but it does not provide information about the presence of resonances at higher orders. We analyze the spectrum of the single-flux Hamiltonian (136) for different two different choices of matrix C and the auxiliary representation A.

A. Case $A = 1$

We begin by analyzing the single-flux Hamiltonian in the case of trivial auxiliary representation $A = 1$. This case is nontopological, as discussed in Sec. V A, but it provides an example of the general behavior of the single-flux energy bands.

For $C = \mathbb{1}$, the S_3 model displays only two single-flux energy bands due to the degeneracy of the masses of the fluxes corresponding to the rotation (c and c^2) and inversion (b, bc and bc^2) elements of the groups. The doubly degenerate rotations have mass $m_c = 2J$, whereas the threefold degenerate inversions have mass $m_b = 0$ [see the definition (20) and the matrices (37)]. Both the bands acquire a bandwidth proportional to μ due to the kinetic energy K.

The spectrum for $C = \mathbb{1}$ is represented in Fig. 5(a). The lowest (inversion) band includes $18(L - 1)$ states corresponding to the six different backgrounds h in (135) and the three degenerate fluxes at mass 0. Some of these states are localized at the edges of the system and they include, for instance, the separate branch at the bottom of the band with a 12-fold degeneracy. The remaining states, instead, can be distinguished into families of 18 states with a degeneracy pattern 8-8-2, except for the 24 state closest to the upper edge of the band, which are instead organized in the degeneracy pattern 8-8-8.
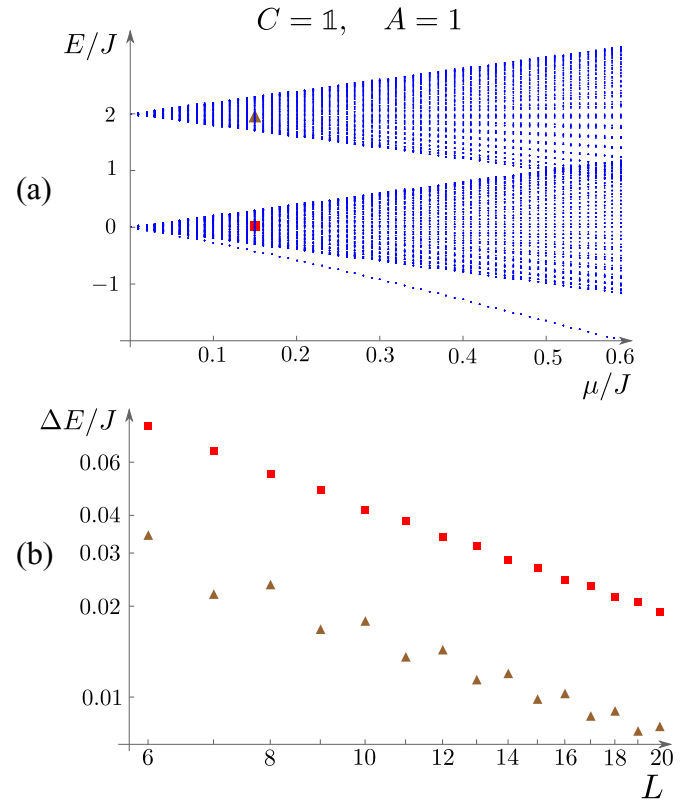

FIG. 5. (a): Spectrum of the single-flux Hamiltonian for $C = \mathbb{1}$ and $A = 1$ for 19 sites. The bottom band consists of the group elements containing inversions, and the top band consists of the rotation fluxes. The branch separating from the lower band consists of 12 exactly degenerate states. (b): Energy splittings in the middle of the two bands for varying system sizes, shown on a logarithmic plot. The red squares indicate splittings between the last set of eight and two degenerate states in the 18-plet in the middle of the lower band, and the brown triangles indicates splittings between the last four and two degenerate states in the 12-plet in the middle of the upper band. In both cases, the energy splitting decays roughly as $1/L$. The splitting between other sets of adjacent degenerate states behave similarly throughout the band.

For $C = \mathbb{1}$, indeed, the first-order resonances in (86) hinder the formation of strong modes, and the states in the lowest band are not arranged in the typical 6-plets. Our numerical analysis shows that both the splitting of the energies within and between the 18-plets of states decay algebraically and approximately as $1/L$ in the system size [see Fig. 5(b)].

The upper band is constituted by the two degenerate rotation fluxes. In this case, the spectrum displays families of 12 states with a typical degeneracy pattern 2-4-4-2, and again all energy differences inside and between these 12-plet families decay algebraically [see Fig. 5(b)].

To split the degeneracies of these the single-flux energy bands for small values of μ/J we introduce a C matrix that fulfills conditions $C1$ and $C2$. In particular, we choose

$$C_1 \equiv \frac{e^{-i\pi/4}}{\sqrt{2}}\left(\mathbb{1} - \frac{i}{\sqrt{3}}\sigma_x + \frac{i}{\sqrt{3}}\sigma_y + \frac{i}{\sqrt{3}}\sigma_z\right). \quad (141)$$

The corresponding masses (in ascending order) are $\{-2, -2/\sqrt{3}, -1 + 1/\sqrt{3}, 0, 1 + 1/\sqrt{3}, 2\}$, and we have
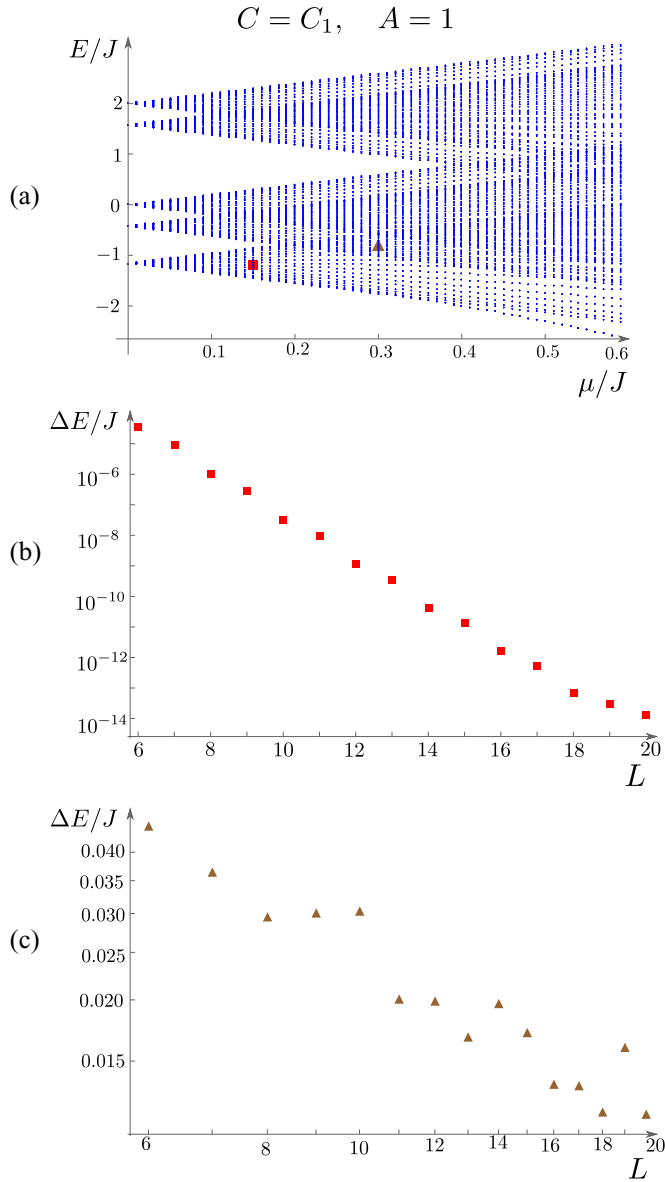
FIG. 6. (a) Spectrum of the single-flux Hamiltonian for $C = C_1$ and $A = 1$ as a function of μ/J for 19 sites. The bands are nondegenerate by construction of C_1. (b) Energy splitting ΔE in units of J as a function of system size L, shown on a semilogarithmic scale; its exponential decay is evident. The splitting is taken between the six quasidegenerate states in the middle of the bottom band at $\mu = 0.15$ [red square in (a)]. (c) Splitting as a function of system size L shown on a logarithmic plot and taken within a region of overlap between the bottom and next-lowest band at $\mu = 0.3$ [brown triangle in (a)]. The splitting decays approximately algebraically, and we conclude that the zero-energy modes are weak.

chosen this matrix in such a way that the gap between the trivial and the first excited fluxes is larger than the gap between the first and second excited fluxes. In this way the predictions of the single-flux Hamiltonian are more accurate for what concerns the lowest band since the transitions with the ground-state manifold and the two-flux states are less relevant than the boundary-term mixing between the first two bands.

The five resulting single-flux bands are well separated for small μ [see Fig. 6(a)] and all the states are now organized into
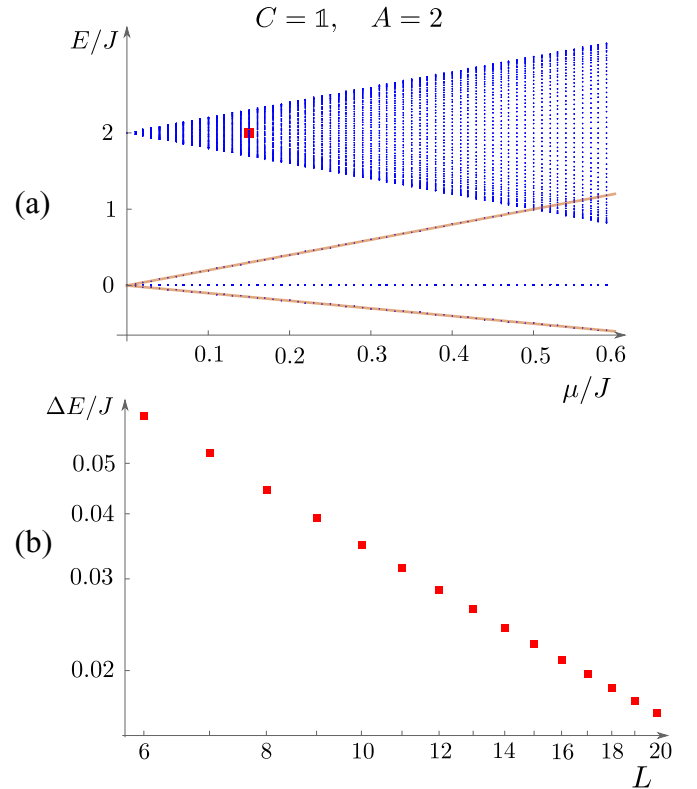

FIG. 7. (a) Spectrum of the single-flux Hamiltonian for $C = \mathbb{1}$ and $A = 2$ for 19 sites. At $\mu = 0$, the states associated with the inversions have zero energy (lowest band). These fluxes have no dynamics in the bulk. At the boundary, however, they mix and the boundary states acquire a finite energy when μ is increased. The energies of these edge states are given by the eigenvalues of the boundary terms (139) and (140): six states acquire the energy $E = 2\mu$ and 12 states the energy $-\mu$. These values are indicated by the straight orange lines. (b) Energy splitting ΔE in units of J shown on a logarithmic plot. The splitting is taken between two sets of fourfold degenerate states in the middle of the top band at $\mu = 0.15$ (red square in the top panel). The splitting is algebraically suppressed in the system size. We conclude that the zero-energy modes are weak.

6-plets separated by gaps scaling as μ/L due to the kinetic energy. For small μ, in the regions where the bands do not overlap, we observe an exponential decay of the splitting of the 6-plets with the system size [see Fig. 6(b)]. The C_1 matrix removes the resonance at the first level of iteration in the definition of the strong-zero energy modes and, consequently, the single-flux spectrum behaves as in the presence of strong modes (whereas states with more than one flux are subject to higher-order resonances). When we consider larger values of μ and we study the spectrum of the states in a region with two overlapping bands, however, a weaker decay reappears [see Fig. 6(c), which approximately shows an algebraic decay] and the division into 6-plets is no longer precise.

B. Case $A = 2$

True topological order is expected to arise when A is non-Abelian, and therefore we consider the case $A = 2$ (the case $A = -1$ is analogous to $A = 1$). For the group S_3, though, the choice $A = 2$ implies that no operator θ_{g_b} corresponding
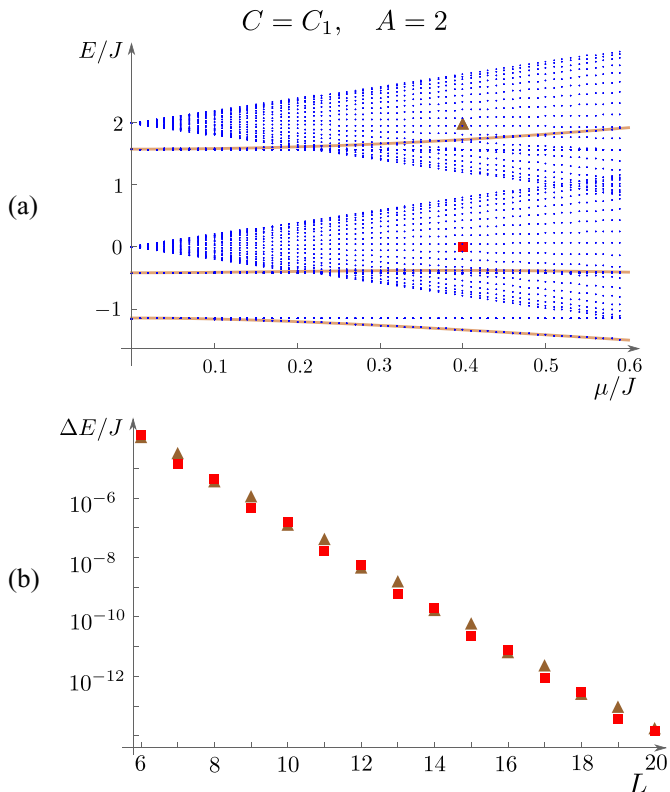
FIG. 8. (a) Spectrum of the single-flux Hamiltonian for $C = C_1$ and $A = 2$ for 19 sites in units of J. The flat bands correspond to the inversions, and the branches separating from these bands correspond to boundary states. In analogy to the situation in Fig. 7, these boundary states have energies derived from (139) and (140) (orange curves), which are not linear in μ in this case. (b): Energy splitting ΔE of two 6-plets in the middle of the two rotation bands at $\mu = 0.4$ (red square and brown triangle in the top panel) shown on a logarithmic plot. ΔE is exponentially suppressed in the system size in both cases.

to the inversion group elements appears in the Hamiltonian, since they have vanishing character in that representation. Consequently, the single-flux inversion bands become flat. This can be seen for both $C = \mathbb{1}$ (Fig. 7) and $C = C_1$ (Fig. 8).

For $C = \mathbb{1}$, the system displays a dispersing band corresponding to the degenerate rotation fluxes, and a flat band corresponding to the zero-energy fluxes. Two sets of edge modes branch from the inversion band, with energy 2μ and $-\mu$, as an effect of the boundary terms T.

The degeneracy structure of the rotation band is slightly different from the $A = 1$ and $C = \mathbb{1}$, as the states in this band are fourfold degenerate with the exception of the states at the edges of the band displaying a twofold degeneracy. The splitting between the fourfold degenerate states is algebraic in the system size [see Fig. 7(b)].

For $C = C_1$, instead, the five bands are well separated. The bands corresponding to the inversions are still dispersionless and, also in this case, branches of edge modes depart from them [see Fig. 8(a)]. The behavior of the rotation bands is analogous to the case $A = 1$; the states are arranged in 6-plets and, for values of μ such that these two bands do not overlap, their splitting is exponentially suppressed in the system size.

VII. CONCLUSIONS

In this work, we defined two models with a global non-Abelian group symmetry. The first is the chiral ladder model for gauge fluxes in Eq. (18). Based on our assumptions on its parameters, this model displays a ferromagnetic symmetry broken phase with $|G|$ degenerate ground states. The second is the model (62) built through dyonic operators whose properties are determined by the symmetry group. The two models are unitarily equivalent through a nonlocal Jordan-Wigner transformation based on the non-Abelian group G. Such transformation maps the ferromagnetic phase of the ladder model into a phase of the dyonic model that displays topological order and weak zero-energy dyonic modes localized on the boundary of the system. This is analogous to the topological one-dimensional chains of Majorana [1] and parafermionic [5] modes and our construction generalizes these systems and defines a new kind of one-dimensional topological order based on discrete non-Abelian symmetry groups.

To examine the properties of the dyonic model, we extended the definition of one-dimensional topological order (see, for example, Ref. [7]) to systems with non-Abelian symmetries. The appearance of topological order in the dyonic model crucially relies on the notion of locality determined by the dyonic modes. For this purpose, the Jordan-Wigner transformation adopted for the definition of the dyonic modes must rely on an auxiliary irreducible representation A, which must be non-Abelian. In case of Abelian auxiliary representations, the dyonic model displays holographic symmetries.

We examined the weak localized dyonic topological modes appearing in the system through a quasiadiabatic continuation technique and we presented a constructive approach to investigate the appearance of strong zero-energy modes. We showed that the definition of strong modes is in general flawed by divergences originating from two kinds of resonances between excited states: besides the resonances appearing in the study of the Abelian models [6,9], the non-Abelian dyonic and ladder models suffer from the degeneracy of states characterized by different permutations of the same set of gauge fluxes. This hinders the formation of strong zero-energy modes unless these degeneracies are removed through the introduction of coupling constants with a weak position dependence.

The gauge-flux ladder models have been inspired by lattice gauge theories and quantum double models. They may display, in general, very rich phase diagrams and it is possible to envision schemes for their quantum simulation in ultra-cold atom setups based on the protocols developed for the quantum simulation of lattice gauge theories [16,17] (see, for example, the proposal [36] for the simulation of systems with S_3 symmetry). The realization of the dyonic model, instead, must rely on topological systems in higher dimensions with one-dimensional edge states with the required G symmetry. Based on matrix-product-state results in Refs. [37–39], it is indeed possible to show that there cannot exists a purely one-dimensional realization of these gapped topological phases of matter.

The systems we built are based on discrete symmetry groups. We observe, however, that the flux-ladder model can be extended to truncated Lie groups through suitable modifications of the operators U in the Hamiltonian (18) [18] (see

Ref. [40] for the specific SU(2) case), and we can envision extensions to quantum groups as well. The generalization of the dyonic models to these scenarios is an interesting open problem which may connect our model to different systems of interacting anyons.

Finally, we point out that the dyonic modes we defined constitute a particular one-dimensional realization of the extrinsic anyonic twist defects studied in the context of two-dimensional symmetry-enriched systems with topological order [32–34]. Based on the analogy with quantum double models, we suppose that their projective non-Abelian braiding statistics is universal for a suitable choice of the symmetry group. The braiding of dyonic modes can be studied by embedding the dyonic models in appropriate tri-junction geometries or two-dimensional systems, thus extending the known results for parafermionic modes [41,42].

ACKNOWLEDGMENTS

APPENDIX A: THE *C* MATRIX IN HIGH-DIMENSION REPRESENTATIONS

In the main text, we proved the existence of a unitary matrix C satisfying Eq. (21) when the representation matrices $D^F(g)$ of G belong to U(2). In this section, we will extend the proof to the case with $D^F(g) \in U(N)$. We will exploit the decomposition $U(N) = U(1) \times SU(N)$, implying that any matrix $U \in U(N)$ is generated by a phase and the generators of $SU(N)$. $SU(N)$ in turn is generated by $N^2 - 1$ traceless, Hermitian matrices T_a satisfying $[T_a, T_b] = i \sum_c f_{abc} T_c$, where f_{abc} are the structure constants of $SU(N)$. These matrices T_a satisfy

$$T_a T_b = \delta_{ab} \mathbb{1} + \frac{1}{2} \sum_{c=1}^{N^2-1} (i f_{abc} + d_{abc}) T_c, \quad \text{(A1)}$$

such that we can write

$$D^F(g) = e^{i\eta_{g,0}\mathbb{1}} e^{it\vec{\eta}_g \cdot \vec{T}} = e^{i\eta_{g,0}\mathbb{1}} (d_{g,0}\mathbb{1} + \vec{d}_g \cdot \vec{T}). \quad \text{(A2)}$$

Here, d_{g0} and $\vec{d}_g$ are in general complicated functions of $\vec{\eta}_g$ and the structure constants. For simplicity, let us consider the case $C \in SU(N)$. We can write

$$C = v_0 \mathbb{1} + \vec{v} \cdot \vec{T}. \quad \text{(A3)}$$

From (A1), we see that

$$K_g = \text{Tr}(C D^F(g)) = e^{i\eta_{g,0}} \left(N v_0 d_{g,0} + N \sum_i v_i d_{g,i} \right)$$

$$= N\mathcal{D}(g) \cdot \mathcal{C}, \quad \text{(A4)}$$

where the N^2 dimensional vectors are defined in analogy with the two-dimensional case:

$$\mathcal{D}(g) = e^{i\alpha_{g0}} \begin{pmatrix} d_{g,0} \\ \vec{d}_g \end{pmatrix}, \quad \mathcal{C} = \begin{pmatrix} v_0 \\ \vec{v} \end{pmatrix}. \quad \text{(A5)}$$

Since

$$1 = \frac{1}{N} \text{Tr}[C^\dagger C] = |v_0|^2 + \sum_i |v_i|^2 = ||\mathcal{C}||^2, \quad \text{(A6)}$$

the vector $\mathcal{C}$ lies on the $(N^2 - 1)$-sphere. The condition $K_g \neq K_h$ amounts to

$$(\mathcal{D}(g) - \mathcal{D}(h)) \cdot \mathcal{C} \neq 0, \quad \text{(A7)}$$

and the demand that this holds for all $g \neq h$ gives at most $n = |G|(|G| - 1)/2$ vectors, which $\mathcal{C}$ cannot be orthogonal to, or in other words, there are n great circles on the $(N^2 - 1)$-sphere which $\mathcal{C}$ cannot lie on. For all the vectors $\mathcal{C}$ that do not belong to these great circles, the corresponding matrix C satisfies the condition (21). If we include a general overall phase to the matrix C, this does not affect v_0 and $\vec{v}$, hence the conditions (A7) are unaffected and the extension to $C \in U(N)$ is straightforward.

APPENDIX B: QUASIADIABATIC CONTINUATION OF THE WEAK ZERO-ENERGY MODES AT FIRST ORDER

By applying the quasiadiabatic continuation technique [7,28,43], we evaluate the first order correction of the weak zero-energy modes of H_J after the introduction of a small perturbation H_μ such that $\mu \ll J$. We consider for simplicity the case $C = \mathbb{1}$.

For the left edge, the unperturbed zero energy mode is $\alpha(1)$. We will calculate $\mathcal{V}(\mu)\alpha(1)\mathcal{V}^\dagger(\mu)$ where the unitary operator $\mathcal{V}(\mu)$ is defined as the path ordered evolution

$$\mathcal{V}(\mu) = \text{Texp}\left[i \int_0^\mu \mathcal{D}(\mu') \, d\mu' \right] \quad \text{(B1)}$$

generated by the operator

$$\mathcal{D}(\mu) = -i \int_{-\infty}^{+\infty} dt \, e^{iHt} \mathcal{F}(\partial_\mu H) e^{-iHt}. \quad \text{(B2)}$$

In the previous relation, $H = H_J + H_\mu$ and the function $\mathcal{F}$ is meant to introduce suitable filter functions [43], depending on the different kinds of excitations of the ground states, to cut off the time the time evolution of $\partial_\mu H$ for large $|t|$. In particular, we adopt

$$\mathcal{F}(\partial_\mu H) = -\sum_r \sum_{h \neq e} F[(m_h - m_e)t] \chi^A(h^{-1}) \theta_h(r), \quad \text{(B3)}$$

where m_g labels the flux masses (20) and $F(t)$ is an imaginary, odd and analytical filter function such that its Fourier transform results in

$$\tilde{F}(\omega) = \int_{-\infty}^{+\infty} dt \, e^{i\omega t} F(t) \approx -\frac{1}{\omega} \quad \text{for} \quad |\omega| \geqslant 1, \quad \text{(B4)}$$

and $\tilde{F}(0) = 0$ [43]. From Eq. (B1), we get

$$\mathcal{V}(\mu)\alpha(1)\mathcal{V}^\dagger(\mu) = \alpha(1) + i\mu[\mathcal{D}(0), \alpha(1)] + \ldots. \quad \text{(B5)}$$

The commutator results in

$$
\begin{aligned}
[\mathcal{D}(\mu = 0), \alpha(1)] &= i \int_{-\infty}^{+\infty} dt \left[e^{iH_Jt} \sum_{h \neq e} F[(m_h - m_e)t] \chi^A(h^{-1})\theta_h(1) e^{-iH_Jt}, U^{\dagger}(1) \right] \\
&= i \int_{-\infty}^{+\infty} dt \, e^{iH_Jt} \left[\sum_{h \neq e} F[(m_h - m_e)t] \chi^A(h^{-1})\theta_h(1) U^{\dagger}(1)\left(\mathbb{1} - D^{\dagger}(h)\right) \right] e^{-iH_Jt} \\
&= i \sum_{h \neq e} \chi^A(h^{-1})\theta_h(1) U^{\dagger}(1)(\mathbb{1} - D^{\dagger}(h)) \int_{-\infty}^{+\infty} dt \, F[(m_h - m_e)t] e^{-iJ(\mathrm{Tr}[U(2)CU^{\dagger}(1)(D^{\dagger}(h)-\mathbb{1})+\mathrm{H.c.}])t}.
\end{aligned} \tag{B6}
$$

We expressed all the terms in the previous relations as a function of the flux operators $U^{\dagger}(1) = \alpha(1)$ and $\chi^A(h^{-1})\theta_h(1) = \mathrm{Tr}_A\,[\beta_h^{\dagger}(2)\alpha_h(1)]D^{\dagger}(h)$. The weak zero-energy modes are defined based on their commutation relation (71) with the Hamiltonian projected on the ground-state manifold. Therefore we can specialize the previous expressions by considering their effect on the ground states of H only. To the purpose of evaluating the first-order correction in (B5), we can consider in turn the effect of the commutator on the ground states of H_J, since dealing with the eigenstates of H would imply the introduction of a further correction of order μ/J based on the relation $P(\mu) \approx P(0) + i\mu[\mathcal{D}(0), P(0)]$, where $P(\mu)$ is the projection operator onto the ground-state manifold for finite μ. Under this assumption, in the case $C = \mathbb{1}$, we obtain

$$
[\mathcal{D}(\mu = 0), \alpha(1)]P(\mu) \approx i \sum_{h \neq e} \chi^A(h^{-1})\theta_h(1) U^{\dagger}(1)(\mathbb{1} - D^{\dagger}(h))P(0) \int_{-\infty}^{+\infty} dt \, F[(m_h - m_e)t] e^{i(m_h - m_e)t} + O(\mu/J). \tag{B7}
$$

After considering this ground-state restriction, by applying Eq. (B4) and considering that $\tilde{F}(1) \approx -1$, we finally obtain

$$
\mathcal{V}(\mu)\alpha(1)\mathcal{V}^{\dagger}(\mu) = U^{\dagger}(1) + \sum_{h \neq e} \frac{\mu}{m_h - m_e} \chi^A(h^{-1})\theta_h(1) U^{\dagger}(1)(\mathbb{1} - D^{\dagger}(h)) + O\left(\frac{\mu^2}{J^2}\right). \tag{B8}
$$

This relation corresponds to Eq. (75) once we express the θ and $U^{\dagger}$ operators in terms of the dyonic modes. We also observe that this first-order correction coincides with the first-order term $\Lambda^{(1)}$ in Eq. (86) when we apply the strong zero-energy mode to the ground-state manifold of H_J in the limit $C \to \mathbb{1}$. The case with a general C matrix in the Hamiltonian can be investigated with the same approach. The final result indeed matches $\Lambda^{(1)}$ in Eq. (86).

For $C = \mathbb{1}$, a similar calculation can be performed for the right edge modes. For this purpose, it is necessary to generalize the functional $\mathcal{F}(t)$. Instead of considering the set of functions $F(m_h - m_e)t$ in Eq. (B3), we define $\mathcal{F}$ based on a set of operators f_J:

$$
\mathcal{F}(\partial_\mu H) = -\sum_r \sum_{h \neq e} F(f_J(h, r)t) \chi^A(h^{-1})\theta_h(r), \tag{B9}
$$

where

$$
f_J(h, r) = H_J - \theta_h(r) H_J \theta_h^{\dagger}(r). \tag{B10}
$$

The role of the operators f_J is to extract the correct spectral gap of the unperturbed Hamiltonian H_J to be associated with each term of $\partial_\mu H$.

The key property in the definition (B9) is that both $\mathcal{F}(\partial_\mu H)$ and the resulting $\mathcal{D}(0)$ commute with the string operator $\mathcal{L}_g(L)$ appearing in $\beta_g(2L)$. By exploiting this property and $[\beta_g(2L), H_J] = 0$, we get

$$
\begin{aligned}
[\mathcal{D}(\mu = 0), \beta_g(2L)]P(\mu) &\approx i \int_{-\infty}^{+\infty} dt \left[e^{iH_Jt} \sum_{r, h \neq e} F[f_J(h, r)t] \chi^A(h^{-1})\theta_h(r) e^{-iH_Jt}, \mathcal{L}_g(L) U^{\dagger}(L) \right] P(0) \\
&= i \int_{-\infty}^{+\infty} dt \left[\sum_{r, h \neq e} e^{if_J(h,r)t} F[f_J(h, r)t] \chi^A(h^{-1})\theta_h(r), \mathcal{L}_g(L) U^{\dagger}(L) \right] P(0) \\
&= i \mathcal{L}_g(L) \sum_{h \neq e} \int_{-\infty}^{+\infty} dt \, e^{if_J(h,L)t} F[f_J(h, L)t] \chi^A(h^{-1})[\theta_h(L), U^{\dagger}(L)] P(0) \\
&= -i \sum_{h \neq e} \mathcal{L}_g(L) U^{\dagger}(L)[D(h) - \mathbb{1}] \int_{-\infty}^{+\infty} dt \, e^{if_J(h,L)t} F[f_J(h, L)t] \chi^A(h^{-1})\theta_h(L) P(0) \\
&\approx i \sum_{h \neq e} \mathcal{L}_g(L) U^{\dagger}(L)[D(h) - \mathbb{1}] \chi^A(h^{-1})\theta_h(L) \frac{1}{m_h - m_e} P(0).
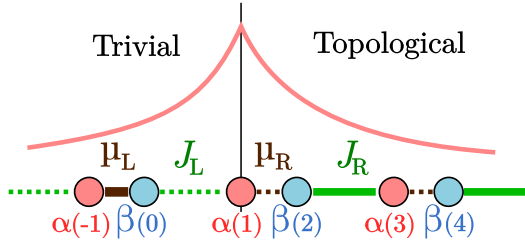\end{aligned} \tag{B11}
$$

FIG. 9. Schematic representation of the interface between trivial ($r < 1$) and topological ($r \geqslant 1$) interface. The dotted/full lines represent weak/strong couplings and the resulting weak zero-energy modes is localized around $\alpha_g(1)$.

Thanks to the definitions (B9) and (B10), the last line holds also for $C \neq \mathbb{1}$ and can be derived by commuting f_J with θ_h and applying it to the projector $P(0)$. We conclude, in general:

$$\mathcal{V}(\mu)\beta_g(2L)\mathcal{V}^\dagger(\mu)$$
$$= \beta_g(2L) + \beta_g(2L) \sum_{h \neq e} \frac{\mu}{m_h - m_e}(D(h) - \mathbb{1}) \operatorname{Tr}_K \operatorname{Tr}_A$$
$$\times [\beta_h^\dagger(2)\alpha_h(1)D^{K\dagger}(h)] + O\left(\frac{\mu^2}{J^2}\right), \tag{B12}$$

which is also consistent with the form of the right zero-energy strong mode (104) applied to the unperturbed ground states.

APPENDIX C: THE WEAK MODES AT THE INTERFACE BETWEEN NONTOPOLOGICAL AND TOPOLOGICAL REGIONS

The analysis in Sec. IV assumes a finite and uniform chain in its topological phase with $\mu \ll J$. For $\mu = 0$, the left zero-energy mode is $\alpha(1)$ which, based on the definition (45), does not carry a Jordan-Wigner string, and, consequently, a group element index. This property is inherited by all the left weak zero-energy modes defined by adiabatic continuation in Appendix B and it holds also for the calculation of the strong zero-energy modes in Sec. IV.

In this appendix, we analyze what happens when we consider a boundary between a nontopological region, located at $r < 1$ and a topological region at $r \geqslant 1$. In this case, the system is infinitely extended in both directions and the Jordan-Wigner strings must be redefined by extending them

to $r = -\infty$: $\mathcal{L}_g(r) = \prod_{x=-\infty}^{r} \Theta_g(x)$ where the product is an ordered product generalizing Eq. (41).

We model the system through the Hamiltonian

$$H = H_L(\mu_L, J_L) + H_R(\mu_R, J_R), \tag{C1}$$

where the left Hamiltonian H_L is defined for $r < 1$ and is in the trivial regime $\mu_L \gg J_L$, whereas the right Hamiltonian H_R is defined in the topological region $r \geqslant 1$ with $\mu_R \ll J_R$ (see Fig. 9). For $\mu_R = J_L = 0$, the operators $\alpha_g(1)$ do not appear in H and constitute zero-energy modes. In the following, we will discuss how these zero-energy modes evolve quasiadiabatically, at first order, when introducing perturbations given by J_L and μ_R.

The unperturbed Hamiltonians $H_L(\mu_L, 0)$ and $H_R(0, J_R)$ commute, since they are defined in nonoverlapping domains. This makes it possible to evaluate the two first-order contributions resulting in Eq. (B5) separately. The contribution given by μ_R coincides with the result in Eq. (B8). Therefore we focus on the introduction of J_L only. For ease of notation, we drop the subscript L referring to the domain $r < 1$. The operator $\mathcal{D}(J = 0)$ is defined as

$$\mathcal{D}(J = 0) = i \int_{-\infty}^{+\infty} dt \, e^{iH_\mu t} F(\Delta t)$$
$$\times \left[\sum_{r < 1} (\operatorname{Tr}[U(r+1)CU^\dagger(r)] + \text{H.c.})\right] e^{-iH_\mu t}. \tag{C2}$$

Since we are interested in the weak modes, the operator Δ represents the gap caused by the application of the plaquette operators over the ground states of H_μ. By using the projectors (28), we can rewrite

$$H_\mu = -\frac{\mu|G|}{\dim A} \sum_{r < 1} \Pi^A(r), \tag{C3}$$

therefore the ground states of H_μ corresponds to states in which all the sites in the ladder model are in an arbitrary state $|Aab\rangle$. We conclude that the gap operator Δ can be defined as

$$\Delta = \frac{\mu|G|}{\dim A} \sum_{r < 1} (\mathbb{1} - \Pi^A(r)). \tag{C4}$$

We observe that the projector over the ground states of H_μ is $P(J = 0) = \prod_{r < 1} \Pi^A(r)$ and it commutes with $\alpha_g(1)$. Therefore, by following the approach in Appendix B, we obtain

$$[\mathcal{D}(J = 0), \alpha_g(1)]P(J) \approx i \int_{-\infty}^{+\infty} dt \, F(\Delta t)e^{i\Delta t}[(\operatorname{Tr}[U(1)CU^\dagger(0)] + \text{H.c.}), \mathcal{L}_g(0)]U^\dagger(1)P(0)$$

$$= -i\frac{\dim A}{\mu|G|}(\mathbb{1} - \Pi^A(0))(\operatorname{Tr}[U(1)CU^\dagger(0)(\mathbb{1} - D^\dagger(g))] + \text{H.c.})\alpha_g(1)P(0), \tag{C5}$$

where we exploited that $\tilde{F}(0) = 0$. The first-order correction to $\alpha_g(1)$ on the trivial region results in

$$\mathcal{V}(J_L)\alpha_g(1)\mathcal{V}^\dagger(J_L) = \alpha_g(1) + \frac{J_L \dim A}{\mu_L|G|}(\mathbb{1} - \Pi^A(0))(\operatorname{Tr}[U(1)CU^\dagger(0)(\mathbb{1} - D^\dagger(g))] + \text{H.c.})\alpha_g(1) + O\left(\frac{J_L^2}{\mu_L^2}\right). \tag{C6}$$

This relation can be fully recast in a local form as a function of the operators $\alpha_g(1)$, $\alpha_g(-1)$ and $\beta_g(0)$ and it suggests that, under quasiadiabatic evolution, the weak zero-energy modes at the interfaces between topological and nontopological regions maintain their locality. A similar approach can be applied to estimate the strong-zero energy modes at such interface. Also, in this case, the left modes acquire a group index g and the result is fully dyonic.

APPENDIX D: INNER TERM OF THE ZERO MODES

In Sec. IV D, we discussed the resonances appearing in the definition of the outer modes $\Lambda_{\text{out},n}$. Here we investigate the behavior of the inner modes. To this purpose, it is necessary to refine our definition of the inner part of the commutators C_n and of the inner modes $\Lambda_{\text{in},n}$.

We introduce the notation $c_{a_1}{}^{a_2}{}_{a_3}{}^{\cdots}{}_{\cdots}$ to label all the terms of the commutator C_n appearing at level $n = \sum_i a_i$ in the iteration process. The set $a_1, a_2, \ldots, a_n$ is an ordered partition of n where lower and upper indices refer to the number of consecutive times that the outer or inner operators θ have been considered in the definition of this contribution of the commutator C_n. In particular, $c_n \equiv C_{\text{out},n}$, whereas all the other contributions belong to $C_{\text{in},n}$.

To define in detail $c_{a_1}{}^{a_2}{}_{a_3}{}^{\cdots}{}_{\cdots}$, let us consider first the second order of iteration. The operator C_2 can be decomposed into

$$c_2 = -\mu \left[\Lambda_1, \sum_{h_2} \theta_{h_2}(2) \right] = C_{\text{out},2}, \tag{D1}$$

$$c_1{}^1 = -\mu \left[\Lambda_1, \sum_{k_1} \theta_{k_1}(1) \right] = C_{\text{in},2}. \tag{D2}$$

The notation for $c_1{}^1$ refers to the fact that, in the first order of iteration, we considered the outermost θ operator available ($\theta_{h_1}(1)$) in this case, whereas in the second order of iteration, we considered the commutator with the inner term $\theta_{k_1}(1)$.

In a similar way, we can define different contributions for the inner part of the strong mode $\Lambda_{\text{in},n}$. In particular, we build the following operators:

$$\lambda_2 = \Lambda_{\text{out},2} \quad \text{such that} \quad [\lambda_2, H_J] = -c_2, \tag{D3}$$

$$\lambda_1{}^1 = \Lambda_{\text{in},2} \quad \text{such that} \quad [\lambda_1{}^1, H_J] = -c_1{}^1. \tag{D4}$$

In the following iteration steps, we can define

$$c_n = -\mu \left[\lambda_{n-1}, \sum_{h_n} \theta_{h_n}(n) \right] = C_{\text{out},n}, \tag{D5}$$

$$c_{n-1}{}^1(r) = -\mu \left[\lambda_{n-1}, \sum_{k_1} \theta_{k_1}(r) \right], \tag{D6}$$

$$c_{n-2}{}^2(r_1, r_2) = -\mu \left[\lambda_{n-2}{}^1(r_1), \sum_{k_2} \theta_{k_2}(r_2) \right]. \tag{D7}$$

More in general, given $\lambda_{a_1}{}^{a_2}{}_{a_3}{}^{\cdots}{}_{\cdots}$, we will define a set of commutators $c_{a_1}{}^{a_2}{}_{a_3}{}^{\cdots}{}_{\cdots}$, increasing the last upper index when
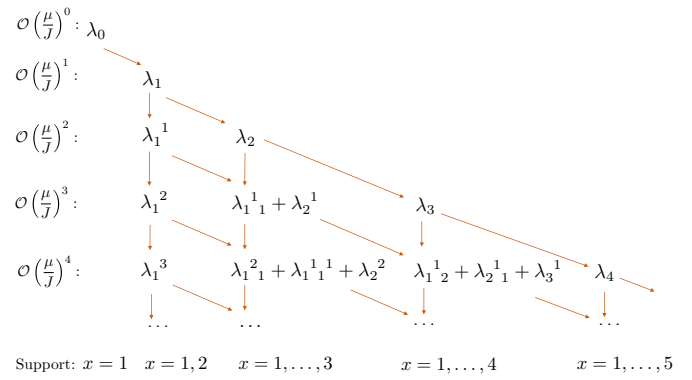

FIG. 10. Diagram of the structure of the terms at each order in $\frac{\mu}{J}$. For a given term, its commutator with H_μ is canceled by the subsequent terms' commutator with H_J. The notation keeps track of which term is derived from this. At each successive order, the support may be extended compared to the previous step, in which case a lower index is added. If the support is unchanged, an upper index is added instead. The sum of all the indices gives the order of the term in $\frac{\mu}{J}$, and the support of a given term is given by the sum of lower indices plus one.

considering the commutator with an inner θ operator, and increasing the last lower index when considering the commutator with an outer θ operator. If the last index is not of the type which is increased, a new index of 1 is added at that position instead.

The construction of $\lambda_{a_1}{}^{a_2}{}_{a_3}{}^{\cdots}{}_{\cdots}$ follows accordingly, based on the relation

$$\left[\lambda_{a_1}{}^{a_2}{}_{a_3}{}^{\cdots}{}_{\cdots}, H_J \right] = -\sum_{r_1 \ldots} c_{a_1}{}^{a_2}{}_{a_3}{}^{\cdots}{}_{\cdots}(r_1, \ldots), \tag{D8}$$

where we are summing over all the possible position indices of the inner part of the commutator.

This construction implies that the modes $\lambda_{a_1}{}^{a_2}{}_{a_3}{}^{\cdots}{}_{\cdots}$ have support in the first $a_{\text{in}} = a_1 + a_3 + a_5 + \ldots$ sites of the flux-ladder model, and they range from $\alpha(1)$ to $\alpha(2a_{\text{in}} + 1)$.

This construction is summarized in Fig. 10. We observe that the order of the indices matters, so each term in Figu. 10 at any given order are in general not equal.

Because of the factor $U^\dagger(1)$ in λ_n there is a difference between $c_n{}^1(1)$ and $c_n{}^1(j)$ for $n \geqslant j > 1$. To get an idea of the structure of all these many terms, it is illustrative to calculate a few of them, and by using (97), we see

$$c_2{}^1(1) = -\frac{\mu^3}{J^2} \sum_{h_1, h_2 \neq e} \sum_{k_1 \neq e} \chi^A(h_1^{-1}) \chi^A(h_2^{-1}) \chi^A(k_1^{-1})$$
$$\times [\tilde{F}_1 F_2 \theta_{h_1}(1) \theta_{h_2}(2) U^\dagger(1) (D^\dagger(h_1) - \mathbb{1}), \theta_{k_1}(1)]$$
$$= -\frac{\mu^3}{J^2} \sum_{h_1, h_2 \neq e} \sum_{k_1 \neq e} \chi^A(h_1^{-1}) \chi^A(h_2^{-1}) \chi^A(k_1^{-1})$$
$$\times (\tilde{F}_1 F_2 \theta_{h_1 k_1}(1) \theta_{h_2}(2) U^\dagger(1) D^\dagger(k_1) (D^\dagger(h_1) - \mathbb{1})$$
$$- \tilde{G}_1(k_1, 1) G_2(k_1, 1) \theta_{k_1 h_1}(1) \theta_{h_2}(2) U^\dagger(1)$$
$$\times (D^\dagger(h_1) - \mathbb{1})), \tag{D9}$$

where

$$\tilde{G}_1(k_1, 1) = \theta_{k_1}(1)\tilde{F}_1\theta_{k_1}^\dagger(1)$$
$$= (\mathrm{Tr}[U(2)CU^\dagger(1)D(k_1)(D(h_1) - \mathbb{1}) + \mathrm{H.c.}])^{-1}$$
$$- (\mathrm{Tr}[U(2)CU^\dagger(1)D(k_1)(D(h_1) - \mathbb{1})D^\dagger(h_2)$$
$$+ \mathrm{H.c.}])^{-1}) \tag{D10}$$

and

$$G_2(k_1, 1) = \theta_{k_1}(1)F_2\theta_{k_1}^\dagger(1)$$
$$= \big(\mathrm{Tr}\big[U(2)CU^\dagger(1)D(k_1)\big(D(h_1 h_2^{-1})-\mathbb{1}\big)+\mathrm{H.c.}\big]$$
$$+ \mathrm{Tr}[U(3)CU^\dagger(2)(D(h_2) - \mathbb{1}) + \mathrm{H.c.}]\big). \tag{D11}$$

The crucial point to notice is that no new conditions are required on the Hamiltonian in order have this term finite. The next order correction $\lambda_2^1(1)$ is also finite, since the only difference from (D9) is that the two terms have an added factor of $([\theta_{h_1 k_1}(1)\theta_{h_2}(2), H_j](\theta_{h_1 k_1}(1)\theta_{h_2}(2))^{-1})^{-1}$ and $([\theta_{k_1 h_1}(1)\theta_{h_2}(2), H_j](\theta_{k_1 h_1}(1)\theta_{h_2}(2))^{-1})^{-1}$, respectively. There is a subtlety we should address however. If for instance

we look at $c_2^2(1, 2)$, there are commutators of the form

$$[\theta_{h_1 k_1}(1)\theta_{h_2 k_2}(2), H_J]$$
$$= (\mathrm{Tr}(U(2)CU^\dagger(1)(D(h_1 k_1(h_2 k_2)^{-1} - \mathbb{1}) + \mathrm{H.c.})$$
$$+ (\mathrm{Tr}(U(3)CU^\dagger(2)(D(h_2 k_2 - \mathbb{1}) + \mathrm{H.c.}))\theta_{h_1 k_1}(1)\theta_{h_2 k_2}(2), \tag{D12}$$

and the above is zero for $k_2 = h_2^{-1}$ and $k_1 = h_1^{-1}$. Therefore, when constructing $\lambda_2^2(1, 2)$, we would only have to sum over the k_1 and k_2 such that $c_2^2(1, 2) \neq 0$.

In conclusion, all the inner terms can be expressed as the sum of terms similar to the outer modes, through a redefinition of the domain and the correct conjugations of the F functions generating suitable G functions. As long as F_n and $\tilde{F}_n$ are bounded, their conjugated counterparts G_n and $\tilde{G}_n$ are as well, and all the inner terms are well-defined to all orders. All the F and G operators assume the general form $(\sum_i (m_{g_i} - m_{h_i}))^{-1}$ in the group element basis, and the only resonances which may appear are the ones described in Sec. IV D. Consequently, the inclusion of the inner modes does not qualitatively modify the general behavior of the decay of the strong modes in the bulk.

[1] A. Y. Kitaev, Phys. Usp. **44**, 131 (2001).
[2] J. Alicea, Rep. Progr. Phys. **75**, 076501 (2012).
[3] M. Leijnse and K. Flensberg, Semicond. Sci. Tech. **27**, 124003 (2012).
[4] C. W. J. Beenakker, Annu. Rev. Condens. Matter Phys. **4**, 113 (2013)
[5] P. Fendley, J. Stat. Mech. (2012) P11020.
[6] A. S. Jermyn, R. S. K. Mong, J. Alicea, and P. Fendley, Phys. Rev. B **90**, 165106 (2014).
[7] A. Alexandradinata, N. Regnault, C. Fang, M. J. Gilbert, and B. A. Bernevig, Phys. Rev. B **94**, 125103 (2016).
[8] F. Iemini, C. Mora, and L. Mazza, Phys. Rev. Lett. **118**, 170402 (2017).
[9] N. Moran, D. Pellegrino, J. K. Slingerland, and G. Kells, Phys. Rev. B **95**, 235127 (2017).
[10] A. Y. Kitaev, Ann. Phys. **303**, 2 (2003).
[11] E. Fradkin and L. P. Kadanoff, Nucl. Phys. B **170**, 1 (1980).
[12] R. Jagannathan, arXiv:1005.4300.
[13] S. S. Bullock and G. K. Brennen, J. Phys. A **40**, 3481 (2007).
[14] M. Burrello, B. van Heck, and E. Cobanera, Phys. Rev. B **87**, 195422 (2013).
[15] M. Koch-Janusz, M. Levin, and A. Stern, Phys. Rev. B **88**, 115133 (2013).
[16] M. Dalmonte and S. Montangero, Cont. Phys. **57**, 388 (2016).
[17] E. Zohar, J. I. Cirac, and B. Reznik, Rep. Progr. Phys. **79**, 014401 (2016).
[18] E. Zohar and M. Burrello, Phys. Rev. D **91**, 054506 (2015).
[19] E. Zohar and M. Burrello, New J. Phys. **18**, 043008 (2016).
[20] E. Cobanera, G. Ortiz, and E. Knill, Nucl. Phys. B **877**, 574 (2013).
[21] J. Kogut and L. Susskind, Phys. Rev. D **11**, 395 (1975).
[22] S. Ostlund, Phys. Rev. B **24**, 398 (1981).
[23] A. Milsted, E. Cobanera, M. Burrello, and G. Ortiz, Phys. Rev. B **90**, 195101 (2014).

[24] Y. Zhuang, H. J. Changlani, N. M. Tubman, and T. L. Hughes, Phys. Rev. B **92**, 035154 (2015).
[25] R. Samajdar, S. Choi, H. Pichler, M. D. Lukin, and S. Sachdev, Phys. Rev. A **98**, 023614 (2018).
[26] A. Keesling *et al.*, arXiv:1809.05540.
[27] E. Cobanera, G. Ortiz, and Z. Nussinov, Adv. Phys. **60**, 679 (2011).
[28] M. B. Hastings and X.-G. Wen, Phys. Rev. B **72**, 045141 (2005).
[29] D. M. Brink and G. R. Satchler, *Angular Momentum* (Oxford University Press, 1993).
[30] Y.-Z. You and X.-G. Wen, Phys. Rev. B **86**, 161107(R) (2012).
[31] M. Barkeshli, C.-M. Jian, and X.-L. Qi, Phys. Rev. B **87**, 045130 (2013).
[32] M. Barkeshli, P. Bonderson, M. Cheng, and Z. Wang, arXiv:1410.4540.
[33] J. C. Y. Teo, T. L. Hughes, and E. Fradkin, Ann. Phys. **360**, 349 (2015).
[34] J. C. Y. Teo, J. Phys.: Condens. Matter **28**, 143001 (2016).
[35] E. Cobanera, G. Ortiz, and Z. Nussinov, Phys. Rev. B **87**, 041105(R) (2013).
[36] J. Bender, E. Zohar, A. Farace, and J. I. Cirac, New J. Phys. **20**, 093001 (2018).
[37] A. M. Turner, F. Pollmann, and E. Berg, Phys. Rev. B **83**, 075102 (2011).
[38] L. Fidkowski and A. Kitaev, Phys. Rev. B **83**, 075103 (2011).
[39] N. Bultinck, D. J. Williamson, J. Haegeman, and F. Verstraete, Phys. Rev. B **95**, 075108 (2017).
[40] E. Zohar, T. B. Wahl, M. Burrello, and J. I. Cirac, Ann. Phys. **374**, 84 (2016).
[41] D. J. Clarke, J. Alicea, and K. Shtengel, Nat. Commun. **4**, 1348 (2012).
[42] N. H. Lindner, E. Berg, G. Refael, and A. Stern, Phys. Rev. X **2**, 041002 (2012).
[43] S. Bravyi and M. Hastings, Commun. Math. Phys. **307**, 609 (2011).

Chapter 6

Epilogue

In this thesis we have investigated aspects of Majorana physics, which are crucial to understand in the practical application of quantum computation. In the four projects we have firstly tackled the problem of modeling the readout dynamics of Majorana qubits, presenting a flexible model which explicitly includes the measurement apparatus. Secondly, we have extensively studied the decoherence rates for noisy ideal Majorana qubits, finding non-Markovian effects that may constitute a significant reduction of readout fidelity persisting at zero temperature. Thirdly, we have introduced and discussed a model generalizing the notion of Majorana zero-energy modes by hosting more complicated dyonic zero-energy modes with richer structure.

Once the experimental milestone of consistent Majorana parity readout has been successfully achieved, we are in position to finally establish whether the putative zero-energy modes found in proximitized nanowires [4, 22, 23, 58] truly stem from Majorana zero-energy modes, by using the procedure of measurement-based braiding. Thus, we are on the verge of possibly proving the existence of a species of quasiparticles that are fundamentally very different from ordinary electrons, phonons and so on. Furthermore, if this is successfully demonstrated, it opens the door for applications of Majorana zero-energy modes in topological quantum computation.

Project A, B and C contribute towards these goals by furthering our understanding of the dynamics of Majorana qubits. These projects complement each other, since a high-fidelity readout has to happen quicker than the information loss. On the other hand, one of the central findings of Project C is that readouts have to be carried out gently, as entanglement with excess bosonic modes lead to visibility- and potentially fidelity loss. In all four projects, there remain open questions suggesting interesting future avenues of theoretical research.

In Project A, we mapped the problem of readouts of Majorana box qubits onto a variation of the spin-boson model. The variation consists in there being two copies of the spin-boson model, corresponding to the two different parity outcomes of the measurement, as well as coherence between the two sectors. On the parity-diagonals therefore, the dynamics is highly detailed in the literature [77], and thus there may very well exist more sophisticated theoretical tools which are immediately applicable to our case. It would be curious to see these methods adapted to also describe the off-diagonals. However, one of the strengths of our project is the simplicity of the results; one can quite easily adapt our theory to describe different setups of reading out parities using a dot.

In the project we dealt with the experimentally relevant readout procedure where the conductance of a capacitively coupled QPC is used to projectively measure the parity of the split dot-Majorana system. We derived a microscopic model for the effective spectral density as seen from the dot-Majorana system, but this complicated expression was unwieldy for the purpose of obtaining workable analytical results, and we approximated the function with a much simpler Ohmic one. Thus, a possible follow-up project would be to numerically tackle the problem of the exact QPC spectral density. In such a numerical study, one could also include other error sources, using the methods outlined in the paper. Essentially, one could include errors of the type studied in Project B and C, as well as a host of other sources of dephasing for a complete quantitative treatment of the dynamics of the readouts.

Another type of readout which is also experimentally relevant, is dispersive readouts. Here, the dot is capacitively coupled to an LC circuit, which is driven. In the steady state configuration, the capacitance

of the dot reflects a shift of the impedance of the system, resulting in a phase- and amplitude shift of reflected and transmitted signals through the circuit. While we modelled the decoherence due to a circuit without driving, the time-dependency of the environment in the driven case leads to non-trivial changes of the effective bosonic spectral function. Treating this problem beyond the rotating-wave approximation would be immensely interesting, and would cover an important open theoretical problem in Majorana qubit readouts.

For Project B and C, we developed a model of the decoherence in an ideal Majorana box qubit subjected to electromagnetic noise. In Project B we used an intuitively simple model, treating the fluctuations as classically varying potentials and calculating the leading order of non-adiabatic contributions to the decoherence. This model relies on temperatures being comparable with the frequencies of the environmental modes, and thus it is maybe not realistic in practical applications. In contrast, in Project C the electromagnetic noise was represented by bosonic modes, which gave us the possibility of calculating that non-Markovian contributions to decoherence at zero temperature when the bare Majorana degrees of freedom are measured projectively. In this case, the true eigenmodes of the system are dressed by the bosons, and the question about the fidelity and visibility loss at zero temperature thus depends on whether or not it is possible to perform a readout of the dressed modes. Here, we stress that the bosonic spectrum is gapless, such that there is no meaningful way of adiabatic operations with respect to the bosonic frequencies. Working out the dynamics of coupling the measurement apparatus and performing the readout in the presence of these bosonic interactions is arguably the main outstanding problem. It appears to be a hard problem as non-Markovian dynamics played an important role. Expanding upon the calculation of the instantaneous zero-energy modes in Project B, it could maybe be possible to calculate the consequences of switching on the dot coupling in a readout experiment, thus paving a way towards solving the problem. Following the techniques of Project B, the formalism could also potentially allow for including noise in the coupling parameters through statistically averaging over such terms.

If topological quantum computation can be proven possible using Majorana bound states, it opens the possibility of using more exotic anyons with complete braiding statistics. In that case, all quantum gates could be implemented in a topologically protected manner, which would for example vastly limit the overhead expected from magic state distillation. Project D contributes to establishing the necessary theoretical groundwork for achieving this very long term goal.

Here, we introduced an abstract model with a local dyonic representation hosting zero-energy modes that generalize the Majorana bound states in the Kitaev model. In contrast with Majoranas, the modes are in general weak zero-energy modes, but we found that adding a spatial dependency on the parameters, for instance through disorder, might make the zero-energy modes strong. We did this through an iterative construction of the zero-energy modes, and one question that went beyond the scope of our study was how far into the excited states disorder would preserve the degeneracy. On one hand, as the system size increases, so does the risk of destructive resonances, but on the other hand, the support of the terms decrease exponentially. It would be an interesting question for a follow-up study to investigate the interplay of these two effects to see whether strong zero-energy modes are possible in principle.

While we understand the fusion rules of the dyonic zero-energy modes, we still don't know their braiding statistics. If this could be figured out, our model could present a paradigmatic framework for collectively describing 1-dimensional systems with anyonic zero-energy modes. Parafermions are naturally described by our model, and it could be interesting to investigate if there can be made a connection with other types of anyons, such as Fibonacci anyons. Also, if the braiding rules of the dyonic zero-energy modes corresponding to any finite groups G is worked out, it could be interesting to investigate what restrictions are necessary on G and its representations in the model, for the dyons to have a computationally complete set of braiding rules.

Collectively the four projects of this thesis expand upon our knowledge of anyonic zero-energy modes, and it is the hope of its author that the findings will help guide experiments as well as theory towards achieving the goal of demonstrating non-abelian anyons. The fields of topological phases of condensed matter and topological quantum computation are very active fields of research, both theoretically and experimentally, and following the developments over the coming years will be very interesting.

Bibliography

[1] David Aasen, Michael Hell, Ryan V. Mishmash, Andrew Higginbotham, Jeroen Danon, Martin Leijnse, Thomas S. Jespersen, Joshua A. Folk, Charles M. Marcus, Karsten Flensberg, and Jason Alicea. Milestones Toward Majorana-Based Quantum Computing. *Phys. Rev. X*, 6(3):031016, aug 2016.

[2] Stephen L Adler. Why decoherence has not solved the measurement problem: a response to p. w. anderson. *Studies in History and Philosophy of Science Part B: Studies in History and Philosophy of Modern Physics*, 34(1):135–142, 2003.

[3] S M Albrecht, E B Hansen, A P Higginbotham, F Kuemmeth, T S Jespersen, J Nygård, P Krogstrup, J Danon, K Flensberg, and C M Marcus. Transport Signatures of Quasiparticle Poisoning in a Majorana Island. *Phys. Rev. Lett.*, 118:137701, 2017.

[4] S M Albrecht, A P Higginbotham, M Madsen, F Kuemmeth, T S Jespersen, J Nygård, P Krogstrup, and C M Marcus. Exponential Protection of Zero Modes in Majorana Islands. *Nature*, 531:206, 2016.

[5] A Alexandradinata, N Regnault, Chen Fang, Matthew J Gilbert, and B Andrei Bernevig. Parafermionic phases with symmetry breaking and topological order. *Physical Review B*, 94(12):125103, 2016.

[6] Jason Alicea and Paul Fendley. Topological phases with parafermions: theory and blueprints. *Annual Review of Condensed Matter Physics*, 7:119–139, 2016.

[7] Alexander Altland and Ben D Simons. *Condensed matter field theory*. Cambridge university press, 2010.

[8] Alexander Altland and Martin R Zirnbauer. Nonstandard symmetry classes in mesoscopic normal-superconducting hybrid structures. *Physical Review B*, 55(2):1142, 1997.

[9] Philip W Anderson. More is different. *Science*, 177(4047):393–396, 1972.

[10] Pavel P Aseev, Jelena Klinovaja, and Daniel Loss. Lifetime of majorana qubits in rashba nanowires with nonuniform chemical potential. *Physical Review B*, 98(15):155414, 2018.

[11] David John Baker, Hans Halvorson, and Noel Swanson. The conventionality of parastatistics. *The British Journal for the Philosophy of Science*, 66(4):929–976, 2015.

[12] Maissam Barkeshli and Jay D Sau. Physical architecture for a universal topological quantum computer based on a network of majorana nanowires. *arXiv preprint arXiv:1509.07135*, 2015.

[13] Sergey Bravyi. Universal quantum computation with the $\nu= 5/ 2$ fractional quantum hall state. *Physical Review A*, 73(4):042313, 2006.

[14] Sergey Bravyi, Matthew B Hastings, and Spyridon Michalakis. Topological quantum order: stability under local perturbations. *Journal of mathematical physics*, 51(9):093512, 2010.

[15] Heinz-Peter Breuer, Francesco Petruccione, et al. *The theory of open quantum systems*. Oxford University Press on Demand, 2002.

[16] Henrik Bruus and Karsten Flensberg. *Many-body quantum theory in condensed matter physics: an introduction.* Oxford university press, 2004.

[17] Xie Chen, Zheng-Cheng Gu, Zheng-Xin Liu, and Xiao-Gang Wen. Symmetry protected topological orders and the group cohomology of their symmetry group. *Physical Review B*, 87(15):155114, 2013.

[18] David J Clarke, Jason Alicea, and Kirill Shtengel. Exotic non-abelian anyons from conventional fractional quantum hall states. *Nature communications*, 4:1348, 2013.

[19] Piers Coleman. *Introduction to many-body physics.* Cambridge University Press, 2015.

[20] Łukasz Cywiński, Roman M Lutchyn, Cody P Nave, and S Das Sarma. How to enhance dephasing time in superconducting qubits. *Physical Review B*, 77(17):174509, 2008.

[21] Mark Wild de Propitius and F Alexander Bais. Discrete gauge theories. In *Particles and fields*, pages 353–439. Springer, 1999.

[22] M T Deng, S Vaitiek, E B Hansen, J Danon, M Leijnse, K Flensberg, P Krogstrup, and C M Marcus. Majorana bound state in a coupled quantum-dot hybrid-nanowire system. *Science*, 354:1557, 2016.

[23] M. T. Deng, C. L. Yu, G. Y. Huang, M. Larsson, P. Caroff, and H. Q. Xu. Anomalous Zero-Bias Conductance Peak in a Nb–InSb Nanowire–Nb Hybrid Device. *Nano Lett.*, 12(12):6414–6419, December 2012.

[24] Fernando Dominguez, Jorge Cayao, Pablo San-Jose, Ramon Aguado, Alfredo Levy Yeyati, and Elsa Prada. Zero-energy pinning from interactions in Majorana nanowires. *npj Quantum Materials*, 2:13, 2017.

[25] Paul Fendley. Parafermionic edge zero modes in $\mathbb{Z}_n$-invariant spin chains. *Journal of Statistical Mechanics: Theory and Experiment*, 2012(11):P11020, 2012.

[26] Lukasz Fidkowski and Alexei Kitaev. Effects of interactions on the topological classification of free fermion systems. *Physical Review B*, 81(13):134509, 2010.

[27] Bernard Field and Tapio Simula. Introduction to topological quantum computation with non-abelian anyons. *Quantum Science and Technology*, 3, 06 2018.

[28] Matthew PA Fisher and Leonid I Glazman. Transport in a one-dimensional luttinger liquid. In *Mesoscopic Electron Transport*, pages 331–373. Springer, 1997.

[29] K. Flensberg. Non-Abelian Operations on Majorana Fermions via Single-Charge Control. *Phys. Rev. Lett.*, 106(9):090503, March 2011.

[30] Eduardo Fradkin and Leo P Kadanoff. Disorder variables and para-fermions in two-dimensional statistical mechanics. *Nuclear Physics B*, 170(1):1–15, 1980.

[31] Liang Fu. Electron Teleportation via Majorana Bound States in a Mesoscopic Superconductor. *Phys. Rev. Lett.*, 104(5):056402, 2010.

[32] Liang Fu. Topological crystalline insulators. *Physical Review Letters*, 106(10):106802, 2011.

[33] Liang Fu and Charles L Kane. Superconducting proximity effect and majorana fermions at the surface of a topological insulator. *Physical review letters*, 100(9):096407, 2008.

[34] Wen Xiao Gang. *Quantum field theory of many-body systems: from the origin of sound to an origin of light and electrons.* Oxford University Press, 2007.

[35] D. Gottesman. The Heisenberg Representation of Quantum Computers. *arXiv:quant-ph/9807006*, 1998.

[36] David J Griffiths and Darrell F Schroeter. *Introduction to quantum mechanics.* Cambridge University Press, 2018.

[37] Matthew B Hastings and Xiao-Gang Wen. Quasiadiabatic continuation of quantum states: The stability of topological ground-state degeneracy and emergent gauge invariance. *Physical review b*, 72(4):045141, 2005.

[38] MB Hastings. Quasi-adiabatic continuation for disordered systems: Applications to correlations. *Lieb-Schultz-Mattis, and Hall conductance*, 2010.

[39] Michael Hell, Jeroen Danon, Karsten Flensberg, and Martin Leijnse. Time scales for Majorana manipulation using Coulomb blockade in gate-controlled superconducting nanowires. *Phys. Rev. B*, 94:035424, 2016.

[40] A. P. Higginbotham, S. M. Albrecht, G. Kiršanskas, W. Chang, F. Kuemmeth, P. Krogstrup, T. S. Jespersen, J. Nygård, K. Flensberg, and C. M. Marcus. Parity lifetime of bound states in a proximitized semiconductor nanowire. *Nat. Phys.*, 11:107, 2015.

[41] Shih-Hao Ho, Sung-Po Chao, Chung-Hsien Chou, and Feng-Li Lin. Decoherence patterns of topological qubits from majorana modes. *New Journal of Physics*, 16(11):113062, 2014.

[42] Mark Howard, Joel Wallman, Victor Veitch, and Joseph Emerson. Contextuality supplies the 'magic' for quantum computation. *Nature*, 510(7505):351–355, 2014.

[43] Adam S Jermyn, Roger SK Mong, Jason Alicea, and Paul Fendley. Stability of zero modes in parafermion chains. *Physical Review B*, 90(16):165106, 2014.

[44] Torsten Karzig, Christina Knapp, Roman M Lutchyn, Parsa Bonderson, Matthew B Hastings, Chetan Nayak, Jason Alicea, Karsten Flensberg, Stephan Plugge, Yuval Oreg, Charles M Marcus, and Michael H Freedman. Scalable designs for quasiparticle-poisoning-protected topological quantum computation with Majorana zero modes. *Phys. Rev. B*, 95:235305, 2017.

[45] Torsten Karzig, Gil Refael, and Felix von Oppen. Boosting majorana zero modes. *Physical Review X*, 3(4):041017, 2013.

[46] Gediminas Kiršanskas, Martin Franckié, and Andreas Wacker. Phenomenological position and energy resolving lindblad approach to quantum kinetics. *Physical Review B*, 97(3):035432, 2018.

[47] A. Yu. Kitaev. Unpaired Majorana fermions in quantum wires. *Phys. Usp.*, 44(10S):131, October 2001.

[48] Christina Knapp, Torsten Karzig, Roman M Lutchyn, and Chetan Nayak. Dephasing of majorana-based qubits. *Physical Review B*, 97(12):125404, 2018.

[49] Christina Knapp, Jukka I Väyrynen, and Roman M Lutchyn. Number-conserving analysis of measurement-based braiding with majorana zero modes. *Physical Review B*, 101(12):125108, 2020.

[50] P. Lafarge, P. Joyez, D Esteve, C. Urbina, and M. Devoret. Measurement of the even-odd free-energy difference of an isolated superconductor. *Phys. Rev. Lett.*, 70:994, 1993.

[51] Jon M Leinaas and Jan Myrheim. On the theory of identical particles. *Il Nuovo Cimento B (1971-1996)*, 37(1):1–23, 1977.

[52] Goran Lindblad. On the generators of quantum dynamical semigroups. *Communications in Mathematical Physics*, 48(2):119–130, 1976.

[53] Netanel H Lindner, Erez Berg, Gil Refael, and Ady Stern. Fractionalizing majorana fermions: Non-abelian statistics on the edges of abelian quantum hall states. *Physical Review X*, 2(4):041002, 2012.

[54] Roman M. Lutchyn, Jay D. Sau, and S. Das Sarma. Majorana Fermions and a Topological Phase Transition in Semiconductor-Superconductor Heterostructures. *Phys. Rev. Lett.*, 105:077001, Aug 2010.

[55] Ryan V Mishmash, Bela Bauer, Felix von Oppen, and Jason Alicea. Dephasing and leakage dynamics of noisy majorana-based qubits: Topological versus andreev. *Physical Review B*, 101(7):075404, 2020.

[56] Gregory Moore and Nicholas Read. Nonabelions in the fractional quantum hall effect. *Nuclear Physics B*, 360(2-3):362–396, 1991.

[57] Niall Moran, Domenico Pellegrino, JK Slingerland, and Graham Kells. Parafermionic clock models and quantum resonance. *Physical Review B*, 95(23):235127, 2017.

[58] V. Mourik, K. Zuo, S. M. Frolov, S. R. Plissard, E. P. A. M. Bakkers, and L. P. Kouwenhoven. Signatures of Majorana fermions in hybrid superconductor-semiconductor nanowire devices. *Science*, 336:1003, 2012.

[59] Evgeny Mozgunov and Daniel Lidar. Completely positive master equation for arbitrary driving and small level spacing. *Quantum*, 4:227, 2020.

[60] F. Nathan and M. Rudner. Universal Lindblad equation for open quantum systems. *arXiv:2004.01469*, 2020.

[61] Chetan Nayak, Steven H. Simon, Ady Stern, Michael Freedman, and Sankar Das Sarma. Non-Abelian anyons and topological quantum computation. *Rev. Mod. Phys.*, 80(3):1083, 2008.

[62] Yuval Oreg, Gil Refael, and Felix von Oppen. Helical Liquids and Majorana Bound States in Quantum Wires. *Phys. Rev. Lett.*, 105(17):177002, October 2010.

[63] Stephan Plugge, Asbjørn Rasmussen, Reinhold Egger, and Karsten Flensberg. Majorana box qubits. *New Journal of Physics*, 19:012001, 2017.

[64] Elsa Prada, Pablo San-Jose, Michiel WA de Moor, Attila Geresdi, Eduardo JH Lee, Jelena Klinovaja, Daniel Loss, Jesper Nygård, Ramón Aguado, and Leo P Kouwenhoven. From andreev to majorana bound states in hybrid superconductor-semiconductor nanowires. *arXiv preprint arXiv:1911.04512*, 2019.

[65] John Preskill. Lecture notes for ph219/cs219: Quantum information. *Accesible via http://www.theory.caltech.edu/people/preskill/ph229*, 2015, 1997.

[66] Lupei Qin, Xin-Qi Li, Alexander Shnirman, and Gerd Schön. Transport signatures of a majorana qubit and read-out-induced dephasing. *New Journal of Physics*, 21(4):043027, 2019.

[67] Diego Rainis and Daniel Loss. Majorana qubit decoherence by quasiparticle poisoning. 85:174533, 2012.

[68] Mathias S Scheurer and Alexander Shnirman. Nonadiabatic processes in majorana qubit systems. *Physical Review B*, 88(6):064515, 2013.

[69] Manuel J. Schmidt, Diego Rainis, and Daniel Loss. Decoherence of Majorana qubits by noisy gates. *Phys. Rev. B*, 86:085414, 2012.

[70] Shun-Qing Shen. *Topological insulators*, volume 174. Springer, 2012.

[71] Michael Tinkham. *Introduction to superconductivity*. Courier Corporation, 2004.

[72] DM Tong, Jing-Ling Chen, JY Huang, LC Kwek, and CH Oh. Kraus representation for the density operator of a qubit. *Laser physics*, 16(11):1512–1516, 2006.

[73] Simon Trebst, Matthias Troyer, Zhenghan Wang, and Andreas WW Ludwig. A short introduction to fibonacci anyon models. *Progress of Theoretical Physics Supplement*, 176:384–407, 2008.

[74] M T Tuominen, J M Hergenrother, T S Tighe, and M Tinkham. Experimental evidence for parity-based 2e periodicity in a superconducting single-electron tunneling transistor. *Phys. Rev. Lett.*, 69(13):1997, 1992.

[75] MT Tuominen, JM Hergenrother, TS Tighe, and M Tinkham. Even-odd electron number effects in a small superconducting island: Magnetic-field dependence. *Phys. Rev. B*, 47:11599, 1993.

[76] Sagar Vijay and Liang Fu. Teleportation-based quantum information processing with majorana zero modes. *Phys. Rev. B*, 94:235446, Dec 2016.

[77] Ulrich Weiss. *Quantum dissipative systems*, volume 13. World scientific, 2012.

[78] AM Whiticar, A Fornieri, ECT O'Farrell, ACC Drachmann, T Wang, C Thomas, S Gronin, R Kallaher, GC Gardner, MJ Manfra, et al. Interferometry and coherent single-electron transport through hybrid superconductor-semiconductor coulomb islands. *arXiv preprint arXiv:1902.07085*, 2019.

[79] Frank Wilczek. Magnetic flux, angular momentum, and statistics. *Physical Review Letters*, 48(17):1144, 1982.